Master's thesis

NTNU
Norwegian University of Science and Technology
Faculty of Natural Sciences
Department of Chemistry

Sara Johnson

Cryoconite Holes as Potential Tools for Environmental Monitoring in the Arctic. A Study of the Accumulation of Atmospherically Deposited Inorganic and Organic Pollutants in Cryoconite Holes from Three Glaciers in Ny-Ålesund.

Master's thesis in Environmental Toxicology and Chemistry
Supervisor: Øyvind Mikkelsen
June 2022

NTNU
Norwegian University of
Science and Technology

Sara Johnson

Cryoconite Holes as Potential Tools for Environmental Monitoring in the Arctic. A Study of the Accumulation of Atmospherically Deposited Inorganic and Organic Pollutants in Cryoconite Holes from Three Glaciers in Ny-Ålesund.

Master's thesis in Environmental Toxicology and Chemistry
Supervisor: Øyvind Mikkelsen
June 2022

Norwegian University of Science and Technology
Faculty of Natural Sciences
Department of Chemistry

NTNU
Norwegian University of
Science and Technology

Abstract

A study of hazardous trace element accumulation in cryoconite from three glaciers in Ny-Ålesund; Austre Brøggerbreen, Vestre Brøggerbreen, and Midtre Lovénbreen, found elevated concentrations of As, Cd, and Pb compared to average upper continental crustal levels. Lead in particular was highly enriched and found to be present at 'moderate' levels of pollution in five of 28 cryoconite samples according to the Norwegian Environmental Agency quality standards for sediment in freshwater. Direct atmospheric deposition and scavenging of elements from replenished cryoconite hole water are likely to be the main sources for accumulation of certain elements in cryoconite. Cryoconite hole water contained a high proportion of Ca, whereas snow deposits sampled from the three glaciers were significantly elevated in Na and Cl, indicating a strong freshwater influence in the former and marine influence in the latter. Both the cryoconite and the overlying water fraction showed large spatial variability within and between the three glaciers analysed. On the whole, the spatial variation in elemental concentrations in cryoconite hole water followed the same pattern as in the cryoconite solid material, suggesting that the main source of elements detected in cryoconite hole water to be a consequence of dissolution from the solid mineral fraction. The low TOC content indicated a significant influence of the mineral fraction in the composition of cryoconite particles which was supported by a dominance of elements Al, Fe, Mg, K, and Ca. Supraglacial material from mud mound deposits on the glacier surface showed similar elemental and carbon content to cryoconite indicating that the origin of these deposits may be from melted-out cryoconite. Polychlorinated biphenyls (PCBs) were not detected in any of the cryoconite sampled, but the presence of a number of polycyclic aromatic hydrocarbons (PAHs) was observed. Given the remote situation of cryoconite holes, their limited exposure to pollutants outside of atmospheric deposition and ability to accumulate certain hazardous trace elements such as Pb and As, cryoconite could be considered an important environmental monitoring tool for changes in emissions and atmospheric transport of contaminants of concern in the Arctic.

Acknowledgements

This thesis is the conclusion of the Master's degree programme "Environmental Toxicology and Chemistry" (ENVITOX) from the Chemistry Department at the Norwegian University of Science and Technology (NTNU). The specialisation in this Master's degree programme is Environmental Chemistry.

Firstly I would like to thank my supervisor Øyvind Mikkelsen for providing me with the opportunity to do this research project in a remote area of Svalbard. I am very grateful for the help and patience throughout the fieldwork, for the analysis of samples for TOC/ROC/TIC and for anion analysis on IC. I am also thankful for his guidance throughout the project.

I would also like to thank Kyyas Seyitmuhammedov for his instruction on the freeze dryer, guidance through the microwave assisted digestion process and analysis of the water and snow samples by ICP-MS. Thank you to Anica Simic for her instruction on microwave assisted digestion in addition to analysis of the cryoconite and supraglacial debris by ICP-MS. This was a major part of the thesis, and it would not have been possible without both their help.

I am also grateful to Susana Villa Gonzalez for her help on GC-MS for PCB analysis, and Sylvia Weging for her instruction on ASE extraction.

Finally, thank you to Hege Bergesen Husebø and Natalia Vylegzhanina for their assistance during both the field and lab work, and to Mathilde Syvertsen and Thomas Walmsley for their help throughout sample preparation.

Table of Figures

List of Tables

Abbreviations

AB	Austre Brøggerbreen
amu	Atomic mass unit
ANOVA	Analysis of variance
ASE	Accelerated solvent extraction
CG	Cryoconite
CH	Cryoconite hole
CRM	Certified reference material
CW	Cryoconite hole water
DIC	Dissolved inorganic carbon
DOM	Dissolved organic matter
d.w.	Dry weight
EI	Electron impact ionisation
EPS	Extrapolymeric substances
ES	External standard
eV	Electronvolt
GC-MS	Gas chromatography – mass spectrometry
GPS	Global positioning system
IC	Ion chromatography
ICP-MS	Inductively coupled plasma – mass spectrometry
IR	Infrared
IS	Internal standard
ISO	International Organization for Standardization
K	Kelvin
LOD	Limit of detection
LOQ	Limit of quantification
LRAT	Long range atmospheric transport
m.a.s.l	Meters above sea level
ML	Midtre Lovénbreen
n	Sample number
n/a	Not applicable
NA	Not available
MB	Method blank
ME	Matrix effect
MF	Matrix factor
MM	Matrix matched
MPa	Megapascal
mya	Million years ago
PCA	Principal component analysis
PC	Principal component
ppm	Parts per million
QA	Quality assurance
QC	Quality control
ROC	Residual oxidisable carbon
RSD	Relative standard deviation
SD	Standard deviation
SGD	Supraglacial debris
SGD-M	Supraglacial debris – mud mounds
SGD- P	Supraglacial debris – plant based
SIM	Selected ion monitoring
SP	Spiked
TIC	Total inorganic carbon
TOC	Total organic carbon
UC	UltraCLAVE
UCC	Upper continental crust
VB	Vestre Brøggerbreen
WGMS	World glacier monitoring service

Al	Aluminium
Al_2O_3	Aluminium oxide
Ar	Argon
As	Arsenic
Ca	Calcium
Cd	Cadmium
Cl/Cl^-	Chlorine/ chloride
CO_2	Carbon dioxide
Cr	Chromium
DCM	Dichloromethane
Fe	Iron
HCl	Hydrochloric acid
$HClO_4$	Perchloric acid
HDPP	High density polypropylene
He	Helium
HF	Hydrofluoric acid
Hg	Mercury
HNO_3	Nitric acid
H_2O_2	Hydrogen peroxide
H_2SO_4	Sulphuric acid
K	Potassium
Mg	Magnesium
Na	Sodium
NH_4ClO_4	Ammonium perchlorate
NO_3^-	Nitrate
OCP	Organochlorine pesticide
PAH	Polycyclic aromatic hydrocarbon
Pb	Lead
PCB	Polychlorinated biphenyl
Pd	Palladium
POP	Persistent organic pollutant
Rh	Rhodium
Sb	Antimony
Si	Silicon
SO_4^{2-}	Sulphate
Zn	Zinc

Table of Contents

1 Introduction

Despite the remoteness of the Arctic and the limited human activity, the region has been exposed to pollution from long distance sources, the majority of which arrive as a consequence of anthropogenic activity from industrial areas and the mid latitudes in the northern hemisphere (1, 2). Transported in the atmosphere as gases or aerosols, to high latitudes via long range atmospheric transport, these contaminants reach the polar region where they are removed from the cold atmosphere via wet or dry deposition and accumulate in the Arctic environment (3-5).

Heavy metals and metalloids such as arsenic (As), cadmium (Cd), and lead (Pb) occur naturally in the environment, the concentrations of which are strongly influenced by the local geology (6-8). Higher than expected concentrations of these elements have been detected in remote locations in the Arctic such as Svalbard, where enrichment in comparison to natural background concentrations has been reported (9, 10). Persistent organic pollutants (POPs) such as polychlorinated biphenyls (PCBs) are synthetic chemicals with only anthropogenic sources and have also been detected in the Arctic (2, 11, 12). The accumulation of such contaminants in biota may result in risks to the health of animals and humans inhabiting the region (1, 3).

The Arctic is sensitive to changes in temperature. Ny-Ålesund in Svalbard has seen a decline in the number of snow days per annum and a warming of 1.35 °C per decade (13, 14). The Arctic contains ~ 44 % of the global glacierised area, and the glacial melting and receding experienced in this region is a consequence of increasing global temperatures (1, 15, 16). Cryoconite holes are small holes found on the surface of glaciers, filled with water and containing a thin layer of mineral and organic matter 'dust' known as cryoconite (17, 18). The holes provide distinctive habitats and are amongst the coldest, most extreme polar freshwater ecosystems on earth (19, 20). Cryoconite has been reported to alter the physical properties of ice, impacting glacier surface albedo, thus potentially contributing to glacier melting (21, 22). Moreover, cryoconite reflect the local atmospheric environment, and accumulate trace elements such as Pb, As, and Cd deposited on the surface of a glacier from local and distant sources (9, 10).

This study focuses on the physical and chemical characteristics of cryoconite holes, their ability to accumulate trace elements, and the potential to use these unique glacial habitats for environmental monitoring of future changes in the distribution and/or sources of long range atmospherically transported contaminants to the Arctic.

2 Theoretical Background

2.1 Svalbard

Svalbard is an archipelago in the Arctic Ocean, located at latitudes of 74º N to 81º N and longitudes of 10º E to 35º E. The archipelago is highly glaciated, with ~ 57 % of the land covered in 1,668 individual glaciers, spanning a total area of 33,775 km^2 and representing approximately 11 % of the total glacierised area of the Arctic (15, 16). Svalbard is comprised of three major islands: Spitsbergen, Edgeøya and Nordaustlandet. Spitsbergen, the largest island, is located between 76º - 80º N, and 10 º - 21º E, and represents approximately 60 % of the glacial area of the archipelago (16). The area of land not covered in glaciers is characterised by a landscape with glacial tills, lakes and bogs, and continuous permafrost, which can reach depths in excess of 500 m in the higher mountains (14, 23, 24). The soil is poorly developed, the area is devoid of trees and vegetation cover, comprised of tundra and alpine species, is low (14, 23).

The climate of Svalbard, in particular the western region, is influenced by the West Spitsbergen Current (WSC); air circulation patterns which bring humid and warm air from lower latitudes into the Arctic; and latitude which results in annual changes in light availability (25, 26). The WSC is the northernmost extension of the Norwegian Atlantic Current (the Norwegian branch of the North Atlantic Current), which transports warm and highly saline water into the Arctic Ocean (26). Large fluctuations in weather can be experienced, especially in winter, as a consequence of significant contrasts in temperature between two large air-masses originating from the Atlantic or Arctic (25, 26). The result is warmer temperatures than those experienced in areas of the same latitude, such as the Canadian and Russian Arctic (23). Precipitation is generally low in Svalbard, with the eastern side of the archipelago experiencing the highest precipitation as a consequence of easterly winds across the Barents Sea (25). The average annual temperature for the period 1971 – 2000 was – 8.7 °C with temperatures of – 16 °C in winter and 0.5 °C in summer (also for the same period). Ny-Ålesund, on the west coast of Spitsbergen experienced higher average temperatures for the same period of – 5.7 °C (14). The polar night begins on 25 October and ends on 17 February in Ny-Ålesund. The midnight sun then appears on 18 April and stays until 24 August (27).

At present the total population of Svalbard is ~ 2,940 which includes the three main settlements of Longyearbyen, Ny-Ålesund and Barentsburg, in addition to Pyramiden and Hornsund, all of which are located on Spitsbergen (28). Longyearbyen, which is the largest settlement on Svalbard, experiences dramatic increases in the number of residents during the tourist seasons (29).

2.2 Glaciers

Glaciers are an important ecosystem on earth, containing approximately 70 % of the earth's fresh water, covering ~ 10 % of the earth's land surface area, as well as providing valuable habitats for a diverse range of microorganisms (18, 30-32). The Randolf Glacier Index (RGI), an inventory of all glaciers (excluding Greenland and Antarctic ice sheets), estimated that the global glacierised area covered 726,800 ± 34,000 km^2 (reported in 2014) with 44 % of this area being represented by the Arctic region. Approximately 5 % of the total global glacierised area is in Svalbard and Jan Mayan (15).

Significant variability in the temperature structure and ice pressure (thermal regimes) of glaciers result in a large variety of glacier types (33). The thermal regime of a glacier influences glacier hydrology; the route surface meltwater takes through or across a glacier; and the type of erosion and deposition of sediment (34). In very simple terms, there are three types of glacier: temperate, cold, and polythermal (33). In temperate glaciers, the entirety of the glacier ice is warm and the temperature is at the pressure melting point, whereas ice in a cold glacier is found at temperatures below the pressure melting point (33, 35). Polythermal glaciers, widely found in Svalbard, are more complex with a thermal regime of both warm and cold ice (16, 33, 36, 37). Large variations in the polythermal structure of glaciers exist, however in general the glacier mostly contains cold ice (below the pressure melting point), with the exception of an area of warm glacier ice (at the pressure melting point) located in the basal layer at the glacier bed (33, 35, 37). The surface (~ 15 m thick) of all three glacier types is susceptible to variability in seasonal temperatures (33, 35).

A glacier can be split into two areas, an accumulation zone and an ablation zone, separated by the equilibrium line (25). In the accumulation zone, snow accumulation exceeds ablation, whereas in the ablation area, melting and/or evaporation exceeds snow accumulation (17, 25). At the equilibrium line, where the net mass balance is zero, ablation and accumulation are equal (25). In the summer melting season, on polythermal glaciers such as those found in Svalbard,

snow melt in the accumulation zone can slowly drain down to the glacier bed and to the groundwater below the permafrost (33, 38, 39). In the ablation zone, meltwater channels can form on the surface of glaciers. In addition, englacial channels can be formed as a consequence of the downwards melting of the surface meltwater channels, leading to englacial drainage networks which follow the gradient of the surface of the glacier. The formation of moulins or crevasses in the glacier can lead to the transport of surface meltwater down to either the englacial channels or to subglacial pathways near to, or at the glacier bed (38, 39). The location of the temperate ice at the glacier bed may impact the drainage through subglacial pathways (39). In contrast, cold polar glaciers are frozen to the glacier bed and hence surface meltwater penetration may be limited to channels near the surface, potentially forming interconnecting passages between cryoconite holes (water-filled holes found on glacier surfaces), or along fractures, that can transport meltwater through to the cold glacier bed (17, 40, 41).

Summer meltwater can transport large volumes of water from a glacier and it has been estimated that melting snow and ice from Svalbard glaciers produce approximately 25 ± 5 km^3 a^{-1} surface run off (38). The meltwater contained within cryoconite holes may also contribute to the surface run-off on glaciers (40). Contained within this meltwater are anions such as sulphate (SO_4^{2-}) and chloride (Cl^-), supraglacial debris called "cryoconite" released from cryoconite holes, and possible, previously deposited pollutants such as PCBs, stored within the glacier ice (9, 39, 42-44). Over the past 30 years, the glacierised area of Svalbard has reduced by ~ 7 %, being an average decrease of 80 km^2 a^{-1} (16). If temperatures continue to rise as a consequence of increase in greenhouse gas emissions, it is estimated that small Arctic glaciers could completely disappear by 2050 (45).

2.3 Trace Elements and Polychlorinated Biphenyls

2.3.1 Polychlorinated Biphenyls (PCBs)

Polychlorinated biphenyls are a group of synthetic organic chemicals with the molecular formula $C_{12}H_{10-n}Cl_n$ (Fig. 2.1) (11). Hydrogen atoms on the biphenyl rings are replaced by between 1 to 10 chlorine (Cl) atoms, and the number and placement of these atoms result in a total of 209 different PCB congeners (46). Each congener is named based on a numbering system proposed by Ballschmiter and Zell (1980), where the congener is identified by a unique number from 1 to 209, the order of which is determined with respect to the original IUPAC

system name (47, 48). Although 209 congeners are possible, it is not expected that all these congeners would have been commercially produced (11).

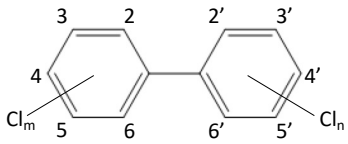

Figure 2.1 *General structure of polychlorinated biphenyls*

The chemical and physical properties as well as biological activity of the congeners differ based on their chemical structure and the number of Cl atoms (48, 49). For example, vapour pressure and water solubility of a PCB congener decreases, whilst viscosity and boiling point increase, with increasing numbers of Cl atoms (50). PCBs are lipophilic, poorly soluble in water, chemically stable, heat resistant and insulating, in addition to having useful flame retardant properties (11, 46, 48, 49). As a consequence, PCBs were used in a number of applications including in electrical capacitors and transformers, as plasticisers and sealants in construction, and in paints, printing inks, and carbonless copy paper (46, 48, 51-54). The properties which made PCBs especially attractive for commercial use, are also the reason for their persistence in the environment (48). The high lipophilicity of PCBs enable them to bind to lipids in tissue, and their resistance to biodegradation results in bioaccumulation, and subsequent biomagnification along food chains (1). It has been suggested that PCBs have endocrine disrupting effects, and can produce possible toxic effects in birds and mammals such as disruption to behaviour and reproduction, brain development, immune system suppression, and disruption of the development of the central nervous system (1, 55, 56).

2.3.1.1 History of PCBs

It has been estimated that global production of PCBs reached ~ 1.3 million tonnes from first commercial production by Monsanto Chemical Corporation in the US in 1930 to its cessation 1993 in former Soviet Union (Russia). It is however expected that this figure could be higher in reality due to a lack of reliable production data from every country. The majority of PCBs appeared to be produced in the northern hemisphere, with Monsanto being responsible for approximately 50 % of global production (50, 57). Individual countries manufactured PCBs under their own trade names such as Aroclor (USA, Japan), Pyroclor (UK, USA), and Kanechlor (Japan) (11).

Due to their persistent nature and adverse impacts on ecosystems and human health, PCBs were one of the 'dirty dozen' persistent chemicals initially added to the Stockholm Convention listing on Persistent Organic Pollutants in 2004, and are regulated under Annex A meaning 'elimination' (with some exceptions) (1, 58, 59). However prior to this, many countries introduced their own regulations restricting and/or banning the use of PCBs and PCB-containing chemicals (except in closed systems) from the late 1970s (11). Although production is now prohibited under the Convention, it was estimated by Breivik et al. (2007), using two different scenarios, that 12.9 % or 16.5 % of the PCBs produced might still be utilised worldwide, the majority within closed systems (57). Emissions of PCBs are therefore still a risk, and due to their persistence, PCBs are still being detected across the globe, including as far north as the Arctic (1, 2, 60).

2.3.1.2 PCBs in the Arctic

Seven indicator PCBs (Fig. 2.2) consist of the most commonly reported congeners in literature due to their abundance in both the environment and composition in technical mixtures such as Aroclor (12, 61). Their sum is often used as an estimation of total PCB contamination in the environment, although it has been suggested that the reliance on these seven indicator PCBs in environmental matrices may result in an underprediction of total PCB contamination (61). Of the seven PCB congeners, the presence of PCB 28, 52, and 180 have been identified in soil in Svalbard (2). Enhancements in atmospheric concentrations of PCBs taken at Zeppelin in Ny-Ålesund, Svalbard have also been identified potentially as a result of long range atmospheric transport of contaminants following biomass burning events (12). A major route of PCBs into the Arctic is via the atmosphere (62). The properties of PCBs which favour atmospheric transport are described in further detail in Section 2.3.3.

Polychlorinated biphenyls have also been reported in biota in Svalbard such as polar bears, arctic foxes, seals, and birds (55, 56, 63, 64). Temporal trend studies for PCBs in the Arctic air and biota showed significant decline before 2000, however since then the decline has slowed (59, 60). For some PCB congeners a rise in concentration has been reported since 2000 in Arctic air which may be due to secondary emissions from, for example, melting ice or oceans (60).

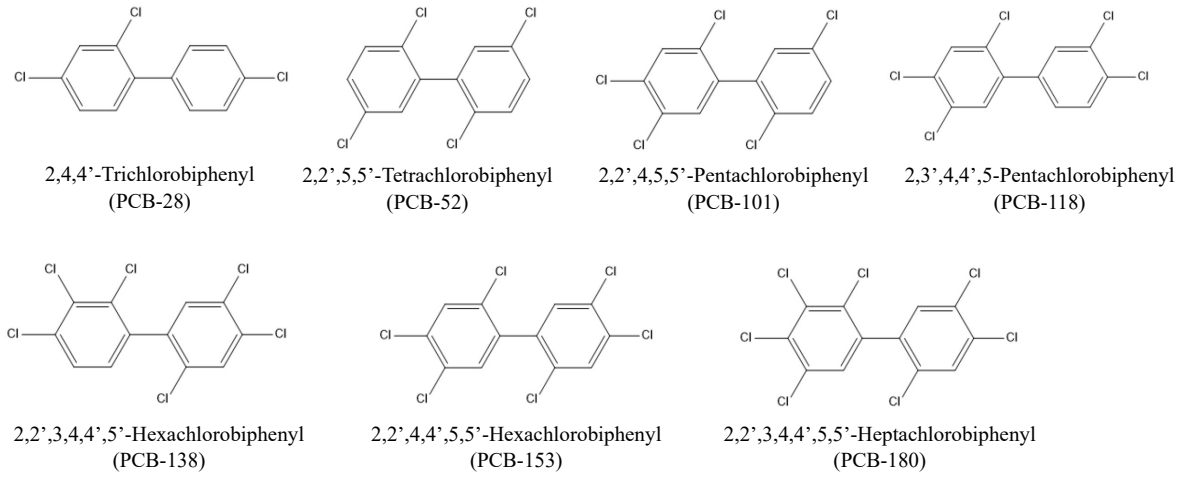

Figure 2.2 *Structures of the seven indicator PCBs analysed, the 'Dutch Seven', including nomenclature and IUPAC numbers.*

Some local PCB contamination exists on Svalbard and Jartun et al. (2009) identified local sources from electrical and building waste and scrap metal from three coal mining settlements on Spitsbergen; Longyearbyen, Barentsburg, and Pyramiden (54). It was suggested that paint and small capacitors were the main sources of PCB contamination (54). Waste dumpsites and chemicals required in old mining machinery may provide additional local sources of PCBs (65). The PCB-138 congener was also observed at the rocket booster impact area in Ny-Ålesund following investigations after sounding rocket launches in 2018 and 2019 (66).

2.3.2 Trace Elements

Of the 118 known elements in the periodic table, 90 occur naturally on earth (6). These naturally occurring elements can be classified into three groups; major, minor, and trace. The trace elements can be further categorised as essential, non-essential, and toxic (6). Large variations occur in both the physicochemical form and magnitude of elements within and between earth compartments and their distribution can be dependent on a number of factors including weathering, solubility, pH, and redox potential (6). Essential elements are those elements which are necessary for physiological and biochemical functions in a living organism and cannot be substituted by other elements to fulfil their role (6, 67). This group includes the elements iron (Fe), zinc (Zn), copper (Cu), manganese (Mn), and cobalt (Co) (67). Non-essential elements are those elements with no proven essential function but can be found in biological tissue such as lithium (Li) and strontium (Sr) (6). The toxic trace elements include mercury (Hg), cadmium

(Cd), and lead (Pb). These elements have no biological function and are toxic even at low concentrations. Arsenic (As) is also considered to be a toxic element in the environment at low concentrations, although it may be essential for some species (6, 67). The toxic elements can bioaccumulate in living organisms and Hg (as methylmercury) has been shown to biomagnify along a food chain (67). There is however, a fine line between essentiality and toxicity, with essential elements also being toxic at high enough concentrations (6).

In the environment, trace elements are present and move both within and between five main compartments or spheres (6). The three spheres where the movement and presence of trace elements are most relevant for the study of cryoconite holes are the geosphere, the hydrosphere, and the atmosphere.

2.3.2.1 Trace Elements in the Geosphere

The earth's crust is the natural origin of trace elements (6). Within the geosphere, the main element in the earth's crust is oxygen which makes up 47.2 % of the total composition, followed by silicon (Si) with a 28.8 % contribution. Aluminium (Al) and Fe represent 7.96 % and 4.32 % respectively, whilst the other major elements: calcium (Ca), sodium (Na), magnesium (Mg), and potassium (K) make up 3.85 %, 2.36 %, 2.20 %, and 2.14 % of the continental crust respectively (8, 68, 69). The trace elements are a much smaller component of the earth's crust. These elements are not commonly found as free elements but incorporated into the mineral fraction of the rock, for example, Zn, As, Pb, and Hg can be present as sulphides, and chromium (Cr) as oxides, and are present at ppm and ppb levels (6, 8, 68, 69).

The mobilisation and distribution of trace elements within the geosphere and into environmental compartments such as the hydrosphere and atmosphere is the consequence of processes such as physical and chemical weathering, and dissolution (6). Natural emissions into the atmosphere via particulate matter and aerosols can occur as a result of volcanic eruptions (representing 40 – 50 % of natural emissions annually of Cd and Hg, and 20 – 40 % of As, Cr, and Pb), forest fires, sea-salt sprays (14 % of As emissions), biogenic sources, and wind-blown soil dusts (> 50 % of Cr emissions and 20 – 30 % of Pb and Zn emissions) (70). Anthropogenic activity has significantly sped up the process of emissions of elements into the atmosphere, water, and soil, and has resulted in wide spread alterations to natural elemental concentrations in all environmental compartments (6). Anthropogenic activities, which include those industries involving high temperature processes such as the burning of fossil fuels (coal and oil), non-

ferrous metal smelters, waste incineration, transportation (with respect to Pb), and to a lesser extent cement production and wood combustion, in addition to mining and aerosol sprays (halo-carbons), result in the release of elements into air, soil, and water (6, 71).

The geosphere also includes soil and sediment compartments. Soils, where trace elements are also found to naturally occur, can become a source of elements to plants, animals, and humans (72). Soil consists of a mineral and organic matter fraction (6). Trace elements can adsorb onto soil components such as clay minerals (generally silicate based), organic matter, such as humic acids, and hydr(oxides) of Fe and Mn via complexation or ion exchange adsorption (72, 73). High surface areas and negatively charged surfaces result in a high ion exchange capacity of the soil, between the positively charged metal ion and the negatively charged surface (72).

Sediment is comprised of silt, clay, sand, and organic matter and can contain significant amounts of trace elements, the majority of which participate in similar interactions as in soil. These interactions include adsorbing onto hydr(oxides) of Fe and Mn, onto the surface of clays, and forming organic complexes of low solubility. Bacteria can also play a role in the speciation of trace elements at the surface-water interface (6). Trace elements found in significant quantities in sediments include Cr, Cd, Pb, Fe, and Mn. In both soil and sediment, the type and availability of ligands, pH, and redox potential play a crucial role in the determination of the chemical forms of the trace elements present in these environments (6).

2.3.2.2 Trace Elements in the Hydrosphere

In marine systems, major elements are found in the order $Na^{+}>Mg^{2+}>Ca^{2+}>K^{+}$. In freshwater systems such as rivers, the elemental order differs slightly with Ca^{2+} being the most dominant ion (6). Trace elements are generally present in low concentrations in their dissolved form in water, with higher concentrations often found accumulated in sediments (6, 74). Trace elements in natural waters can be found in various organic and inorganic, dissolved and particulate forms (Table 2.1) (74). The dissolved forms are defined practically, as those species that can pass through a 0.45 μm filter (75). Dissolved forms include free metal ions (hydrated, i.e. coordinated with water molecules), ion pairs, inorganic and organic complexes, and smaller inorganic and organic colloids. Inorganic and organic complexes consist of metal ions electrostatically or covalently bonded with, for example, carbonate, bicarbonate or hydroxide groups (inorganic), or for example fulvate or humic acids (organic). Chelation, complexation of metal ions by covalently bonding with multidentate ligands (i.e. multiple ligands on the same

molecule coordinate with the metal ion), can produce stable complexes in water (74). In the particulate phase, trace elements can be present as large colloids or bound to solid surfaces (74).

Colloids play an important role in the transport and regulation of trace element concentrations in natural waters as a consequence of their high surface area and charge (76). Colloidal particles are defined based on a size range of 1 nm to 1 μm (75). They are highly complex and can vary significantly in type. For example, colloids in freshwater can consist of oxides of Mn and Fe, biological debris, colloidal humic acid, fulvic compounds, clays and minerals such as kaolinite, aluminosilicates, and silica (75, 76). Colloids participate in a number of different reactions, resulting in a dynamic system with a continuously changing composition. Metal ions can interact with colloids via charged surfaces or via inorganic or organic ligands present on the colloidal surface. Colloids can aggregate with other particles to form larger colloids, which if sufficiently large and unstable can coagulate, transporting the metal ions from the water column to the sediment (75, 76).

Dissolved organic matter (DOM) is also present in natural waters and can have a significant impact on the presence, solubility, transport, bioavailability, and toxicity of trace elements via complexation of the metal ion (77). The composition of DOM is complex and contains a heterogeneous mixture of organic molecules, both allochthonous (derived outside of the aquatic environment) and autochthonous in origin (derived within the aquatic environment) (77, 78). The DOM can include humic and fulvic acids, extrapolymeric substances (EPS), proteins, and carbohydrates (77, 78). Humic and fulvic acids can represent a substantial portion of dissolved organic carbon (a component of DOM) in natural waters, and can complex with metal cations such as Pb^{2+}, Cu^{2+}, and Hg^{2+} through phenolic and carboxyl groups present on the humic substances (74).

Table 2.1 *Summary of the speciation of metal ions in natural waters with lead as an example (74, 76).*

Speciation	Description	Lead Example	Medium
Free metal ion[a]	$M \cdot aq^{n+}$ The metal ion is not found as a free ion i.e M^{n+} in water, but found co-ordinated with H_2O molecules	$Pb{\cdot}aq^{2+}$	Dissolved, in solution
Inorganic complexes[a]	Complexation with Cl^-, OH^-, $HCO_3^{2-}$to form inorganic complexes	$PbCl^+$	Dissolved, in solution
Organic complex with natural acid[a]	For example complexation with humic and fulvic acids via chelation	Pb-Hum	Suspension
Colloidal complexes[a,b]	Metal ion adsorbed onto colloids such as iron oxides or aluminium silicates	Pb^{2+} - $Fe(OH)_3$	Colloidal; dissolved or particulate phase depending on colloidal particle size
Adsorbed to surfaces[a]	For example metal bound to decomposing organic matter, or clay particles	Pb – Organic matter	Solid particulate matter
Ionic solid[a]	Metal ion held within a lattice structure, for example within the clay mineral structure	$PbCO_3$	Solid particulate matter

[a] Stumm & Morgan 1996: Metal Ions in Aqueous Solution: Aspects of Coordination Chemistry (74).
[b] Stumm & Morgan 1996: Particle-Particle Interaction: Colloids, Coagulation, and Filtration (76).

The pH of the water also plays an important role in the speciation and thus the transport of trace elements (74). In freshwater, the majority of Pb is present as Pb^{2+} at pH 6, whereas at pH 8, Pb is predominantly in the form $PbCO_3$(aq). However the dominating Zn species in freshwater at both pH 6 and 8 is Zn^{2+} (74). The pH can also affect the speciation of trace elements in the presence of DOM such as humic and fulvic acids, with the capacity to complex with metals such as Pb, As, Fe, and Cd changing based on pH (77).

2.3.3 Trace elements and PCBs in the Atmosphere: Long Range Atmospheric Transport

Global transport of pollutants can occur via a number of pathways including the transfer of contaminants over long distances via ocean currents, sea ice, rivers and the atmosphere (1). Long range atmospheric transport (LRAT) is responsible for the presence of volatile and semi volatile contaminants in the Arctic (1, 3).

The Arctic haze, a term introduced in the 1950s to describe the reduced visibility observed during flights in the High Arctic, is a clear and visible result of the accumulation of anthropogenic contaminants from outside sources reaching the pristine Arctic atmosphere (1). The dominant source of the particulate matter causing the Arctic haze is believed to originate from Eurasia and is reported to consist mainly of sulphates, with soot and to a lesser extent dust making up the remainder (1). Heavy metals and organochlorine contaminants are transported to the Arctic either as gases or adhered to particles in aerosols, for example in sea-salt spray or wind-blown dust (3-5). Aerosols can travel long distances depending on a number of physical and chemical properties including size, mass, and shape of the aerosol (4). Once in the Arctic, aerosol particles containing contaminants are deposited on the surface of, for example, glaciers either by wet or dry deposition (4). Dry deposition is the direct transfer of gases or particles from the atmosphere to the surface, as result of gravitational settling (4, 79). Wet deposition of heavy metals is the result of processes such as in-cloud and sub-cloud scavenging in which particles can be incorporated into snow (4, 79). Finally, the cold temperatures promote condensation, slowing the evaporation of POPs from water, and thereby supporting the partitioning of contaminants from the atmosphere to the Earth's surface (62).

Pollutants are transported to the poles because volatile chemicals evaporate from the earth's surface in warm temperature regions (tropical and sub-tropical), where they migrate in the atmosphere as aerosols and gases, partition from a gaseous phase to a non-gaseous phase, condense and deposit onto surfaces such as soil and water in colder regions at higher latitudes such as the Arctic and Antarctica (62). A number of processes by which contaminants are transported in the atmosphere to the Arctic have been proposed, including "global distillation" or fractionation, the "grasshopper effect", and the "single hop". Contaminants are separated or fractionated as they are transported to higher and colder latitudes relative to their volatility, resulting in a "global fractionation", with more volatile and mobile contaminants migrating faster than pollutants with lower volatility (5, 62). The term "grasshopper effect" has been used to describe the jump-like movement of POPs from the release point at warmer temperatures, to higher cooler latitudes. The transport of the contaminants follows an alternating pattern of migration and deposition in line with annual variations in temperatures in the mid-latitude regions (62). Some contaminants are insufficiently volatile to be re-volatilised after deposition into soil or water. These contaminants can only reach the Arctic through a "single-hop" process, where once emitted into the atmosphere, deposition does not take place until the

contaminant has reached the cold temperatures in the Arctic region (80). An inverse relationship can be observed between the concentration of mobile volatile contaminants and latitude (62).

The cooler temperatures at higher latitudes provide a number of conditions favourable for the deposition and accumulation of contaminants. The cooler temperatures slow the natural degradation process, thereby increasing the persistence of contaminants such as POPs. Furthermore, the adsorption of contaminants to particulate matter present in the atmosphere is preferred at cool temperatures (62). Temperature therefore plays a vital role in determining the extent to which POPs and heavy metals enter the Arctic atmosphere and deposit on its surface (81).

A combination of physicochemical properties are required for a contaminant to reach the Arctic and accumulate in soil, vegetation or water (81). Firstly the chemical must be present in the atmosphere, either by processes such as direct emission or evaporation, at considerable concentrations in the source region (80). Secondly, the contaminant then needs to be sufficiently volatile and persistent to survive in the atmosphere, without degradation, for potentially long periods of time during transport from the source region to the Arctic (5, 80, 81). Thirdly the contaminant then needs to have the correct physicochemical properties to enable deposition onto the surface of the Arctic region, and to then be retained once deposited (80, 81). For example, if a contaminant is highly volatile it may be easily transported to the Arctic, but will stay in the Arctic atmosphere and may never be deposited onto the surface (80). The properties of contaminants are therefore important as not all volatile chemicals will reach the poles. Many contaminants will be retained by compartments such as soil and sediment following a deposition step or degraded either at the point of release, or whilst moving to higher latitudes (62, 80).

The mobility of a contaminant can be determined using three partition coefficients which describe the equilibrium partitioning between water, air and octanol. These coefficients are: the octanol-water (K_{OW}) partition coefficient, octanol – air (K_{OA}) partition coefficient, and the air-water (K_{AW}) partition coefficient. The K_{OW} can be determined from K_{OA}/ K_{AW} and is a measure of a chemical's lipophilicity/hydrophilicity (80, 82). The mobility of PCBs and the corresponding transport characteristics are presented in Table 2.2 along with examples of PCBs and related log K_{OA}, Log K_{OW} and temperature of condensation (T_C) values for each PCB example.

Table 2.2 *Properties for PCB mobility. The mobility of PCBs allocated into four groups ranging from low to high, including their general deposition patterns. Examples of PCBs in each mobility category are provided, including details of partition coefficient values for log K_{OA} and log K_{OW}. The temperature of condensation (T_C) is displayed in °C. Information provided in the table is adapted from Wania & Mackay (1996) and Wania (2003). The partition co-efficient values are extracted from Li et al. (2003) (62, 80, 83).*

Mobility[a]	Transport Characteristics[b]	No. of Cl Atoms[a]	PCB Example	Log K_{OA}[c]	Log K_{OW}[c]	Temperature of Condensation[d] (T_C)
Low	Generally found at high concentrations close to emission source. Deposition over evaporation favoured.	8 - 9	PCB 194	11.13	7.76	+ 37 °C
Relatively Low	Deposit and accumulate at mid-latitudes.	4 - 8	PCB 153	9.44	6.87	+ 10 °C
Relatively High	Deposit and accumulate in polar regions. Show bioaccumulation potential. Partition to compartments such as soil, vegetation, snow and water.	1 - 4	PCB 28	7.85	5.66	- 22 °C
High	Highly volatile substances, do not favour deposition even in the Arctic. Globally dispersed in the atmosphere.	0 - 1	PCB 3	6.78	4.65	~ - 50 °C

[a] Wania & Mackay (1996) (62).
[b] Transport characteristics information extracted from Wania & Mackay (1996) and Wania (2003) (62, 80).
[c] Data extracted from Li et al. (2003). The Log K_{OA} and Log K_{OW} values are presented at 25 °C from final adjusted values (FAV) (83).
[d] Temperature of condensation information extracted from Wania & Mackay (1996), NILU Report (84).

The seasons play a key role in contaminant transport to the Arctic. In the winter season low pressure areas form over the Atlantic Ocean (Icelandic Low) and northern Pacific (Aleutian Low), and high pressures are established over the continent (Siberian High) (85). These high and low pressure areas result in the movement of air masses (along with contaminants) leading to a mean circulation out of northern Eurasia, into and across the Arctic, and through to North America (1, 86). The Arctic front, which acts as a barrier between the cold near-surface (lower troposphere) of the Arctic and the rest of the atmosphere, can expand down to as far south as 40° N in winter as a consequence of the Siberian high pressure system, leading to areas of Eurasia being within the Arctic air masses (1, 87, 88). As a consequence, Eurasia is believed to account for more than half of the air transported contaminants reaching the Arctic, driven by the high pressure systems moving air northwards and significant point sources in northern Russia (1). However in summer, changes in pressure systems lead to the disappearance of high pressure cells over the continent, and weakening of low pressures over the oceans (85). As a consequence, transport slows, being approximately half the speed of the winter months, and the

mean circulation changes to movement from the North Atlantic Ocean, through the Arctic and to the north Pacific Ocean (86). In the summer months, the Arctic front contracts and the air masses are restricted to just the polar region (87).

Global changes in climate can alter temperature, weather patterns, and ocean currents (85). Changes in the global climate can alter the steps a contaminant takes on its journey to the Arctic, including the time spent in the terrestrial and aquatic environment. These alterations could lead to changes in the mixture of contaminants reaching northerly latitudes through for example alterations in degradation and concentration of contaminants, as well as either expediting transport to higher latitudes or causing delays (85). Even if only a small proportion of contaminants reach the poles, these environments are susceptible to high concentrations of contaminants, due to the smaller areas they cover in comparison to mid-latitude regions (62).

2.4 Cryoconite Holes

2.4.1 An Introduction to Cryoconite Holes

Cryoconite is derived from Greek, meaning ice dust (89). The term "cryoconite" was first used in 1870 by the Arctic explorer A. E. Nordenskiöld during a crossing of the Greenland ice cap, with reference to particulate matter found in holes or depressions on the surface of the glacier (18). In an article from 1883 regarding an expedition to inland Greenland, Nordenskiöld described the particles in the bottom of water cavities: "*At the bottom a layer of kryokonite one to four millimetres in thickness is deposited, which has often, by organisms and by the wind, been formed into little balls*" (Nordenskiöld 1883, p726) (90).

The discovery of cryoconite holes consequently became of particular interest to explorers and scientists in the early twentieth century (18). In the last two decades there has been a significant increase in research on cryoconite holes, especially with respect to microbial communities present in the holes (19, 20, 91, 92), the biogeochemistry of cryoconite (93, 94) and cryoconite hole hydrology (40, 95). The last 10 years has seen the emergence of a number of studies on the accumulation of atmospherically deposited heavy metal and radionuclides by cryoconite (9, 10, 43, 96-98). To date, research is scarce with respect to the potential existence of PCBs in cryoconite holes, and no studies have been found regarding PCB concentrations in cryoconite in the Arctic. Just one study has been identified, which investigated the potential for microbial degradation of PCBs in cryoconite and which identified 18 PCB congeners in alpine cryoconite

holes from Jamtalferner glacier in Austria (99). It was suggested that the average concentrations detected in cryoconite were 100 times higher than PCB concentrations found in contaminated glaciers (99).

Cryoconite are most commonly found at the bottom of cryoconite holes in the ablation zone of glaciers worldwide (22, 33, 100). Studies have reported finding cryoconite holes on glaciers at high latitudes in Antarctica and the Arctic, including Greenland and Svalbard (9, 10, 22, 40, 92-94, 97, 98, 100-102). Cryoconite holes have also been found at mid-latitudes including the Himalayas and temperate regions of the high Alps, the Tien Shan (China) and the Tibetan Plateau, as well as on glaciers in British Colombia, Canada (21, 22, 43, 96, 98, 103, 104). Cryoconite, however, are not only restricted to holes in the ablation zone of glaciers but have been observed directly on the surface of a Himalayan glacier; as dry deposition coined 'cryoconite mantles'; and in supraglacial stream deposits (22, 33, 105).

There are three types of cryoconite holes; open, closed, and submerged holes, as shown in Fig. 2.3 (33).

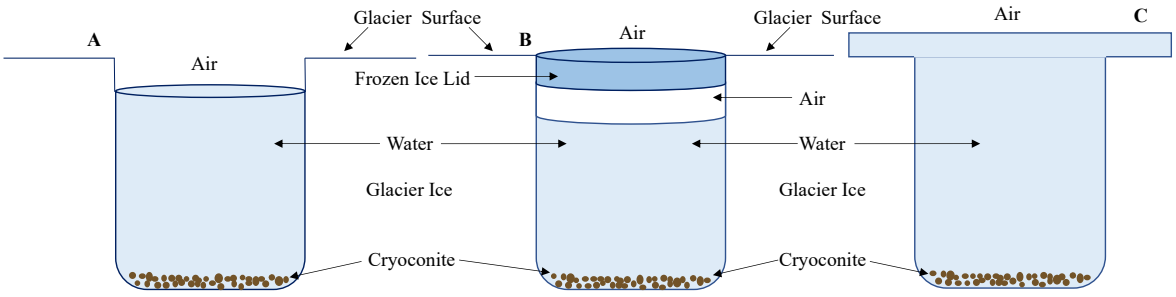

Figure 2.3 *Schematic of the three types of cryoconite holes: (A) open cryoconite hole, as found in the Arctic; (B) closed cryoconite hole with frozen lid, as found in Antarctica; (C) submerged cryoconite hole (figure adapted from Hodson et al. (2008)) (33).*

2.4.2 Cryoconite Biogeochemistry

The cryoconite particulate matter found at the bottom of cryoconite holes are both organic and inorganic in nature. The dominant component of cryoconite is the inorganic matter fraction, making up an estimated 84 – 99 % of the total particle mass (dry weight), with the remainder comprised of microorganisms, organic matter, and anthropogenic particles such as black carbon, radionuclides, heavy metals, and POPs (9, 10, 22, 31, 94, 99).

Mineral fragments mainly containing silicates, such as quartz, phyllosilicates (for example mica), tectosilicate (for example plagioclase or potassium feldspar), and clay minerals (for example illite and kaolinite) can make up the majority of the inorganic fraction (101, 106). Material can be transported to the surface of the ice locally, for example by wind, the release of inorganic matter stored within the glacier as a result of melting, and redistribution from coastal processes (101, 106, 107). The mineral fraction can also be impacted by more distant sources where fine particles in the high atmosphere are transported long distances and deposited on the surface of large glaciers, such as deposition from desert dust storms and micrometeorites (space dust) (106, 108). The minerology can thus vary between cryoconite, resulting in a high level of geochemical heterogeneity even within a glacier's surface (31, 94, 101).

The minerology of cryoconite can affect its physical properties (colour and reflectivity) as well as potentially impacting the organic matter (OM) component (22, 91). The OM fraction of cryoconite is comprised of living microorganisms and their dead and decomposing components. The OM fraction can be both autochthonous, i.e. generated by photosynthesis within the holes, or allochthonous, i.e. sourced from outside the holes, such as material transported by wind and deposited on the glacier surface from local areas of high OM content such as soils and proglacial wetlands (102, 109).

The OM content is also considered to play a crucial role in both the physical and chemical characteristics of cryoconite (22, 94, 100, 103, 110). Indeed the extent of OM content is considered to influence the size and shape of cryoconite, with a positive relationship being reported between photoautotrophic microorganism number and cryoconite granule size (94, 103). The OM content of cryoconite has been found to vary both on a local and global scale ranging from ~ 3 % from Canada Glacier, Antarctica, to as much as 38 % in Blåsen, Scandinavia (100, 111). Organic carbon (OC) content, can make up a fraction of OM and is typically found at ~ 1 – 4 % dry weight in cryoconite (102, 112). The OM composition has also been found to vary across a glacier surface (113). Langford et al. (2011) reported higher quantities of OM rich in carbohydrate and related products of humification in cryoconite from the centre of Aldegondabreen glacier, Svalbard in comparison to the glacier edge (113).

2.4.3 Cryoconite Biology

Cryoconite holes are unique habitats for microorganisms (21, 103, 111). Microbial communities are present in both cryoconite hole water and cryoconite, although to a lesser

extent in the former (19). Microbial communities have an important role to play within cryoconite holes such as nutrient cycling, carbon fixation, and hole and cryoconite granule formation (18, 19, 93, 114). Furthermore, the microbial communities can also have an indirect impact on the physical characteristics of glacier surfaces via the lowering of the surface albedo, as a consequence of their role in aggregate formation (21, 93).

A wide variety of microorganisms have been identified in cryoconite holes including cyanobacteria, green algae, heterotrophic bacteria, viruses, fungi, rotifers, tardigrades, and diatoms (18-20, 30, 91, 92). Microorganisms colonise the holes through deposition of air-borne particles of biological origin onto the glacier surface or via cryoconite hole water replenishment from melting ice or glacial streams (17, 92, 115). Photoautotrophic bacteria (primary producers via photosynthesis) and heterotrophic bacteria (consumers that source their energy from organic compounds) dominate in cryoconite (19, 31, 91, 114). Of the photoautotrophs, cyanobacteria dominate, with filamentous cyanobacteria reported to make up 90 - 99 % of the total photoautotrophic microorganisms (94, 102, 112).

Spatial variability has been observed when comparing the minerology, OM content and structure of the cryoconite aggregates, both within a glacier and between glaciers locations (91, 94, 113). The heterogeneity in aggregate structure and composition promotes variability in microbial communities contained within cryoconite holes (94). For example some cryoconite have been found to be dominated by heterotrophic bacteria as opposed to the cyanobacteria often found in higher abundance (94).

A significant role of microorganisms in cryoconite holes is their contribution to the formation of cryoconite granules. A number of studies have observed filamentous cyanobacteria covering the outer, or near surface region of the cryoconite granule, as opposed to the interior (21, 93, 94). It has been proposed that filamentous cyanobacteria bind particulate matter to form aggregates by two processes; mechanical and chemical binding. The cyanobacteria mechanically bind the aggregates by entangling and weaving together the constituent particles thereby providing a structural support for the granules (93, 94). Chemical binding occurs through interactions between the mineral surface and a substance like glue with cohesive properties produced by microorganisms, known as extracellular polymeric substances (EPS) (93, 94, 116). Langford et al. (2010) identified high concentrations of polysaccharides, a form of carbohydrate and a major component of EPS, near or on the surface of the granules, associated with photoautotroph clusters (94, 116).

Granules with a low abundance of filamentous cyanobacteria are perhaps more fragile and as a consequence easily disintegrated into their constituent parts (93, 94). As such there appears to be a positive relationship between the size of cryoconite granules and the number of photosynthesising microorganisms present in the cryoconite holes (94). The aggregation of the particulate matter into cryoconite granules, driven by the binding properties of the filamentous cyanobacteria, is likely to increase the residence time of cryoconite on the surface of the glacier (93). The larger granules are more likely to settle than the finer particulate matter which is more easily transported down the glacier by supraglacial streams and meltwater (94). The increased residence of the granules contributes to the reduction in the surface albedo of the glacier, unless limited by heterotrophic bacteria or by the removal of these cryoconite granules from the surface by glacial meltwater (21, 22, 93, 106, 114). Microorganisms can therefore play an indirect role in glacier melting and the spatial variability in glacier surface albedo (93).

2.4.4 Cryoconite Morphology

Cryoconite granules are quasi- spherical in shape consisting of aggregated particles of both biotic and abiotic nature as discussed in Section 2.4.2 and 2.4.3 (100). A study by Rozwalak et al. (2022) compared the colour and morphology, in addition to organic matter content, cyanobacteria and algae composition, and geochemistry of cryoconite from 33 glaciers worldwide (100). The size and shape of the cryoconite granules were found to vary to a significant extent between geographical locations as well within a glacier. Cryoconite granules differed in size from on average 0.32 ± 0.12 mm on Gulkana Glacier in Alaska, to 7.21 ± 3.11 mm on Austerdalsbreen in Norway, with an overall range across the sampled glaciers of 0.1 – 12 mm (100). Zarsky et al. (2013) reported cryoconite mean size as large as 110 ± 35 mm on Aldegondabreen, Svalbard (91). This significant variation in granule size may be the result of local conditions such as glacial slope, geology, atmospheric deposition, and the balance maintained between the rate of microbial growth, aggregation of particulates, and erosion (91). The spherical shape observed in many particles could be due to a dense coverage of the granules by filamentous cyanobacteria in addition to the physical force created from the movement of meltwater (21, 103).

Cryoconite granules with a number of different internal structures have been observed (103). Four distinct structures were identified by Takeuchi et al. (2010) which include: (i) granules consisting of a large mineral particle at the centre, (ii) granules comprised of sub-granules (i.e.

smaller aggregated granules), (iii) granules made up of layers of organic material and (iv) granules with no distinct structure (i.e. no layering observed) (103). Granules with distinct layers were most commonly found, and it was suggested that these layers probably originated from the annual growth activity of cyanobacteria (21, 103). A layered structure was also reported by Hodson et al. (2010) in cryoconite granules studied from Longyearbreen in Svalbard, which was suggested to be driven by incorporation of sediment from a variety of sources (93). The variation in the potential sources of the mineral fraction may therefore provide an explanation for the diversity of mineral fragment sizes reported within cryoconite granules across the globe (108). For example, the particulate matter making up cryoconite granules from Longyearbreen included fine silt particles which measured on average 22 – 25 μm in diameter, whereas granules from Midtre Lovénbreen in Svalbard had a high sand content, with higher mean sizes of 80.5 μm in comparison (93, 94). These small fragments are likely to be deposited on the glacier surface as a result of aeolian processes, in contrast to the cryoconite granules, whose larger sizes make this transport process less likely (93).

The growth rate for cryoconite granules studied on the Yala Glacier in the Himalayas was suggested to be approximately 400 μm per annum (21). The layers within the granules could be an indication of the age of the cryoconite, and it was suggested that the seven layers identified in some cryoconite granules from Ürümqi glacier in the Tien Shan could represent a maximum cryoconite age of seven years (103). A granule threshold size of approximately 3 mm in diameter was proposed by Takeuchi et al. (2001) (21). The size and age of granules could be limited by breakdown due to freezing and transportation of particles in addition to the ability of the cyanobacteria filaments to bind the granules and the adhesiveness of the organic matter (21, 93, 94, 103).

The life cycle of a granule has therefore been proposed by Takeuchi et al. (2010) which includes annual growth during the summer melting season by filamentous cyanobacteria, followed by aggregation with neighbouring granules producing larger particles (103). Once the granules reach a threshold size, they fragment into smaller pieces, which then regrow during the melt season to create new granules. This life cycle of growth and disintegration may span multiple years (103). The summer melting season is expected to be the only season when the cyanobacteria can grow, as photosynthesis is not possible due to the thick snow cover on the glacier surface, and/or the lack of sunlight in the polar regions during the winter months (21).

2.4.5 Cryoconite Colour and the Impact on Surface Albedo

Colour variations occur as a consequence of differences in the light absorbency of cryoconite. Colours such as pale or dark brown, black, or grey have been reported, and this colouration has been found to differ among glaciers worldwide (22, 100, 106). The colour of cryoconite can be influenced by both the mineral and OM fractions to differing extents. The mineral fraction has been observed to range in colour from transparent or white, through to brown or black (21, 22, 106). The OM content can be near transparent, or near opaque, and can range from green to black (94, 100). The age of the aggregate may influence the colour of the OM in the cryoconite granules, in addition to the presence of black carbon (94). The dark coloured amorphous OM (general term; humic substances) identified in cryoconite is suggested to result from the presence of bacteria which decompose old microorganisms and other organic particulate matter contained within the cryoconite (21, 117). The dark colour of the OM may be a consequence of the presence of conjugated bonds in humic substances which absorb visible light (118).

The components of cryoconite (mineral fragments and organic matter) influence its reflectance (22). Cryoconite are suggested to lower the surface albedo (i.e. the reflectance) of a glacier, and as a result, promote melting of the glacier surface (21, 22). An experiment performed on the surface of a glacier, which compared the surface albedo of a clean glacier with no cryoconite, to one covered in cryoconite, found that the surface albedo was between ~ 20 – 40 % lower in the cryoconite covered ice (21). The lower reflectance of the ice was due to the higher light absorbency of the cryoconite. A comparison of cryoconite to windblown material, sourced from the surrounding rock and believed to be mostly comprised of mineral fragments and small amounts of plant fragments and considered to be the origin of the cryoconite, found the windblown material to have a higher spectral albedo and therefore a lower light absorbency than the cryoconite granules (21). It was also found that OM, carbon and nitrogen content were all lower in windblown particles compared to cryoconite (21). Another study reported a significant negative correlation between humic substances and the reflectance of the cryoconite, but a lack of significant correlation between cryoconite reflectance and total OM, nitrogen and carbon content (22). It was proposed that the level of light absorbency and thus the reflectance of the cryoconite and as a consequence its colouration, is related to the quality, not quantity of the OM (22). It is therefore the OM content contained within cryoconite, which substantially increased once deposited on the glacier surface, that has the largest influence on the reduction of the glacier surface albedo and the colour of the cryoconite (21, 22, 106).

2.4.6 Cryoconite Hole Formation

Cryoconite holes form as a result of melting caused by the deposition and accumulation of wind-blown dust and organic material on a glacier surface. The sizes of the holes can be determined in part by sediment distribution on the ice surface (40, 107).

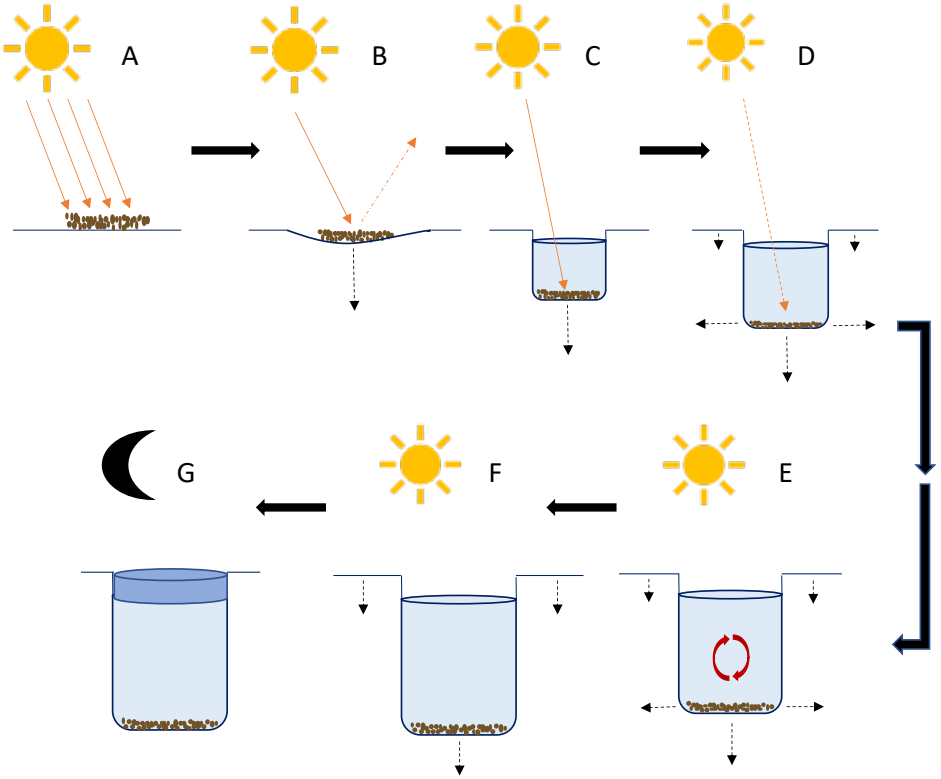

Figure 2.4 *Formation of cryoconite holes. Flow diagram shows the absorption of solar radiation (yellow line) by accumulated sediment leading to the formation of cryoconite holes via downwards and horizontal melting (dotted black line). The cryoconite is depicted as brown material at the bottom of the hole, the water is pale blue and the frozen ice lid is dark blue. The red circular arrows in image (E) represent the circulation of heat energy. The final image (G) represents a frozen hole in winter in the Arctic. Image adapted from MacDonell and Fitzsimons (2008); and Cook et al. (2016) (107, 108).*

In simple terms sediment (inorganic and organic material) is deposited onto the glacier surface (as described in Section 2.4.2) where it accumulates, aided by deformities in the ice which trap particulate matter (17, 89). On steep sloped glaciers or those with very high melt rates, the sediment may be washed off the glacier surface before hole formation is achieved (119, 120). The dark coloured cryoconite sediment, which has a lower albedo than the surrounding clean glacier ice, absorbs short wavelength solar radiation (Fig. 2.4, A). This solar radiation is converted to thermal energy which preferentially melts the underlying ice, and as a

consequence, the sediment sinks into the surface of the glacier (Fig. 2.4, B) (17, 21, 108, 120). Melting occurs in both vertical and horizontal directions, resulting in the formation, deepening and widening of the cryoconite holes (Fig. 2.4 C,D). During hole formation the particulate matter redistributes across the bottom of the hole to fill the new space created (108). As the vertical melting caused by the cryoconite occurs at a faster rate than the glacier surface ice ablation, the hole deepens (40). As the hole depth increases, meltwater fills the space and as a result, heat energy transfer is dominated by convection (Fig. 2.4, E) (according to McIntyre (1984), as cited in MacDonell & Fitzsimons (2008)) (107). The effectiveness of the heat transfer is then dependent on the conductivity and ability of the water to circulate the heat energy in the hole (107, 120). With depth, less solar radiation reaches the bottom of the cryoconite hole, and more heat is conducted away from the base of the hole at a faster rate, as a result of the colder temperatures of the deeper ice (40, 108). Eventually an equilibrium depth is reached when the rate of hole deepening slows, at which point the rate of downward melting is equal to the rate of glacier surface ablation (Fig. 2.4, F) (40, 120).

In addition to energy generated from solar radiation, some metabolic energy generated by microbial processes such as photosynthesis also contribute to the formation of cryoconite holes, although to a much lesser extent (18). Experiments performed in the field demonstrated that cryoconite holes were 10 % shallower when micro-organisms in the cryoconite holes were killed (according to McIntyre (1984), as cited in Fountain et al. (2004)) (40). In the polar regions, during winter months when no solar radiation is available for melting or photosynthesis, the water in cryoconite holes typically freezes (Fig. 2.4, G) (17).

Ultimately, cryoconite hole decay is caused by melting of the glacial ice, destruction of the holes as a result of the formation and growth of supraglacial glacier drainage channels through the cryoconite hole, or by the formation and accumulation of ice on the cryoconite walls, resulting in a reduction in size until the hole is no longer present (according to McIntyre (1984), as cited in Samui et al. (2018)) (94, 95, 105). The survival of cryoconite holes for more than one season is therefore dependent on a number of factors, including the appropriate conditions for the cryoconite sediment to melt the underlying glacier ice at a faster rate than the glacier surface ice ablation (120).

2.4.7 Cryoconite Hole Hydrology and its Impact on Nutrient and Ion Concentrations

Cryoconite holes are separated into two major classes, those with and without frozen lids (Fig. 2.3) (33). The summer season conditions influence the surface temperature of the glacier and hence the melting of the ice lid (33). Cryoconite holes with open lids are most commonly found in temperate locations and on glaciers in the Arctic (9, 10, 97, 98). Cryoconite holes characterised by frozen lids are found in Antarctica, and are the consequence of a surface energy balance that means glacier surface ice in the ablation zone remains below the freezing point of water (92, 95).

Cryoconite holes with open and closed lids are reported to have very different chemical and biological properties (92, 95, 115, 121, 122). Atmospheric and water exchange processes occurring in open cryoconite holes affect microbial, carbon, nutrient, and elemental accumulation within the holes as a consequence of removal and replenishment of water from glacier meltwater run-off, the exchange of gases, and exposure to atmospheric deposition (33, 92, 115, 121). Closed cryoconite holes are isolated from water and gas exchange. As a result, fluctuations in nutrients and accumulation of major ions are significantly influenced by processes occurring within the holes, such as melting, freezing, weathering of debris and microbial activity (92, 123).

Within the cryoconite holes, deposition of inorganic solutes from marine aerosols, dissolution of solutes from cryoconite sediment along with photochemical and biological reactions of microbes is proposed to occur. These processes result in the presence of ions such as Na^{+}, Ca^{2+}, Cl^{-}, SO_4^{2-} and nitrate (NO_3^{-}), nutrients, dissolved inorganic carbon (DIC), organic carbon, and microorganisms in the cryoconite hole water (93, 95, 121-123). Constituents of cryoconite holes can be gradually transported down a glacier via the recharging of water from upstream, and the subsequent draining of cryoconite hole water downstream across a glacier surface (102). The lack of complete isolation of open cryoconite holes, and the consequential redistribution of cryoconite hole water and material over a glacier surface, may lead to homogenisation of microbial communities between holes as a result of inter-hole mixing (33, 115, 121).

The age of a cryoconite hole can be determined, for hydrologically isolated holes only, using chloride (40). Chloride is not modified by biological activity within a cryoconite hole and is thus a useful tracer ion (107). Fountain et al. (2004) proposed a calculation which compared the

concentration of Cl^- ions in cryoconite hole water to that of the surrounding ice (40). Cryoconite hole depth and cross sectional area are also required in addition to the melt rate at the floor of the cryoconite hole to determine age (40).

2.5 Supraglacial Debris

Supraglacial debris in addition to cryoconite contained within cryoconite holes can be found on glaciers. Rockfalls, and mixed snow and rock avalanches, may result in the formation of lateral, medial, and terminal moraines (32, 33, 112, 124, 125). Hodson et al. (2008) reported the presence of a mounds of what was believed to be cryoconite debris, containing thick layers of dark organic matter (33). This debris was suggested to be frequently found on glaciers in Svalbard, especially on those with a more gentle slope. In contrast to the processes that result in the formation of cryoconite holes, the thick layers of organic matter contained within the debris insulate the underlying ice, preventing melting, thus leading to the formation of the mound-like structures with cracked surfaces. The structure of the mounds can lead to an anaerobic environment within the debris, resulting in conditions and rates of respiration which differ from those within open cryoconite holes (33).

2.6 Snow

Snow is an important sink for both soluble and insoluble, naturally and anthropogenically released impurities (4, 126-128). The impurities present in snow are either the result of dry deposition directly onto the snow surface or via snowfall as a consequence of the scavenging and incorporation of species from the atmosphere (79). By analysing ice cores on glaciers, which are composed of accumulated snow, it is therefore possible to determine the atmospheric chemistry of the time when snow deposition occurred (1). Thus snow chemistry can be key to understanding the transport of natural and anthropogenic, organic and inorganic contaminants and is dependent on both the source of the impurities, and the air masses that transport the aerosols containing these impurities, both long and distant (4, 126-128). Given that the Svalbard archipelago is surrounded by ocean, the strong marine influence can lead to high concentrations of major ions such as Cl^-, SO_4^{2-} and Na^+, mainly as a consequence of sea-salt particle transport (126, 129). Dust from the local rock can also be a natural source of ions such as Mg^{2+} and Ca^{2+} in snow (126, 129, 130). Long range atmospheric transport of pollutants is described in detail in Section 2.3.3.

During the winter season from October to May, most of the Svalbard archipelago is covered in snow, however temperatures have been increasing at 1.35 °C per decade in Ny-Ålesund, and the number of days in the snow season has been decreasing (13, 14). Across the whole of the Svalbard archipelago the duration of the snow season decreased by ~ 20 days (from 340 to 320 snow days) between 1958 – 2017 (14). The annual snow season is also important for the mass balance of glaciers, which have been affected significantly by the changing climate in Svalbard (131, 132).

2.7 Ny-Ålesund Rocket Launches

Svalbard Rocket Range (Svalrak) is located close to the airport, approximately 1.2 km from Ny-Ålesund town (Fig. 2.5) and may be a local source of pollution to the surrounding environment (66). Five sounding rockets were launched in 2018, 2019, and 2021; two on 7 December 2018, one on 26 November 2019 and one on 10 December 2019 (133). The launch of the Japanese rocket on 4 November 2021 occurred after sampling in August 2021 (133). The rocket launches were part of a 12 rocket research project called "Grand Challenge Initiative – Cusp" (GCI-Cusp), an international collaboration between Norway, the United States and Japan. The project consisted of 9 missions, and 12 rocket launches, 4 from Svalrak in Ny-Ålesund, Svalbard, and 5 from Andøya Space Centre (133).

Sounding rockets are designed for scientific testing and experimental research missions. The rockets generally use solid propellants due to their easy handling and storage, in addition to simplicity, high thrust at low cost, and density properties which are important when dealing with compact size requirements (134). Solid propellants usually consist of a fuel, an oxidiser and other ingredients including a binder, catalyst and curing agent (135). The most commonly used solid rocket propellants comprise of an aluminium fuel, along with an oxidiser such as ammonium perchlorate (NH_4ClO_4). Binders, for example hydroxyl-terminated polybutadiene (HTPB), can be included in the solid rocket motor (135, 136). The binder provides a matrix structure in which the fuel and the oxidiser are held (135). The curing agent impacts the physical properties of the propellant, and is responsible for solidification and hardening of the binder. Finally, a catalyst can be used to modify the rate of burning of the propellant, an example being iron oxide (66, 135).

The primary combustion products of the emission on launch include among others: hydrochloric acid (HCl) generated from NH_4ClO_4, aluminium oxide (Al_2O_3), carbon dioxide (CO_2), and water (136, 137). In addition to combustion emissions, debris is also left behind in the area surrounding the launch site from booster rocket break-up following the launch. The debris can include material used for insulation in addition to paint chips, metal and electrical equipment (66, 137). The rocket booster impact area locations are shown in Fig. 2.5 at 78º 54.59' N, 11º 49.41' E and 78º 55.33' N, 11º 49.43' E along with the locations of the three neighbouring glaciers (66). The base of glaciers Vestre Brøggerbreen, Austre Brøggerbreen and Midtre Lovénbreen are approximately 2.6, 2.8 and 5.5 km from the launch site respectively.

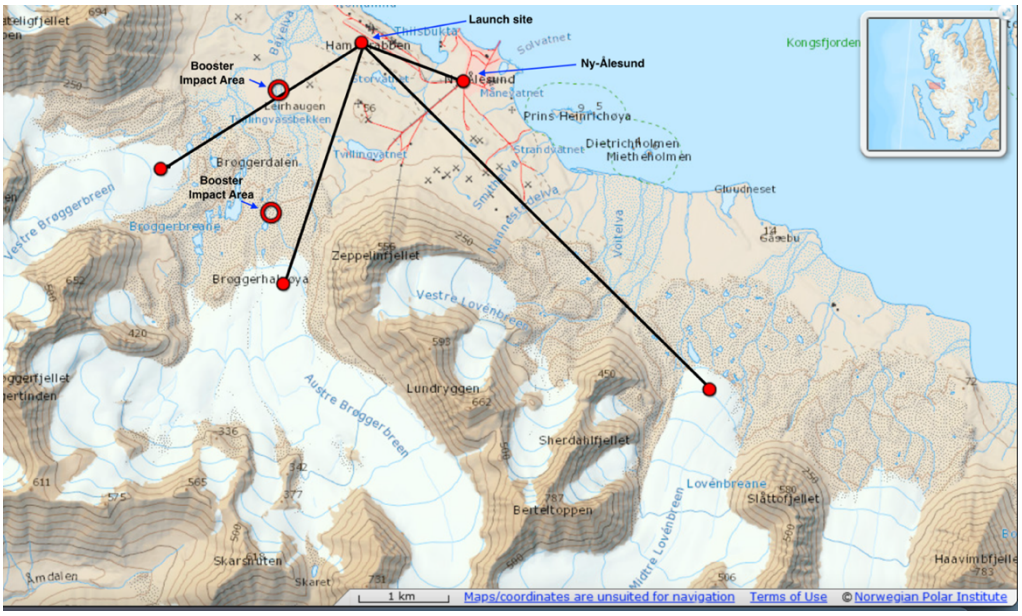

Figure 2.5 *Locations of the sounding rocket launch site and booster impact areas demonstrating proximity of launch site to surrounding glaciers Austre and Vestre Brøggerbreen and Midtre Lovénbreen. Map adapted from Aas et al. (2021) report on the "effects of rocket launches in Ny-Ålesund, 2018-2019" using TopoSvalbard maps from the Norwegian Polar Institute n.d (66, 138).*

Contamination at a local level can be caused by the generation of clouds of dust (ground clouds) on launch, which can then be transported from the launch site by the wind. Furthermore, atmospheric interactions with the rocket exhaust vapour trail can result in local transport of the exhaust emissions (136). The size of the local deposition area depends on meteorological conditions including wind direction, speed, and humidity (137, 139). Within ground clouds, turbulence created by the rocket exhaust results in atomisation of water. The coagulation of water droplets and the scavenging of Al_2O_3 and HCl occurs, producing droplets with a very low pH which can be carried within the ground cloud until deposition via fall out (139). Fallout has been reported up to 22 km from a launch site (139). A NASA Technical report from 1983 on

the environmental effects of the first five space shuttle flights found elevated levels of Al, Cr, Cd, and Mn, and decreased concentrations of Fe in soil at the launch pad site (140).

The immediate effects of the rocket launches in Ny-Ålesund including potential trace metal and POP contamination were analysed by Aas et al. (2021) (66). The study provided information on atmospheric, snow, and overbank sediment environmental analysis performed in the area surrounding the rocket launch location on the days of the launches in 2018 and 2019. Increased levels of Al and Fe were found, in addition to elevated concentrations of two chlorinated organic pollutants in 2018 and the sum of dioxins in 2019 (66).

2.8 Aims and Hypothesis

The overarching objective of this study was to assess the potential for cryoconite holes to be used for environmental monitoring of air deposited contaminants in the Arctic. This objective was achieved through (i) the evaluation of the chemical composition of cryoconite from three land terminating glaciers: Austre Brøggerbreen, Vestre Brøggerbreen, and Midtre Lovénbreen in Ny-Ålesund, with a particular focus on the trace elements As, Cd, Cr, Pb, and Zn; (ii) the determination of enrichment levels of the selected elements in cryoconite in comparison to the continental crust, including a comparison of elemental concentrations to literature on cryoconite from Svalbard; (iii) the comparison of the concentrations of the selected elements to other matrices in Svalbard; and (iv) the comparison of the accumulation of trace elements in cryoconite hole water and snow to investigate the influence of glacier melting on cryoconite accumulation. In addition, potential local and long range sources of the selected elements, including the possible impact from the rocket launches from Svalrak, have been discussed. Heterogeneity of cryoconite within and between glaciers have been analysed, and the chemical and physical properties of cryoconite were compared to other supraglacial debris in order to investigate the fate of cryoconite following melt out. Finally, new research was performed to determine the presence of PCBs in cryoconite sampled from the three glaciers. This information could provide current data on background concentrations for future environmental monitoring.

The following hypotheses have been established for this study:

(a) Elements including Cd, Pb, Zn, and As are found at higher concentrations in cryoconite material compared to the upper continental crust indicating accumulation, and a potential local or long range source outside the local rock.

The null hypothesis states that concentrations of heavy metals and metalloids including Cd, Pb, Zn, and As in cryoconite will be influenced by natural sources and will be present within those levels identified in the continental crust.

(b) There is a heterogenous distribution in the physical and chemical properties of cryoconite holes within Midtre Lovénbreen, Austre Brøggerbreen, and Vestre Brøggerbreen.

The null hypothesis states the presence of a homogeneous distribution in the physical and chemical characteristics of cryoconite holes within Midtre Lovénbreen, Austre Brøggerbreen, and Vestre Brøggerbreen.

3 Analytical Theory

3.1 Sample Preparation

A number of pre-treatment techniques were required to prepare the samples for elemental analysis by inductively coupled plasma – mass spectrometry (ICP-MS), PCB determination by gas chromatography – mass spectrometry (GC-MS), and total organic carbon (TOC), residual oxidisable carbon (ROC), and total inorganic carbon (TIC) determination via combustion. The techniques described in Sections 3.1.1 – 3.1.3 include freeze drying, microwave digestion, and accelerated solvent extraction (ASE).

3.1.1 Freeze Drying

Freeze drying, or lyophilisation, is a process of drying under vacuum, via sublimation and desorption of ice or other frozen solvent molecules (141). A low pressure is needed for sublimation, below the triple point of water (611.657 Pa, 0.01 ºC) (142, 143). Heat energy is then required to enable sublimation of the ice to a gas (141). There are three steps in the freeze drying process, the first being the freezing of the sample, followed by primary and secondary drying (141). The material being dried must be properly frozen prior to lyophilisation. In the primary stage, the pressure is reduced to below the triple point of water to enable sublimation. In the secondary stage, heat is added under vacuum to enable the desorption of the water molecules (141, 143). The ISO standard relevant to freeze drying of soil and sediment samples is *ISO 16720:2005 standard – Soil quality – pre-treatment of samples by freeze-drying for subsequent analysis* (144).

3.1.2 Microwave Assisted Digestion for Environmental Purposes

Microwave assisted digestion is a sample preparation technique used for elemental analysis of solid samples by ICP-MS, which requires samples to be in solution rather than in a solid state (145). The technique has been shown to effective in the digestion of matrices such as soils and sediments containing silicates and organic substances. Short digestion times are also an advantage (146). Two types of microwave assisted digestion exist: open and closed vessel systems. A closed vessel system has the advantage of minimising external contamination,

including cross contamination between samples, requires smaller volumes of acid, enables the use of high pressures and temperatures, and has demonstrated good recoveries for volatile elements (146-148). Thus closed systems are of particular use for trace elemental analysis where contamination risk is high and limited sample is available for analysis (147). Different acids and acid mixtures have been used to obtain the optimal dissolution of target analytes, including combinations of acids such as nitric acid (HNO_3), hydrofluoric acid (HF), hydrochloric acid (HCl), sulphuric acid (H_2SO_4), perchloric acid ($HClO_4$), and hydrogen peroxide (H_2O_2) (148). Nitric acid, frequently used for digestion, has the advantage of being a strong oxidising agent with the ability to dissolve organic samples. The majority of elements are soluble in the HNO_3, although silicates are only partially soluble and require HF for digestion (148). On the other hand, elements such as the lanthanides can have low solubility or are insoluble in HF, and the selection of the acid required for digestion is therefore dependent on the target analyte (148). In accordance with ISO standard *ISO 16729:2013(E) – Soil quality – digestion of nitric acid soluble fractions of elements*, although HNO_3 is known to not dissolve the entire environmental sample, it is considered adequate for the majority of environmental studies (149).

In microwave assisted digestion, microwave energy is absorbed by the solution only (not the vapour phase), resulting in heating of the liquid phase. A thermal non-equilibrium is established between the liquid and vapour phase which enables high temperatures to be achieved in the liquid at relatively low pressures (147). In a closed system these higher temperatures and pressures can be reached. This enables the boiling point of HNO_3 to increase above its normal boiling point, resulting in an increase in the oxidising strength of the acid, and shorter decomposition and dissolution times (148).

3.1.3 Accelerated Solvent Extraction (ASE)

Analysis of environmental samples by GC requires the exchange of a sample from a solid to a liquid matrix (150). Accelerated solvent extraction (ASE) is a method used to extract analytes from a solid matrix at elevated pressures and temperatures above the boiling point of the liquid solvent (151). It has been found to successfully extract PCBs and PAHs without thermal degradation, producing comparable recoveries to other frequently used extraction methods such as Soxhlet extraction (151). An advantage of ASE is the time it takes for extraction, and the smaller volumes of solvent required (151, 152). While other extraction methods such as Soxhlet

extraction use large volumes of solvent (150 – 500 mL) and can take 4 – 48 h, ASE extraction can take less than 30 minutes depending on the parameters, and requires significantly smaller volumes at ~ 1.5 times the extraction cell volume (15 – 40 mL) (153). Elevated pressure enables the extraction solvent to reach temperatures above boiling point whilst remaining in the liquid phase (151). Moreover, elevated temperature and pressure can weaken the interactions between the solute and the matrix, increase solubility, and improve extraction efficiency by increasing the contact between the sample and the solvent, forcing the solvent into pores within the matrix where the target analytes may be located (151).

The main components of ASE are a stainless steel extraction cell which contains the solid sample, an oven, pumps for the delivery of solvent, nitrogen gas, and an extract vial (151). The solid sample, loaded into an extraction cell, is added to a preheated oven where it is filled with an extraction solvent such as DCM, at temperatures between 50 – 200 ºC and pressures between 500 – 3000 psi (151). During the static extraction process, the solvent is held within the extraction cell for a specific length of time, at a preselected temperature and pressure (154, 155). This process can be repeated for the required number of static cycles, with each cycle using fresh solvent (155, 156). After extraction, the sample is rinsed with fresh solvent followed by a purging step whereby a compressed gas such as nitrogen purges the extract from the extraction cell and into the collection container (153).

Purification steps can also be combined with extraction to remove compounds that may interfere with analyte detection (152). For the use of non-polar solvents such as DCM, a drying agent such as diatomaceous earth is required to mix with the sample matrix to ensure the sample is sufficiently dry prior to extraction, thereby removing interference from water and improving extraction efficiency (154). Diatomaceous earth can also act as a dispersing agent, preventing particle aggregation (152, 154). Copper can be added to remove sulphur from the sample which is co-extracted with PCBs and can therefore cause interference in detection (152, 157). Activated alumina is added to the extraction cell for the removal of lipids (154).

3.2 Analysis

Four different analytical techniques were used for elemental analysis, PCB determination, anion determination, and TOC/ROC/TIC measurement of cryoconite, water, snow and supraglacial

debris samples. A theoretical background of each analytical process, ICP-MS, GC-MS, ion chromatography (IC), and combustion are presented in Sections 3.2.1 – 3.2.4.

3.2.1 Inductively Coupled Plasma - Mass Spectrometry (ICP-MS)

Inductively coupled plasma mass spectrometry (ICP-MS) has been used since 1983 for trace elemental determination in environmental samples and is suitable for a number of different matrices including rock, sediment, soil, vegetation, and water (145). The success of ICP-MS over other analytical techniques such as Flame Atomic Emission and Flame Atomic Adsorption is its low detection limits, wide analytical range, and multi-element capabilities, enabling the measurement of multiple elements simultaneously at low concentrations, down to parts per trillion (ppt) levels (158, 159). The ICP-MS technique also has the advantage of relatively simple sample preparation and small sample weight requirements, in addition to short analysis times (145, 159).

An ICP-MS instrument is made up of an ICP which creates the ion source, and a mass spectrometer (MS) which detects and quantifies the ions (159). The instrument has six main compartments, (i) a sample introduction system, (ii) a plasma source (ICP), (iii) an interface region through which the ions are extracted, (iv) an ion optics region which focuses the ions through lenses, (v) a mass analyser which separates the ions based on their mass to charge (m/z) ratio, and (vi) a detector (159).

The sample introduction system requires samples to be in a liquid form (145). The sample introduction system comprises an autosampler, a peristaltic pump, a nebuliser, and spray chamber (159). The peristaltic pump transports the sample to the nebuliser, where the sample is transformed into an aerosol (145, 159). The spray chamber then removes large aerosol droplets which can cause plasma overload (impacting analytical performance) or extinguish the ICP-torch, so that only a fine aerosol remains (with size of ~ <10 μm) which usually represents 1-5 % of the sample (145, 158, 159).

Plasma source: the aerosol is then injected into the plasma where the analytes are ionised (145). The plasma is a mixture of electrons and positively-charged argon (Ar) ions, generated by a spark (high voltage discharge) and an electromagnetic field in the ICP-torch (159). The ICP torch is made up of three tubes, surrounded by a copper coil, each containing a flow of Ar gas; one to deliver the sample aerosol to the plasma, the second to deliver Ar used to generate the

plasma, and the third to cool the torch and prevent melting due to the high temperatures generated by the torch (160). An electromagnetic field is induced in the torch by a high frequency alternating current created by a radio frequency generator connected to the copper coil. The electromagnetic field accelerates the ions and electrons formed by the spark, causing multiple collisions between the electrons, ions and Ar atoms (159, 160). The high energy generated from these collisions results in temperatures of up to approximately 10000 K in the plasma (159). Within the hot plasma, desolvation and vaporisation of the analyte compounds occurs, followed by atomisation and finally ionisation (145).

Interference region: the ions, neutral atoms, and photons from the plasma are then transferred into the interface region, which is used to enable the coupling of the ICP with the MS (158, 159). Within the interface region, there are two cones: a sampler and a skimmer cone, which are used to extract the analyte ions (159). A vacuum applied in the interface region accelerates the ions through the two cones from atmospheric pressure in the plasma region to an area of lower pressure and high vacuum maintained in the interface region (158).

Ion optics: the ions are then focused into a beam using electrostatic lenses (ion optics) which is then directed towards the mass analyser. The ion optics also separate out any neutral species or photons present thereby preventing transportation of these species to the detector (158, 159).

The mass analyser used in this study is the triple quadrupole mass analyser and is comprised of two quadrupoles separated by a collision cell (159). The collision reaction cell is used to remove interferences (158). The quadrupoles, four metal rods in a square positioning, act as filters to separate the target analyte ions according to their m/z ratios. This separation is achieved by applying a specific radio frequency alternating current (AC), direct current (DC) potential combination to the four metal rods, thus allowing only ions with the appropriate m/z ratio to pass through the quadrupole and towards the *detector* where they are measured and quantified (159).

Limitations of ICP-MS analysis include spectroscopic interferences. These include isobaric, doubly charged ions, or polyatomic ion interferences (4, 158). Isobaric interferences are formed from isotopes of different elements with the same mass such as Cd^+ and Pd^+ which both have an atomic mass of 106 amu (4). Doubly charged ion interference results from the production of ions with a double charge and the same m/z ratio as a singly charged target ion. For example Pb^{2+} has a mass of 206 amu and a m/z ratio of 103, and Rh^+ has an atomic mass of 103 amu,

with the same m/z ratio (4). Polyatomic interferences result from the formation of ions with more than one atom (usually between the sample and Ar, the carrier gas), which then have the same ratio as the target ion (4). An example of this is the formation of ArO^+ which has the same atomic mass as Fe^+ at 56 amu (145). These interferences can be removed in the collision reaction cell using tuning modes such as O_2, H_2 and He (161). Other interferences can result from tailing, where overlaps form between peaks in the spectra (159).

Matrix effects can also cause interferences leading to enhancement or suppression of the analyte signal (145, 159). Matrix effects are described in Section 3.3.4

3.2.2 Gas Chromatography - Mass Spectrometry (GC-MS)

Gas chromatography–mass spectrometry (GC-MS) is an analytical technique frequently used in the separation and detection of semi-volatile and volatile organic contaminants from complex matrices in environmental samples (150, 162). The combination of GC with MS provides highly efficient separation from the GC along with highly specific and sensitive selective detection from the electron ionisation (EI) MS (150, 163). Detection limits can be achieved at sub ng levels, appropriate for the detection of organic pollutants such as PCBs in environmental samples (150, 164). GC-MS has been used for the separation and detection of PCBs in matrices including soil, sediment, vegetation, water, and biological samples (2, 162, 164).

A GC-MS instrument is separated into several components: (i) carrier gas supply, (ii) sample injector, (iii) separation column, (iv) oven, (v) interface area, (vi) mass spectrometer, and (vii) detector (165).

A carrier gas (mobile phase) is used to carry the sample through the column and to the mass spectrometer. The mobile phase is an inert gas such as helium (He) which is often used for capillary columns, such as those used in this study (165, 166). The gas is supplied at a controlled pressure to establish a steady flow rate to the sample injector (165, 166).

Sample injection: the sample must be in a liquid form for injection into the GC, and is often dissolved in a volatile solvent (150, 165). A syringe collects the sample at a typical volume of 1 µL (165). There are two types of injection, split and splitless (165). Splitless injection is more appropriate for analysis of trace levels of contaminants, as split injection can cause a loss of target analyte as a result of venting of a large proportion of the sample to avoid overloading of the column (166). The liquid sample is injected into a heated injection port, at temperatures of

between 250 – 300 ºC resulting in flash vaporisation, whereby the sample is transformed from a liquid to a vapour state (165, 167). The inert carrier gas then transports the vapourised sample into the column (167). At the head of the column, the sample then undergoes reconcentration (166). This process is required to improve efficiency of separation and avoid the adverse effects of large solvent volumes on the column, such as the creation of broad peaks on elution (166).

In the separation column, the compounds are partitioned between the He gas mobile phase and a liquid stationary phase. In capillary columns, also known as open tubular columns, the stationary phase consists of an inert solid support (usually fused silica) covered in a high molecular weight, high boiling point liquid (165, 166). Each compound in the sample then partitions to a different extent as a consequence of differences in volatility, resulting in separation (165). The choice of liquid stationary phase is important for separation of target analytes. For example a low-polar liquid stationary phase is required for the separation of PCBs, such as 5 % diphenyl/ 95 % dimethyl polysiloxane (168).

Oven: The capillary column is held within an oven. Temperature programming is an important part of GC analysis and is of particular use for separating compounds with a large range of boiling points (166). Using a temperature programme to increase temperature enables the faster elution of higher boiling point analytes after the lower boiling point analytes have been eluted (165). Once the analytes are eluted from the column, the carrier gas stream transports the sample through an interface to the mass spectrometer (169).

The Interface region is important because of the different pressure requirements for GC and MS operation. The GC works at atmospheric pressure, whereas very low pressures are required for the MS (169).

Mass spectrometer and detector: The EI detector is one of the most commonly used detectors in MS (150). Electrons (typically with an energy of 70 eV) collide with the gaseous sample resulting in the production of both fragments and molecular ions (162). The ionised fragments are then focused through a quadrupole into a detector (150). Ions are separated through a quadrupole as described in Section 3.2.1 in ICP-MS, but for a single quadrupole only. A mass spectrum is produced showing the signal intensity against the m/z ratios for each compound (150). The EI spectra have high reproducibility therefore enabling the use of libraries containing reference spectra held on computers for identification of unknown compounds (162). However one disadvantage of EI is the production of a high degree of fragmentation which can reduce

sensitivity when the measurement of small amounts of target analyte is required (162). There are two types of scanning mode, full scan and SIM (single ion monitoring) mode. In SIM mode it is possible to achieve low detection limits compared to when monitoring a full spectra of ions (163).

The GC-MS technique however has its limitations, one being that it cannot determine involatile, unstable or thermally labile compounds which decompose at high temperatures, due to the high temperatures required for the mobile gas phase (163). In addition, contamination can occur at the injection port walls, or from the septum that then bleeds onto the column, resulting in the introduction of impurities into the sample, or adsorption of sample onto the walls of the injection port (166).

3.2.3 Ion Chromatography

Ion chromatography (IC), also known as ion-exchange chromatography, is a liquid-solid analytical technique to separate charged ions in a solution, and is the preferred method for analysing anions in water (165, 170). Advantages of IC over analytical techniques such as stripping voltammetry or gravimetry is the high sensitivity and precision, short analysis time, and low sample volume requirements (170, 171).

In IC, the ions are separated based on selective exchange between a solid stationary phase such as silica or a polymer resin with charged ionic functional groups, and a mobile phase (165, 172). In an anionic exchange system, the negatively charged ions (E^-) in the eluent (i.e. the mobile phase) are displaced from the stationary phase by the negatively charged ions in the sample (A^-), resulting in ion exchange. The sample ions (A^-) are then retained on the stationary phase, until they are displaced again by the eluent ions (172). The following equilibrium is established in equation [1]:

$$SP\text{-}R^+ - E^- + A^- \rightleftharpoons SP\text{-}R^+ - A^- + E^- \qquad [1]$$

Where SP is the stationary phase, and R^+ is the charged functional group. Different anions within the sample are retained on the solid stationary phase to varying extents, depending on their affinity to the functional groups, resulting in separation. For example those anions that only weakly bind to the stationary phase will elute first (165).

The IC set up is similar to that of high performance liquid chromatography (HPLC), and consists of several components including a pump, sample injector, guard column, analytical column, detector, and computer software to process the signal (165). The sample is injected into the mobile phase (eluent) after the pump (which pumps the mobile phase through the instrument), but prior to the columns. A guard column can be added to filter and remove any particulate matter present in the sample, and to remove interferences (165). The mobile phase then passes through the analytical column where analytes are separated. On leaving the column, the target analyte is detected with a conductivity detector, and a chromatogram is produced with the signal as a function of retention time (165).

3.2.4 Total Organic Carbon, Residual Oxidisable Carbon, Total Inorganic Carbon Determination

Total organic carbon (TOC400), residual oxidisable carbon (ROC), and total inorganic carbon (TIC900) content of a dry homogenised sample can be determined using stepwise combustion with oxygen gas. The temperature programme is set to 400 °C to determine the biologically labile organic carbon, 600 °C for ROC, and 900 °C for TIC (173, 174). An autosampler is used to introduce the samples into the combustion furnace, which then transports the samples through the different temperature zones for the determination of each carbon form (175). Carbon in the sample is combusted to CO_2 which is then transported by the oxygen carrier gas to the infrared (IR) detector where the CO_2 concentration is measured (173). The TOC400, ROC, and TIC900 content of the sample can then be determined, the sum of which represents the total carbon content (TC) (173).

A number of errors can occur during analysis. For example, both the sample weight and the particle size are important in order to ensure complete combustion. If the weight is too high, suffocation may occur, and if the particle size is too small, oxygen will not be able to completely penetrate into the sample, both of which lead to incomplete combustion (173). The crucibles used for holding the sample must also be cleaned with dilute HCl and heated in excess of 900 °C to remove any potential contamination. Crucible contamination can occur from organic material or from metal oxides which can react with CO_2 to produce metal carbonates (173). Contamination may cause a positive error leading to higher than actual C content determination.

3.3 Quality Control and Quality Assurance

Quality control (QC) and quality assurance (QA) are important in environmental analytical chemistry, especially with respect to the sampling, storage, pre-treatment, analysis, and quantification of trace levels of pollutants with a high risk of contamination. Poor QA/QC can lead to misleading results and incorrect decisions with respect to environmental management (176). It is therefore important that robust QA programs are implemented as part of any analytical protocol, with all decision making, actions, and checking performed, so as to ensure the reliability and accuracy of the results and to enable the detection and correction of problems that occur (176, 177). A QA processes should include the use of: calibration, equipment maintenance, standard reference materials with reported values, replicate samples, and skilled personnel (178, 179). Protocols should be clear and validated, results should be monitored and critiqued and corrections should be made where quality standards have not been met (178, 179). Interlaboratory comparisons can also be used to determine acceptable accuracy levels (177).

Quality control relates to the measures taken to monitor and evaluate QA procedures. Quality control is performed throughout the entire process from initial sampling, through to data handling and analysis of results, including collection and handling of samples, transportation, storage and preparation for analysis (176). A QC procedure is important to ensure the precision, accuracy and thus the validity of a result. For example QC could be used to prevent errors as a result of contamination or sample loss during sample preparation and analysis (178, 180, 181). The QC measures can include: collection of duplicate samples, analysis of certified reference materials (CRMs), field and method blanks, matrix effects and recoveries, and the use of solvent blanks to measure the cleanliness of analytical equipment (176). The International Organisation for Standardisation (ISO) provides standard procedures for every step of the environmental management process (182).

3.3.1 Quality Control in Sampling

Sampling methods were carried out where possible, within the resource and time limitations of the fieldwork, following International Organization for Standardization (ISO) standards for the various sample types including supraglacial debris, cryoconite, water, and snow. The ISO 5667 series of standards provide a detailed guide for the steps involved in water and sediment sampling. Although the samples collected from cryoconite holes were not directly described,

the closest ISO standards were selected to plan, collect representative samples, minimise contamination and improve quality. The ISO standards selected include guidance on fieldwork planning and design (ISO 5667-1:2020), guidance on bottom sediment sampling from lakes (ISO 5667-12:2017), water sampling from lakes (ISO 5667-4:2016) and snow sampling (ISO5667-8:1993) (183-186). Standards were also selected for guidance on the handling, preservation, and transport of sediment (ISO 5667-15:2009) and water (ISO 5667-3:2018) (187, 188). Finally the ISO standard 5667-14:2014 describes QA and QC measures with respect to the sampling and handling of water samples (189).

Prior to fieldwork, planning is essential to ensure sampling errors are reduced, representative samples are collected, suitable sampling equipment and containers are utilised, and sources of contamination are controlled or prevented (189). To avoid contamination, care should be taken when collecting water samples to avoid disturbance of the underlying sediment, disposable gloves should be worn and sampling materials should be sufficiently cleaned (184). For water samples, sample containers and sampling equipment should be rinsed up to three times from the water body to be sampled, (184). Metal free plastic containers should be used for trace elemental analysis of water and sediment samples to avoid metal contamination (187, 188). Preservation of the water samples is required to stabilise the sample so that no alterations in chemical composition occur between sampling and analysis which may impact the analytical results. Filtration of water samples for elemental analysis is required to remove biological material or particulate matter, and is performed on site using 0.45 μm filters (184, 188). Irreversible adsorption of metals dissolved in water onto the surface of the collection container can alter the concentrations of elements within the sample. Preservation with HNO_3 to a pH of 1-2 is required for elemental analysis in accordance with ISO 5667-3:2018 (188). Water samples should be refrigerated at 3 ± 2 ºC during storage. Parameters such as conductivity should be ideally measured in the field (188). Sediment samples should be kept cool during transport and frozen at temperatures of at least -18 ºC until dry and after which samples can be stored at ambient temperature (187). Samples should also be clearly labelled with a unique naming system which includes sample date and location, so as to ensure later identification of samples. Other details such as time, GPS location, sample description, sampling conditions, and any treatment/ preservation should be documented for future reference (188).

3.3.2 Blanks

Blanks are used to detect points of contamination in the analytical process from fieldwork through sample preparation to analysis (190, 191). Three major types of blanks include field, method, and reagent blanks. Field blanks are taken into the field and exposed to the environment where the samples are collected, without coming in contact with the sample itself. These blanks are used to detect trace levels of potential contamination in sampling and transport steps (190). Method blanks are used to identify background laboratory contamination through the sample preparation steps and are exposed to the exact procedures the sample is subjected to (191). Reagent blanks are used to monitor the purity of the reagent by detecting any trace levels of components that may produce positive errors in the final quantification of the target analyte (190). In addition, the frequent analysis of solvent blanks in, for example GC-MS analysis, can be used to detect any carry forward of analyte from a previous sample as a result of adherence to the analytical instrument (192). Any analytes detected in the blank indicate contamination and corrections may be made when calculating the analyte concentration in the sample by deduction of the blank (190).

3.3.3 Limit of Detection and Limit of Quantification

The limit of detection (LOD) and limit of quantification (LOQ) are estimations used to define the limits of a procedure. The LOD is defined as the lowest analyte concentration in a sample that can be reliably detected by an analytical procedure, i.e. it is the smallest concentration of an analyte that can be reliably distinguished from a blank (where the analyte is absent) (177, 193). Concentrations of an analyte above the LOD may not however be accurately quantifiable, and an LOQ should therefore be estimated which is significantly above the LOD (177). The LOQ is defined as the smallest concentration of an analyte that can be determined with a defined degree of precision by an analytical procedure (194).

There are several methods for estimating the LOD and LOQ. The LOD is often calculated based on the signal-to-noise ratio, where the noise represents fluctuations in the background signal of the instrument, which is the instrument signal generated from a blank measurement (194, 195). Another method is to calculate the LOD based on the standard deviation of the response and the slope of the calibration curve, i.e. $LOD = 3.3\sigma/S$, where S is the slope and σ is the standard deviation of the response (158). The method used to calculate the LOQ is dependent on the

method used for the estimation of the LOD, and is often estimated using the equation LOQ = 10σ/S (158).

3.3.4 Standards, Matrix Effects, and Recoveries

Standards, substances containing a known accurate quantity of a compound, are used in QC to determine the accuracy and precision of a method and can also be used for instrument calibration (196). There are three main types of standards: certified reference materials (CRMs), external standards (ESs), and internal standards (ISs) (196).

Certified reference materials are standards with reported certified levels of analyte in a material with a similar matrix and analyte concentration to the sample (178, 197). The concentrations of target analytes measured using an analytical technique such as ICP-MS are compared against the reported certified concentrations to determine performance of the procedure (178, 198).

External standards contain a known concentration of the target analytes, and can be used for calibration of an analytical instrument as well as quantitation, via the establishment of calibration curves (196). External standards can include the 'Dutch Seven' PCBs (Fig. 2.2) which are often used in PCB analysis of environmental samples (12, 61). A calibration curve is established by analysing a range of concentrations of the external standard in a pure solvent, separately from the sample (196). At least five to six concentrations are required for a calibration curve, which is plotted as the response from the detector (for example peak area) as a function of concentration (178, 196).

Internal standards contain analytes that are chemically similar to the target analyte, but are unlikely to be found in the sample (199). Internal standards can be used in the calculation of recoveries, to correct for matrix effects, for calibration, and for quantitation of the target analyte in a sample (159, 196, 200). The internal standard is added at a constant concentration (ideally similar to the expected concentration of the target analyte) to all samples, as well as the recovery, matrix effect samples and calibration solutions (159, 196, 200). An internal standard must also be chemically stable and have a similar retention time to the target analytes. As such more than one internal standard is often used when analysing for multiple analytes (196). Fluorinated PCBs, which contain a fluorine atom on the biphenyl ring (Fig. 3.1) can be used as internal standards for PCB determination, such as 3'-Fluoro-2,4,4'-Trichlorobiphenyl (3'-F-PCB-28) and 5'-Fluoro-2,3',4,4',5-Pentachlorobiphenly (5'-F-PCB-118) (201).

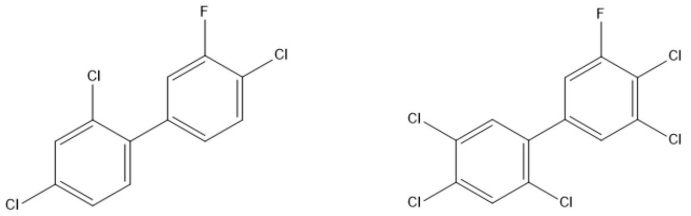

3'-Fluoro-2,4,4'-Trichlorobiphenyl (3'-F-PCB-28)

5'-Fluoro-2,3',4,4',5-Pentachlorobiphenyl (5'-F-PCB-118)

Figure 3.1 *Chemical structures of two fluorinated PCB internal standards; 3'-F-PCB-28 and 5'-F-PCB-118.*

Using the internal standard method, calibration curves can be produced where the relative response (area of the analyte/ area of the IS) is plotted as a function of the concentration of the analyte in the calibration solutions (196).

Many analytical techniques require the sample containing the target analytes to be in a simpler form than that of the often complex environmental matrices (199). As a consequence, extraction procedures and other sample preparation techniques are performed, and in each step target analyte may be lost, or remain behind in the original matrix, resulting in lower than actual concentrations being determined (199). This can lead to incorrect quantification and interpretation of results if no corrections are made to compensate for these losses (199). The recovery of a technique can assess the efficiency of the entire procedure, and can be used to account for losses when calculating the concentration of the target analyte (2, 199). Recovery calculations are based on a comparison between measured concentrations of an analyte added (spiked) to a matrix sample pre- and post-extraction (199). Pre-extraction spiked samples are hereafter named 'spiked (SP) samples' and post-extraction spiked samples are named 'matrix match (MM) samples'. There are two types of recoveries: absolute and relative recoveries (200). Absolute recoveries (%) ($R_{abs.}$) can be calculated using equation [2]:

$$R_{abs.}(\%) = \frac{(Area\ A_{SP} - Area\ A_{MB})}{(Area\ A_{MM} - Area\ A_{MB})} \times 100 \qquad [2]$$

where Area A_{SP} is the peak area of the analyte (A) in the pre-extraction spiked matrix sample, and Area A_{MM} is the peak area of the analyte (A) in the post extraction spiked matrix sample (200). Area A_{MB} is the peak area of the analyte in the method blank, and is deducted to account for any contamination from the method. Recoveries can also be calculated for each target analyte using internal standards (IS) (200). By comparing the signal from the analyte in the pre

and post extraction spiked samples relative to the signal from the IS in both the pre- and post-extraction spiked samples, it is possible to determine the relative recovery. Relative recovery (%) ($R_{rel.}$) can be calculated using equation [3]:

$$R_{rel.}(\%) = \frac{\left(\frac{Area\ A_{SP}}{Area\ IS_{SP}} - \frac{Area\ A_{MB}}{Area\ IS_{MB}}\right)}{\left(\frac{Area\ A_{MM}}{Area\ IS_{MM}} - \frac{Area\ A_{MB}}{Area\ IS_{MB}}\right)} \times 100 \qquad [3]$$

where Area IS_{SP} is the peak area of the internal standard in the pre-extraction spiked matrix sample, and Area IS_{MM} is the peak area of the internal standard in the post-extraction spiked matrix sample (200). Area IS_{MB} is the peak area of the internal standard in the method blank and is deducted to account for any contamination in the analytical procedure.

Matrix Effects occur as a result of interference of the sample matrix with the detection of target analytes. Interference from co-extracted constituents can lead to either signal enhancement or suppression in a chromatogram (202). This can have an impact on the accuracy of the quantification of the target analyte in a sample, and may lead to misinterpretation of results, either by over or underestimating contamination levels (202, 203).

In GC-MS, the main matrix effects occur at the inlet and/or column (202). Signal enhancement is caused by matrix co-extracts which bind to active sites in the inlet, thus competing with the target analyte binding. As a consequence more target analyte is eluted in comparison to a standard solution of target analytes in a pure solvent, leading to enhancement of the signal and thus overestimation of the analyte concentration (202, 204). Signal suppression is a consequence of non-volatile matrix components binding and accumulating on the active sites in the inlet and/or column, leading to the creation of a larger number of active sites (203). These additional active sites lead to a reduction in analyte elution and a lower analyte response in comparison to the standard solution of target analytes in pure solvent (203). One method of reducing matrix effects is to ensure adequate clean up steps in sample preparation are performed to remove interferences (202). In addition, a number of calibration methods can be used to compensate for matrix effects which include the standard addition calibration method, the use of matrix match standards or isotopically labelled internal standards (202, 203).

Calculation of a matrix factor (MF) can be used to identify the presence of matrix effects, with an MF > 1 indicating signal enhancement, an MF < 1 indicating suppression, and a MF = 1 indicating a lack of matrix effect (202). The MF can be calculated by comparing the peak area

of the analyte in a post-extraction matrix matched sample to the peak area of the analyte in a standard solution in pure solvent (such as ethyl acetate) using equation [4]:

$$MF = \frac{(Area\ A_{MM} - Area\ A_{MB})}{Area\ A_{SS}} \qquad [4]$$

Where Area A_{SS} is the peak area of the target analyte in a standard solution in pure solvent (202).

The matrix effect (ME) can be calculated from the MF using equation [5]:

$$ME\ (\%) = (MF - 1)\ \times\ 100 \qquad [5]$$

Matrix effects are given as a percentage, where a negative percentage ME indicates signal suppression, and a positive percentage indicates signal enhancement (200).

In ICP-MS, matrix effects are also observed and are the result of non-spectroscopic interferences (159). Space-charge effects which cause a reduction in ion transmission to the detector can occur, leading to suppression of the signal (159, 160). In addition to the strategies mentioned for GC-MS, dilution of the sample may also be used to reduce matrix effects (159).

3.4 Statistics

The statistical methods and tools used in this study include the calculation and use of mean, median, sample standard deviation, and assessment for normal distribution. Significant differences between groups have been determined and correlations have been calculated in addition to the use of principle component analysis (PCA) to statistically analyse the data obtained from the analytical techniques described in Section 3.2.

3.4.1 Mean

The mean ($\bar{x}$) of a data set is the arithmetical average of the given data, and is the best statistical tool for data with a symmetrical distribution. In this case, the mean provides a representation of the central tendency of the entire set of data (180). The mean is defined by equation [6]:

$$\bar{x} = \frac{\sum_i x_i}{n} \qquad [6]$$

where n is the number of data in the set and x_i is the individual result (180).

3.4.2 Median

The median, the central number in a set of data ordered from smallest to largest, is used rather than the mean to provide a representation of the central tendency of the entire data when it is not possible to make assumptions on data distribution (180).

To calculate the median, data is sorted by increasing magnitude. If n is odd, then the position of the median value is found using $\frac{1}{2}(n+1)$. If n is even, the position of the median value is determined using the midpoint between the equations $\frac{1}{2}\ n$ and $\left(\frac{1}{2}n+1\right)$ (180).

3.4.3 Standard Deviation

The standard deviation (σ) of a data set describes the dispersion or spread of data relative to the mean (180). For example a low standard deviation (SD) means that the data is close to the mean value. The standard deviation is calculated using equation [7]:

$$\sigma_{n-1} = \sqrt{\frac{\sum_i (x_i - \bar{x})}{(n-1)}} \qquad [7]$$

where $\bar{x}$ is the mean, n is the number of results, and x_i is the individual result (180). Standard deviation is often represented as relative standard deviation, measured as a percentage (180). The relative standard deviation (RSD) is defined by equation [8]:

$$RSD\ (\%) = \frac{\sigma_{n-1}}{\bar{x}} \times\ 100 \qquad [8]$$

3.4.4 Distribution of Data

In order to determine the applicable statistical test required for analysis of data, it is important to first determine the normality of the data set. This is because different statistical tests are required for data that is not normally distributed. Parametric tests such as one-way ANOVA, assume normal distribution whereas non-parametric tests such as Mann-Whitney U test and Kruskal-Wallis test do not assume normality of data (205). The distribution of a data set can be determined using the Shapiro-Wilk test (206).

A normal or Gaussian distribution is symmetrical and bell-shaped with the peak forming above the mean (207). A normal distribution assumes that replicate measurements will follow the same pattern, with variations being both positive and negative as a result of uncertainties in the measurement procedure (180). A standard deviation of ± 1 SD around the mean represents 68 % of the data, with ± 2 SD representing 95 % and ± 3 SD representing 98 % of the data (207). As such, the majority of the data will be dispersed within 1 SD of the mean.

3.4.5 Correlations

Correlations show the strength of an association or relationship between two or more continuous variables (180). A linear correlation (i.e. a straight line) is the simplest method to describe the relationship between two variables, with the correlation coefficient representing the strength of the association (208). In a linear correlation, an increase or decrease in one variable is proportional to the change in the other variable (208). The correlation coefficient has a value range from + 1 to - 1. A value close to + 1 represents a strong positive correlation, with + 1 being a perfect linear relationship between the two variables (180, 208). A correlation coefficient value close to – 1 indicates a strong negative correlation, i.e. as one variable decreases, the other increases (208). A value of 0 indicates a lack of correlation between the two continuous variables (180). A scatter plot can be used to provide a visual representation of the data from which the correlation coefficient has been calculated (180). This is important because incorrect conclusions may be drawn based on the value of the correlation coefficient, especially when there is a non-linear relationship between the variables (180).

Two types of correlation include the Pearson's correlation and the non-parametric Spearman rank correlation (208). The choice of correlation depends on a number of assumptions including the normality of the data. A non-parametric Spearman correlation can be used for data which is not normally distributed (208).

3.4.6 Principal Component Analysis

Principal Component Analysis (PCA) is a useful tool for analysing and interpreting large complex datasets with vast numbers of samples and variables (209, 210). The aim of the PCA is to provide a more descriptive visualisation of the data, which enables sample classification and identification of patterns and trends in data, such as similarities (e.g clustering) or

differences between samples, and identification of outliers (209-212). The PCA lowers the dimensionality of the data, through identification of new uncorrelated variables (209, 210). The new variables are called principal components (PCs). These PCs are linear combinations of the variables in the original data, which represent a summary of specific features, whilst at the same time maintaining the statistical information (209, 210, 212). The number of PCs is the smaller of either the number of samples or variables. However in general, not all the PCs will be used for data interpretation, as most of the variance will likely be explained by at least the first two PCs (209, 212). The aim is to achieve the most meaningful summary of the data whilst using the lowest number of PCs (212).

A two dimensional scatter plot is produced where PC1 accounts for the largest variation in the data, and PC2 being the second largest variation (210). The PCA can also show clusters which can be used to identify correlations between samples, for example where the samples are clustered together they are correlated by the total percentage variation represented by the two PCs (211).

4 Materials and Methods

In this section, details have been provided on locations and methods for collection of cryoconite, cryoconite hole water, snow, and supraglacial debris. Detailed procedures for sample pre-treatment and analysis have also been presented. Pre-treatment methods with respect to freeze drying, sample homogenisation, microwave assisted digestion, ASE, concentration and solvent exchange, and filtration have been described. Analytical procedures and specifications for GC-MS, ICP-MS, combustion, and IC have been set out for PCB determination, elemental analysis, TOC/ROC/TIC, and anion determination respectively. A full list of sample pre-treatment and analytical techniques performed on each sample is presented in Table A.2.1 in the Appendix.

4.1 Fieldwork

4.1.1 Study Area

Sampling was performed near Ny-Ålesund (78º55' N, 11º55' E), located on the north side of the Brøggerhalvøya peninsula on the west coast of Spitsbergen (Fig. 4.1 A). Ny-Ålesund, previously an old coal mining settlement, is now the location of an international research station with a population varying from ~ 200 in the summer, to ~ 25 in the winter months (65). With the exception of the research station, a small airport, and local transport within the town, there is little activity in Ny-Ålesund. Local sources of contamination include the airport, fuel storage areas, an old dumpsite at Thiisbukta, the sewage outlet and the remains of the former coal mining operations (65). Coal was mined in Ny-Ålesund from 1917 to 1962 with approximately 1.43 million tonnes of coal being exported (26). Remnants of the mining operations are still visible in the local landscape, and wind-blown coal dust is a potential source of heavy metal contamination to the local area (65). Elevated levels of contaminants such as equivalent black carbon and sulphur dioxide from emissions generated by tourist cruise ships to Ny-Ålesund have also been documented (213). Nonetheless, the remote location and limited local sources of pollution have established the area as an ideal location for the determination of background pollution levels in various environmental compartments in the Arctic (2).

Average temperatures in Ny-Ålesund for the period from 1972 to 2021 ranged from - 6.12 °C (in 1980) to - 2.76 °C (in 2017). The average temperature in Ny-Ålesund in 2021 was - 3.01 °C,

with July being the warmest month and March the coldest, recording average temperatures of 5.5 °C and - 11.6 °C respectively (214, 215). Large fluctuations in temperature during a year have been observed in the area, and in 2021 temperatures ranged from a maximum of 12.0 °C in August down to as low as - 24.6 °C in March (214). Annual precipitation for the period from 1972 to 2021 ranged from 358 mm (in 1981) to 565 mm (in 2016). In 2021, the annual precipitation was 496 mm (216).

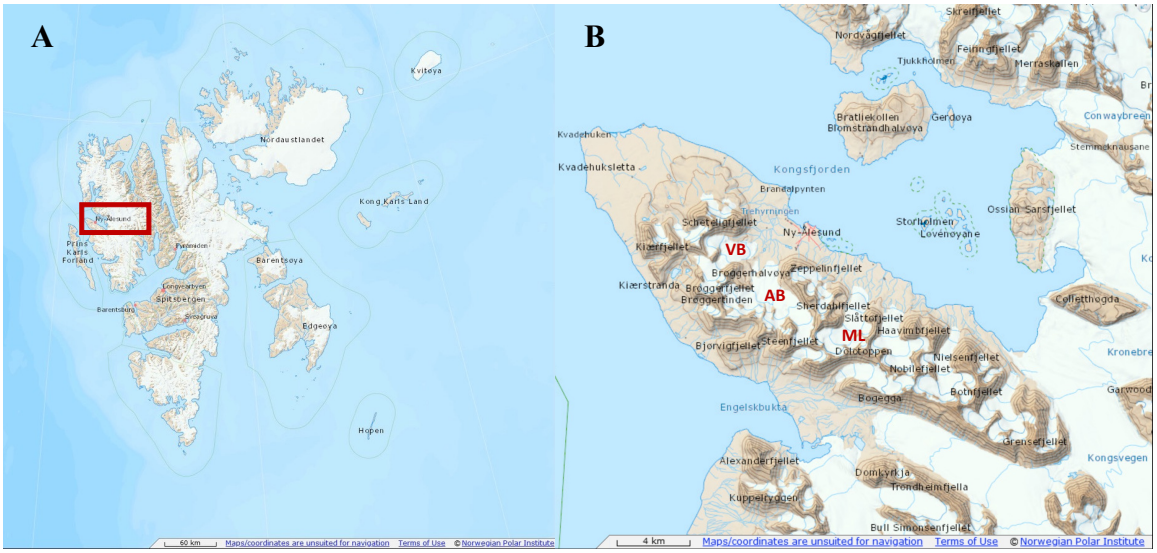

Figure 4.1 *Maps of Svalbard. Map (A) shows the location of Ny-Ålesund on the Svalbard archipelago; Map (B) shows the study locations: VB, AB, and ML near Ny-Ålesund. Glaciers are marked on the map as follows: VB represents Vestre Brøggerbreen, AB is Austre Brøggerbreen, and ML represents Midtre Lovénbreen. Source: Norwegian Polar Institute n.d (138).*

Sampling was conducted during the Arctic summer from 23rd to 30th August 2021 on three land terminating glaciers located within 5 km of Ny-Ålesund (Fig. 4.1B & Fig. 4.2). Austre Brøggerbreen (AB) is a cold supraglacial polar glacier whilst Midtre Lovénbreen (ML) and Vestre Brøggerbreen (VB) are polythermal glaciers (31, 33). The glaciers AB and ML have been surveyed extensively since 1966 and 1968 respectively and are listed on the World Glacier Monitoring Service (WGMS) (131, 132). Both AB and ML have been documented as showing active receding, with mass balance values in 2020 of - 1744 and - 1574 respectively, as reported by J Kohler with the Norwegian Polar Institute (132). Midtre Lovénbreen is documented to show accelerated mass loss rates, with thinning rates being more than 4 times higher for the period 2003 – 2005 compared to the period 1936 – 1962 (131). It has been reported that the glacier terminus of both snouts of VB has receded by 197.5 m and 70.1 m since 2010 (217).

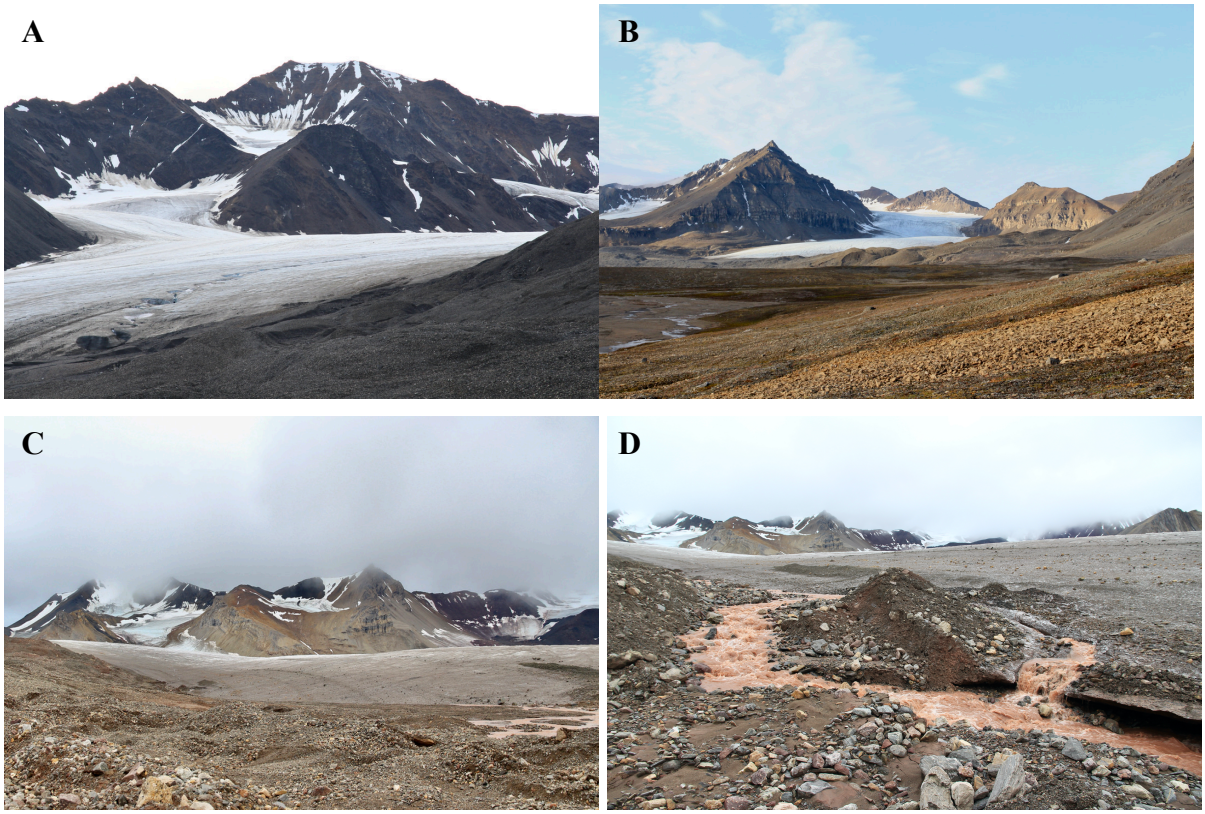

Figure 4.2 *Images of glaciers where sampling of cryoconite, snow, and supraglacial debris took place. (A) Midtre Lovénbreen; (B) Vestre Brøggerbreen; (C) Austre Brøggerbreen; (D) glacial river water flowing from the base of Austre Brøggerbreen.*

Austre Brøggerbreen is located approximately 3 km from Ny-Ålesund, at 78º54' N, 11º50' E. The glacier covers an approximate area of 6 km^2, and lies at an altitude of between 80 to 680 meters above sea level (m.a.s.l) according to data from Kohler (2013) as cited in Schuler et al. (2020) (131). It was estimated that 7.3% of the glacier was covered in supraglacial debris in 2020 (124). Vestre Brøggerbreen is located ~ 3.5 km from Ny-Ålesund, at 78º54' N, 11º46' E. The glaciated area lies between 30 to 468 m.a.s.l and covers an area of ~ 3.53 km^2 (217). It was estimated in 2020 that 15.2% of the glacier was covered in supraglacial debris (124). At approximately 4.5 km from Ny-Ålesund, Midtre Lovénbreen is the furthest of the three glaciers from the settlement, at 78º53' N, 12º03' E. The glacier covers an area of ~ 5.4 km^2 (218). Midtre Lovénbreen lies at an altitude similar to both AB and VB of between 50 to 690 m.a.s.l, according to data from Kohler (2013) as cited in Schuler et al. (2020) (131). Approximately 6 % of the surface of the glacier is covered by cryoconite holes (12 holes m^{-2}) (10, 19). The melting ice and snow from AB and VB is transported via Bayelva river to Kongsfjorden. The Bayelva basin, covering approximately 31 km^2 has an annual total mean runoff of 30 x 10^6 m^3 a^{-1} (38).

Svalbard has an interesting and varied geology resulting from its position below sea level for a significant portion of the planets' history. This situation has resulted in large amounts of sedimentation of materials such as carbonates, sand, and clay which thereafter formed stratified rock. This stratification has revealed that the archipelago has rock from each period in the geological history of the earth (219).

The local geology of the areas surrounding the glaciers ML, AB, and VB is important for understanding the composition of cryoconite. The structure and composition of cryoconite is described in detail in Section 2.4. There is a large variation in the geology of the local area surrounding the three glaciers which consist of rock from the Lower and Middle Proterozoic (2500 – 1000 million years ago (mya)), Upper Proterozoic (1000 – 570 mya), as well as Carboniferous (360 – 290 mya), and Permian periods (290 – 245 mya), with small areas from the Tertiary period (65 – 2 mya). During the transition from the Cretaceous to Tertiary periods (~ 145 – 2 mya), large amounts of thrusting resulted in older carboniferous rock being pushed over the younger Tertiary coal containing beds (219, 220).

The geology surrounding ML contains basement rock from the Precambrian era (> 570 mya), covering the Lower and Middle Proterozoic periods as well as Upper Proterozoic period (219, 220). The upper section of the glacier is surrounded by basement rock from the Lower and Middle Proterozoic period. The lithology consists of garnet-mica schist and quartz-carbonate schist, in addition to quartzite and carbonate beds. Some areas of marble can also be found (Fig. 4.3, Table 4.1). On both the east and west sides of the lower section of the glacier, rock from the Upper Proterozoic period is found comprising phyllite, carbonate, and quartzite (7, 220). The composition, including chemical formulas, of each rock type are presented in Table 4.2.

Austre Brøggerbreen, which is situated between ML and VB is surrounded by differing rock types between the western and eastern side of the glacier, as identified in Fig. 4.3, and Table 4.1. The upper eastern section of the glacier shares the same rock lithology as ML, with basement rock containing phyllite, carbonate, and quartzite in addition to garnet-mica schist, quartz-carbonate schist and marble (7, 220). In the lower eastern area and to the upper western side of AB, the rock is from the Carboniferous and Permian period (within the end of the Palaeozoic era) (220). The lithology is a mixture of chert, siliceous shale, sandstone, limestone, dolomite, anhydrite, gypsum, carbonate breccia, carbonate rock, conglomerate, shale, and calcareous sandstone (7, 221).

The geology of VB is similar to that of the western side of AB (Fig. 4.3), and is surrounded by rock from the Carboniferous and Permian period as described for AB (7, 220). At the bottom of AB and VB, areas of shale, siltstone, sandstone, coal, and conglomerate are found from the Tertiary period (yellow and orange colours on Fig. 4.3, Table 4.1) (7).

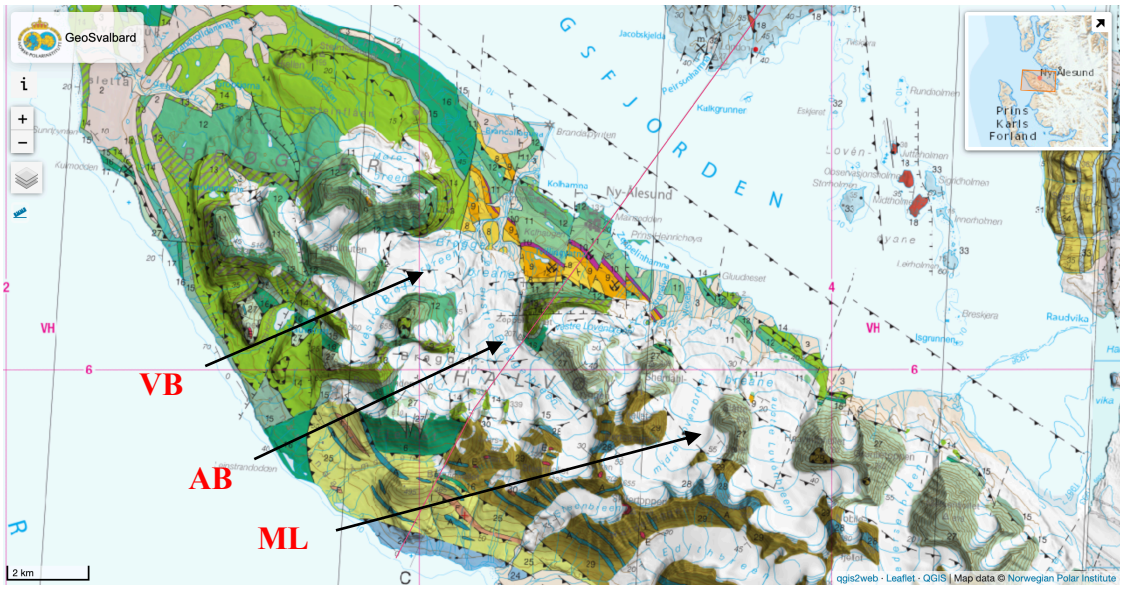

Figure 4.3 *Geological map of the Brøggerhalvøya peninsula on Svalbard. Differences in the lithology of the rock surrounding the three glaciers: Midtre Lovénbreen (ML), Austre Brøggerbreen (AB), and Vestre Brøggerbreen (VB) can be identified by the different colourations. Source: Norwegian Polar Institute, GeoSvalbard n.d. (7).*

Table 4.1 *Summary key for the geological map of the Brøggerhalvøya peninsula on Svalbard. The numbers in the coloured boxes represent the numbering on the GeoSvalbard map. Numbers 27-29 cover the area surrounding Midtre Lovénbreen (ML) and the upper eastern section of Austre Brøggerbreen. In general, the numbers 11 – 16 cover the area surrounding Vestre Brøggerbreen (VB) and the lower eastern and upper western section of Austre Brøggerbreen (AB). Numbers 8 – 10 cover the lower section of Austre and Vestre Brøggerbreen. Data is extracted from the GeoSvalbard map by Hjelle et al. (1999), and it should be noted that the below table is a summary, and some variation exist between the map and below summary depending on area selected (7).*

Colour	Rock/Mineral type	Colour	Rock/Mineral type
[27]	Phyllite, quartzite	[8]	Sandstone, shale, conglomerate
[29]	Garnet-mica schist, quartz carbonate schist	[9]	Sandstone, shale, coal
[28]	Marble	[10]	Shale, siltstone, sandstone
[14]	Carbonate rock/ calcareous sandstone	[16]	Conglomerate, sandstone, shale
[11]	Chert, siliceous shale, sandstone, limestone	[12]	Dolomite, limestone, anhydrite/gypsum, carbonate breccia
[13]	Carbonate rock		

Table 4.2 *The composition of rocks and minerals found on Brøggerhalvøya surrounding Midtre Lovénbreen, Austre Brøggerbreen, and Vestre Brøggerbreen.*

Rock/ Mineral Name	Rock/ Mineral Type	Rock/ Mineral Composition
Amphibole	Mineral	$((Mg, Fe, Ca, Na)_{2-3}(Mg, Fe, Al)_5(Si, Al)_8O_{22}OH_2)$ (222)
Anhydrite	Mineral	$CaSO_4$ (223)
Biotite	Mineral	$H_2K(MgFe)_3Al(SiO_4)_3$ (222)
Calcite	Mineral	$CaCO_3$ trigonal crystal. The other calcium carbonate form is Aragonite (rhombic crystal system) (223)
Coal	Mineral	Compact mineral containing C, O, H, S, and N (Bituminous and anthracite coal) (222)
Dolomite	Mineral	$(CaMg(CO_3)_2)$ (223)
Feldspar	Mineral	Mineral group containing mostly $NaAlSi_3O_8$ (albite), $CaAl_2Si_2O_8$ (anorthite), and $KAlSi_3O_8$ (orthoclase) (222, 224)
Garnet	Mineral	$Ca_3Al_2(SiO_4)_3$ (222)
Gypsum	Mineral	$CaSO_4 \cdot 2H_2O$ (223)
Hematite	Mineral	Fe_2O_3 (222)
Kyanite	Mineral	$3Al_2O_3$, $2SiO_2$ (222)
Mica	Mineral	A group of aluminosilicates containing K/Na, Fe/Na and on rare occasions Li or Cr (e.g. muscovite and biotite) (222)
Muscovite	Mineral	$KAl_2(OH)_2AlSi_3O_{10}$ (common mica) (225)
Quartz	Mineral	SiO_2 (223)
Sericite	Mineral	Mica-type phases containing muscovite & illite (225)
Staurolite	Mineral	$Fe_2Al_9O_7(OH)(SiO_4)_4$ (222)
Talc	Mineral	Granular/ fibrous rock of $3MgO$, $4SiO_2H_2O$ (222)
Chlorite	Clay mineral	Stacking of 2:1 negatively charged layers balanced by a single octahedral positively charged interlayer. Structure: $(R^{2+},R^{3+})_3(Si_{4-x}Al_x)O_{10}(OH)_2$ where R^{2+} can be Mg^{2+}, Fe^{2+}, Mn^{2+}, and Ni^{2+}; R^{3+} can be Al^{3+}, Fe^{3+}, Cr^{3+} (226, 227)
Illite	Clay mineral	$K_{0.65}Al_{2.0}Al_{0.65}Si_{3.35}O_{10}(OH)_2$ (225)
Kaolin	Clay mineral	$Al_2Si_5O_5(OH)_4$ (226)
Montmorillonite	Clay mineral	Phyllosilicate: $(M^+_y \cdot nH_2O)(Al^{3+}_{2-y}Mg^{2+}_y)Si^{4+}_4O_{10}(OH)_2$ containing for example Na, K, Ca, Mg, Fe, Al (226)

Rock/ Mineral Name	Rock/ Mineral Type	Rock/ Mineral Composition
Marble	Metamorphic	Primarily calcite and/or dolomite, and some minor minerals. Minor mineral impurities can provide different colourations (228)
Phyllite	Metamorphic	Consists of minerals: chlorite, microcrystalline quartz, muscovite, and sericite (micas) (228)
Quartzite	Metamorphic	Mostly monomineralic containing quartz (> 90 %). Can also consist of small amounts of minerals: mica, chlorite, garnet, feldspar, and amphibole (228)
Schist	Metamorphic	Rock showing clear schistosity (layering), mostly comprised of chlorite, talc, garnet, quartz, micas, feldspar, kyanite, and staurolite (222)
Carbonates	Sedimentary	Mostly composed of carbonate minerals such as limestone and dolostone (mostly consisting of dolomite) (229)
Chert	Sedimentary	Also known as hornfels; chert is the general name for solid-silicon rock containing quartz in a microcrystalline or cryptocrystalline form (230)
Conglomerate	Sedimentary	Fragments of various rocks and minerals (coarse – pebble shaped) contained in a finely grained cementing material (222)
Limestone	Sedimentary	Mostly aragonite and calcite (different crystal structures of $CaCO_3$). Also includes marine fragments (coral) and silica (flint and chert) (222)
Sandstone	Sedimentary	Mostly composed of quartz and/or feldspar. Also includes other mineral compositions such as hematite (222, 230)
Shale	Sedimentary	Includes clay minerals such as kaoline, chlorite, illite, and montmorillonite, as well as aluminosilicates (222)
Siltstone	Sedimentary	Clay and quartz (222)

Table 4.2 continued: The composition of rocks and minerals found on Brøggerhalvøya surrounding Midtre Lovénbreen, Austre Brøggerbreen, and Vestre Brøggerbreen.

4.1.2 Sample Collection

In all, 90 samples were collected across the three glaciers. Cryoconite and cryoconite hole water (CW) were sampled from cryoconite holes (CHs) at ten sampling locations on both AB and VB and eight sampling sites on ML. Cryoconite holes were sampled at various altitudes across the glacier surfaces, ranging from 92 to 267 m.a.s.l, representing the lower part of each of the three glaciers. Isolated cryoconite holes with no observable flowing water were those selected for sampling. All sampling locations surrounding Ny-Ålesund are presented in Fig. 4.4. The locations of the cryoconite hole and snow sampling sites on ML, AB, and VB are presented in Fig. 4.5 – 4.7. A summary of the sample types, number of samples, and location are presented in Table 4.3. Further detailed information is presented in Table A.1.1 in the Appendix.

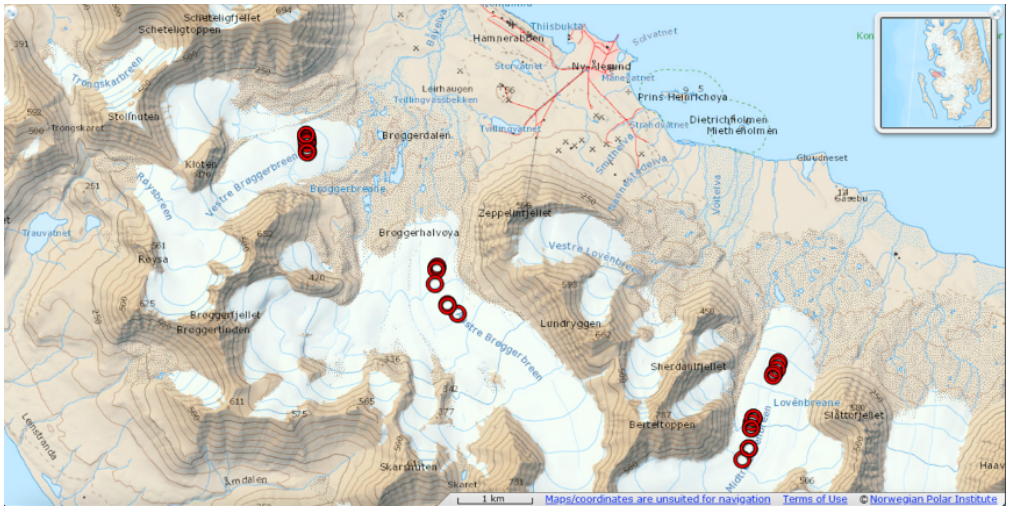

Figure 4.4 *Map of sampling locations on three glaciers and their locations in relation to Ny-Ålesund. From right to left: Midtre Lovénbreen (ML), Austre Brøggerbreen (AB), and Vestre Brøggerbreen (VB). Sampling locations marked in red circles. Source: Norwegian Polar Institute n.d. (138).*

Table 4.3 *A summary of type, location, and number of samples (n) collected. The sample reference and sample no. have also been provided*

Sample Type	Sample Location	n	Sample Reference	Sample No.
Cryoconite	Midtre Lovénbreen	8	1a - 8a	1 – 8
Cryoconite	Austre Brøggerbreen	10	AB1a - AB10a	9 – 18
Cryoconite	Vestre Brøggerbreen	11[a]	VB1a - VB10a & VB9b	19 – 29
Cryoconite hole water	Midtre Lovénbreen	8	1 - 8	30 – 37
Cryoconite hole water	Austre Brøggerbreen	10	AB1 - AB10	38 – 47
Cryoconite hole water	Vestre Brøggerbreen	10	VB1 - VB10	48 – 57
Snow	Midtre Lovénbreen	10	MLS1 - MLS10	58 – 67
Snow	Austre Brøggerbreen	8	ABSN1 - ABSN8	68 – 75
Snow	Vestre Brøggerbreen	7	VBSN1 - VBSN7	76 – 82
Supraglacial debris	Midtre Lovénbreen	5	ML1 - ML4 & 9a	83 – 87
Supraglacial debris	Austre Brøggerbreen	3	ABS1 - ABS3	88 – 90

[a] Ten cryoconite holes sampled on VB, two samples taken from one hole, with sample reference VB9a and VB9b.

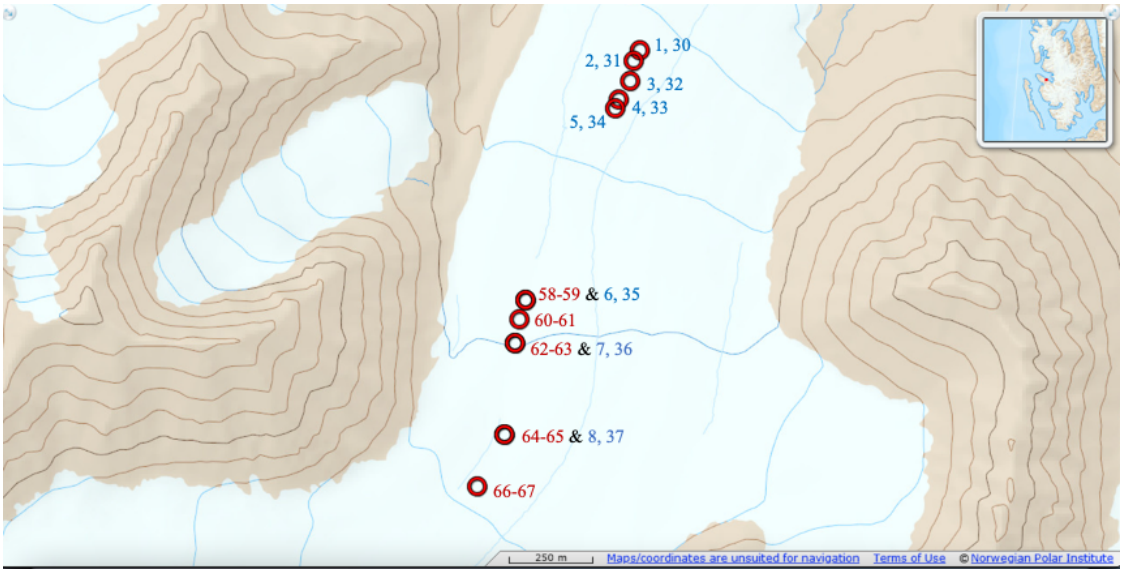

Figure 4.5 *Snow and cryoconite hole sampling locations on Midtre Lovénbreen. Snow samples are numbered in red, and cryoconite hole water and cryoconite samples are numbered in blue. Details on sample name, sample no., type, and GPS coordinates are presented in Table A.1.1 in the Appendix. Source: Norwegian Polar Institute n.d. (138).*

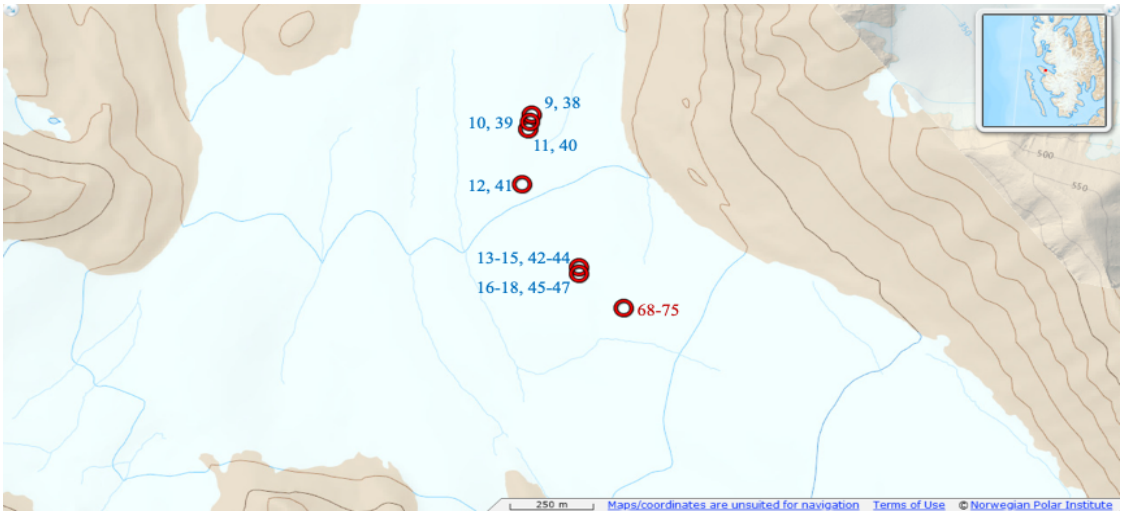

Figure 4.6 *Snow and cryoconite hole sampling locations on Austre Brøggerbreen. Snow samples are numbered in red, and cryoconite hole water and cryoconite samples are numbered in blue. All snow samples were taken at the same GPS coordinates. Details on sample name, sample no., type, and GPS coordinates are presented in Table A.1.1 in the Appendix. Source: Norwegian Polar Institute n.d. (138).*

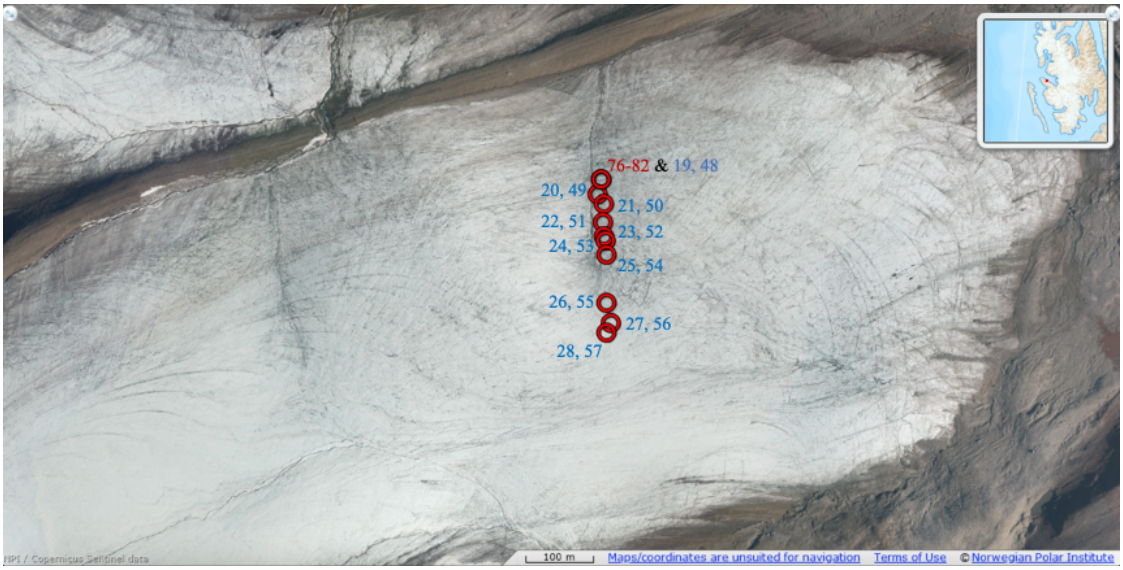

Figure 4.7 *Snow and cryoconite hole sampling locations on Vestre Brøggerbreen. Snow samples are numbered in red, and cryoconite hole water and cryoconite samples are numbered in blue. All snow samples were taken at the same GPS coordinates. Details on sample name, sample no., type, and GPS coordinates are presented in Table A.1.1 in the Appendix. Source: Norwegian Polar Institute n.d. (138).*

Water samples were collected from cryoconite holes using a sterile plastic syringe (20 mL HSW HENKE-JECT) and transferred into 50 mL sterile HDPP plastic sampling tubes (Centrifuge Tubes, VWR Chemicals, USA). Both syringe and sampling tube were cleaned twice with water from the sampling hole before collection. Nitrile gloves were used whilst sampling. Samples were stored outside at atmospheric temperature of ~ + 5 ºC during fieldwork, and then stored in the refrigerator at + 5 ºC on return to the laboratory. Water samples were filtered into 15 mL plastic sampling tubes (Centrifuge Tubes, VWR Chemicals, USA) using a plastic syringe (20 mL HSW HENKE-JECT) and 0.45 µm filter with a polyethersulphone membrane (VWR Chemicals, USA). A new filter was used for each sample, and the syringe cleaned between each filtration with the sample. The sampling tube was also cleaned three times with the sample before final sample filtering. Filtered samples were made up to a volume of 10 mL for later analysis. In accordance with ISO 5667-3:2018 samples were preserved using nitric acid to a pH of 1 – 2 for elemental analysis (188). A total of 3 drops of concentrated HNO_3 were added to the filtered sample to a concentration of 0.1 M immediately after filtration. Samples for SO_4^{2-} and Cl^- determination did not require preservation with HNO_3 (188).

Particulate matter was collected from cryoconite holes using either a plastic 50 mL HDPP sampling tube (Centrifuge Tubes, VWR Chemicals) or a plastic syringe (50 mL HSW HENKE-JECT). Both sampling tube and syringe were cleaned with water from the cryoconite hole prior to sample collection. Samples were deposited into metal free plastic cc cups and stored at

atmospheric temperature of approximately + 5 ºC during fieldwork, and in the freezer at - 26 ºC on return to the laboratory. Examples of cryoconite holes sampled are presented in Fig. 4.8.

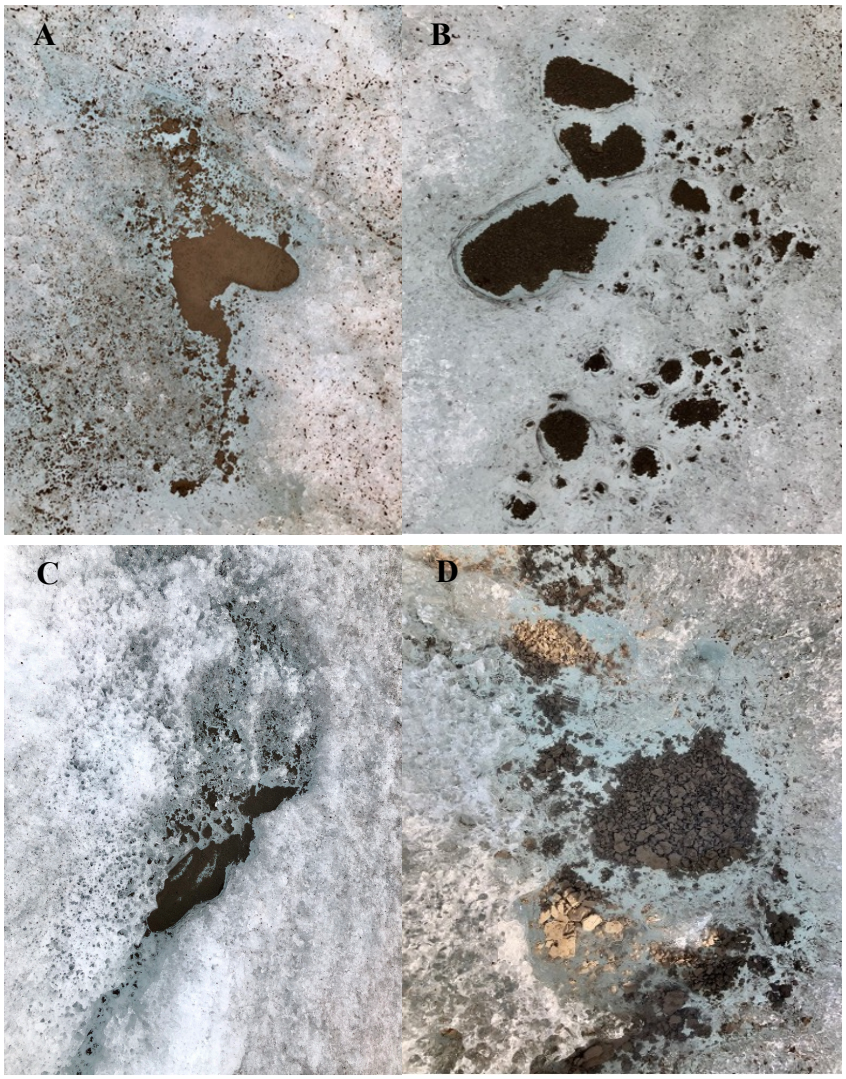

Figure 4.8 *Images of cryoconite holes sampled on the three glaciers. Images show differences in colour and variations in cryoconite hole shape. Images (A) & (B) Cryoconite holes on Austre Brøggerbreen; (C) cryoconite hole on Midtre Lovénbreen; and (D) cryoconite hole on Vestre Brøggerbreen.*

Snow samples were collected from deposits remaining on the surface of the three glaciers (Fig. 4.9). A total of 25 samples were collected across the three glaciers, at seven locations with altitudes ranging from 92 to 285 m.a.s.l. Snow samples were collected into sterile plastic 50 mL HDPP tubes (Centrifuge Tubes, VWR Chemicals) by removing the top 2 cm of snow using a sterile sampling tube followed by collection of snow from the cleared surface into the same tube. Snow samples were allowed to thaw overnight, after which the water was filtered using the same method as described for cryoconite hole water samples.

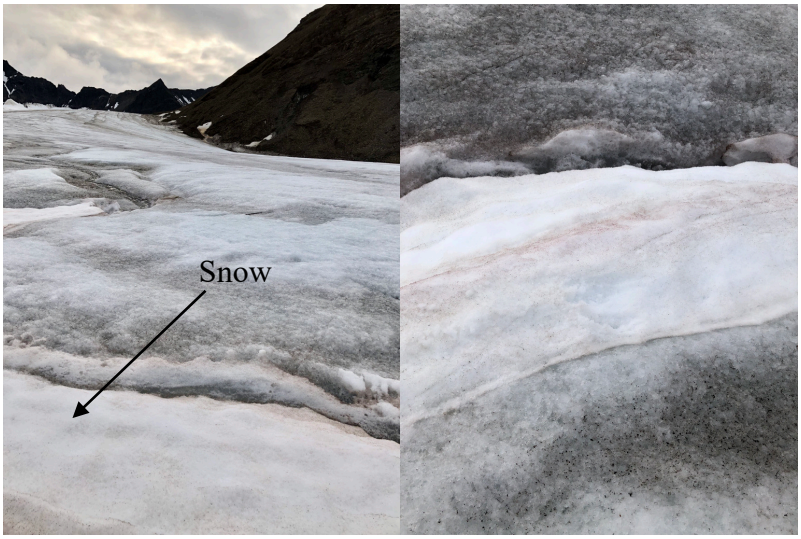

Figure 4.9 *Images of snow collected on Midtre Lovénbreen. Only small patches of snow remained at the end of August at the lower levels of the glacier.*

Supraglacial debris samples were collected from small mud mound deposits and isolated pieces of debris found on the glacier surface (Fig. 4.10 – 4.11). A total of seven samples were collected across ML and AB. Samples were collected in metal free plastic cc cups, sterile 50 mL HDPP plastic tubes (Centrifuge Tubes, VWR Chemicals) or PE-LD Ziplock bags. No debris deposits were found in the sampling area on VB.

Figure 4.10 *Supraglacial debris collected from the surface of Austre Brøggerbreen.*

Figure 4.11 *Supraglacial debris collected from the surface of Midtre Lovénbreen.*

Parameters: conductivity and temperature measurements were recorded in the field using a WTW Multi 350i meter with probe, details of which are presented in Table B.1.1 in the Appendix. The pH and redox potential fluctuated significantly and as a consequence it was not possible to obtain an accurate reading of either parameter in the field.

Photographs were taken at each sampling location documenting the shape of the cryoconite holes in addition to the colour and texture of cryoconite sediment. GPS co-ordinates and altitude readings were also recorded and are presented in Table A.1.1 in the Appendix.

4.2 Sample Pre-treatment

4.2.1 Freeze Drying

Frozen cryoconite (samples 1 - 29) and supraglacial debris (samples 83 - 90) were freeze dried to remove water content prior to further analysis. Those samples collected in PE-LD Ziplock bags and 50mL HDPP tubes were transferred to metal free plastic cc cups prior to drying (samples 86, 88-90). In order to reduce cross-contamination, lids were removed, and plastic wrap film (Wrapmaster 1000 clingfilm refills) was placed on top of each cc cup, ensuring a small gap to allow water vapour to be released during the drying process. The frozen samples were freeze dried under vacuum using a Christ Alpha 1-4 LD plus instrument, at a pressure of 0.94 mbar and a temperature of - 21 ºC for 52 hours. Final drying was performed at a pressure

of 0.09 mbar and a temperature of - 43 ºC for approximately 1 hour until pressure fluctuation was minimal. Dried samples were stored at room temperature.

4.2.2 Sample Homogenisation

The majority of cryoconite samples were of sufficient homogeneity that no additional homogenisation was required prior to the sample pre-treatment steps. For those samples that required homogenisation, homogeneity was achieved by grinding the samples using a mortar and pestle. For QC procedures, the mortar and pestle were cleaned between samples three times with both soap and water, followed by rinsing with MilliQ water. Where organic matter remained on the equipment, the mortar and pestle were also rinsed with acetone and air dried.

4.2.3 Microwave Assisted Digestion

Cryoconite and supraglacial debris required digestion prior to elemental analysis by ICP-MS. Samples were decomposed using a Milestone UltraCLAVE high performance microwave reactor (Milestone GmbH, Leutkirch, Germany) with a temperature, pressure and power gradient as presented in Table A.3.2 in the Appendix. All samples were digested using suprapur 50 % v/v HNO_3. The base load was prepared using 300 mL ultrapure water (~ 18.2 MΩ·cm, ELGA PURELAB Chorus water purification system), 30 mL 30 % hydrogen peroxide (H_2O_2, AnalaR NORMAPUR, VWR Chemicals, USA) and 2 mL 96 % sulphuric acid (H_2SO_4, suprapur, Merck, Germany).

Samples were weighed to between 250 and 350 mg into Teflon vials to which 9 mL (2 times 4.5 mL) of suprapur 50 % v/v HNO_3 (prepared using a Milestone SubPUR Subboiling distillation system) was added. Digestion was performed in two batches. Following digestion, samples were diluted with ultrapure water (~ 18.2 MΩ·cm, ELGA PURELAB Chorus water purification system) to a weight of approximately 109.8 g (to achieve a final HNO_3 concentration of ~ 0.6 M) into a plastic bottle, and transferred to 15 mL plastic HDPP tubes (VWR centrifuge tubes) for ICP-MS analysis. Digested samples were then stored at room temperature. Exact weights used for digestion are presented in Table A.3.1 in the Appendix.

Quality control procedures included the preparation of procedural blanks and the use of CRM in both batches. In batch 1, containing cryoconite samples, three procedural blanks were prepared with 9 mL of suprapur 50 % v/v HNO_3 only, and four CRMs. Duplicates were prepared

for each of the CRMs; MESS - 4 marine sediment (LOT G 4169010, serial CC 567306 from National Research Council Canada) and Modas – 2 bottom sediment (M-2 BotSed, 50 g for trace analysis, No. 0382). In batch 2, containing supraglacial debris, two blanks containing 9 mL of suprapur 50 % v/v HNO_3 and two CRMs were prepared using MESS-4 marine sediment. All surfaces were covered in plastic wrap (Wrapmaster 1000 clingfilm refills) to reduce risk of contamination during sample preparation. No utensils were used to measure out samples, with the exception of sample 87, where a spatula wrapped in plastic wrap was used. The dilution bottle was rinsed three times with ultrapure water (~ 18.2 MΩ·cm, ELGA PURELAB Chorus water purification system) between sample dilutions to minimise cross contamination. The volume of HNO_3 was confirmed at the start of sample preparation using a measuring cylinder to ensure a volume of 4.5 mL.

4.2.4 Accelerated Solvent Extraction (ASE)

The accelerated solvent extraction (ASE) method was used for the extraction of PCBs from solid cryoconite samples. The extraction followed Pintado-Herrera et al. (2016) protocol with modifications from Weging (2021) (152, 231).

Stainless steel 22 mL Thermo Scientific extraction cells were used for extraction of PCBs from cryoconite samples. The extraction cells were loaded in the following order: two cellulose filters, followed by ~ 2 g of activated copper powder, ~ 2 g of activated alumina (Al_2O_3), sample mixture, and lastly activated Ottawa sand. A cellulose filter was used to separate each of the individual layers (with the exception of Ottawa sand), as demonstrated in Fig. 4.12. The Ottawa sand was used to fill the remaining space in the extraction cell. The cell cap was then firmly screwed in place to seal the sample and resins inside. Ottawa sand and diatomaceous earth were activated prior to extraction by heating at 400 ºC for 4 hours in a porcelain crucible using a Carbolite oven (Carbolite ELF 11/6 (201)). Details and specifications of the materials used in the ASE process are presented in Table A.4.1 in the Appendix.

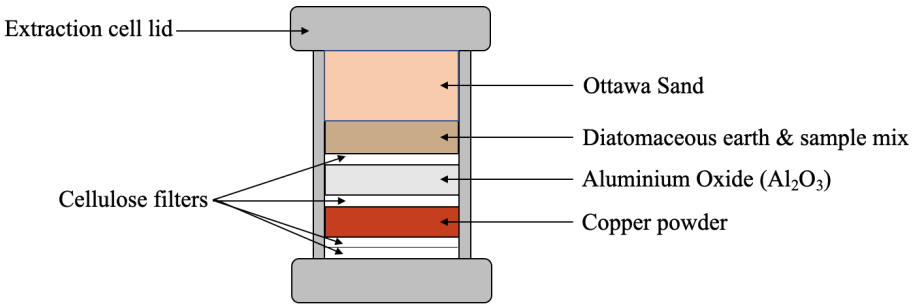

Figure 4.12 *Extraction cell set up for accelerated solvent extraction.*

The sample mixture was prepared using 0.5 g of cryoconite sample, ~ 2 g of activated diatomaceous earth to which 50 µL of each internal standard (IS) were added. The mixture was left to stand until the solvent in the IS had evaporated, then mixed thoroughly with a glass rod. Fluorinated PCBs: 3-fluoro-2,4,4'-trichlorobiphenyl (3'-F-PCB), and 5-fluoro 2,3',4,4',5 pentachlorobiphenyl (5'-F-PCB) were used as internal standards, and the 'Dutch Seven' PCBs were used as external standards (ES) (Fig. 2.2). Internal PCB standards were prepared in ethyl acetate by adding 10 µL of 3'-F-PCB and 100 µL of 5'-F-PCB to 990 µL and 900 µL of ethyl acetate respectively, to achieve IS solutions with a concentration 1 µg mL^{-1}. The ES was prepared with 10 µL 'Dutch Seven' stock solution and 990 µL of ethyl acetate to achieve an ES solution with a concentration of 1 µg mL^{-1}.

The prepared extraction cell was added to a heated Thermo Scientific™ Dionex™ ASE™ 150 Accelerated Solvent Extractor. The extraction solvent used was dichloromethane (DCM) and the system parameters were set at a temperature of 100 ºC and pressure of 1500 psi. The extraction run time was 24 minutes per sample, with a static time of 5 minutes and three static cycles per run. In addition, a nitrogen purge time was set at 60 s and a nitrogen purge volume of 60 %. The total solvent volume per sample was approximately 35 mL. Amber and clear 60 mL glass collection vials were used for the extractant. Clear collection vials were wrapped in aluminium foil to prevent exposure to sunlight following extraction. Samples were stored in the freezer at - 26 ºC until the concentration and solvent exchange step.

Quality control procedures included the preparation of method blanks and CRM, in addition to samples for recovery and matrix effects testing. Five method blanks were prepared; three at the start of the extraction process, followed by two method blanks between cryoconite samples and quality control samples (CRM, recoveries and matrix effects samples). The method blanks were prepared in the same way as the cryoconite samples, however without the cryoconite material.

Three reference materials were prepared using 0.5 g of 'PCB congeners in soil' certified reference material, exact details of which are presented in Table A.4.1 in the Appendix.

To test recoveries, nine samples were prepared, containing 0.5 g of a cryoconite mixture. The cryoconite mixture contained ~ 0.35 g of each of the cryoconite samples being analysed, so as to obtain a mixture containing representation by 100 % of the samples. All recovery sample mixtures were spiked with 50 µL of IS. Three samples were also spiked 50 µL of ES, and three with 100 µL of ES, to give 50 and 100 ng of target analyte respectively ('Dutch 7' PCBs) prior to extraction. These recovery samples are referred to as pre-extraction spiked samples. Full details of sample preparation volumes and weights are presented in Table A.4.2 in the Appendix. To study potential effects of the matrix on PCB quantification, four matrix effect samples were prepared. In this case, the samples were prepared using 0.5 g of the cryoconite mixture, without the addition of IS or ES prior to extraction. These samples are referred to as post-extraction spiked samples.

Working surfaces were covered in aluminium foil to reduce potential contamination. All equipment in contact with the sample, including glass rod, metal spatula and glass beaker were cleaned three times with each soap and water, MilliQ water, and acetone between samples. The extraction cells were cleaned three times with acetone only. The extraction cell cleaning steps with water were removed due to issues with respect to moisture found in the method blank extracts. It was suspected that water had not been completely removed from the cells following the cleaning phase. The use of acetone only for cleaning the extraction cells was therefore determined to be the most efficient method given the time restrictions. The ASE system was rinsed three times at the start of each daily run with the DCM solvent, after solvent replenishment, and between each sample type change (for example between samples and CRM). The rinse extraction cell contained only resins.

4.2.5 Concentration and Solvent Exchange

Concentration, followed by solvent exchange, was performed on the extracts collected from ASE to ensure the use of an appropriate solvent for GC-MS analysis. Exact specifications of the materials and chemicals used are presented in Table A.5.1 in the Appendix. Dichloromethane in the ASE extracts was concentrated down to approximately 2 mL using a Biotage TurboVap LV Evaporator. The vials were held in a water bath at a temperature of 35 ºC under a gentle stream of nitrogen gas at a pressure of 5 psi. Following concentration, the

solvent was changed to ethyl acetate, added at a volume of 10 mL, by rinsing the vial walls so as to minimise loss of analyte. The solution was filtered using a 25 mm 0.2 µm nylon membrane filter with syringe, concentrated down to a volume of 1 mL, and transferred to amber vials required for GC-MS analysis using disposable glass pipettes. Following solvent change and concentration of ethyl acetate, matrix match extracts were spiked with IS and ES (post-extraction spiking). Two matrix match samples were spiked with 50 µL ES, and two with 100 µL ES to give 50 ng and 100 ng of PCB target analytes respectively. All four matrix match samples were spiked with 50 µL of each IS (3' and 5'-F PCBs). The final prepared samples were stored in the freezer at - 26 ºC prior to GC-MS analysis.

For QC purposes, one concentration method blank was prepared for each run. The concentration blank contained ~ 35 mL of DCM only and was evaporated in the TurboVap with a total of nine extracted samples. The same procedure was used for the concentration method blank as the other extracts. A total of six concentration blanks were prepared for the six concentration and solvent exchange batches.

4.2.6 Filtration

Prior to analysis by IC and ICP-MS, the methods for which are described in Sections 4.3.2 – 4.3.3, refrigerated water and snow samples were filtered so as to remove any particulate matter larger than 0.45 µm that may interfere with the analytical instruments. Filtration was performed using a 20 mL HENKE-JECT plastic syringe (Henke Sass Wolf, Germany) connected to a 25 mm syringe filter with a 0.45 µm polyethersulphone membrane (VWR Chemicals, USA). The syringe was first rinsed with ~ 3 mL of the sample. The filter and collection tubes were then rinsed three times with 1 – 2 mL of filtered sample following which the collection tubes were filled with filtered sample up to the required volume for IC and ICP-MS analysis. A new filter was used for each sample. Cryoconite hole water and snow samples prepared for elemental analysis by ICP-MS were filtered during the fieldwork as described in Section 4.1.2. Cryoconite hole water and snow samples prepared for anion determination using IC were filtered just prior to analysis.

4.3 Analysis

4.3.1 Gas Chromatography - Mass Spectrometry (GC-MS)

Cryoconite samples were analysed for PCBs by GC-MS following freeze drying, extraction, concentration, and solvent change procedures described in Sections 4.2.1, 4.2.4 and 4.2.5 respectively. Analysis was carried out on an Agilent Technologies 7890A GC system coupled to an Agilent 5975 single quadrupole mass spectrometer. Target compound separation was performed using a Thermo Scientific^{TM} TraceGOLD TG-5MS GC Column (ThermoFisher Scientific), low polar phase 5 % diphenyl/ 95 % dimethyl polysiloxane. The GC parameters are presented in Table 4.4. Mass spectrometry detection was set to SIM (selected ion monitoring) mode. Electron impact ionisation was selected for the ionisation mode, at 70 eV. Calibration solutions were prepared at concentrations of 0.5, 5, 10, 30, 50, and 100 ng mL^{-1} using 'Dutch 7' PCB standards (Fig. 2.2), dissolved in ethyl acetate, also containing 50 ng mL^{-1} of 3'- and 5'-F-PCB IS.

Table 4.4 *Parameters for the analytical measurement of PCBs in cryoconite samples by GC-MS.*

GC parameters	
Model	Agilent 7890A gas chromatograph
Autosampler	GCPal (CTC Analytics AG, Switzerland)
Column	Thermo Scientific^{TM} TraceGOLD TG-5MS GC Column (ThermoFisher Scientific) Length: 30 m Inner diameter: 0.25 mm Film thickness: 0.5 µm
Carrier gas	Helium gas, at a rate of 1 mL min^{-1}
Transfer line and injection port temperature	290 ºC
Injection volume	1 µL splitless
Temperature programme	50 ºC for 2 min; temperature increase at 25 ºC min^{-1} to 250 ºC 250 ºC for 1 min; temperature increase at 3 ºC min^{-1} to 286 ºC 286 ºC for 3 min; temperature increase at 8 ºC min^{-1} to 308 ºC 308 ºC for 1 min; temperature increase at 1 ºC min^{-1} to 310 ºC 310 ºC for 3 min
Sample analysis time	34.75 min

For QC/QA purposes, method blanks prepared at both the ASE and evaporation and solvent exchange steps to identify any potential contamination from the method itself, were analysed by GC-MS. In addition a reagent blank of ethyl acetate was run every ten samples in order to identify any carry over from the previous sample or contamination in the column. The 10 ng

mL^{-1} calibration solution was run after the reagent blanks for identification and quantification of contamination.

4.3.2 Inductively Coupled Plasma - Mass Spectrometry (ICP-MS)

Elemental analysis of all samples (snow, water, cryoconite, and supraglacial debris) was performed on an 8800 Triple Quadrupole inductively coupled plasma mass spectrometry (ICP-MS) system (Agilent, USA). The ICP-MS parameters used for the snow/water and cryoconite/supraglacial debris samples are presented in Table 4.5. Tune modes O_2 and H_2 were used for removal of interferences. Internal standards used are presented in Table A.6.1 in the Appendix.

The quality of the data was evaluated through use of procedural blanks and CRMs, both of which were prepared using the same analytical procedures. For snow and water samples, method blanks and MilliQ water blanks were prepared in triplicate. Method blanks were prepared using ultrapure water (~18.2 MΩ·cm) from an ELGA PURELAB Chorus water purification system, filtered through 25 mm syringe filter with 0.45 µm polyethersulphone membrane as described in Section 4.2.6. MilliQ water blanks were prepared using MilliQ water only, collected from the ICP-MS laboratory. Concentrated HNO_3 was added to both blank types to a final HNO_3 concentration of 0.1 M. Cryoconite and supraglacial debris blanks were prepared as described in Section 4.2.3.

Table 4.5 *ICP-MS parameters for cryoconite hole water, snow, cryoconite, and supraglacial debris samples. Details include general parameters and gas flow in H_2 and O_2 modes.*

ICP-MS Parameters	Cryoconite Hole Water & Snow	Cryoconite & Supraglacial Debris
General Parameters		
RF Power:	1600 W	1550 W
Nebuliser Gas:	0.77 L min^{-1}	0.78 L min^{-1}
Makeup Gas:	0.40 L min^{-1}	0.40 L min^{-1}
Sample depth:	8.0 mm	8.0 mm
Ion lenses:	s-lens	x-lens
H_2 mode		
H_2 gas flow:	6.0 mL min^{-1}	4.4 mL min^{-1}
He gas flow:	1.5 mL min^{-1}	1.2 mL min^{-1}
O_2 mode		
O_2 gas flow:	0.675 mL min^{-1}	0.525 mL min^{-1}
He gas flow:	1.5 mL min^{-1}	

4.3.3 Ion Chromatography (IC)

Filtered cryoconite hole water and snow samples were analysed for the presence of selected anions using ion chromatography (IC). The anions analysed included fluoride (F^-), Cl^-, nitrite (NO_2^-), bromide (Br^-), NO_3^-, phosphate (PO_4^{3-}), and SO_4^{2-}. Anion separation was achieved using a Metrosep A Supp 7 – 250/4.0 column with an anion eluent of Na_2CO_3 at a concentration of 3.6 mM. Parameters were set at a temperature of 45.0 ºC, pressure between 9.85 and 9.97 MPa, and eluent flow rate of 0.7 mL min^{-1}, at a run time of 38 mins. Detection was performed using the Metrohm IC with MagIC Net 3.2 software and a conductivity detector 940 Professional IC Vario.

Blanks of ultrapure water from an ELGA PURELAB flex 3 water delivery system were used for QC purposes. Standards were used to establish calibration curves at concentrations of 0.2, 0.5, 1.0, 2.0, 5.0, and 10.0 ppm.

Samples were only filtered where particulate matter could be observed by eye. All snow samples were filtered. Cryoconite hole water samples did not require filtering with the exception of five samples: 36, 38, 42, 52, and 54 where clear particulate matter was observed at the bottom of the sample tubes. Collection tubes were prepared with between 12 – 15 mL of sample for analysis. A limited volume of snow samples were available, therefore to ensure sufficient sample for analysis, the syringe used for filtering was cleaned with MilliQ water between samples, rather than the sample itself. This method was in contrast to that described in Section 4.2.6. The filter and collection tubes were cleaned with sample as described in Section 4.2.6. Where there was insufficient sample volume, the samples were diluted with ultrapure water from the ELGA PURELAB flex 3 purification system to a total volume of 15 mL prior to analysis. No dilution was required for cryoconite hole water samples. Dilution factors have been recorded for snow samples: 77, 79, 80, and 82 from VB in Table B.8.2 in the Appendix.

4.3.4 Total Organic, Residual Oxidisable, and Total Inorganic Carbon Content Determination

All supraglacial debris and 12 cryoconite samples (four cryoconite samples per glacier) were analysed for total organic carbon (TOC), residual oxidisable carbon (ROC), and total inorganic carbon (TIC). Samples were first freeze dried to remove water and homogenised where required, as described in Sections 4.2.1 and 4.2.2 respectively. Homogenisation was performed

to achieve a particle size of between 0.05 mm and 1 mm required for proper combustion process. Determination of TOC, ROC and TIC was performed in accordance with DIN 19539 method (173). In short, a weight of between 75 to 125 mg of sample was measured using a ceramic spatula into ceramic crucibles (2SN100370 pkg/20). Total organic carbon, ROC, and TIC content were determined via combustion of samples at 400, 600 and 900 ºC respectively using ultra-pure grade, 99.995 % purity oxygen gas to produce CO_2. An infrared (IR) detector was used to measure the concentration of CO_2 generated.

For calibration, a total of seven points over a range of 0.2 - 3mg C abs, were used to establish the calibration curve using the calibration standard DIN A. The standards were prepared to weights of: 10, 25, 50, 75, 100, 125, and 150 mg. The calibration standard contained 2 % carbon in each TOC, ROC, and TIC form. The standard contained calcium carbonate (12.00 % carbon content), carbon black (100 % carbon content) and ammonium oxalate monohydrate (16.90 % carbon content), in addition to aluminium oxide. This is in accordance with Skalar (173). Exact weights and results for the calibration are presented in Table B.7.1 in the Appendix. A mean accuracy of 100 ± 3 % was achieved for TOC and 99 ± 9 % for both ROC and TIC.

For QC purposes the crucibles were handled with metal tweezers to avoid potential contamination resulting in a positive error from hands during sample preparation. The ceramic spatula was washed with soap and water, followed by MilliQ water, and dried with dust-free paper between each sample to avoid cross contamination. Crucibles were acid washed with dilute HCl solution and ignited prior to use. Blanks were run using empty crucibles. The QC results are presented in Table B.7.2 in the Appendix.

4.4 Data Treatment

Data processing and production of box plots and graphs was performed using Microsoft Excel Version 16.58. Topographical maps modified to show sample locations were provided by the Norwegian Polar Institute (138). Statistical analysis was performed using Microsoft Excel and SPSS Statistics (IBM SPSS Statistics Version 28.0.1.0) (142). Principal Component Analysis was performed on Aspen Unscrambler V12.1. The Shapiro-Wilk test was used to determine normal distribution. Where data was normally distributed, the one-way ANOVA followed by Tukey's HSD post-hoc test was used to determine the presence of significant differences between three or more means. For comparison of two means with non-normally distributed

data, the Mann-Whitney U test was used. For comparison of three or more means with non-normally distributed data, the Kruskal-Wallis test, followed by Dunn's post hoc test with Bonferroni correction was used. Non-parametric Spearman correlation was used to identify significant correlations between elements. The significance level was set at $p < 0.05$ for all statistical tests.

5 Results

In order to understand the elemental composition of cryoconite holes (CHs), their accumulation ability and the influence of the surrounding environment, the results obtained from ICP-MS, GC-MS, IC, and combustion, for elemental analysis, PCB, anion, and TOC/ROC/TIC determination respectively have been presented for cryoconite, supraglacial debris (SGD), snow, and cryoconite hole water (CW).

5.1 Cryoconite and Supraglacial Debris

5.1.1 General Observations on Cryoconite and Supraglacial Debris

5.1.1.1 Colour and Size Categories of Cryoconite

Based on observations made during sampling, as presented in Table B.2.1 in the Appendix, cryoconite were classified into four general size groups: (i) cryoconite comprised of fine particulate matter (fine and very fine); (ii) cryoconite containing a mixture of fine and granular sized particles with fine particles dominating; (iii) cryoconite containing a mixture of fine and granular sized particles with granular particles dominating; and (iv) cryoconite containing granular sized particles. A large proportion of the cryoconite holes contained a mixture of sized particles, usually with one size dominating. Particulate matter appeared finer in cryoconite holes from AB in comparison to VB. Cryoconite from ML were mostly comprised of a mixture of particle sizes with finer particles dominating, although two samples were found to contain just granular particulate matter.

Cryoconite were grouped into six main colour categories: pale grey, grey, dark grey, cream, brown, and red-brown. Cryoconite varied in colour both within and between the three glaciers. Cryoconite sampled from AB showed a large amount of colour variation of red-brown, pale grey and grey, and were generally lighter in colour than cryoconite from VB, where the majority were brown. Cryoconite from ML were all grey, varying between hues of grey and dark grey.

5.1.1.2 Supraglacial Debris

Supraglacial material excluding samples collected from cryoconite holes were grouped into three main categories based on observations made in the field. Supraglacial debris was found

in small mounds, examples of which are presented in Fig. 4.10 in Section 4.1.2 The mounds were low in number within the study area of each glacier, and just four samples were available for collection on ML and AB, and have been referred to hereafter as supraglacial debris - mounds (SGD-M). The second type consisted of individual isolated pieces of debris collected from the glacier surface, as presented in Fig. 4.11, Section 4.1.2, all of which had observable plant content, and are referred to hereafter as SGD-P. A total of three SGD-P samples were collected across AB and ML. The final category of SGD was a sample collected from a small stream on the surface of ML (sample 87). As a consequence of glacier surface conditions on VB, the sampling area was limited and no SGD was identified within the area. Observations of the physical properties of SGD samples are presented in Table B.2.1 in the Appendix. Of the four SGD-M samples, three had a granular form and were dark brown in colour, whilst the final was black and consisted of fine particulate matter. The three SGD-P samples varied in colour between brown, dark brown, and black.

5.1.2 Elemental Composition of Cryoconite and Supraglacial Debris

A total of 64 elements were analysed in cryoconite and SGD samples by ICP-MS. Despite the shape and colour heterogeneity of the cryoconite, some general patterns were observed in the proportions of major elements, trace elements, heavy metals and metalloids, and rare earth elements (REE) between sample types and locations (Fig. 5.1). A total of nine elements were selected for further analysis. The elements Pb, As, Cd, and Cr were selected due to their hazardous nature and anthropogenic source (1, 6). Lead and Cd (in addition to Hg which was below detection in all samples) are considered by the Arctic Monitoring and Assessment Programme (AMAP) to be elements of most concern in the Arctic, and even at low concentrations, these elements can be toxic (1). Zinc was selected as it has both natural and anthropogenic sources and is subject to long range atmospheric transport (1). Aluminium, Fe, Ca, and Mg were selected due to the parent rock influence (Table 4.2).

No method blank correction was made for the nine selected elements. Of the five method blanks analysed at least four of five contained the elements As, Cd, Cr, Pb, and Zn at concentrations below the detection limit. For elements Al, Fe, Mg, and Ca, the average blank concentration was less than 1 % of both the mean cryoconite and SGD concentrations, hence blank corrections were not performed prior to further analysis.

The certified reference material MESS-4 Marine sediment from the National Research Council Canada was analysed by ICP-MS following microwave assisted digestion. The relevant elements were compared to certified values reported for the CRM in order to verify measurement efficiency. The results of the QA procedures are presented in Table 5.1 and were in reasonable agreement (average of 87 % accuracy) with certified reported values. The limit of detection (LOD), calculated as $3\sigma/S$, is also presented in Table 5.1 for cryoconite and SGD following conversion from $\mu g\ L^{-1}$ to $\mu g\ g^{-1}$. Aluminium and Fe were detected at lower concentrations than reported for the CRM. This is a assumed to be a consequence of the use of HNO_3 in the microwave assisted digestion step, which did not dissolve the entire sample.

Table 5.1 *Quality assurance results for analysis of selected elements Al, Fe, Ca, Mg, Zn, Pb, As, Cd, and Cr by ICP-MS. Limit of detection (LOD) is reported in $\mu g\ g^{-1}$. Measured concentrations of selected elements in MESS - 4 marine sediment (LOT G 4169010, serial CC 567306 from National Research Council Canada) reported in $\mu g\ g^{-1}$ for both the mean and 2 x standard deviation (SD). The certified levels reported for the CRM are reported on a dry weight mass in $\mu g\ g^{-1}$ with 95 % confidence (CI) (198). In order to obtain reproducibility and determine accuracy of results, four reference material samples were analysed. Accuracy was determined based on the measured concentration as a percentage of certified reported elemental concentrations.*

		Measured MESS-4		Certified MESS-4		
Element	LOD	Mean	2 SD	Certified	95 % CI	Accuracy
	$\mu g\ g^{-1}$	$\mu g\ g^{-1}$	$\mu g\ g^{-1}$	$\mu g\ g^{-1}$	$\mu g\ g^{-1}$	%
Al	0.002	59500	4450	79100	2000	75.3
Fe	0.003	32700	803	37900	1600	86.3
Ca	0.006	12300	531	13100	600	94.2
Mg	0.008	14500	318	15800	1200	91.5
Zn	0.003	138	4.03	147	6	93.8
Pb	0.0004	19.2	0.543	21.5	1.2	89.2
As	0.0004	18.7	1.67	21.7	2.8	86.2
Cd	0.0000	0.231	0.0287	0.28	0.04	82.4
Cr	0.0005	81.2	4.45	94.3	1.8	86.1

The proportions of the major elements (Fig. 5.1), which are those elements expected to be present in high quantities in the local rock (as described in Table 4.2), were on the whole present in similar proportions in cryoconite and SGD across the three glaciers. The exception being cryoconite from VB (VB(CG)) where three of the ten samples collected from the glacier contained higher concentrations of Ca and Mg compared to the remaining seven samples.

The proportions of trace elements were also relatively consistent across sample types and locations. The largest fluctuations in concentrations were observed for Mn, which also has a local rock influence (Table 4.2). Observable differences were however noted in the proportions

of heavy metals and metalloids especially Cr and Pb, although As appeared relatively consistent across the groups and locations.

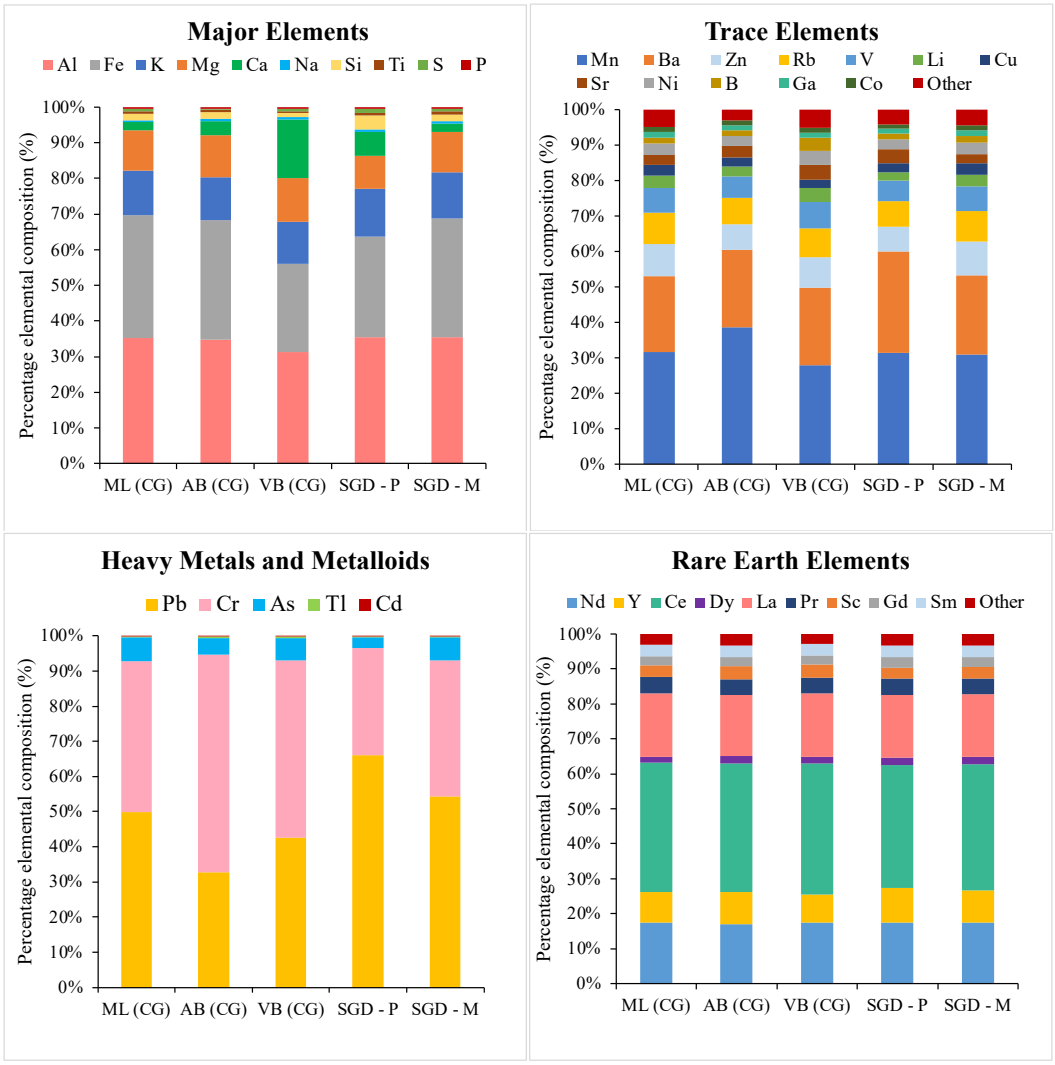

Figure 5.1 *Percentage elemental composition of cryoconite and supraglacial debris categorised by major elements, trace elements, heavy metals and metalloids, and rare earth elements. Percentage composition calculated based on mean concentrations of each element. Cryoconite (CG) are split by location where ML = Midtre Lovénbreen, AB = Austre Brøggerbreen, and VB = Vestre Brøggerbreen. Percentage elemental composition results for supraglacial debris (SGD) are separated into supraglacial debris with observable plant content (SGD-P) and supraglacial debris from small mounds (SGD-M).*

The proportion of REE showed very similar trends across all sample types and locations. The REE were generally enriched in contrast to the Earth's crust, where concentrations are typically 137 – 242 µg g^{-1} (this study: mean total concentration was 334 µg g^{-1}) (232). These findings are in contrast to those reported by Rozwalak et al. (2022) which found a general depletion in the concentration of REE across cryoconite worldwide, with the exception of two glaciers including Austerdalsbreen in Norway, where the sum of REEs was 274 µg g^{-1} (100).

Just eight of the 64 elements analysed represented 98 % of the total elemental composition of the cryoconite. On average, Al and Fe were the dominating elements with 33.3 % and 30.4 % contribution to total element composition respectively (Fig 5.9). Magnesium and K contributed 11.6 % and 12.1 % respectively, with Ca as the next largest contributor at 7.6 %. The continental crust is dominated by these elements, after oxygen and silicon (which make up 76 % of the upper continental crust) (8, 68, 69). The elements that dominated the composition of SGD-M and SGD-P were similar both in type and extent to those found in cryoconite. Aluminium made up 35.0 % and 34.9 %; and Fe, 33.0 % and 27.9 % of the composition of SGD-M and SGD-P respectively. Potassium contributed 12.8 % and 13.1 %; and Mg, 11.1 % and 9.1 % to SGD-M and SGD-P respectively. On average, the percentage of Ca in SGD-M was lower at 2.3 % compared to SGD-P (6.7 %). The proportion of Si was on average just 1.6 % of the cryoconite composition, with similar proportions observed in SGD (1.9 % of SGD-M, and 3.9 % of SGD-P). The Si contribution was significantly lower than initially expected given that Si is the second most abundant element in the upper continental crust after oxygen (8, 68, 69).

A summary of the mean ± SD and concentration range of each of the nine selected elements in the 28 cryoconite and seven SGD samples are presented in Table 5.2. Elemental concentrations in each of the 28 cryoconite and eight SGD samples analysed are presented in Table B.3.1 and B.3.2 in the Appendix. Concentrations of selected elements were above the LOD in all samples (Table 5.1). A total of eight SGD samples were collected, however sample 87 taken from a small glacial stream on ML was excluded from further analysis due to the large differences in concentrations calculated compared to all other samples. The final sample volume after freeze drying was just 7.3 mg, which was significantly lower than the weight required for microwave assisted digestion (250 to 350 mg). As a consequence the sample was diluted ~ 35 times compared to all other samples. On conversion from $\mu g\ L^{-1}$ to $\mu g\ g^{-1}$ elemental concentration ranged between 133 – 357 % higher in sample 87 compared to the average concentrations found in all other SGD samples. The small weight and low concentrations analysed (prior to conversion to $\mu g\ g^{-1}$) could lead to errors in concentration determination, hence this outlier has been removed from further statistical tests.

The mean concentrations of selected elements in cryoconite were found in the following decreasing order: Al>Fe>Mg>Ca>>Zn>Cr>Pb>As>>Cd. The mean concentrations in SGD-M followed a similar order but with Pb detected at higher concentrations than Cr: Al>Fe>Mg>Ca>>Zn>Pb>Cr>As>>Cd. In SGD-P samples, mean Pb concentrations were also higher than Zn, resulting in the following order: Al>Fe>Mg>Ca>>Pb>Zn>Cr>As>Cd>>Cd.

Table 5.2 *Elemental concentrations of nine selected elements in cryoconite and supraglacial debris samples collected from three glaciers located in the Ny-Ålesund area. Concentrations displayed as mean ± SD, and include the range between minimum and maximum concentrations. The 'n' represents the total number of samples. Concentrations displayed in µg g^{-1}. Samples were analysed by ICP-MS. Supraglacial debris is represented by SGD – M (supraglacial debris from mounds) and SGD – P (supraglacial debris with observable plant content).*

Element		Cryoconite (n = 28)	SGD-M (n = 4)	SGD – P (n = 3)
Al	Mean ± SD	40300 ± 5240	40700 ± 4950	26300 ± 20300
	Range	31600 – 52100	34300 – 46300	4640 – 45000
Fe	Mean ± SD	36800 ± 7860	38400 ± 4080	21000 ± 14300
	Range	14000 – 47800	35300 – 44400	5040 – 32800
Ca	Mean ± SD	9220 ± 27800	2650 ± 771	5010 ± 3100
	Range	2010 – 151000	1790 – 3340	1810 – 7,990
Mg	Mean ± SD	14000 ± 7310	12900 ± 731	6860 ± 4180
	Range	8730 – 48900	11900 – 13600	2230 – 10300
Zn	Mean ± SD	87.8 ± 10.2	103 ± 13.8	52.1 ± 32.3
	Range	60.6 – 101	90.6 – 123	15.6 – 77.0
As	Mean ± SD	7.14 ± 2.35	9.54 ± 2.81	3.23 ± 2.59
	Range	2.77 – 11.9	7.07 – 13.6	0.378 – 5.44
Cd	Mean ± SD	0.119 ± 0.0926	0.0920 ± 0.0202	0.0993 ± 0.0624
	Range	0.0432 – 0.532	0.0736 – 0.117	0.0605 – 0.171
Cr	Mean ± SD	61.2 ± 5.71	57.0 ± 7.33	32.9 ± 23.9
	Range	52.5 – 84.1	47.4 – 64.7	6.45 – 53.0
Pb	Mean ± SD	50.0 ± 25.0	79.7 ± 23.4	71.2 ± 78.4
	Range	8.33 – 135	60.5 – 111	8.83 – 159

The concentration of elements was observed to fluctuate considerably between cryoconite samples (Table 5.2). For example, Ca and Mg concentrations in cryoconite ranged from 2010 to 151000 µg g^{-1}, and from 8730 to 48900 µg g^{-1} respectively. In the trace elements, large variations between samples were detected for Pb and Cd, with Pb concentrations ranging between 8.33 – 135 µg g^{-1}, and Cd concentrations ranging between 0.0432 – 0.532 µg g^{-1}. In contrast Cr and Zn, demonstrated much lower concentration ranges. Sample 25 collected from a cryoconite hole on VB was found to be responsible for the large variations in Ca, Mg, Cd, and Pb observed, containing the maximum concentrations of Ca, Mg, and Cd from the 28 cryoconite sampled. Sample 25 also contained the lowest concentration of Pb (8.33 µg g^{-1}) of all 28 cryoconite analysed. Large variations were observed for SGD-P samples, where an RSD of over 60 % was noted for all nine elements. However, given the small sample size of three, it is difficult to draw a reasonable conclusion as to the reason for the large variability.

Similar concentrations of most elements were observed between cryoconite and SGD-M, with the exception of Pb and Ca. The mean ± SD concentrations of both these elements were however

influenced by sample 25 as previously noted. Given the small sample size, it is not possible to determine the statistical significance of any differences between cryoconite and SGD-M.

5.1.3 Elemental Enrichment in Cryoconite

5.1.3.1 Elemental Composition of Cryoconite and Supraglacial Debris Between Colour Categories

A large heterogeneity in the colour of cryoconite and SGD was observed on the surface of ML, AB, and VB, thus a comparison of elemental concentrations between colour categories with respect to the nine selected elements is presented in Fig. 5.2. On the whole, the major elements in each colour category followed the same order as described in Section 5.1.2, where the mean concentration across all cryoconite followed the order Al>Fe>Mg>Ca. One clear exception was the cream coloured sample (sample 25) where Ca represented 61 % of the total elemental composition across the 9 elements. The mean concentration of Fe (41600 ± 3130 μg g^{-1}) was slightly higher than Al (41000 ± 1800 μg g^{-1}) in the grey coloured material although the differences were minor. Concentrations of Mg and Ca appeared relatively consistent across the colour groups (excluding cream).

For the trace elements, across all colour groups with the exception of the cream sample and the darker colours: dark grey, dark brown, and black, the general trend in concentration followed the order Zn>Cr>Pb>As. Dark brown and black (SGD-P and SGD-M samples) and dark grey (cryoconite) samples contained elevated concentrations of Pb compared to the other colour categories, with concentrations being either very similar or in some cases higher than Zn. Average Pb concentrations in the darker cryoconite and SGD samples was 86.5 μg g^{-1} compared to the average Pb concentrations in the other colour categories combined of 42.7 μg g^{-1}.

Chromium levels were found to be elevated in the cream coloured sample than in the other colour categories, this was also the case for Cd. Chromium concentrations in all grey, brown and red-brown samples appeared to be relatively similar. Arsenic was also found at relatively consistent concentrations across the colour categories, although slightly elevated in the darker coloured cryoconite (dark grey mean: 9.98 ± 1.39 μg g^{-1}) and lower in the pale grey cryoconite (mean: 2.97 ± 0.282 μg g^{-1}). As a result of the small sample sizes for the majority of the colour groups, it was not possible to test the differences in elemental concentrations for statistical significance. In addition, the cream coloured category contained only one sample and as a

consequence it is not possible to draw an accurate conclusion as to the reason for the very different elemental concentrations in this colour.

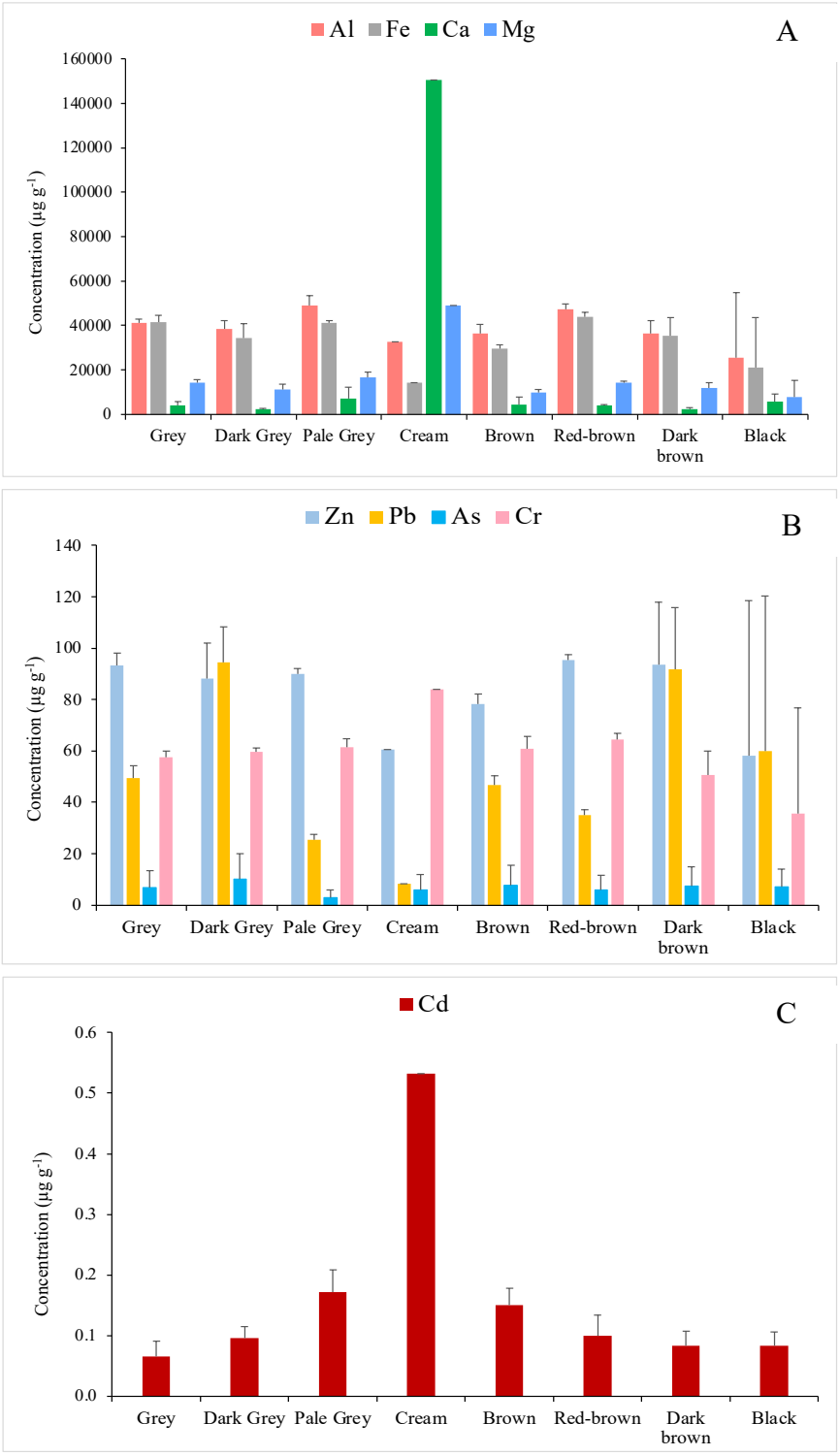

Figure 5.2 *Concentrations of selected elements detected in cryoconite and supraglacial debris categorised by colour. Elements in plot (A): Al, Fe, Mg, and Ca; plot (B): Zn, Pb, As, and Cr; and in plot (C): Cd. All concentrations are presented in µg g^{-1}. The number of samples in each colour category is: grey (n = 10), dark grey (n = 4), pale grey (n = 2), cream (n = 1), brown (n = 8), red-brown (n = 4), dark brown (n = 4), and black (n = 2).*

5.1.3.2 Enrichment of Elements in Cryoconite in Comparison to the Upper Continental Crust

A study by Singh et al. (2013) analysed the elemental composition of cryoconite from four cryoconite holes on Midtre Lovénbreen, a summary of which is included in Table B.4.1 in the Appendix (10). The study made a comparison of the concentrations of trace elements in cryoconite to those in the continental crust using the crustal composition based on the refraction seismic profile of Western Europe and Canada according to Shaw et al. (1967, 1976) and Wedepohl (1995) (8, 10, 68, 69). A similar comparison is presented in Fig. 5.3 in order to evaluate the rock influence on the concentrations of elements in cryoconite and to aid in the identification of potential sources outside of the local geology.

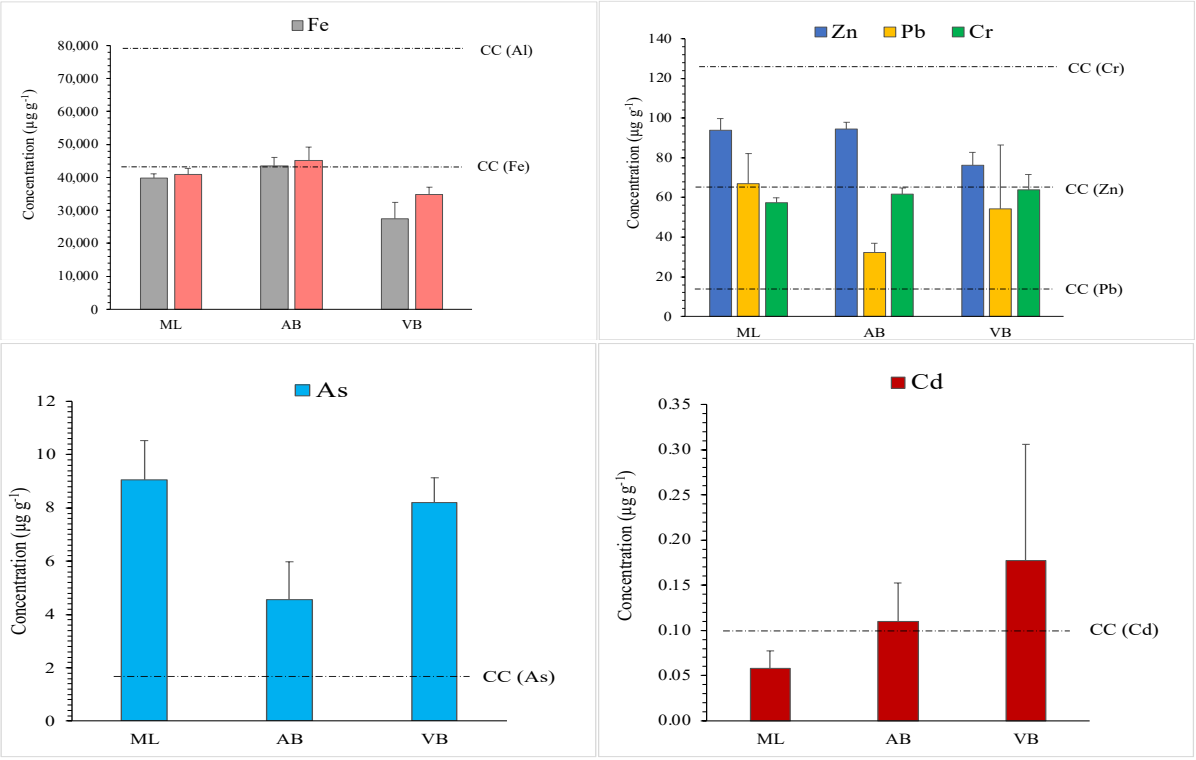

Figure 5.3 *Comparison of elemental concentrations detected in cryoconite to continental crustal levels. Error bars show standard deviation in the data. The dotted horizontal line named "CC" is the concentration found in the continental crust according to Shaw et al. (1967, 1976) and Wedepohl (1995) (8, 68, 69).*

Aluminium concentrations were well below upper continental crust (UCC) levels of 79600 ppm in all samples. Calcium was found at concentrations below continental crustal levels (38500 ppm) in all but one sample (sample 25) which contained Ca at ~ 4 times crustal levels. Concentrations of Mg were below crustal levels (22000 ppm) in all but one sample (sample 25) which was found at ~ 2 times crustal levels. Iron concentrations were below crustal levels

(43200 ppm) in all cryoconite from ML and VB, however 50 % of samples from AB demonstrated elevated concentrations above the continental crust. Crustal concentrations for all elements are according to Shaw et al. (1967, 1976) and Wedepohl (1995) (8, 68, 69).

To determine the extent of elemental enrichment, enrichment factors (EFs) were calculated by comparing the concentrations of each of the elements As, Cd, Cr, Pb, and Zn to the concentrations present in the UCC. Each of the elemental concentrations were normalised relative to Al. The EFs are presented in Table 5.3 and 5.4 displayed by location, for cryoconite only, and sample type respectively. An EF > 1 shows enrichment compared to the continental crust, however given the variations in crustal composition an EF > 2 has been chosen to represent enrichment.

Table 5.3 *Enrichment factors (EFs) for cryoconite based on the upper continental crust levels according to Shaw et al. (1967, 1976) and Wedepohl (1995), for the elements Zn, Pb, Cr, As, and Cd normalised to Al.Mean, minimum (min), and maximum (max) EF reported for each glacier, where ML = Midtre Lovénbreen, AB = Austre Brøggerbreen, and VB = Vestre Brøggerbreen (8, 68, 69).*

	ML (n = 8)			AB (n = 10)			VB (n = 10)		
	Mean	Min	Max	Mean	Min	Max	Mean	Min	Max
Zn	2.80	2.61	3.02	2.58	2.15	2.98	2.68	2.27	2.85
Pb	8.75	6.92	11.8	3.89	2.65	4.75	8.28	1.37	20.6
Cr	0.883	0.858	0.911	0.863	0.772	0.911	1.16	1.08	1.63
As	10.3	9.06	13.5	4.74	2.84	7.24	11.0	8.47	12.0
Cd	1.13	0.795	1.83	1.91	1.14	3.46	4.11	1.98	13.0

Table 5.4 *Enrichment factors (EFs) for cryoconite and supraglacial debris (SGD) separated into those collected from mounds (SGD-M) and those with observable plant content (SGD-P). The EF is calculated based on upper continental crustal levels according to Shaw et al. (1967, 1976) and Wedepohl (1995), normalised relative to Al for the elements Zn, Pb, Cr, As, and Cd. Mean, minimum (min), and maximum (max) EF values reported (8, 68, 69).*

	Cryoconite (n = 28)			SGD-M (n = 4)			SGD-P (n = 3)		
	Mean	Min	Max	Mean	Min	Max	Mean	Min	Max
Zn	2.68	2.15	3.02	3.13	2.67	3.59	2.96	2.10	4.12
Pb	6.85	1.37	20.6	10.4	8.07	12.9	15.0	5.46	29.3
Cr	0.975	0.772	1.63	0.886	0.846	0.941	0.822	0.744	0.878
As	8.57	2.84	13.5	10.8	9.66	13.7	5.52	3.82	8.71
Cd	2.47	0.795	13.0	1.80	1.45	2.23	5.34	1.65	11.3

Several elements in cryoconite were elevated in concentration compared to the UCC (EF > 2). Chromium was however found to be depleted in comparison to the continental crust in all cryoconite and SGD samples, with an EF range of 0.772 – 1.63 and a mean EF of 0.975 for cryoconite. Elevated concentrations of Zn were determined in 27 of 28 cryoconite samples, and

was found to be slightly enriched, with an EF of between 2.15 and 3.02 (mean EF = 2.68). Similar enrichment was also observed in SGD-M and SGD-P with mean EFs of 3.13 and 2.96 respectively. Arsenic was found at elevated concentrations above the continental crust in all 28 cryoconite and was also highly enriched, with EFs ranging from 2.84 to 13.5. Cryoconite from VB showing the highest mean As enrichment with an EF of 11.0. Supraglacial debris (SGD-M) was found to have the highest enrichment in As of the three sample types with a mean EF of 10.8 compared to 8.57 for cryoconite and 5.52 for SGD-P. Lead was elevated in 27 of 28 cryoconite samples and was highly enriched, particularly in samples from ML and VB. Lead was found to be more highly enriched in SGD samples than in cryoconite, with EF of 10.4 and 15.0 for SGD-M and SGD-P respectively. Cadmium concentrations were elevated in 14 of 28 cryoconite samples, with 90 % and 50 % of the samples being higher than UCC levels in cryoconite from VB and AB respectively. All samples from ML were depleted in Cd. The EF of Cd in cryoconite ranged from 0.795 to 13.0, with cryoconite from VB showing the highest enrichment (mean EF 4.11). Cryoconite and SGD-M samples showed lower mean enrichment compared to SGD-P which had a mean EF for Cd of 5.34.

5.1.4 Total Organic Carbon, Residual Oxidisable Carbon, and Total Inorganic Carbon Content of Cryoconite and Supraglacial Debris

Cryoconite and SGD samples were analysed for TOC, ROC, and TIC by combustion. The objective of this analysis was to gain more understanding of the characteristics of cryoconite and SGD collected from the surface of the three neighbouring glaciers in Ny-Ålesund. Results of the analysis were also utilised to consider the potential influence of TOC, ROC, and TIC on the concentration of trace elements and PCBs.

A comparison of the levels of TOC, ROC, and TIC in cryoconite was performed using Kruskal-Wallis test and Dunn's post hoc test with Bonferroni correction as a result of non-normal distribution. Normality was tested using the Shapiro-Wilk test ($p < 0.05$). The percentage by weight carbon content of TOC, ROC, and TIC in cryoconite across all sampling locations is presented in Fig. 5.4. The two outliers denoted by coloured circular markers were from cryoconite on VB. A statistically significant difference was present between TOC, ROC and TIC ($p < 0.001$, Kruskal-Wallis test) with TIC being significantly lower than TOC ($p = 0.000$, Dunn's post hoc test with Bonferroni correction, adjusted significance value). Mean TOC in cryoconite was 1.6 %, whilst ROC (graphitic carbon, coal or soot) and TIC (carbonates) showed mean vales of 0.44 % and 0.70 % respectively (174, 233).

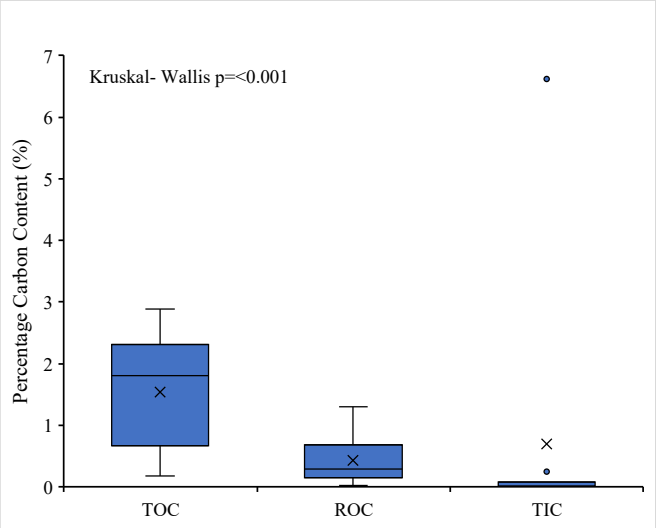

Figure 5.4 *Total organic carbon (TOC), residual oxidisable carbon (ROC), and total inorganic carbon (TIC) content in cryoconite presented as box and whisker plots. Carbon content is reported in percentage by weight in cryoconite material. A total of n = 12 cryoconite were analysed, with n = 4 per study location, Midtre Lovénbreen, Austre Brøggerbreen and Vestre Brøggerbreen. The circular points represent outliers, the 'x' denotes the mean and the line within the box represents the median.*

A comparison of TOC, ROC and TIC content in cryoconite by location is presented in Table 5.5. The mean TOC content in cryoconite from ML was 2.2 %. Total organic carbon content in AB and VB was slightly lower, although at a similar magnitude, of 0.73 % and 1.7 % respectively.

Table 5.5 *TOC, ROC, and TIC percentage composition by weight in cryoconite and supraglacial debris. Cryoconite samples grouped by location, Midtre Lovénbreen (ML), Austre Brøggerbreen (AB) and Vestre Brøggerbreen (VB). Supraglacial debris grouped by type, where SGD-M represents mud mound samples, and SGD – P represents samples with high plant content. Sample number given by 'n'. Mean ± standard deviation (SD) given as percentage by weight of TOC, ROC and TIC.*

	Cryoconite (ML) Mean ± SD	Cryoconite (AB) Mean ± SD	Cryoconite (VB) Mean ± SD	SGD-M Mean ± SD	SGD-P Mean ± SD
n	4	4	4	4	3
TOC (%)	2.2 ± 0.51	0.73 ± 0.44	1.7 ± 1.0	2.1 ± 0.27	18 ± 15
ROC (%)	0.46 ± 0.25	0.12 ± 0.078	0.75 ± 0.41	0.43 ± 0.15	0.44 ± 0.13
TIC (%)	0.018 ± 0.00	0.078 ± 0.12	3.3 ± 4.7[a]	0.013 ± 0.0050	0.015 ± 0.0071[b]

[a]Two samples were found to have a TIC content below LOD.
[b] One sample was found to have a TIC content below LOD.

The TIC content in cryoconite was consistently low in all samples across all locations with the exception of sample 25 from VB which was found to have a TIC content of 6.6 %, considerably higher than the mean TIC content of the remaining cryoconite samples at 0.040 %. If it is

assumed that total carbon (TC) is the sum of TOC, ROC and TIC, then TOC represents on average 73 % of the TC content.

The TOC, ROC, and TIC content in SGD-M was comparable to cryoconite, in particular cryoconite from ML (Table 5.5). The SGD-P samples were however found to contain significantly higher TOC content than all other samples (mean: 18 ± 15 %). The TIC and TOC levels in SGD-P were however comparable to cryoconite and SGD-M. The elevated TOC in SGD-P is expected given the high plant content observed.

5.1.5 Organic Pollutants in Cryoconite

Chemical analysis of seven indicator PCBs (congeners 28, 52, 101, 118, 138, 153, and 180) was performed by GC-MS with EI, in SIM mode. The objective was to identify and quantify PCBs in cryoconite sampled from ML, AB, and VB. All PCBs analysed were indistinguishable from background noise in all cryoconite samples. The quality control procedures have been reviewed to investigate the potential reasons for unquantifiable PCB results.

A number of polycyclic aromatic hydrocarbon (PAH) peaks were also detected in the cryoconite samples by GC-MS. The cryoconite samples were run using calibration standards containing both the seven PCB and 16 PAH external standards and fluorinated PCB and PAH internal standards, and thus identification of PAH peaks was possible. Peaks were identified for naphthalene (NAP), phenanthrene (PHEN), fluoranthene (FLTH), and pyrene (PYR), details of which are included in Tables B.10.1 and B.10.2 in the Appendix. However samples were not spiked with PAH internal standards, and no recovery or ME testing was performed. Thus the concentrations of PAHs detected in this study cannot be accurately quantified, as QC procedures were not in place to correct for losses during sample pre-treatment or the effect of the matrix for concentration determination.

5.1.5.1 Quality Control

PCB standard solutions were analysed using the 'Dutch Seven' indicator PCBs (ES), dissolved in ethyl acetate at concentrations of 0.5, 5, 10, 30, 50, and 100 ng mL^{-1} with fluorinated PCB internal standards 3'-F-PCB-28 and 5' – F-PCB-118 at concentrations of 50 ng mL^{-1}. Standard solutions were used to produce calibration curves to analyse for linearity in the method. All PCBs showed linearity within the range of 0.5 – 100 ng mL^{-1} and with an $R^2 > 0.98$ (coefficient

of determination, Table 5.6). The calibration curves for each PCB are presented in Fig. B.10.1 in the Appendix.

Measurements of PCB concentrations determined using the certified reference material 'PCB congeners in Soil' (Sigma Aldrich, SQC068 – 50 g, Lot#LRAA7458) were compared to reported values from Sigma Aldrich (Table 5.7) (234). The measured concentrations of PCBs in the CRM were on average just 50 % of the reported values. Loss of PCBs could have occurred through the extraction process. In addition, matrix effects may have led to signal suppression. Due to the age of the reference material (expiry 2017), the lower Mw PCBs such as PCB 28 and 52 may have been lost as a result of their volatility.

Table 5.6 *Calibration results from GC-MS analysis of seven target PCBs using standard solutions of 0.5, 5, 10, 30, 50, and 100 ng mL^{-1} 'Dutch Seven' ES dissolved in ethyl acetate.*

Analyte	Internal Standard	R^2	Slope (a)
PCB 28	3'-F-PCB-28	0.984	0.082
PCB 52	3'-F-PCB-28	0.985	0.054
PCB 101	5'-F-PCB-118	0.998	0.107
PCB 118	5'-F-PCB-118	0.997	0.153
PCB 138	5'-F-PCB-118	0.997	0.115
PCB 153	5'-F-PCB-118	0.998	0.108
PCB 180	5'-F-PCB-118	0.998	0.107

Table 5.7 *Quality assurance results for analysis of seven target PCBs by GC-MS. A comparison of reported concentrations of PCBs in certified reference material 'PCB Congeners in Soil' to measured values extracted using ASE and analysed by GC-MS (234). Mean measured concentrations of PCBs in 'PCBs congeners in soil' reference material reported in ng g^{-1}. The certified levels for the CRM are reported in µg kg^{-1} (both being equivalent), with a 95 % confidence interval (CI). In order to obtain reproducibility and determine accuracy, reference materials were analysed in triplicate. Accuracy was determined based on the measured concentration as a percentage of certified reported PCB concentrations.*

PCB	Measured	Reported (PCB Congeners in Soil)				
	Concentration ng g^{-1}	Concentration µg kg^{-1}	CI (95%)	SD	Acceptance Interval	Accuracy %
PCB 28	63.0	150	5.08	22.5	82.5 – 218	42
PCB 52	16.8	43.7	1.48	6.56	24.0 – 63.4	38
PCB 101	35.9	93.5	3.17	14.0	51.4 – 136	38
PCB 118	121	257	8.72	38.6	141 – 373	47
PCB 138	112	85.6	2.91	12.8	47.1 – 124	130
PCB 153	34.1	312	10.6	46.8	172 – 452	11
PCB 180	66.1	163	5.53	24.5	89.7 – 236	41

In order to assess the efficiency of the extraction method, the cryoconite matrix was spiked with PCB target analytes prior to extraction, and post extraction at two concentrations, 50 and 100 ng mL^{-1} to give analyte levels of 50 and 100 ng. Pre-extraction spiked samples were prepared

in triplicate and post extraction spiked samples were prepared in duplicate. The absolute and relative recoveries are presented in Table 5.8 and Fig. 5.5. Mean absolute recoveries were considered to be within an acceptable range, from 84 to 88 % for the low fortification (50 ng mL^{-1}) and 83 to 93 % for the high fortification (100 ng mL^{-1}). The relative recoveries were also considered to be within an acceptable range, from 91 to 95 % and 82 to 102 % for the low and high fortification levels respectively.

Table 5.8 *Absolute and relative recoveries (R_{abs} and R_{rel}) of PCB target analytes in cryoconite analysed by GC-MS. The 'Dutch Seven' target PCBs, were analysed at 50 and 100 ng mL^{-1} fortification levels. Mean recoveries and RSD are presented as a percentage (%).*

	ES (50 ng mL^{-1})				ES (100 ng mL^{-1})			
	R_{abs} (%)		R_{rel} (%)		R_{abs} (%)		R_{rel} (%)	
Analyte	Mean	RSD	Mean	RSD	Mean	RSD	Mean	RSD
PCB 28	83.5	5.39	92.5	3.31	82.9	8.17	82.4	5.40
PCB 52	83.9	4.19	93.1	4.42	84.3	8.19	83.9	5.45
PCB 101	84.4	4.97	91.0	7.05	85.8	8.91	93.9	2.28
PCB 118	84.9	6.28	91.3	5.66	88.8	8.55	97.3	2.52
PCB 138	88.3	5.68	95.1	6.24	93.0	8.22	102	1.97
PCB 153	84.7	7.01	91.1	4.36	90.2	8.32	98.8	3.31
PCB 180	87.5	8.39	94.1	5.67	91.2	8.36	99.9	3.17

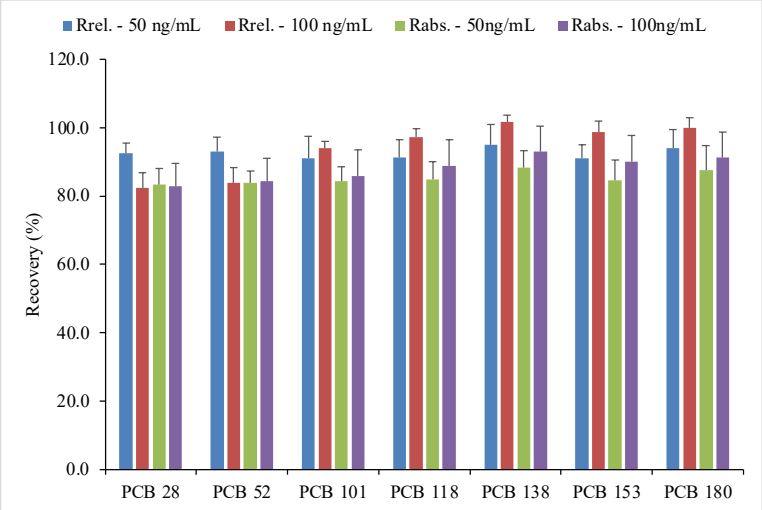

Figure 5.5 *Relative ($R_{rel.}$) and absolute ($R_{abs.}$) recoveries for seven PCB target analytes in cryoconite at 50 and 100 ng mL^{-1} fortification levels. Values were calculated using pre-extraction spiked matrix samples (n = 3) and post-extraction spiked samples (n=2). The error bars represent the standard deviation.*

5.1.5.2 Matrix Effects

The matrix effect was assessed through a comparison of response of the analyte in a post-extraction spiked sample to that of the response of the analyte in ethyl acetate solvent only. Matrix match (post-extraction spiked samples) were prepared in duplicate at each of the low

and high fortification levels (50 and 100 ng mL^{-1} respectively). The MEs are presented in Table 5.9 and Fig. 5.6. The matrix effect at both low and high fortification levels was significant in this study, at a mean value of - 51.8 % and - 57.5 % respectively.

Table 5.9 *Matrix effects of the seven PCB target analytes in cryoconite presented as percentages for mean, standard deviation (SD) and RSD for the two fortifications, 50 and 100 ng mL^{-1}.*

	Matrix Effect (50 ng mL^{-1})			Matrix Effect (100 ng mL^{-1})		
Analyte	Mean (%)	SD (%)	RSD (%)	Mean (%)	SD (%)	RSD (%)
PCB 28	-51.3	0.907	-1.77	-55.7	3.49	-6.27
PCB 52	-53.7	0.424	-0.789	-58.4	2.96	-5.07
PCB 101	-52.4	1.25	-2.39	-57.2	3.38	-5.92
PCB 118	-49.1	2.32	-4.73	-56.6	3.29	-5.81
PCB 138	-53.6	2.07	-3.87	-60.4	3.07	-5.08
PCB 153	-52.1	1.80	-3.45	-58.5	2.66	-4.55
PCB 180	-50.4	3.25	-6.44	-55.7	2.69	-4.83

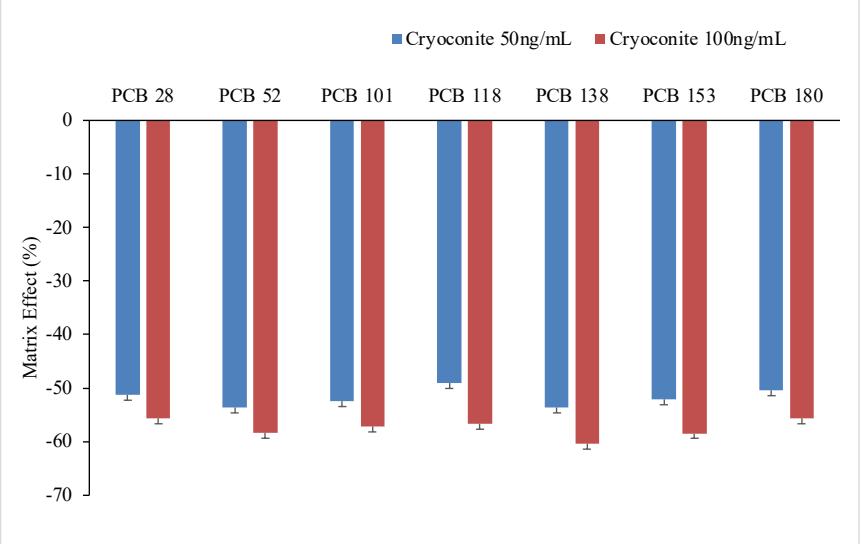

Figure 5.6 *Mean matrix effects of the seven PCB target analytes in cryoconite extracts at 50 and 100 ng mL^{-1} fortification levels as percentages. Error bars represent the standard deviation.*

5.2 Cryoconite Hole Water and Snow

5.2.1 General Observations of Cryoconite Hole Water and Snow

No observable suspended particulate matter was noted in CW. The temperature of the water in the CHs ranged from 0.0 ºC to 1.7 ºC with an mean temperature of 0.5 ºC which was within the range of those measured by Singh et al. (2013) from CHs located on ML (mean temperature range - 1.9 ºC to + 0.2 ºC) (10). The conductivity of CW ranged from 1.2 to 36.7 µS cm^{-1} with

a mean conductivity of 4.4 μS cm^{-1}. A full list of temperature and conductivity measurements for each cryoconite hole is presented in Table B.1.1 in the Appendix.

Sampling took place late in the summer season and consequently the majority of snow on the surface of the three glaciers had melted at the lower altitudes, leaving only small patches of old snow remaining. Given the scarcity of snow in the sampling areas, it was not possible to obtain an altitude gradient for snow sampling on both AB and VB, and samples were collected from just one GPS location on both AB and VB. It was however possible to locate a number of patches of snow on ML and samples were collected from five GPS locations.

5.2.2 Elemental Composition of Cryoconite Hole Water and Snow

A total of 62 elements and seven anions were analysed by ICP-MS and IC respectively in CW and snow samples. A visual representation, provided in Fig. 5.7, presents the percentage composition of elements detected in CW and snow, categorised by locations: ML, AB, and VB, grouped into the major elements, trace elements, heavy metals and metalloids, and REE. Eleven elements and three anions were selected for further statistical analysis. These elements included the major elements and anions in water: Na, Mg, Ca, Cl, chloride (Cl^-), and sulphate (SO_4^{2-}) (6, 74). Trace elements: As, Cd, Cr, and Pb were selected due to their hazardous nature and anthropogenic source (Hg was below detection in all samples) (1, 6). Zinc was selected as it has both natural and anthropogenic sources and is subject to long range atmospheric transport (1). Finally Fe and Al were included in water and snow analysis due to their influence from the parent rock (Table 4.2) and for comparison with cryoconite sediment samples. Nitrate was also detected.

For QC, method blanks and solvent (MilliQ water) blanks were analysed by ICP-MS. Of the elements selected for further analysis, Pb and As concentrations in the snow and water were below the LOD in all six method blanks, and no blank correction was required. The average concentrations of elements Ca, Mg, and Na in the method blanks was less than 5 % of the mean elemental concentration in CW and snow samples, hence no blank correction was performed. Zinc and Cr concentrations in the blanks were at levels above 5 % of their respective mean elemental concentrations in water and snow, thus blank correction was performed. Limits of detection were calculated based on $3\sigma/S$, where 'σ' is the standard deviation of the response, and 'S' is the slope of the calibration curve. The LODs were calculated as follows: Na = 162 ng L^{-1}, Cl = 94.6 μg L^{-1}, Ca = 25.3 ng L^{-1}, Mg = 0.350 ng L^{-1}, Al = 2.47 ng L^{-1}, Fe = 2.34 ng L^{-}

^{1}, As = 2.81 ng L^{-1}, Cd = 0.00 ng L^{-1}, Cr = 4.67 ng L^{-1}, Pb = 3.23 ng L^{-1}, and Zn = 5.01 ng L^{-1}. All samples contained concentrations of Na, Ca, Mg, Al, Fe, and Zn above the LOD. Chlorine concentrations were < LOD in 61 % of CW and 16 % of snow samples. Lead concentrations were below the LOD in 46 % and 25 % of CW and snow samples respectively. Chromium concentrations were below detection in 68 % and 52 % of CW and snow samples respectively, whereas just 8 % of snow samples contained Cd concentrations below LOD following blank correction. Finally, As concentrations were below detection in 11 % of CW and 24 % of snow samples.

The proportions of the major elements detected in snow and CW showed significant variation between sample types and locations (Fig. 5.7). On the whole, the major elements in snow were dominated by Na and Cl. In contrast, cryoconite hole water samples were dominated by Ca, with variations observed in the proportions of sulphur (S), Mg, and Cl across the locations. Snow from VB contained a higher proportion of Ca and Si compared to the other locations, this was also the case for CW, although to a lesser extent for Si. Sulphur content in CW was more dominant in ML compared to Ca. A large variability was also observed in the trace element composition both between sample types and locations. In particular, Al, Fe, Mn, and strontium (Sr) fluctuated in CW between locations. The proportions of Fe and Mn in snow were relatively consistent, with larger variations observed in Zn and Al between glaciers. Observable differences were also noted in the proportions of heavy metals and metalloids especially with respect to Pb and Cr. The proportion of Pb was higher in CW from ML in comparison to AB and VB which showed relatively similar heavy metal and metalloid proportions. In contrast, in snow, Pb was present in higher proportions from AB compared to the other two locations. Chromium appeared to be very dominant in snow from VB. Finally the proportions of the REE were consistent across the sample types and locations with only minor fluctuations observed, consistent with the findings from the cryoconite particulate matter.

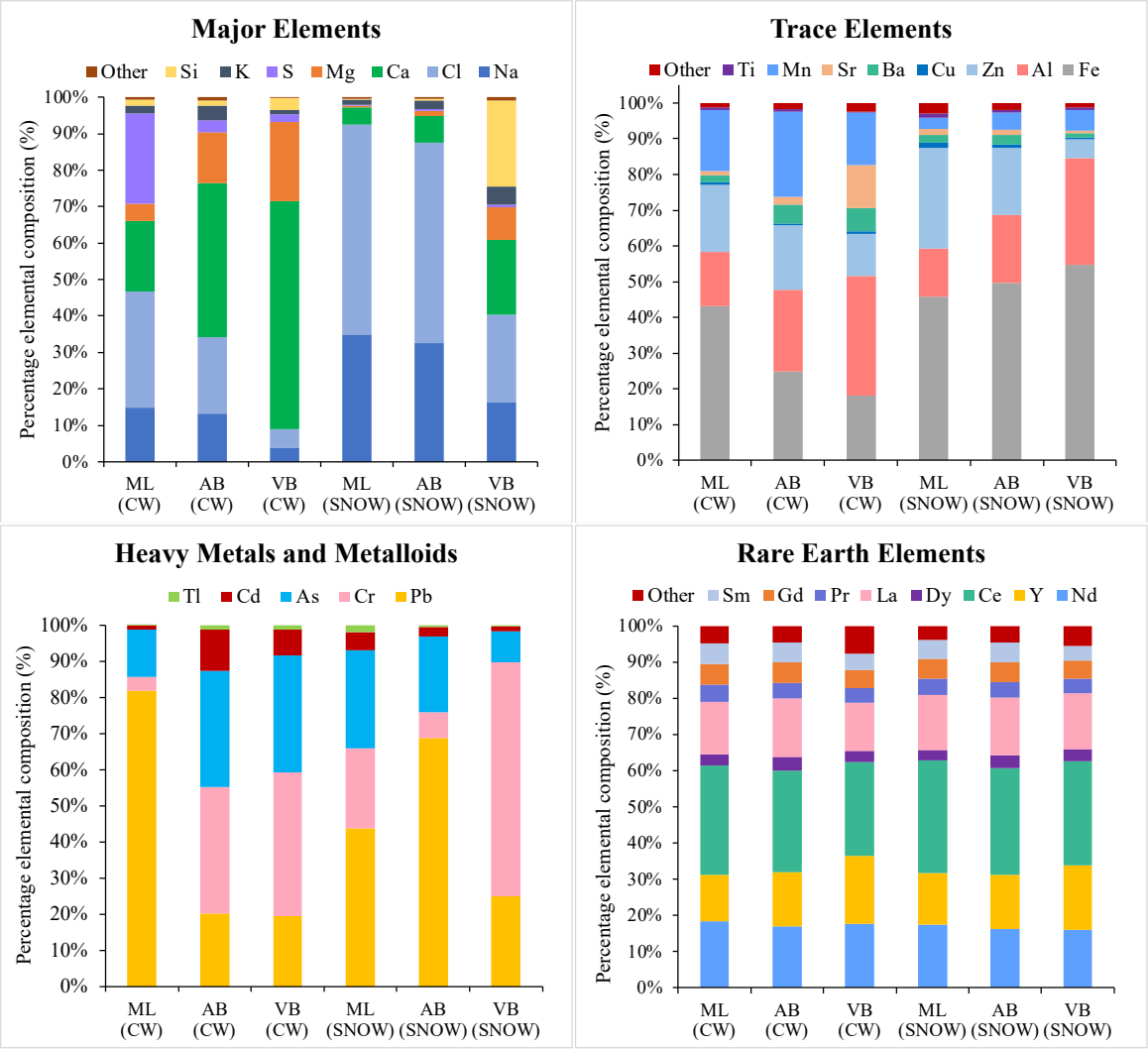

Figure 5.7 *Percentage elemental composition of cryoconite hole water, and snow, categorised by major elements, trace elements, heavy metals and metalloids, and rare earth elements. Percentage composition calculated based on mean concentrations of each element. Cryoconite hole water (CW) and snow split by location where ML = Midtre Lovénbreen, AB = Austre Brøggerbreen and VB = Vestre Brøggerbreen.*

Seven elements contributed 98.6 % and 98.8 % to the total composition (of the 62 elements analysed) in CW and snow samples respectively. The pie charts in Fig. 5.8 present the overall proportions of the elements detected in both CW and snow, and show clear differences in composition. In CW, Ca was the most dominant element and represented 56.4 % of the mean total elemental composition, but in contrast contributed just 8.2 % to the composition of snow. The next dominant elements in CW were Mg and Cl, at a 19.2 % and 9.1 % contribution respectively. Sodium represented just 5.8 % of CW mean composition, but was the second most dominating element in snow at 30.7 %, with Cl being the most dominant at 50.6 % of the mean total elemental composition. Sulphur, Si, and K contributed 3.9 %, 2.9 %, and 1.6 % to the composition of CW respectively. Similar proportions of Si and K were also observed in snow

(4.3 % and 2.3 % respectively), but S was less dominant at only 0.5 % of the mean total elemental composition. Magnesium was also detected at lower mean concentrations in snow and represented just 2.2 % of the total elemental composition.

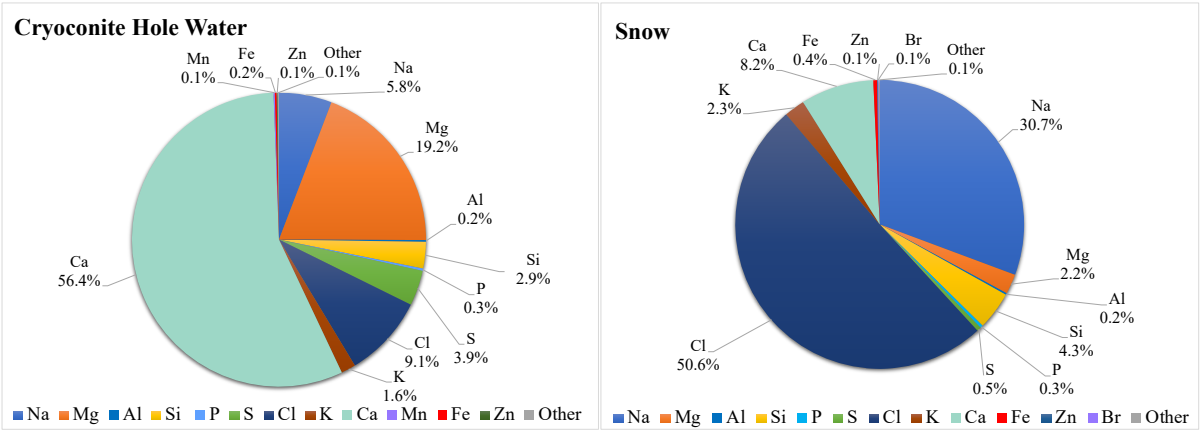

Figure 5.8 *Pie charts representing the major elemental contributions to cryoconite hole water and snow from 62 elements analysed by ICP-MS.*

A summary of the concentrations of the elements in snow and CW is presented in Table 5.10, the full detail of which is presented in Tables B.9.1 and B.9.2 in the Appendix. The mean elemental concentrations in snow samples followed in descending order: Cl>Na>>Ca>>Mg>>Fe>Al>Zn>>Cr>Pb>As>>Cd, which is contrast to the elements detected in CW: Ca>>Mg>Cl>Na>>Fe>Al>Zn>>Pb>Cr>As>>Cd. In the trace elements, the concentrations of Al, Fe, and Zn in CW were two orders of magnitude higher than Cr and Pb, which were an order of magnitude more concentrated than Cd and As. Differences in the mean elemental concentrations between CW and snow were analysed using Mann-Whitney U test (where data was not normally distributed) and the t-test (for normal distribution). Significance for all tests was set at $p < 0.05$.

Table 5.10 *Concentrations of eleven selected elements determined in cryoconite hole water and snow collected from three glaciers located near Ny-Ålesund. Concentrations are presented as mean ± standard deviation (SD) and include the range between minimum to maximum concentrations. The 'n' represents the total number of samples. Concentrations displayed in µg L^{-1} for all elements with the exception of As and Cd which are reported in ng L^{-1}. Samples were analysed by ICP-MS. Snow and cryoconite hole water with the same letters, represented by [a] and [b], were not significantly different from each other (Mann-Whitney U test and t-test, $p < 0.05$).*

Element	Cryoconite Hole Water (n = 28)		Snow (n = 25)		p
	Mean ± SD	Range	Mean ± SD	Range	
Na	52.8 ± 33.6[a]	3.03 – 141	254 ± 132[b]	22.1 – 443	<0.00001
Cl	82.4 ± 49.8[a]	< LOD – 211	419 ± 225[b]	< LOD - 759	<0.00001
Ca	513 ± 1100[a]	29.1 – 5530	67.8 ± 41.7[a]	17.3 – 205	0.123
Mg	175 ± 355[a]	3.20 – 1700	18.5 ± 23.8[b]	1.75 – 93.4	0.0114
Al	1.75 ± 1.47[a]	0.315 – 7.71	1.56 ± 1.54[a]	0.03 – 5.56	0.147
Fe	1.83 ± 0.647[a]	0.756 – 3.13	3.38 ± 2.89[b]	0.436 – 13.3	0.0318
As[**]	8.21 ± 5.28[a]	< LOD – 21.3	5.69 ± 3.51[b]	1.41 – 12.8	0.0268[*]
Cd[**]	1.68 ± 1.47[a]	0.277 – 5.46	0.867 ± 0.611[a]	< LOD – 2.13	0.0583
Cr	0.0106 ± 0.0167[a]	< LOD – 0.0774	0.0248 ± 0.0477[a]	< LOD – 0.205	0.234
Pb	0.0179 ± 0.0282[a]	< LOD – 0.106	0.0163 ± 0.0124[a]	< LOD – 0.0456	0.264
Zn	1.09 ± 0.474[a]	0.185 – 2.24	0.855 ± 0.613[b]	0.101 – 2.35	0.0450

[*] T-test used to determine significance
[**] Reported in ng L^{-1}

Significant differences were observed between snow and water samples for elements: Na, Cl, Mg, Fe, As, and Zn as presented in Table 5.10. No significant differences were identified in the mean concentrations of three of the toxic elements in snow and CW; Cd, Cr, and Pb with p values of 0.0583, 0.234, and 0.264 respectively. Cryoconite hole water samples contained on average significantly higher Zn concentrations than snow with mean concentrations of 1.09 µg L^{-1} and 0.855 µg L^{-1} in CW and snow respectively ($p = 0.0450$, Mann-Whitney U test). Arsenic was also found at significantly higher concentrations in CW than snow ($p = 0.0268$, t-test). For those elements with a rock influence, Al concentrations were not significantly different between sample types. However, Fe levels were significantly higher in snow than CW with mean concentrations of 3.38 µg L^{-1} and 1.83 µg L^{-1} respectively ($p = 0.0318$, Mann-Whitney U test). For those elements with a large marine influence, Na and Cl were significantly higher in snow than CW with concentrations of 254 ± 132 µg L^{-1} and 419 ± 225 µg L^{-1} in snow, and 52.8 ± 33.6 µg L^{-1} and 82.4 ± 49.8 µg L^{-1} in CW respectively. The trend in Mg concentrations were found to be the reverse, with higher concentrations in CW compared to snow.

A detailed list of all anions detected in individual samples is presented in Tables B.8.1 and B.8.2 in the Appendix along with a sample of ion chromatograms (Fig. B.8.1 – B.8.7 in the Appendix). Peaks in the ion chromatograms were only observed for three of the seven anions; Cl^-, SO_4^{2-}, and NO_3^-. The LOD for each of the three anions was calculated using the calibration

curves: Cl^- = 0.456 mg L^{-1}, SO_4^{2-} = 1.70 mg L^{-1}, and NO_3^- = 0.827 mg L^{-1}. In comparison to snow samples where NO_3^- peaks were detected in 14 of the 24 samples, NO_3^- was detected in just one CW sample (all of which were at concentrations below the calibration range and LOD). In contrast, SO_4^{2-} peaks were detected in 27 of 28 CW samples but in only nine of 24 snow samples. In all cases, SO_4^{2-} was however detected at levels below the LOD. However 20 of 27 CW samples showed SO_4^{2-} concentrations within the calibration range, although SO_4^{2-} concentrations were below the calibration range in all snow samples. Chloride peaks were observed in 26 of 28 CW samples, but concentrations were below the LOD in all samples, and within the calibration range in just one. In contrast, Cl^- peaks were detected in all 24 snow samples on the ion chromatogram, with concentrations within the calibration range for 19 of 24 samples, but only above the LOD in seven samples, four of which were from snow sampled from ML.

5.3 Cryoconite Holes

5.3.1 Comparison of the Elemental Composition of Cryoconite and Cryoconite Hole Water

The elemental composition of the cryoconite was compared to that of the overlying water, presented as pie charts in Fig. 5.9 and 5.10. Large differences were observed in the proportions of the major elements between the two matrices. Whilst Fe and Al represented the majority of the composition of the cryoconite sediment (30 % and 33 % respectively), over half of the elemental composition of the hole water was from Ca (56 %). In comparison, both Fe and Al contributed just 0.2 % of the elemental composition of CW, and Ca represented just 7.6 % of the elemental composition of the cryoconite particulate matter. The proportion of K was also higher in cryoconite than the overlying water at 12.1 % and 1.6 % respectively. The contribution by Mg was found to be relatively similar between the two matrices at 11.6 % and 19.2 % in cryoconite and water respectively. With respect to those elements with a sea spray and snow melt influence, Na and Cl were found at 5.8 % and 9.1 % respectively in cryoconite hole water, but only Na was detectable in the sediment, representing just 0.6 % of the mean total elemental composition of the cryoconite particulate matter.

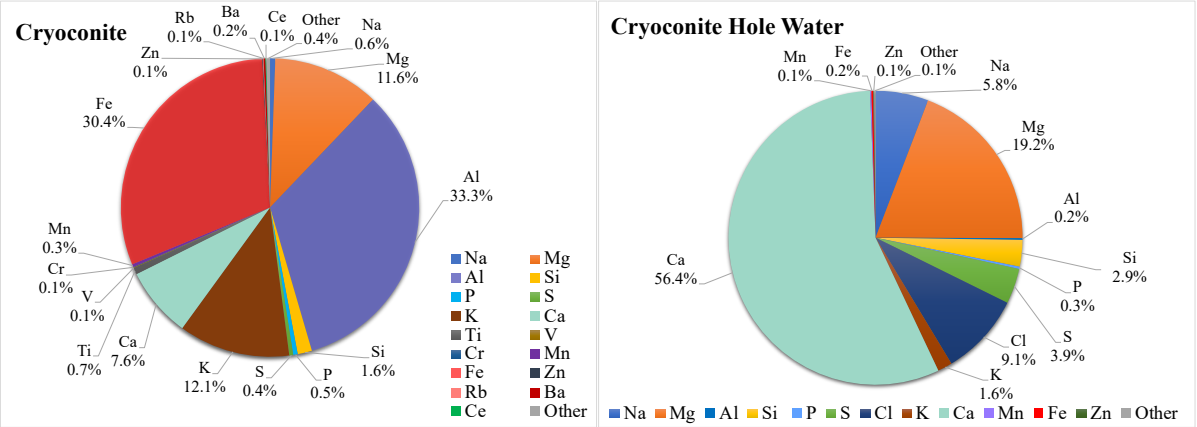

Figure 5.9 *Pie charts representing major elemental contributions to cryoconite and cryoconite hole water.*

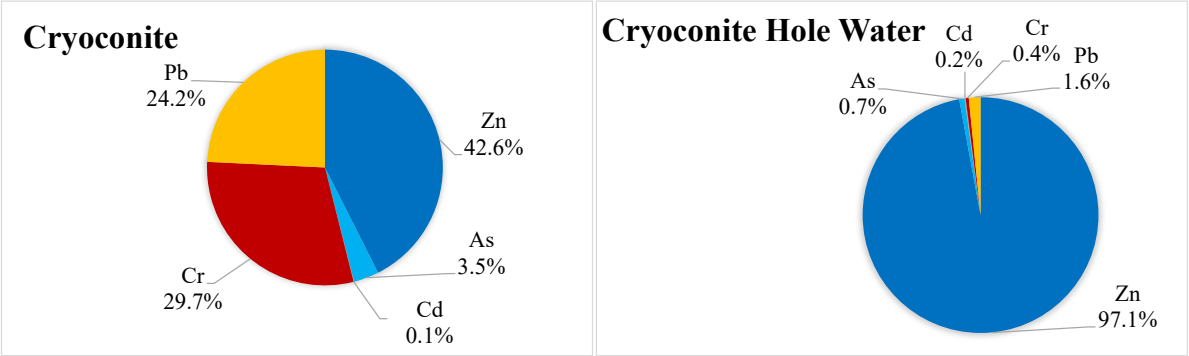

Figure 5.10 *Pie charts representing the percentage composition of the heavy metals and metalloids in cryoconite and cryoconite hole water.*

Large differences in the proportion of hazardous elements As, Cd, Cr, Pb, and Zn detected in cryoconite and the overlying water was observed (Fig. 5.10). Whilst Zn contributed 43 % to the heavy metals and metalloids in cryoconite, it represented 97 % of the composition in water. Chromium and Pb were on a proportional basis, significantly lower in CW in comparison to the sediment, at just 0.4 % and 1.6 % respectively. Arsenic made up a slightly higher proportion of the hazardous elements in cryoconite compared to the water at 3.5 % compared to 0.7 %. The proportion of Cd however was higher in CW compared to the underlying sediment, although still at low levels in both.

5.3.2 Variation in Elemental Composition of Cryoconite Holes Between Glacier Locations

In order to determine the extent to which elemental concentrations in cryoconite differ between locations, comparisons were performed between the three glaciers: ML, AB, and VB. A total

of eight cryoconite holes were sampled from ML, ten from AB, and ten from VB. The mean concentration of the nine selected elements from cryoconite particulate matter at each location is presented in Table 5.11. The mean concentrations of elements in cryoconite from VB are presented both including and excluding sample 25. The mean concentrations of the nine selected elements in CW, excluding Na and Cl, which are more dominant in the snow than CW, are presented in Table 5.12. Statistical tools were used to identify the presence of a statistically significant difference in the mean elemental concentrations between the three glacier locations. Significance was determined using the one-way ANOVA with Tukey HSD post hoc test or Kruskal-Wallis followed by Dunn's post hoc test with Bonferroni correction depending on the normality of the data. Normality was determined using the Shapiro-Wilk test. Significance for all tests was set at $p < 0.05$.

In cryoconite, the mean concentrations of all nine elements sampled showed a statistically significant difference between locations ($p < 0.001$ in all cases with the exception of Cr where $p = 0.009$ and Ca where $p = 0.01$, Kruskal-Wallis test). The mean concentrations of all elements in CW with the exception of Zn also showed statistically significant differences between the locations. Box and whisker plots for all elements excluding Ca and Mg are presented in Fig. 5.11. Box and whisker plots for Ca and Mg in cryoconite are presented in Fig. B.5.1 and B.5.2 in the Appendix.

Table 5.11 *Elemental concentrations determined in cryoconite collected from Midtre Lovénbreen (ML), Austre Brøggerbreen (AB), and Vestre Brøggerbreen (VB) in Ny-Ålesund, Svalbard. Mean concentration ± standard deviation (SD) reported in μg g^{-1} for elements Al, Fe, Ca, Mg, As, Cd, Cr, Pb, and Zn. Mean concentrations with the same letters are not statistically significantly different (Kruskal-Wallis and Dunn's post hoc test with Bonferroni correction; and one-way ANOVA with Tukey HSD post hoc test (p < 0.05)).*

Element	ML Mean ± SD μg g^{-1}	AB Mean ± SD μg g^{-1}	VB Mean ± SD μg g^{-1}	VB* Mean ± SD μg g^{-1}
Al	41000 ± 1690^{a}	45200 ± 4050^{b}	34900 ± 2090^{c}	35200 ± 2050
Fe	39800 ± 1310^{a}	43500 ± 2470^{a}	27500 ± 4870^{b}	29000 ± 1200
Ca	2600 ± 146^{a}	5270 ± 2190^{b}	18500 ± 46500^{a}	3800 ± 3070
Mg	13000 ± 366^{ab}	15200 ± 1490^{b}	13600 ± 12500^{a}	9630 ± 1270
As	9.06 ± 1.45^{a}	4.55 ± 1.44^{b}	8.19 ± 0.941^{a}	8.45 ± 0.524
Cd	0.0583 ± 0.0189^{b}	0.110 ± 0.0429^{a}	0.177 ± 0.128^{a}	0.138 ± 0.0318
Cr	57.3 ± 2.55^{a}	61.6 ± 3.30^{ab}	63.9 ± 7.75^{b}	61.7 ± 3.38
Pb	66.9 ± 15.3^{a}	32.3 ± 4.46^{b}	54.1 ± 32.4^{a}	59.2 ± 29.9
Zn	93.7 ± 5.93^{a}	94.5 ± 3.54^{a}	76.3 ± 6.52^{b}	78.0 ± 3.66

* Excluding sample 25

Table 5.12 *Elemental concentrations determined in cryoconite hole water collected from Midtre Lovénbreen (ML), Austre Brøggerbreen (AB), and Vestre Brøggerbreen (VB) in Ny-Ålesund, Svalbard. Mean concentration ± standard deviation (SD) reported in μg L^{-1} for elements: Al, Fe, Ca, Mg, Cr, Pb, and Zn. Elements Cd and As are reported in ng L^{-1}. Elemental concentrations below the LOD were assigned a value of 0.5 x LOD to determine mean values. Mean concentrations with the same letters are not statistically significantly different (Kruskal-Wallis and Dunn's post hoc test with Bonferroni correction; and one-way ANOVA with Tukey HSD post hoc test (p < 0.05)).*

Element	ML Mean ± SD μg L^{-1}	AB Mean ± SD μg L^{-1}	VB Mean ± SD μg L^{-1}	VB* Mean ± SD μg L^{-1}
Al	0.839 ± 0.329^{a}	1.65 ± 0.888^{b}	2.58 ± 2.02^{b}	2.01 ± 0.959
Fe	2.40 ± 0.663^{a}	1.79 ± 0.564^{ab}	1.40 ± 0.312^{b}	1.42 ± 0.323
Ca	41.2 ± 8.86^{a}	152 ± 196^{ab}	1250 ± 1630^{b}	776 ± 652
Mg	9.97 ± 6.17^{a}	50.2 ± 82.5^{a}	431 ± 508^{b}	290 ± 258
As**	7.91 ± 4.14^{a}	3.58 ± 1.85^{b}	13.1 ± 4.10^{c}	12.2 ± 3.08
Cd**	0.666 ± 0.274^{a}	1.28 ± 1.33^{a}	2.90 ± 1.37^{b}	2.62 ± 1.10
Cr	$<LOD^{a}$	0.00947 ± 0.0122^{ab}	0.0185 ± 0.0235^{b}	0.0119 ± 0.0118
Pb	0.0500 ± 0.0359^{a}	0.00224 ± 0.00140^{b}	0.00788 ± 0.00905^{b}	0.00858 ± 0.00932
Zn	1.04 ± 0.383^{a}	1.31 ± 0.481^{a}	0.908 ± 0.489^{a}	0.988 ± 0.443

* Excluding sample 25
** Reported in ng L^{-1}

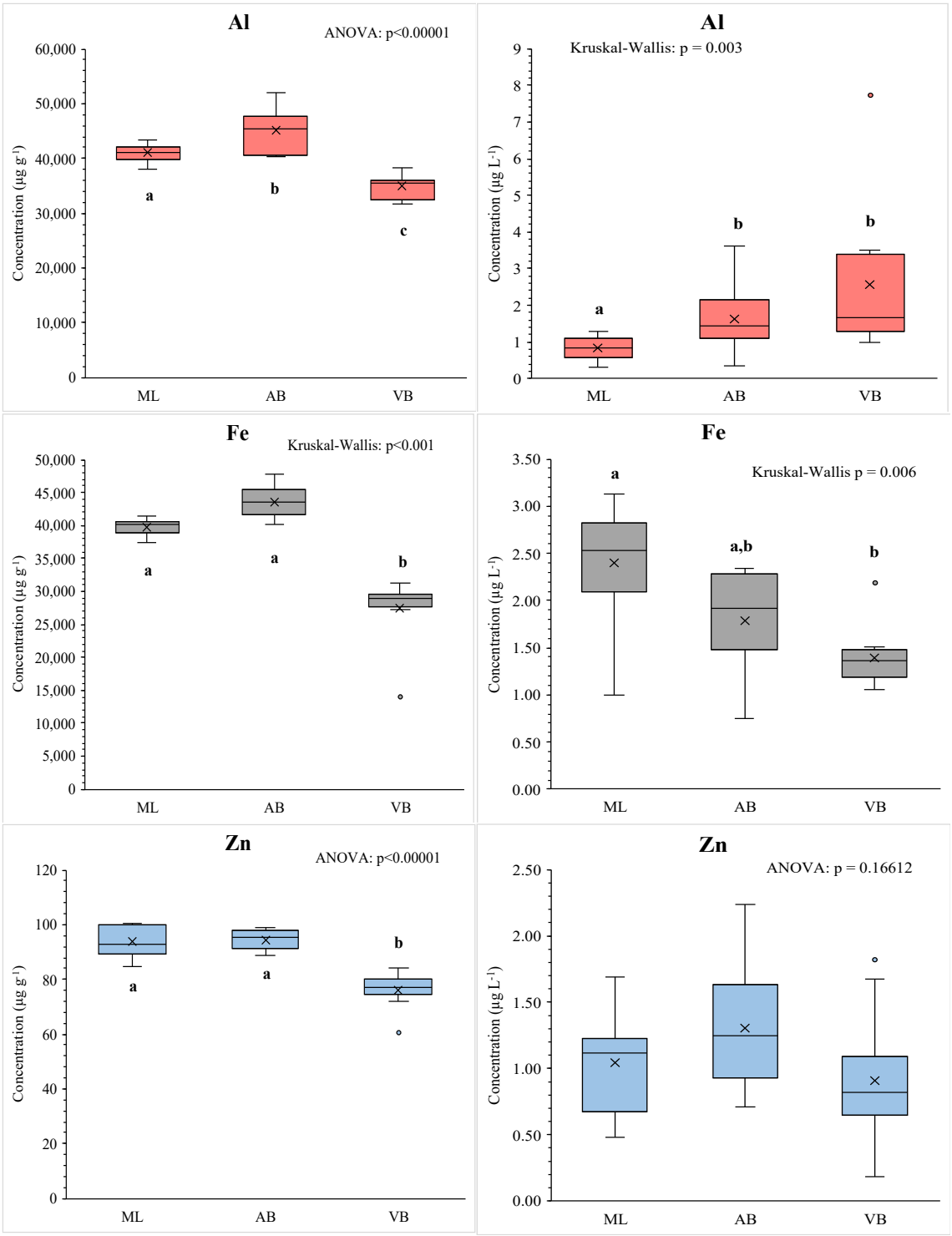

Figure 5.11 *Comparisons in the concentrations of selected elements determined in cryoconite and cryoconite hole water. Box and whisker plots presenting for elements Al, Fe, As, Pb, Cd, Cr, and Zn determined in cryoconite (left) and cryoconite hole water (right) collected from three glaciers near Ny-Ålesund, Svalbard. The three glaciers are represented by ML = Midtre Lovénbreen, AB = Austre Brøggerbreen, and VB = Vestre Brøggerbreen. Concentrations of all elements in cryoconite are in µg g^{-1} and concentrations of all elements in cryoconite hole water are in µg L^{-1}. Study locations with the same letter were not significantly different (one-way ANOVA and Tukey's HSD post hoc test, $p < 0.05$; and Kruskal-Wallis and Dunn's post hoc test with Bonferroni correction, $p < 0.05$). The mean is represented by the 'x', the median by the line within the box, and the interquartile range by the box itself. Outliers are identified as circular coloured markers.*

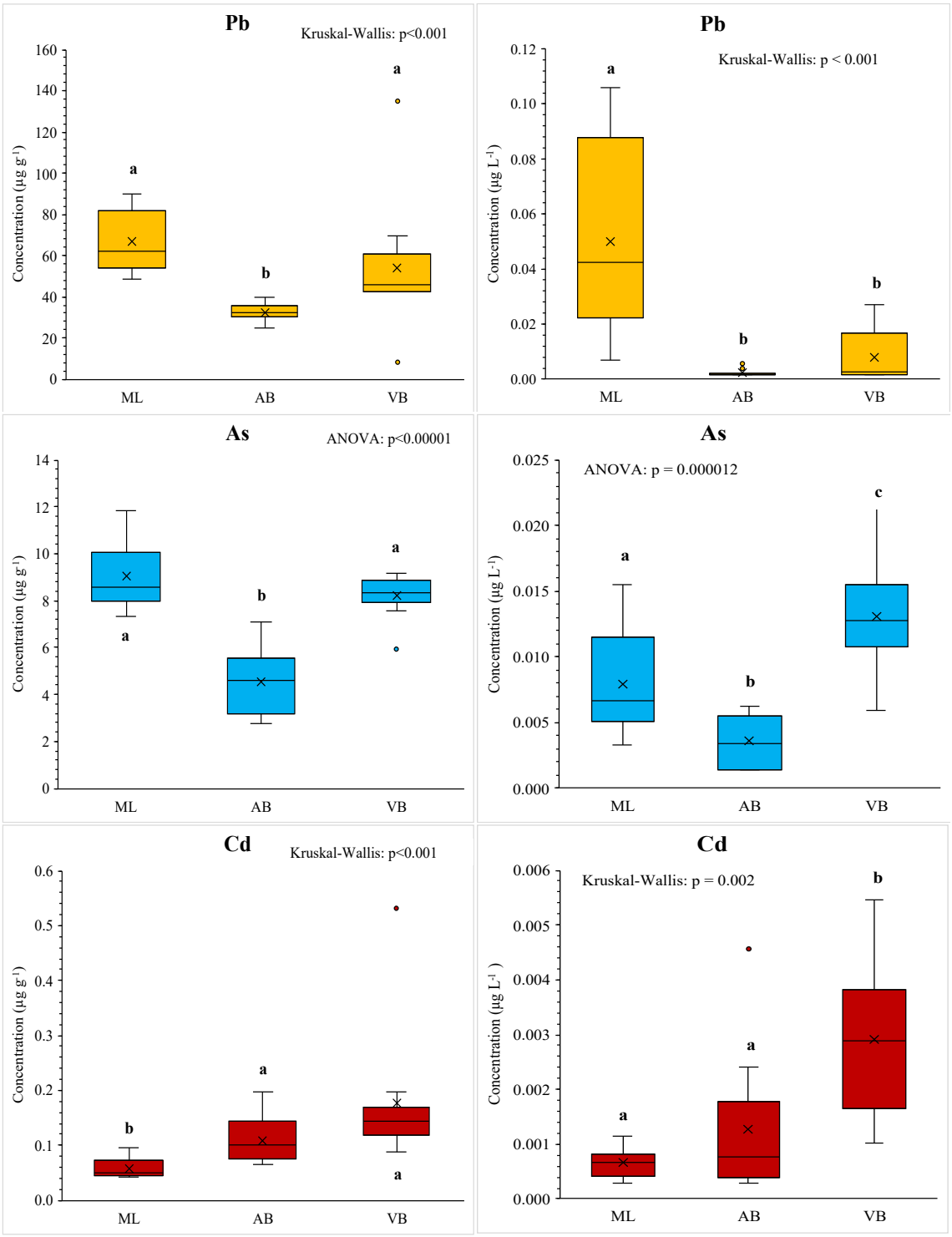

Figure 5.11 continued: Box and whisker plots presenting comparisons in the concentrations of Al, Fe, As, Pb, Cd, Cr, and Zn determined in cryoconite (left) and cryoconite hole water (right) collected from three glaciers near Ny-Ålesund, Svalbard.

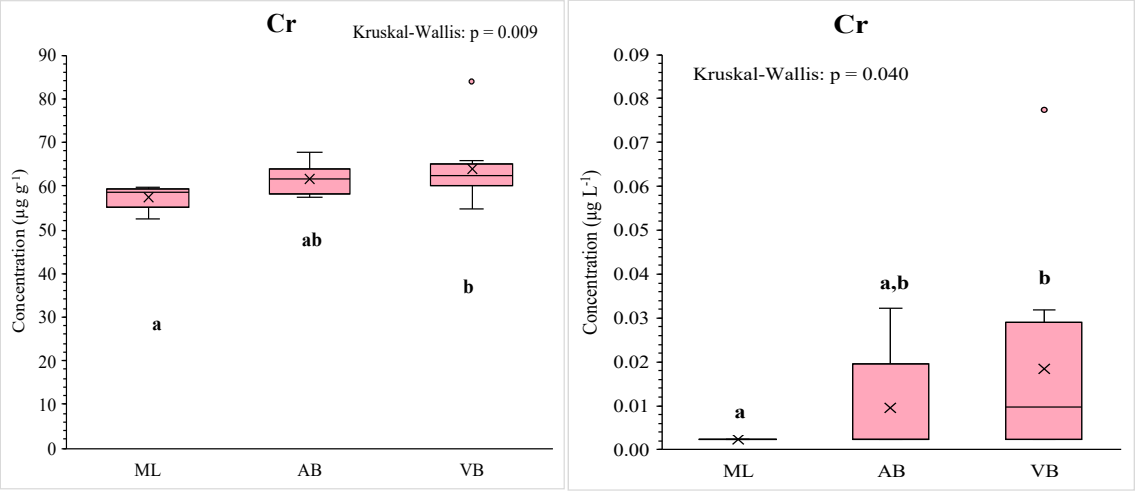

Figure 5.11 continued: Box and whisker plots presenting comparisons in the concentrations of Al, Fe, As, Pb, Cd, Cr, and Zn determined in cryoconite (left) and cryoconite hole water (right) collected from three glaciers near Ny-Ålesund, Svalbard.

Trends in elemental concentrations across the three glaciers were observed in cryoconite particulate matter, although this was not the case for CW. For example, Fe and Zn appeared to follow a similar trend, with cryoconite from VB showing statistically significantly lower concentrations of Fe and Zn compared to ML and AB. Lead and As also appeared to follow the same trend in concentrations across locations, with cryoconite from AB showing statistically significantly lower concentrations of Pb and As compared to ML and VB. For both Cd and Cr, there was no significant difference between AB and VB ($p = 0.384$ and $p = 1.00$ respectively, Kruskal-Wallis and Dunn's post hoc test with Bonferroni correction). A significant difference was however noted between ML and VB, with cryoconite from ML containing on average significantly lower concentrations of Cd and Cr compared to those from VB ($p = 0.000$ and $p = 0.008$ respectively, Kruskal-Wallis and Dunn's post hoc test with Bonferroni correction). The mean concentration of Al was found to be statistically significantly different across all locations, with cryoconite from AB containing the highest, and cryoconite from VB, the lowest concentrations of Al.

Similarities were also observed in trends in elemental concentrations in cryoconite and CW between locations. For example, concentrations of Cd were lower in ML compared to VB in both CW and sediment. Concentrations of As and Pb were also lower in both cryoconite and CW from AB compared to ML. Concentrations of Fe were higher in both cryoconite and the overlying water from ML compared to VB. However, a trend between locations was not observed in the concentrations of Al in cryoconite and CW.

The concentrations of Cr and Pb were low in CW, and in many cases below the LOD. Chromium was not detected in any CW samples from ML, and only in 3 samples from AB, and 6 from VB. No significant difference was identified in Cr concentrations between AB and VB ($p = 0.639$, Kruskal-Wallis and Dunn's post hoc test with Bonferroni correction). Lead was detected in all 8 CW samples from ML, but only in 2 samples from AB, and 5 from VB. A significant difference was detected in Pb concentrations in CW between ML and VB ($p = 0.00700$, Kruskal-Wallis and Dunn's post hoc test with Bonferroni correction), but no significant difference between AB and VB ($p = 0.756$, Kruskal-Wallis and Dunn's post hoc test with Bonferroni correction).

As a consequence of the similarities in trends observed in elemental concentrations in cryoconite between locations, a non-parametric Spearman correlation test was performed (due to non-normal distribution of elements Fe, Ca, Mg, Pb, Cd and Cr) in order to identify significant correlations between elements in cryoconite. The results of the non-parametric Spearman correlation test are presented in Table 5.13. The results exclude sample 25 as it was found to have large differences in composition, and may therefore distort the results of the test. The results of the non-parametric Spearman correlation for all 28 samples for reference is presented in Table B.6.1 in the Appendix.

Iron, Al, Mg, and Zn demonstrated a strong statistically significant correlation with each other. Iron and Mg were also both significantly correlated to Ca. Arsenic was found to be strongly and positively correlated with Pb ($R^2 = 0.932$, $p < 0.001$), showing the strongest correlation between all elements. Both Cd and Cr correlated with each other ($R^2 = 0.557$, $p = 0.003$), and were not strongly or positively correlated with any of the other selected elements.

The results of principal component analysis for cryoconite and supraglacial debris are presented in Fig. 5.12 by location and elemental concentration for PC-1 and PC-2 which represent 44 % and 21 % of the variance respectively. Clear clusters were observed in the score plot between the three locations, with the elemental composition of cryoconite and SGD from AB being the most similar to samples from ML than VB. The loadings plot showed strong associations between antimony (Sb) and As, as well as between those elements dominating in minerals such as Fe, Al, and K. Cadmium did not appear to be associated with any of the other elements. Cryoconite and SGD from AB appeared to be associated with the rock elements, whereas VB appeared to be more associated with Pb and selenium (Se).

Table 5.13 *Non-parametric Spearman correlation between concentrations of elements determined in cryoconite by ICP-MS.The correlation coefficient is represented by R^2. Statistically significant correlations with a p value < 0.05 are represented by * and statistically significant correlations with a p value < 0.01 are represented by **. Sample size of n = 27(excludes sample 25) in all correlation tests. Statistically significant correlations are in bold.*

		Al	Fe	Ca	Mg	Zn	Pb	As	Cd	Cr
Al	R^2									
	p									
Fe	R^2	**0.789****								
	p	<0.001								
Ca	R^2	0.351	**0.546****							
	p	0.073	0.003							
Mg	R^2	**0.788****	**0.912****	**0.672****						
	p	<0.001	<0.001	<0.001						
Zn	R^2	**0.664****	**0.792****	0.329	**0.707****					
	p	<0.001	<0.001	0.094	<0.001					
Pb	R^2	**-0.403***	**-0.499****	**-0.733****	**-0.627****	-0.087				
	p	0.037	0.008	<0.001	<0.001	0.665				
As	R^2	**-0.402***	**-0.548****	**-0.667****	**-0.678****	-0.123	**0.932****			
	p	0.037	0.003	<0.001	<0.001	0.542	<0.001			
Cd	R^2	-0.180	-0.324	0.261	-0.162	**-0.430***	**-0.413***	-0.199		
	p	0.369	0.099	0.188	0.420	0.025	0.032	0.320		
Cr	R^2	0.193	-0.056	-0.032	-0.093	-0.229	-0.179	0.004	**0.557****	
	p	0.335	0.783	0.873	0.645	0.251	0.370	0.986	0.003	

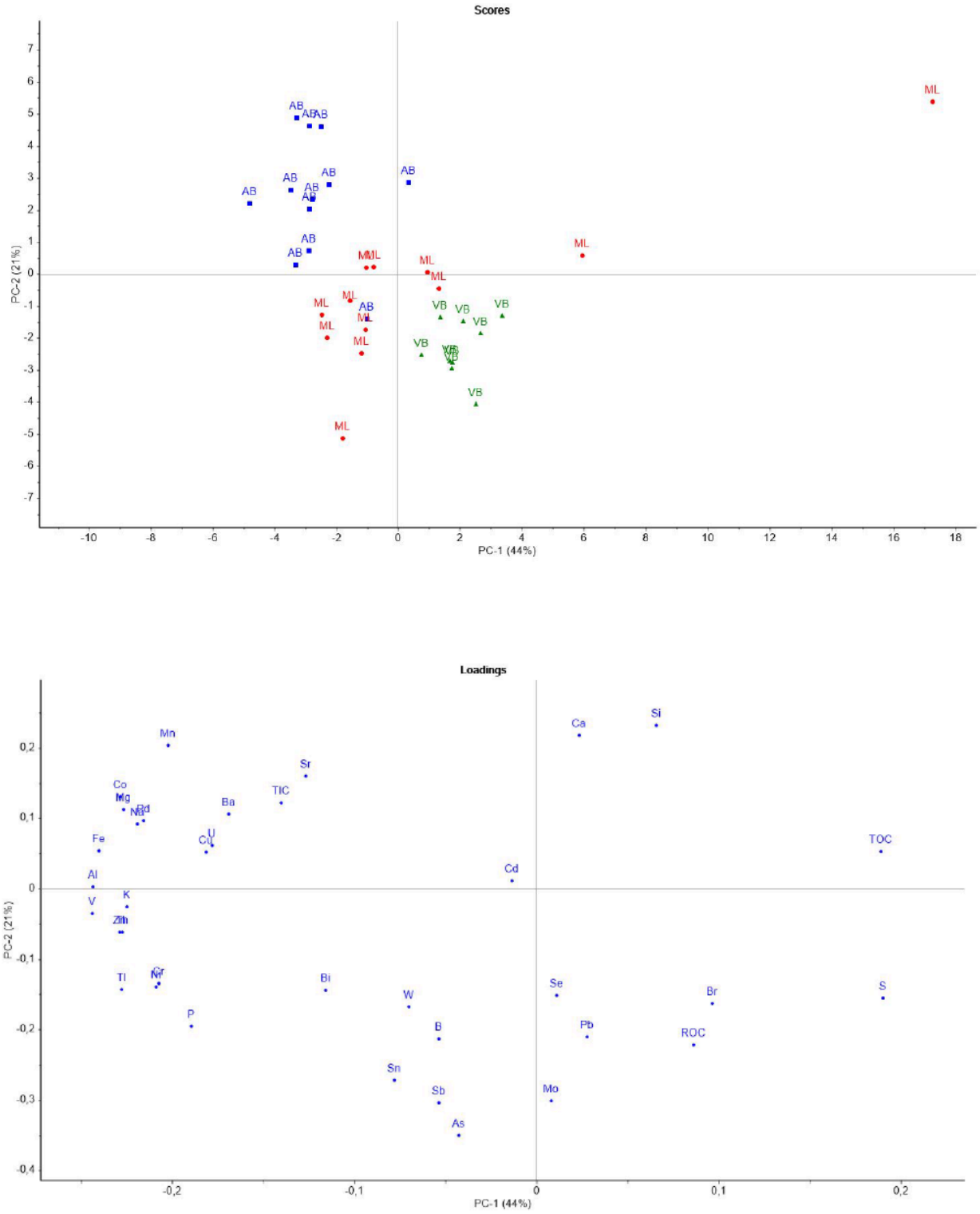

Figure 5.12 *Principal Component Analysis (PCA) score and loadings plot for cryoconite and supraglacial debris. The PC1 and PC2 make up 65 % of the total data variance. The loadings plot shows the original variable influence (the elements analysed) and the score plot shows the cryoconite and supraglacial debris samples by glacier location.*

6 Discussion

6.1 Accumulation of Trace Elements and Organic Pollutants in Cryoconite

On the whole, measured concentrations of all selected elements in this study were found to be within a similar range to four studies of cryoconite from Svalbard and two glaciers across the globe, with some exceptions (Table B.4.1 in the Appendix) (9, 10, 96-98). It should be noted that a number of different analytical techniques were used in the studies presented in Table B.4.1 to measure the elemental composition of the cryoconite, and therefore a direct comparison is not possible. However the reported concentrations across the studies provide an indication of the general magnitude of elements contained within the cryoconite studied. The techniques used for each study are indicated by letters in Table B.4.1.

6.1.1 Major Elements in Cryoconite

Elemental analysis indicated that Al and Fe were the most dominant elements present in cryoconite. These elements, along with Ca and Mg which were also found to be present at high concentrations, exist at high levels in the upper continental crust (UCC) (8, 68, 69). However, the general order in which the major elements were present in cryoconite differed to the UCC composition. The elements in cryoconite followed the order: Al>Fe>K>Mg>Ca>Si>Na, whereas the UCC composition follows the order: Si>Al>Fe>Ca>Mg>Na>K (8, 68, 69). Several reasons can explain the differences observed. Firstly the crustal composition is based on the refraction seismic profile of Western Europe and Canada, and as such is not specific to Svalbard (8). Variability is expected, especially given the complexity of the Svalbard geology, which contains rock reflecting each period in the geological history of the earth (219). The lithology of the local rock surrounding ML, AB, and VB includes among others: dolomite, sandstone, limestone, quartzite, anhydrite, garnet, gypsum, mica, calcite, and phyllite, as described in Section 4.1.1, which are composed of elements: Fe, Al, K, Ca, Mg, and Si to varying degrees (Table 4.2). The dominance of Al and Fe is in agreement with reported findings from several studies on cryoconite from both Svalbard and worldwide as presented in Table B.4.1 in the Appendix (9, 10, 97, 98, 235). These results indicate that the composition of cryoconite is heavily influenced by rock and mineral dust.

Secondly, concentrations of Si in cryoconite were lower than expected, which is assumed to be due to the use of HNO_3 for sample digestion. Unlike HNO_3, HF is considered to be one of the most effective acids for dissolving silicates (236). Consequently, digestion of the entire cryoconite was not achieved, an observation confirmed by the presence of visible precipitation following digestion. It could be assumed that the remaining residue was made up of Si based minerals. Indeed a number of studies report the mineral fraction of cryoconite to be dominated by silicates, especially quartz (93, 101, 102). Furthermore, high concentrations of Si were reported in a study by Baccolo et al. (2017) which used instrument neutron activation analysis (INAA) to determine elemental concentrations in cryoconite from a glacier in the Swiss Alps (96). The study reported Si concentrations of 215 – 370 mg g^{-1} (this study: 0.347 – 2.92 mg g^{-1}), which were an order of magnitude higher than the concentrations of Fe determined, 27.7 – 50.5 mg g^{-1} (this study: 14.0 – 47.8 mg g^{-1}) (96). Although the use of HF would have dissolved a larger fraction of the cryoconite, the objective of this study was to consider the use of CHs for environmental monitoring purposes. Silicates are not considered to be mobile in aqueous environments, and it is therefore less likely that these cryoconite components will have an impact on the levels of pollution transported by cryoconite hole water from the glacier (149). Thus the use of HF for microwave digestion to dissolve the remaining cryoconite particulate matter was not considered to provide relevant additional knowledge for the objective of this thesis and was not utilised.

The crustal composition according to Shaw et al. (1967, 1976) and Wedepohl (1995) can be used as a guide to understand the rock and mineral influence on the elemental composition of cryoconite, the details of which are included in Table B.11.1 in the Appendix (8, 68, 69). However caution must be taken when interpreting the results because as discussed, some variability between the composition of the continental crust and Svalbard geology is likely. The concentrations of the major earth elements in cryoconite: Al, Mg, and Ca were well below the UCC concentrations, thus rock and minerals are considered to be the main source of these elements. Iron was detected at concentrations below the UCC in cryoconite from ML and VB, however 50 % of samples from AB contained elevated concentrations of Fe. Iron enrichment may be due to a particularly high input of iron oxides, for example hematite (Fe_2O_3), from the red sandstone of the local parent rock, indicating some variation to the average UCC levels (Section 4.1.1) (221, 222). A red colour was also observed in the glacial river running from AB as presented in Fig. 4.2D, which was in contrast to the grey-brown coloured glacial river water running from VB and ML. Snow samples analysed for Fe on AB and ML in 2018 and 2019

showed a contribution from the rocket launch at Svalrak. On AB, a contribution for Fe was reported of 11 % and 12 % in 2018 and 2019 respectively, and a 6 % and 27 % contribution on ML in 2018 and 2019 respectively, compared to annual deposition (66). It is possible, given the proximity of AB to the launch site (Fig. 2.5), that some Fe deposited onto the glacier following launch was scavenged from the melting snow by cryoconite (96). However it is not possible to trace the source of the Fe, and concentrations of Fe in cryoconite from ML were not elevated above crustal concentrations, thus it is more likely that the elevated Fe is due to specific local geology.

6.1.2 Trace Element Accumulation

The elements As, Cd, Cr, Pb, and Zn were present in cryoconite at substantially lower concentrations than the major elements, which is in agreement with Wedepohl (1995) which reports ppm levels of trace elements in the continental crust (8).

Chromium

Chromium concentrations determined in cryoconite indicated depletion compared to crustal levels (Fig. 5.3). With a mean EF of 0.975, and a range of 0.772 – 1.63 (Table 5.4), it is probable that the Cr contribution to cryoconite was of geological origin. Indeed erosion of the terrestrial environment enhances the volumes of wind-borne dust and soil particulate matter which may account for > 50 % of the natural Cr atmospheric load (1, 70). Singh et al. (2003) also reported Cr concentrations in cryoconite from Midtre Lovénbreen to be well below continental crustal levels (10). Chromium is not reported to be amongst those elements that are subject to LRAT and it is therefore likely that the Cr in cryoconite was derived from local sources (237). The local rock surrounding the glaciers includes phyllite, quartzite, schist and shale, all of which contain varying quantities of the clay mineral chlorite, which can contain Cr^{3+} within its mineral structure (226). The Cr accumulated within cryoconite was found to be present at 'background' levels in 16 of 28 samples (all eight samples from ML, and four from both AB and VB) according to the Norwegian Environmental Agency quality standards for sediment in freshwater. The remaining 12 cryoconite samples were within 'good' levels (238).

Zinc

Zinc concentrations were found to be elevated compared to crustal levels in 96 % of samples, however the generally low EF of 2.68 indicated only a slight enrichment (Table 5.4). Although enriched compared to the UCC, it is possible that the variability in local geology is responsible

for the elevated concentrations. Furthermore, Zn was found to be highly and positively correlated with Al, Fe, and Mg (R^2 = 0.66, 0.79, and 0.71 respectively, $p < 0.001$ for all elements) (Table 5.13), and was also clustered with Al, K, Fe, and V in the PCA plot (Fig. 5.12) also indicating correlation with earth elements and a similar rock origin. Weathering of rock, resulting in wind-borne dust and soil particulate matter may account for 20 – 30 % of natural Zn emissions into the atmosphere (1, 70). Lokas et al. (2016, 2019) also reported only slight enrichment in Zn levels in cryoconite from two glaciers in Svalbard, with concentrations ranging from 84 to 108 μg g^{-1} and 60 to 98 μg g^{-1} respectively (Table B.4.1 in the Appendix) (9, 97). The concentrations of Zn in cryoconite were attributed to natural sources (9). In contrast, Singh et al. (2013) identified elevated concentrations of Zn above UCC levels in all cryoconite sampled from Midtre Lovénbreen (concentrations ranged from 132 to 150 μg g^{-1}) and attributed this enrichment to other natural sources and/or anthropogenic activity (10). Zinc concentrations in this study ranged from 60.6 to 101 μg g^{-1}, and were within the range of those reported by Lokas et al. (2016, 2019) (9, 97). Given the low EF, correlation with other major crustal elements, and similar concentrations to other studies where natural sources have been proposed, it is probable that the main Zn contribution to cryoconite in this study is of geological origin. The Zn accumulated within cryoconite was found to be present at background levels in 15 of the 28 cryoconite samples, according to the Norwegian Environmental Agency quality standards (three samples from ML, two from AB and all ten from VB). The remaining 13 cryoconite contained 'good' levels of Zn (238).

Cadmium

Cadmium concentrations were found to be elevated in 50 % of cryoconite from AB, and 90 % from VB. All cryoconite from ML contained concentrations of Cd below UCC levels (Fig. 5.3), suggesting that the Cd contribution to cryoconite from ML is of geological origin. Enrichment factors for cryoconite from the three glaciers (Table 5.3) showed natural levels from ML (EF = 1.13), slight enrichment in cryoconite from AB (EF = 1.91) and a higher enrichment in cryoconite from VB (EF = 4.11). In addition, Cd was not found to correlate with any of the major earth elements (Al, Fe, Mg, and Ca), and was only strongly correlated with Cr (Table 5.13). Although Cd is present in ores with Pb, Zn, and Cu, it was not found to be correlated with either Zn or Pb (Table 5.13), and no association was identified in the PCA with any other elements (Fig 5.12) (239). It is likely, due to the low enrichment of Cd in cryoconite from AB, that Cd contribution on AB was also of natural rock origin. However, these findings suggest that cryoconite from VB were influenced by a source outside of the local rock, either natural or

anthropogenic. Singh et al. (2013) found elevated concentrations of Cd in just one sample from ML and also attributed the Cd contribution to natural sources (10). The concentrations ranged from 0.043 to 0.145 μg g^{-1} which is comparable to this study (0.0432 to 0.196 μg g^{-1}) after excluding sample 25 which contained an unusually high concentration of Cd (0.532 μg g^{-1}) compared to all other samples (10). In contrast, Lokas et al. (2016) reported much higher Cd concentrations ranging from 0.065 to 1.529 μg g^{-1}, and proposed that the Cd contribution was from anthropogenic activity (9).

Natural sources of Cd into the atmosphere include sea-salt spray, volcanic eruptions and biogenic sources. However it is estimated that only 5 – 18 % of Cd released into the atmosphere is from natural sources (70). Possible local anthropogenic sources of Cd contamination could result from fossil fuel combustion, mining, landfill, local traffic, or the use of Cd metal as an anticorrosion agent (10, 65, 71, 240). In addition elevated Cd, (as well as Cr, Al, and Mn) was reported in a NASA Technical report from 1983, in the soil surrounding the launch pad of space shuttle flights in the United States (140). Although the rocket type was different, if Cd was a component of the sounding rockets, debris from the rocket boosters may contaminate the surrounding area leading to elevated Cd levels. The majority of snow sampled during the rocket launches contained Cd below detection (66). However overbank sediment samples collected in August 2020 were highly elevated in Cd at the booster impact area located between AB and VB (Fig. 2.5) with reported concentrations of 0.63 and 16 mg kg^{-1} (66). It is possible that Cd in overbank sediment near the booster area may have been transported along with dust particles onto the glacier surface of VB and/or AB resulting in eventual Cd enrichment in cryoconite following snow melt. Although it is not possible to trace, the rocket launches could thus be an additional source of Cd contamination to the glaciers.

Cadmium can also be transported long distances in the atmosphere. The dominant source area for LRAT emissions received in the Arctic is from Eurasia, and it is modelled that between 5 – 10 % of Cd, along with Pb, As, V, and Zn emissions reach the High Arctic from the region (1). Non-ferrous smelters such as those located in Northern Russia, for example in the Norilsk region or on the Kola Peninsula, are a major source of Cd (3, 71). Other sources of Cd may include waste incineration of Cd containing products such as batteries, or materials with Cd based pigments, metal coatings, and alloys (71, 240). Overall, although enriched, Cd concentrations present in cryoconite were found at 'background' levels in 27 of the 28 samples according to the Norwegian Environmental Agency (238).

Arsenic

Arsenic concentrations in all cryoconite were elevated compared to the UCC. Of all the polluting elements, As showed the highest mean enrichment of 8.57, with a maximum EF of 13.5 (Table 5.4). Cryoconite from ML and VB were particularly highly enriched (Table 5.3) indicating either a natural source outside of the local rock, or a significant level of contamination from local and/or long range anthropogenic sources. Arsenic was also found to be highly correlated with Pb (Table 5.13) indicating a possible similar source of contamination. Mean As concentrations in this study of 7.14 ± 2.35 μg g^{-1} (range: 2.77 – 11.9, Table 5.2) were similar to those reported by Singh et al. (2013, 2017) for cryoconite sampled from ML, AB, and VB (Table B.4.1 in the Appendix) (10, 98). Reported concentrations of As in cryoconite from AB and VB ranged from 3.6 to 5.3 μg g^{-1}, and from 5.0 to 5.7 μg g^{-1} respectively, whereas As concentrations in cryoconite from ML were slightly higher and ranged from 11.0 to 14.2 μg g^{-1} (10, 98). Concentrations of As in cryoconite from Svalbard were lower than in cryoconite from the Swiss Alps and Himalayas, which may be due to closer proximity to anthropogenic point sources in Eurasia (1, 96, 98).

Local sources of As contamination may include coal burning activities to generate heat and electricity, the old mining area and landfill (65, 71). With respect to LRAT of contaminants, the non-ferrous metal industry and fossil fuel combustion processes which release heavy metals and metalloids such as As into the atmosphere are a potential source of contamination (71). Arsenic can also be used in wood preservatives; and the manufacture, use, and release via waste incineration may also provide a long distance source of As contamination into the atmosphere (240). In the PCA plot (Fig. 5.12), As was clustered with antimony (Sb). Contamination of both elements is found together in the environment, often in areas of mining activity. This indicates a potential long distance mining source (241). It should be noted that although As was highly enriched, the concentrations present in the cryoconite were at 'background' levels in all samples according to The Norwegian Environmental Agency (238).

Lead

Lead was found to be the most contaminating of all the heavy metals and metalloids analysed in this study with five of the 28 cryoconite samples containing Pb at 'moderate' levels of pollution according to the Norwegian Environmental Agency. Only one cryoconite sample contained background levels of Pb (238). Elevated concentrations of Pb were found in 96 % of cryoconite samples. Lead was highly enriched in cryoconite from both ML and VB with a maximum EF of 20.6 in cryoconite from VB (Table 5.3). Although cryoconite from AB were

found to be enriched in Pb, it was to a much lesser extent, with a mean EF of 3.89. As discussed, Pb and As were highly correlated, indicating a potential similar source outside of the local geology. Lead concentrations were higher compared to other studies from Svalbard that also reported elevated Pb concentrations in cryoconite. Concentrations of Pb in cryoconite in this study ranged from 8.33 to 135 μg g^{-1}, compared to 49.9 to 85.1 μg g^{-1} reported by Singh et al. (2013), 16.3 to 82.7 μg g^{-1} reported by Lokas et al. (2016), and 19.9 to 97.7 μg g^{-1} reported by Lokas et al. (2019) (9, 10, 97). Concentrations of Pb in this study were also higher than those reported for cryoconite from AB and VB by Singh et al. (2017), as presented in Table B.4.1 in the Appendix (98).

Concentrations of Pb were found to be particularly elevated in the dark coloured cryoconite samples (dark grey colour found in two cryoconite from ML, and two from VB). A mean Pb concentration of 94.6 μg g^{-1} was measured compared to the remaining lighter coloured cryoconite (mean Pb concentration 42.5 μg g^{-1}). Organic matter (OM) in the form of humic substances, which have been proposed to affect the optical characteristics of cryoconite, may well be responsible for the darker colouration of these samples (22). Lokas et al. (2016) found a significant correlation between Pb and OM (9). In addition, soil Pb sorption ability has been reported to increase with OM content, in addition to clay, $CaCO_3$ content, and pH (242). Thus the elevated Pb concentrations in the dark coloured samples could be due to the affinity for Pb to adsorb to OM. This is supported by lower Pb concentrations found in the two lighter colour categories (pale grey and cream) where a mean Pb concentration of 19.7 μg g^{-1} was measured across the two groups. Total organic carbon (TOC) a component of OM was analysed in cryoconite and SGD, but did not appear to have an influence on Pb levels. For example, SGD samples (no. 85-86, 88) were all dark in colour, measured a TOC content of 1.79 %, 34.6 %, and 15.3 %; and Pb concentrations of 111 μg g^{-1}, 8.83 μg g^{-1}, and 159 μg g^{-1} respectively (TOC content was not measured in the dark grey cryoconite samples thus cannot be used as a comparison) (Tables B.2.1, B.3.2 and B.7.2 in the Appendix). These finding suggest that OC content itself may not have an impact on the Pb accumulation in cryoconite. However OM is comprised of not just OC, but also nitrogen (N), oxygen, and hydrogen, and Pb^{2+} has a high affinity to N and S ligands, thus the dark OM may still provide an explanation for the trend in Pb concentrations across colour groups (74). Unfortunately the OM content was not analysed in this study, thus corroboration is not possible.

A major source of Pb is still from leaded, low leaded, and unleaded vehicle fuel, although a large decrease has been seen in atmospheric levels of Pb since the introduction of unleaded

gasoline in developed countries. Some countries, however, may still use leaded gasoline as fuel (3, 240, 243). Lead is also emitted from non-ferrous metal production, as discussed for Cd and As, as well as from waste incineration (71). The anthropogenic influence on the concentration of Pb in cryoconite may well be significant, with Lokas et al. (2016) reporting the anthropogenic Pb fraction in cryoconite from the Hornsund area in Svalbard to range between 29 to 95 % (9).

A summary of the discussion for each trace element has been presented in Table 6.1. The results indicate that selected trace elements accumulate in cryoconite leading to enrichment over continental crustal levels. Lead showed the highest contamination.

Table 6.1 *Summary of findings from the analysis of elemental enrichment in cryoconite.*

Level of enrichment is classified as depleted, for those elements that are not enriched compared to the upper continental crust; minor for those elements or glaciers where only low levels of enrichment were observed; and highly enriched for those elements with large enrichment factors. Locations are represented by ML (Midtre Lovénbreen, AB (Austre Brøggerbreen), and VB (Vestre Brøggerbreen).

Element	Cr	Zn	Cd	As	Pb
Enriched?	No	Yes	Yes	Yes	Yes
Extent of Enrichment	Depleted: All	Minor: All	Depleted: ML Minor: AB, VB	Minor: AB Highly: ML, VB	Minor: AB Highly: ML, VB
Correlation with Other Elements[a]	Cd only	Al, Fe, Mg	Cr only	Pb; (and Sb in PCA plot)[b]	As
Contamination Level[c]	Background: 16 Good: 12	Background: 15 Good: 13	Background: 27 Good: 1	Background:28	Background: 1 Good: 22 Moderate: 5
Possible Sources	Geological[d]	Geological[d]	Geological (ML) Other natural[e]; Local[f]: Rocket booster debris, local traffic, landfill; LRAT[g]: Non-ferrous smelting, waste incineration	Local[h]: coal burning, old mining activity, landfill; LRAT[i]: non-ferrous smelting, fossil fuel combustion, wood preservatives, mining	Local[j]: vehicle fuel; LRAT[j]: vehicle fuel, non-ferrous smelting, waste incineration

[a] Data extracted from non-parametric Spearman correlation results in Table 5.13.
[b] Data extracted from PCA plot in Fig. 5.12.
[c] Contamination levels determined using the Norwegian Environmental Agency quality standards for sediment in freshwater (238).
[d] Nriagu (1989); AMAP (1997) (1, 70).
[e] Nriagu (1989) (70).
[f] Aas et al. (2021); Singh et al. (2013); Jarup (2003); Granberg et al. (2017); Nriagu & Pacyna (1988) (10, 65, 66, 71, 240).
[g] AMAP (2002); Nriagu & Pacyna (1988) (3, 71).
[h] Granberg et al. (2017); Nriagu & Pacyna (1988) (65, 71).
[i] Nriagu & Pacyna (1988); Jarup (2003); Hiller et al. (2012) (71, 240, 241).
[j] AMAP (2002); Jarup (2003); Nriagu & Pacyna (1988); Pacyna & Pacyna (2001) (3, 71, 240, 243).

6.1.3 Organic Pollutants

The analysis of cryoconite showed no detectable accumulation of PCBs. Despite PCB-138 contamination being identified in overbank sediment close to the sounding rocket launch debris (Fig. 2.5), the small sample size in the study by Aas et al. (2021) prevented a conclusion as to whether the rocket launches had generated local PCB pollution (66). The findings of this study could indicate that the rocket launches did not contribute to PCB pollution on the three glaciers. However given the high matrix effects (MEs) observed, and the fact that just seven PCB congeners were analysed, it is also not possible to conclude that no PCB contamination occurred.

The MEs in this study were significantly larger than the MEs reported by Weging (2021) (from which the extraction and GC-MS procedure was based) for the same PCB target compounds in soil (- 1 to - 9 % and - 1 to 9 % for 50 ng mL^{-1} and 100 ng mL^{-1} fortification respectively) (231). The high negative MEs indicate signal suppression, and may be the result of contamination in the inlet and/or column through the absorption of non-volatile compounds such as humic substances which may be present in the OM component of a cryoconite matrix (21, 22, 203). Thus the high MEs may be due to inadequate clean up steps compared to those required for the cryoconite matrix. Furthermore, the chromatograms showed a large amount of background noise suggesting a 'dirty' sample (202). Substantial clean up steps may help reduce the MEs, however they can be time consuming, increase the risk of contamination especially when analysing for trace levels of pollutants and may also result in loss of target analyte (203). Consideration must therefore be taken when determining the procedures to reduce the effects of the sample matrix.

Mean absolute recoveries were considered to be within an acceptable range (> 83 %) for the low and high fortification levels (Table 5.8). The recoveries were within a similar range to those reported by Weging (2021) from which the extraction method used in this study was based (231).

Only one study to date analysing PCBs in cryoconite has been located. Weiland-Bräuer et al. (2017) used multiple clean up and concentration steps prior to analysis of cryoconite for the presence of PCBs, PAHs, and various organochlorine pesticides (OCPs) by high resolution gas chromatography/ high resolution mass spectrometry (99). The additional washings, concentration, and clean up steps serve to remove impurities that may interfere with the GC-MS analysis, and concentrate the target analytes to a potentially detectable level (202). It is

possible that the additional procedures may have reduced the effect of the matrix in this study and potentially enabled the determination of the PCBs. Method development was outside the scope, however future development of the method would be interesting to determine the necessary clean up steps, optimal sample weight, and solvent mixture required to reduce the effect of the cryoconite matrix on PCB determination. In total, Weiland-Bräuer et al. (2017) detected 18 PCB congeners in alpine cryoconite sampled from Jamtalferner glacier in Austria. The cryoconite contained a mean concentration of 0.8 ng g^{-1} dry weight PCBs, and ranged from 12 to 3,847 pg g^{-1} dry weight (99). A number of studies analysing PCBs in other matrices have been performed in close proximity to the Ny-Ålesund settlement in Svalbard. Aslam et al. (2019) analysed for PCBs in organic soil and vegetation in Ny-Ålesund, where PCB-28 was detected in one vegetation sample at a concentration of 6.7 ng g^{-1} dw. In organic soil, PCB-52 was detected in two samples and PCB-180 in four samples, at a mean concentration of 2.9 and 4.9 ng g^{-1} dw respectively (2). Thus in general, if detected above the LOD, very low concentrations of PCBs have been measured in soil and vegetation matrices in the area.

A significant correlation was determined by Nam et al. (2008) between TOC and PCBs in background soils in the UK and Norway suggesting a high affinity for PCBs to organic carbon (244). The mean TOC content of cryoconite in this study was low, at just 1.55 %, which may also provide a reason as to the undetectable concentrations of PCBs in cryoconite, and the low concentrations reported by Weiland-Bräuer et al. (2017) in comparison to levels reported in soil and vegetation by Aslam et al. (2019) (2, 99).

The detection of PAHs however indicates the ability for cryoconite to accumulate these organic contaminants. The incomplete combustion of most organic materials such as fossil fuels is the main origin of PAHs, and as such the contaminant group can be derived from both anthropogenic and natural sources (245). Local sources of PAHs in Ny-Ålesund may include coal dust from the old mining site, the dumpsite at Thiisbukta, and the fuel storage area, all of which have also been discussed as potential sources of trace elements and PCBs (65). Other local sources could relate to fuel combustion, vehicle exhaust, in addition to wood burning activities (245). Future analysis and quantification of PAHs in cryoconite from Ny-Ålesund may provide useful background levels for future monitoring of this environmental contaminant group.

6.2 Cryoconite Hole Water and Snow and the Influence of Cryoconite on Elemental Concentrations

6.2.1 Major Elements and Anions in Cryoconite Hole Water and Snow

The major elements present in CW were in contrast to those in snow (Fig. 5.7 and 5.8). The presence of high concentrations of Ca relative to other elements analysed in CW indicates a freshwater input (Table 5.10) whereas the dominance of Na and Cl in snow indicate a strong marine influence (6). The snowpack in Svalbard has been reported to be heavily influenced by the ions in sea-salt (Na^+ and Cl^-) which evaporate into the air from the surrounding oceans and are then transported to Svalbard (128). Indeed the PCA plot also showed a tight clustering of Na and Cl indicating a high correlation, particularly in the snow samples (Fig. B.12.1 in the Appendix). Sea salt aerosols in snow are also believed to be the primary source of Cl^- ions in CW following snow melt (40). Halite minerals (NaCl) and NaCl/silicate aggregates have also been reported in cryoconite, which on dissolution may also represent a portion of the Na and Cl ions present in CW (95, 104). The statistically significantly higher concentrations of Na and Cl present in snow compared to CW (Table 5.10) and the separate clusters observed in the PCA plot between the two sample types (Fig. B.12.1 in the Appendix) provide an indication that the water present in cryoconite holes is not generated solely from melted snow. The conductivity of CW (mean 4.4 µS cm^{-1}) was also found to be low compared to snow, where mean conductivities of 32 µS cm^{-1} have been reported (128). It has been suggested based on stable isotope ^{18}O and D signatures, that the source of CW is in fact meltwater generated from the melting glacier surface (92).

Although the concentrations of SO_4^{2-} and Cl^- were below the LOD, the estimated LOD values in this study were much higher than those calculated in other studies (although it should be noted that different eluent and IC analytical equipment were used) (20, 95). A number of methods can be used to calculate estimated LODs (Section 3.3.3), thus the higher LOD estimations in this study could be due to the method selected (193). Even despite the high LOD estimations, concentrations of the major ions in CW were low, indicating a lack of opportunity for ions to accumulate in CW (95). In cryoconite holes, Cl^- ions act conservatively only when isolated from the hydrological system on a glacier and as a consequence, are affected only by the increase in the age and depth of the cryoconite holes (40). It is possible that where the CHs were hydrologically linked, discharge of solutes may occur leading to the depletion of Cl^- ions as well as Na^+, K^+, Mg^{2+}, Ca^{2+}, SO_4^{2-}, and NO_3^- (95). This process would occur in the summer

months when the cryoconite holes are open to the atmosphere, and may explain the low concentrations of ions observed in this study (33). Stibal et al. (2008) noted a drop in the conductivity of CW from the start to the end of the ablation season, with values of ~9 μS cm^{-1} measured at the start of the period, compared to 3 – 5 μS cm^{-1} in the later half of the melting season, the latter values are in accordance with conductivity measurements taken in this study (102). The reduction in conductivity may be due to replenishment of CW with supraglacial meltwater during the ablation season, thereby removing accumulated solute present in the CW which originated from cryoconite debris dissolution (102). A competing process is the recharging of ions in CW as a consequence of direct deposition of airborne particles and aerosol salts into the open holes, as well as replenishment of solutes from melted snow and ice transported from higher up the glacier, and concentration increases following evaporation (92, 96, 123).

Nitrate levels were low in both CW and snow. The low nutrient concentrations in cryoconite meltwater have been discussed in a number of studies. Takeuchi et al. (2001) reported NO_3^- concentrations between 0 - 0.04 mg L^{-1} in cryoconite meltwater from the Yala Glacier in the Nepalese Himalayas (21). Studies of microorganisms and cryoconite hole water in Svalbard have reported similar findings, with NO_3^- concentrations being below detection in the majority of samples (20, 91). Nitrate concentrations were also reported to be very low, if above detection limits, in surface glacier ice and supraglacial meltwater from Aldegondabreen in Svalbard (91).

The concentrations of SO_4^{2-} ions were found to be higher in cryoconite compared to Cl^-, with the reverse being true for snow (Table B.8.1 and B.8.2 in the Appendix). The dissolution of minerals such as calcite ($CaCO_3$), dolomite ($CaMg(CO_3)_2$), anhydrite ($CaSO_4$), and gypsum ($CaSO_4 \cdot 2H_2O$) (Table 4.2) present in the local geology and thus expected to be present in cryoconite could lead to the enrichment of ions such as Mg^{2+}, Ca^{2+}, and SO_4^{2-} above Cl^- in CW (7, 95). Indeed concentrations of Mg were statistically significantly higher in CW compared to snow (Table 5.10). A larger concentration range was also observed for Ca in CW of 29.1 – 5530 μg L^{-1}, compared to a much lower concentration range in snow of 17.3 – 205 μg L^{-1}, although no significant difference was identified between the two sample types ($p = 0.123$, Mann-Whitney U test). In addition, cryoconite holes with high concentrations of Ca and Mg present in the cryoconite sediment also contained elevated concentrations in the overlying water relative to the other samples, and generally showed higher conductivity. Calcium and Mg have also been found to have a significant marine source in snow as well as in glacier ice cores (126,

246). This suggests that some of the Ca and Mg present in CW may also be derived from sea-salt aerosols, especially given the proximity of the glaciers to Kongsfjorden.

6.2.2 Trace Elements in Cryoconite Hole Water and Snow

No comparable literature has been found on the concentrations of trace elements in cryoconite hole water. As such, concentrations have been compared to glacier ice cores, given the similarities discussed in Section 6.2.1. Literature reporting on the concentrations of trace elements in snow in Svalbard provide differing units making comparison a challenge. In this case, the concentrations of polluting elements in snow were compared to CW to understand the potential influence of snow on cryoconite hole water concentrations following snow melt.

Concentrations of Cr and Pb were generally found to be low in both CW and snow. Chromium concentrations in CW and snow were below detection in 68 % and 52 % of the samples respectively. Cryoconite hole water and snow contained Pb concentrations below detection in 46 % and 28 % of samples respectively. Similar findings were also reported by Singh et al. (2015) in ice cores from surface and subsurface ice on Midtre Lovénbreen (246). Although incomparable units were used, the majority of snow samples reported by Aas et al. (2021) from the Ny-Ålesund area also contained Cr and Pb concentrations below detection, thus supporting the findings from this study (66).

No significant differences were identified in Cr and Pb concentrations between the two sample types (Table 5.10). The low concentrations of Cr in snow and CW samples may be due to the presence of Cr in the +3 oxidation state form which has a low solubility at pH > 5 in soil, and has been found to strongly adsorb to soil particles (239). Although a different matrix to cryoconite, soil particles also contain a mineral and organic matter fraction, and given the lack of literature studying the interactions between cryoconite and the overlying water, interactions between soil and water have been used in this study to consider the processes occurring at the cryoconite solid-water interface (6). Adsorption of Cr(III) to clay minerals and Mn and Fe oxides occurs at a fast rate, and with increasing organic matter content and pH, adsorption increases (73). In contrast, Cr present in water in the oxidation state +6 is soluble in water and can be found in the form CrO_4^{2-} (247). Similarly, Pb also has a high affinity for particulate matter and adsorbs to Mn and Fe oxides as well as clay minerals and OM, and has poor solubility in water (73, 239, 242). The carbonate content of soil can also play a role in the solubility of Pb (thus also assumed to be the case for cryoconite) (247). It is therefore likely

that any Pb^{2+} and Cr^{3+} ions present in the CHs are adsorbed to the negatively charged surfaces in the cryoconite particulate matter and immobilised, rather than being present in the overlying water. Thus the statistically similar, and low concentrations of Cr and Pb in CW and snow would be expected unless mobilised into the water phase by the presence of high concentrations of, for example DOM, present in the dissolved fraction (77, 247).

In line with the low solubility of Cr and Pb, CW and snow samples were less polluted than cryoconite according to the Norwegian Environmental Agency quality standards for freshwater. Lead concentrations were at background levels in 60 % of snow and 71 % of CW samples. Those samples that contained Pb at 'good' levels included eight CW (seven of which were from ML) and ten snow samples (six from AB and four from VB) (238). Chromium was found at background levels in all CW samples, and 92 % of snow samples. The two snow samples at 'good' pollution levels were both from VB (238).

No significant difference was found in Cd concentrations between snow and CW (Table 5.10). However concentrations of Cd were lower than those reported by Singh et al. (2015) in ice cores from ML, which ranged from 0.0007 to 0.0217 ppb compared to 0.000277 to 0.00546 μg L^{-1} in CW in this study (246). Cadmium was found at background levels in all snow samples and 23 of the CW samples, the remaining five samples were found to be at a 'good' level, over 0.003 μg L^{-1} (238). The solubility of Cd in water is also influenced by the presence of clay, organic matter, and $CaCO_3$ in addition to pH (242). At low Cd^{2+} activity, the main adsorption process is via ion exchange (73). Concentrations of Cd present in CW or snow can be influenced by the presence of other ions such as Ca^{2+} and Zn^{2+} which can preferentially adsorb to sites on the surface of soil components such as clays, thus resulting in desorption of Cd^{2+} ions, and may lead to higher concentrations of Cd^{2+} in CW (73, 248, 249). As for Pb and Cr, the statistically similar concentrations of Cd in snow and CW may therefore be due to the affinity of Cd for components with the cryoconite matrix, or dust particles within snow which would remove Cd from the water phase.

Arsenic concentrations on the other hand were found to be significantly higher in CW than snow (Table 5.10) but in both sample types concentrations of As were at background levels (238). Concentrations of As in CW ranged from below detection to 0.0213 μg L^{-1} (Table 5.10) and were found to be within the range of those reported in ice cores by Singh et al. (2015) of below detection to 0.0410 ppb (246). Zinc concentrations were also found to be statistically significantly higher in CW although not to a great extent. Concentrations of Zn in CW were

also lower than those reported in ice cores, with concentrations ranging from 0.185 to 2.24 µg L^{-1} in CW (Table 5.10) compared to 0.38 to 49.59 ppb in ice cores from ML (246). Zinc concentrations were at background levels in 20 of the snow samples and 22 of the CW samples. The remaining five snow samples and six CW samples were found at 'good' levels (1.5 – 11 µg L^{-1}) (238).

As for Pb, Cd, and Cr, it is probable that the cryoconite present in cryoconite holes influence the concentrations of As and Zn present in CW. In this case sediment dissolution processes may dominate adsorption processes leading to the statistically higher concentrations found in CW in comparison to snow. Both Zn and As were detected in the cryoconite solid material, with As concentrations in particular being elevated over UCC average concentrations (Fig. 5.3). Arsenic is most commonly found in water environments in oxidation states +3 and +5 (247). Arsenate, As(V), solubility is dependent on pH. At low pH's the negatively charged $HAsO_4^{2-}$ species is attracted to the positively charged surface of metal oxides such as hematite (239). Thus cryoconite with a high content of Fe and Al oxides, as well as clay, and calcium could be expected to impact the mobility of As, with a high content leading to likely adsorption of As by cryoconite resulting in a reduction in the concentration of the metalloid in the CW (239). However arsenite (As(III)) only weakly adsorbs to soils and presence of As in the 3+ oxidation state would therefore be expected to lead to higher concentrations of As in CW (239). Thus competing processes occur, with the solubility of As being influenced by speciation, which is dependent on pH, and presence of a reducing or oxidising environment and may explain the differences between snow and CW (239).

A higher proportion of Zn (97 %) was present in CW (relative to the other heavy metals and metalloids analysed) in comparison to the proportion found in the cryoconite solid material (43 %) (Fig. 5.10). As discussed, Cr and Pb have a high affinity for particulate matter and are often present for only a short time in the dissolved phase, thus explaining the lower proportion of Cr and Pb in CW compared to cryoconite (247). In contrast, Zn is often found as Zn^{2+} in water, particularly in the freshwater pH range from 6 – 8, and has a relatively low tendency to form organic or inorganic complexes which may explain the higher proportion of Zn in CW (relative to the other heavy metals and metalloids) compared to the solid material (74, 247). Overall, the solubility of Zn and As (III), and possible dissolution processes from the cryoconite solid material may be responsible for the higher concentrations of Zn and As in CW in comparison to snow.

The elements Fe and Al which dominated in cryoconite (Fig. 5.9), were found at much lower proportions in the overlying water and snow (Fig. 5.8). In CW, Fe and Al contributed just 0.2 % to the overall elemental composition (Fig. 5.8). This is due to the low solubility of Fe and Al oxides at environmental pHs in soil (250). No significant difference was identified in the concentrations of Al in snow and CW (Table 5.10). However significantly higher concentrations of Fe were found in snow. The mean concentration of Fe in snow from VB was much higher (6.83 μg L^{-1}) than from the other two glaciers (AB = 3.11 μg L^{-1}, ML = 1.19 μg L^{-1}) which were comparable to CW (mean Fe concentration in CW: 1.83 μg L^{-1}). Only one sample location was available for sampling snow on VB and it is therefore possible that the elevated Fe concentrations on the snow patch may have been result of the deposition of wind-blown dust high in Fe based minerals from the surrounding environment onto the specific area sampled (106).

The lower concentrations of As, Zn, and Cd in CW compared to ice cores may be due to adsorption of solutes from the surrounding water by cryoconite, or dilution of solutes by glacier meltwater that replenishes the water in the cryoconite holes (96, 102). Given that glaciers in Svalbard are receding, the higher concentrations of As, Cd, and Zn reported by Singh et al. (2015) in the ice cores could result in high concentrations of these elements being released into glacier meltwater during melting events (217, 246). These contaminating elements may then be scavenged by cryoconite leading to elevated concentrations of elements such as As, Cd, and Zn in cryoconite in the future (43).

The sources of the polluting elements Zn, Cd, and As are likely to be similar to those discussed for cryoconite in Section 6.1.2. The elements are all subject to long range atmospheric transport and can reach the surface of a glacier by direct dry deposition, or via scavenging from the atmosphere during the creation of snow, or by falling snow (1, 79). The general findings of the study of CW and snow indicate that the concentrations of the polluting elements in the two sample types were very similar. Based on these findings, it is unlikely that snow melt would have a significant impact on the concentrations of elements such as Pb, Cr, Cd, and As in the dissolved phase in CW. However as a consequence of the low quantities of snow remaining on the glaciers in the sampling area, limited spatial variability in samples was achieved. It is therefore possible that the snow sampled was not representative of the snow composition across the glacier at the beginning of the melting season, and consequently it is not possible to

confidently conclude on the impact of snow melt on the concentrations of elements found in cryoconite holes.

6.3 Cryoconite Holes as Potential Tools for Environmental Monitoring in the Arctic

As discussed in Section 6.1, the results of this study show that cryoconite can accumulate certain elements, leading to large levels of enrichment. Direct atmospheric deposition has a key role in this accumulation (96). In addition, the scavenging of contaminating elements from dissolved particulate matter and colloidal particles in glacier meltwater by cryoconite may also play a significant role in the accumulation of inorganic and organic pollutants (43, 96).

In the summer ablation season, snow and glacier ice melt, resulting in the mobilisation of contaminants (most likely also of atmospheric origin) stored within the glacier ice and snow (96). This meltwater is transported down the glacier to the ablation zone, where cryoconite holes are situated (43, 96). The meltwater replenishes the holes, providing contaminants which can then be scavenged by the cryoconite material and thus immobilised (43). As discussed in Section 6.2.2, certain elements have high affinities for components of cryoconite such as organic matter (for example: EPS) and clay minerals, and it is likely that these components have a significant influence on the levels of elemental accumulation (43, 96). Extrapolymeric substances (EPS) are secreted by microorganisms such as cyanobacteria. These substances can protect the cells, enabling survival in extreme conditions (116). The EPS contain heteropolysaccharides, with carbonyl and carboxyl functional groups (116, 251). In addition, cyanobacteria also produce EPS with sulphate groups, a functional group not present in EPS produced by other bacteria (251). These functional groups contribute to the negatively charged nature of EPS (252). The affinity of metal ions towards the negatively charged groups on the EPS may thus provide an explanation for the high accumulation of some elements in cryoconite such as Pb, and Cd which also have a high affinity for S ligands (116, 252).

The age of the cryoconite is not easily determined, especially for cryoconite holes that are not isolated from the atmosphere (92, 96). It is however possible that cryoconite could survive several years of freeze-thaw cycles within cryoconite holes which could enable accumulation of elements over long periods of time (40, 96).

A comparison of the concentrations of As, Cd, Cr, Pb, and Zn in cryoconite determined in this study has been compared to other matrices sampled in Ny-Ålesund and Adventdalen (located near the main settlement of Longyearbyen). The full details of the mean concentration and range for each matrix have been presented in Table B.11.1 in the Appendix. Cryoconite have been compared to mineral and organic soil, vegetation, lichen, Bayelva overbank sediment, Ny-Ålesund coal, and Kongsfjorden sediment, in order to understand differences in the accumulation ability of cryoconite in comparison to other matrices studied in Svalbard (2, 8, 10, 23, 68, 69, 235, 253, 254).

Zinc concentrations in cryoconite were within the range reported in most matrices, including surface and mineral soil, vegetation, lichen, and organic soil, but were higher than overbank sediment and Ny-Ålesund coal deposits. Chromium concentrations in cryoconite were generally higher in both mean and range than surface and mineral soil, vegetation, lichen, and organic soil from Ny-Ålesund. However similar concentrations were reported in organic soil from Adventdalen and Kongsfjorden sediment. Arsenic concentrations in cryoconite were within a similar range to surface and mineral soil. Vegetation and lichen from Ny-Ålesund, Bayelva overbank sediment and Ny-Ålesund coal were all reported to contain lower concentrations of As compared to cryoconite, although not to a large extent. In contrast, concentrations of As were much higher in organic soil, and to a lesser extent in vegetation from Adventdalen. Cadmium concentrations in cryoconite were generally lower than reported in vegetation, for example the mean Cd concentration in cryoconite was 0.119 $\mu g\ g^{-1}$ compared to 0.54 $\mu g\ g^{-1}$ and 0.63 $\mu g\ g^{-1}$ in vegetation from Ny-Ålesund and Adventdalen respectively (2). Surface soil, Bayelva overbank sediment, and Kongsfjorden sediment also contained higher concentrations of Cd compared to cryoconite. Only mineral soil was found to contain similar concentrations of Cd to cryoconite (23). Finally mean Pb concentrations determined in cryoconite samples were higher than in all other matrices, including a higher minimum to maximum ranges.

The findings suggest that certain elements such as Pb accumulate to a much greater extent in cryoconite compared to other matrices, and cryoconite may therefore be a useful monitoring tool to analyse atmospheric deposition of Pb. Cryoconite may also be a useful monitoring tool for As, given the elevated concentrations above most matrices, except mineral soil. On the other hand, cadmium appears to accumulate to a higher extent in organic matter such as vegetation and organic soil, thus matrices with a higher OM content may be more suitable for monitoring Cd levels.

An advantage of cryoconite over other matrices is the remote location in which they are found, which is less impacted by sources outside of atmospheric deposition (97). For example, concentrations of contaminating elements in soils and vegetation may be impacted by other sources such as terrestrial animals, migratory birds, or direct anthropogenic releases to soil and/or water and surface run-off (65, 97, 255, 256). In contrast, the concentrations of contaminating elements in cryoconite may be impacted by glacier meltwater derived from melting snow and ice, as discussed, but the main exposure route is likely to be the same, i.e. atmospheric deposition (96, 126).

6.4 Heterogeneity of Cryoconite Holes

Variability in both the physical and chemical properties of cryoconite holes was observed in this study. In this section, potential explanations have been proposed and discussed for the heterogeneity of cryoconite holes both within and between the three glaciers.

6.4.1 General Observations (Shape, Size, Cryoconite Colour, and Morphology)

Cryoconite holes (CHs) were found to cover areas of the lower section of the three glaciers: ML, AB, and VB. Some CHs were completely isolated whereas others appeared to be interconnected with a number of other holes. The shape and size of CHs varied both within and between glaciers, and were rarely spherical. With the exception of three CHs sampled on VB, CHs were open to the atmosphere at the time of sampling (August 2021). The frozen lids covering three holes sampled on VB were thin and easily broken, suggesting possible freeze over as a consequence of lower night temperatures. Sampling of CHs on VB took place in the morning, compared to late afternoon sampling on AB and ML, thus it is possible that any temporary frozen lids on CHs from AB and ML may have melted during the day prior to sampling.

Variability in CH diameter, depth, and surface area was also observed by Lokas et al. (2016) and Webster-Brown et al. (2015) both within and across glacier locations (9, 92). The variations observed in hole shape may be the result of sediment dynamics within the holes. The thickness of the sediment layer can influence the rate of melting and hole depth. For example, the thicker the sediment and the larger the area covered, the deeper and wider the hole becomes (up to a threshold thickness) (40, 119, 257). The equilibrium depth can differ from location to location

as a consequence of variations in the input of energy received by glaciers (107). The type of glacier ice, cryoconite hole hydrology, the position of the holes on the glacier, and the local topography, may all affect melting patterns and could contribute to the observed heterogeneity in hole shape in this study ((according to McIntyre (1984), as cited in Cook 2016) (108, 258).

A large amount of colour variation in cryoconite was also observed, both within and between the three glaciers. Cryoconite from ML were all grey, varying between hues of grey and dark grey, which is in agreement with reported observations by Rozwalak et al. (2022) where cryoconite from ML were categorised towards the lighter end of the grey scale (100). The rock colour surrounding ML was predominantly dark grey and surrounding VB, predominantly brown, both reflected in the general colour of the cryoconite from these glaciers. The rock surrounding AB was much more varied in colour, containing both dark and light rock, including the red-brown colour which was observed in both the cryoconite and glacial river at AB (Fig. 4.2 A – D). The general cryoconite colours observed in this study are thus influenced by the colour of the surrounding rock, which is in agreement with several reports which suggest that the colour of the cryoconite is influenced in part by the mineral fraction, the majority of which is expected to be derived from local rock sources (21, 22, 101). Other factors can also influence cryoconite colour. The existence and concentration of OM is also proposed to have a significant influence on the darkness of the cryoconite, the presence of a higher quality of humic substances leading to a darker colouration (22, 94). Differences in the extent of weathering of rock dust within CHs can also change the colour of the particulate matter following for example oxidation reactions (100). Thus weathering could also lead to colour variations in cryoconite within a glacier surrounded by the same local geology.

Cryoconite particle sizes varied from very fine to granular sized particulate matter. Takeuchi et al. (2010) and Rozwalak et al. (2022) identified a number of different cryoconite structures, and proposed that the presence of granular cryoconite in holes reflects perhaps the older age of the CH and the higher cyanobacterial content (100, 103). The cyanobacteria which, through mechanical and chemical processes, form granules by entangling and ‘gluing’ particulate matter together, using EPS excreted by the cells, may thus be influential in the size of the cryoconite found in this study (93, 94, 116). It has also been suggested that variations in mineral composition may result in heterogeneity in the composition of bacterial communities found within the cryoconite. For example, fine debris may promote a higher abundance of microorganisms in comparison to coarser debris due to higher surface area available for interactions between the microbial cells and the mineral fragments (91, 94, 112). Although

contrasting findings were reported by Edwards et al. (2011) regarding cryoconite sampled from AB (31).

It could be postulated that cryoconite sampled from AB, which were generally finer in size, were younger in age than those sampled on VB and ML, and as such the cyanobacterial community was less established, resulting in shorter time for growth and entanglement of the particles. Alternatively the holes sampled may have contained a lower content of cyanobacteria in comparison to other microorganisms (94). However the presence and composition of microbial communities was not analysed in this study, thus assumptions can only be made with respect to the presence and abundance of cyanobacteria. It is also possible that more particles in CHs from AB had reached a maximum size and disintegrated or broken down as consequence of freezing and transportation across the glacier surface resulting in mixtures of finer and larger particles (21, 93).

In conclusion, there are many interconnecting factors such as the mineral, OM content, microbial community structure and abundance, weathering, and other physical processes which may influence the size and colour of cryoconite particles within CHs (21, 22, 93, 94, 100). The factors identified may vary both within and between glaciers, hence the large heterogeneity in size and colour of cryoconite observed.

6.4.2 Variability in Elemental Concentrations in Cryoconite within a Glacier

Variability in elemental concentrations in cryoconite was observed within each glacier, although no clear trends were identified based on location of sample within each study site. Elements such as Ca, Mg, Pb, Cd, and As showed large standard deviations (Table 5.2), whereas elements such as Cr and Zn had much lower variability. Statistically significant differences in concentrations of elements determined in cryoconite sampled from holes on the same glacier in Svalbard has been published previously (10). For example, Singh et al. (2013) reported Cd concentrations in cryoconite on ML to range from: 0.043 to 0.144 μg g^{-1} (cryoconite from ML in this study: 0.043 – 0.095 μg g^{-1}) and Pb concentrations to range from 49.87 to 85.08 μg g^{-1} (cryoconite from ML in this study: 48.8 – 90.2 μg g^{-1}) (10).

The heterogeneity in the crustal elements (Ca and Mg) contained within the cryoconite may be due the deposition of different natural sources of wind-blown mineral debris (101, 113). The spatial variability in the concentrations of heavy metals and metalloids in cryoconite, such as

Pb, As, and Cd which have previously discussed as having natural and/ or anthropogenic sources outside of the local crust, may be the result of variations in the age of each of the CHs leading to differences in the extent of accumulation (96). For example, newly established CHs are exposed to the atmosphere for a shorter duration, resulting in lower levels of element accumulation compared to older holes (97). It could therefore be expected that the spatial variability across a glacier changes on a yearly basis due to the formation of new CHs from new wind-blown mineral deposits.

Additionally cryoconite holes may melt or be destroyed by supraglacial channels (105). The consequence could be either the release of cryoconite from the glacier to the wider proglacial environment, or the redistribution of older cryoconite material, and microbial communities via supraglacial meltwater transport across the glacier surface to form new or join previously established CHs (43, 97, 107, 115, 121). Thus the spatial variability may also be influenced by the extent and route of supraglacial streams (31). The variation in elemental concentrations between holes may also be a consequence of heterogeneity in the distribution of microbial communities between holes (94). Those holes with a high biomass of cyanobacteria may lead to higher accumulation of those elements with a high affinity for EPS (116, 252).

6.4.3 Variability in Elemental Concentrations in Cryoconite Holes Between Glaciers

Variability in the concentrations of elements present in cryoconite holes between glaciers was also observed in this study. Clear clusters were noted in the PCA plots for the three glaciers (Fig. 5.12) and significant differences were observed in the selected elements in both cryoconite and cryoconite hole water between locations (Fig. 5.11).

As discussed in Section 6.1, the source of the major elements in cryoconite (Al, Fe, Ca, and Mg) and the trace elements Zn and Cr, is likely to be of geological origin, from rock and mineral dust. It is plausible that a significant source of the inorganic fraction originates from local rock (101). The rocks surrounding the three glaciers exhibit both similarities and differences in geology. Midtre Lovénbreen shares a similar geology to the upper eastern section of AB, and VB shares a similar geology to the western side of AB, as described in Section 4.1.1 (Fig. 4.3). Whilst the rock surrounding ML is dominated by aluminosilicates such as garnet mica schist, quartzite, and phyllite; carbonate rock in the form of marble, carbonate beds, and quartz carbonate schist are also present which incorporate the elements Ca and Mg into the mineral

structure. The rock surrounding VB, and a section of AB, also contains aluminosilicates, however a large variety of carbonate and sulphate based rock containing Ca and Mg is present in the local geology of VB which is not reflected in the rock surrounding ML, such as limestone, dolomite, anhydrite, calcareous sandstone, and gypsum (Section 4.1.1) (7).

Given the large variation in rocks and minerals surrounding the three glaciers which can contain a variety of elements to differing extents, it is not possible to identify a single specific rock source for the cryoconite sampled (100). In addition, the minerology of the cryoconite were not analysed, thus assumptions have been made based on geological data from the Norwegian Polar Institute (Fig. 4.3) (7). However some patterns were observed, which may be explained by the overall dominance of, for example, carbonate based rock compared to aluminosilicate based rock. As a consequence, significant differences may be expected in the major elemental concentrations in cryoconite from ML compared to VB. Based on the location of AB (Fig 4.1), elemental concentrations in cryoconite from AB would be expected to bridge the gap between the two glaciers. For elements: Al, Fe, Zn, Cd, and Cr (Fig 5.11) the expected trend was observed. On the other hand, the PCA plot (Fig 5.12) did not show this trend, with the AB cluster being separated from VB by ML, suggesting elemental concentrations in cryoconite from VB were more similar to ML, than AB. The elements Pb and As (Fig. 5.11); and Ca, and Mg (Fig. B.5.1 & B.5.2) followed the trend shown in the PCA plot, with statistically similar concentrations of these elements measured in cryoconite from ML and VB in comparison to AB.

Major Elements

The concentration of Al was significantly higher in cryoconite from AB and ML compared to VB, reflecting the dominance of aluminosilicate based rock surrounding the two glaciers. The Al concentration in cryoconite from AB was also found to be significantly higher than in cryoconite from ML, which may be due to the larger variation in rock type surrounding AB. The significantly higher Fe concentrations in cryoconite from ML and AB, may be due to the presence of a higher proportion of minerals containing Fe^{2+} and Fe^{3+} ions such as chlorite, amphibole and mica. As previously discussed, the red sandstone observed in rock surrounding AB may be high in the Fe containing mineral hematite, thus higher concentrations of Fe would be expected in cryoconite from AB. In general this was the case, although Fe concentrations in cryoconite from AB were not statistically significantly higher than from ML.

As mentioned, the concentrations of Ca and Mg in cryoconite across the three glaciers did not reflect the expected pattern. Given the dominance of carbonate based rock surrounding VB and part of AB, significantly higher concentrations of Ca and Mg in cryoconite from AB and VB would be expected over ML. However, no such significant differences were observed (Fig. B.5.2). Large standard deviations were noted in the concentrations of Ca in cryoconite from AB and VB, which given the small sample size makes the interpretation of results less reliable. In contrast, a much smaller standard deviation was observed in the concentration of Ca in cryoconite from ML (2600 ± 146 μg g^{-1} from ML; compared to 18500 ± 46500 μg g^{-1} in VB, Table 5.11). Three of the ten cryoconite samples collected on VB had higher concentrations of Ca than the remaining seven cryoconite, with concentrations of 10200 μg g^{-1}, 8000 μg g^{-1} and 151000 μg g^{-1} compared to a mean of 2290 ± 288 μg g^{-1} across the remaining seven samples (Table B.3.1). The cryoconite containing higher levels of Ca may have been formed from wind-blown mineral debris from Ca based rock surrounding VB whereas as discussed in Section 6.4.2 it is possible that the other seven cryoconite may have been formed from wind-blown debris from the other rock/mineral types present in the local area (101, 113). The high concentrations in some cryoconite from VB indicate that an influence from the local rock is still present.

Given the close proximity of the three glaciers, it is possible that wind-blown dust, which forms a substantial part of cryoconite found on each glacier, may originate from the rock surrounding any of the three glaciers (21). This could therefore explain the differences observed in elemental concentration compared to the original expectations.

Trace Elements

Of the trace elements in cryoconite, Zn and Cr were discussed in Section 6.1 to have a strong crustal influence. Zinc concentrations followed the same trend across locations as Fe with significantly higher concentrations observed in cryoconite from ML and AB compared to VB (Table 5.11). A study by Singh et al. (2017) also reported lower concentrations of Zn in cryoconite from VB compared to AB (98). Given that Zn correlated strongly with Fe (Fig. 5.12, Table 5.13), a similar source may be responsible for the Zn measured in cryoconite across the three glaciers. Zinc is commonly found with sulphur as sphalerite; however Zn and S were found at opposite sides of the PCA plot, indicating a lack of association (Fig. 5.12). This suggests that Zn may be present in a different form (239).

In contrast, Cr was found to be present at statistically significantly higher concentrations in cryoconite from VB compared to ML, with AB bridging the gap between the two locations

(Fig. 5.11). This trend also supports a potential local rock source, given the shared geology of AB with ML and VB. In the PCA plot (Fig. 5.12), Cr was found to be closely associated with nickel, both of which can be present in the mineral structure of chlorite. Chlorite can be found in quartzite and phyllite (Table 4.2), which is present in the rock surrounding ML; but also in shale which is present both in the rock surrounding AB and VB, and at the bottom edge of the two glaciers (Fig. 4.3, yellow and orange colours). Cryoconite sampled on VB were located in the lower section of the glacier (Fig. 4.7), and it is possible that the area sampled may be influenced by wind-blown dust from the lower proglacial area, thus providing a potential explanation for the higher concentrations of Cr in cryoconite from VB.

The elements Pb, As, and Cd were discussed in Section 6.1 as having a source other than of geological origin, either natural or anthropogenic, leading to elevated concentrations over UCC levels. Thus the local geology cannot be used as an explanation for trends observed between glaciers. Cadmium concentrations were enriched in cryoconite from VB. In fact, concentrations of Cd were found to be statistically significantly higher in cryoconite from VB compared to ML (Fig. 5.11). Potential reasons for the elevated concentrations of Cd have been discussed in Section 6.1.2. Concentrations of Pb and As on the other hand were found to be statistically significantly higher in cryoconite from ML and VB, than AB.

Glaciers ML and VB are approximately 6.5 km apart, separated by AB. The lower concentrations of Pb and As in cryoconite collected from AB may be the result of reduced binding affinity of Pb and As as opposed to different local sources impacting ML and VB separately. As previously discussed, Pb has been found to be significantly correlated with OM (9). In addition to OM, clay and carbonate content are also believed to contribute to increased sorption ability of Pb in soils (242). The local geology of AB is similar to both ML and VB, thus the mineral influence on binding (clay and carbonate) may not be the main cause of the lower Pb and As concentrations in AB cryoconite. It is perhaps more likely that lower levels of OM may result in a lower sorption efficiency of Pb in cryoconite from AB. Indeed, Edwards et al. (2011) reported statistically significantly lower percentage organic content, sediment primary production and respiration rates in cryoconite holes from AB compared to ML and VB (31). The lower primary production suggests a lower content of cyanobacteria, and as a consequence lower levels of EPS, which may explain the finer sized particles in addition to a reduced binding capacity for elements such as Pb^{2+} (93, 94, 116, 252). Although the OM content of the cryoconite is not known in this study, the darker colouration of two cryoconite from ML and two from VB, as previously discussed, indicates a potential elevated OM content in the

form of humic substances, which also have an affinity for Pb. Thus it is possible that the differences in the bacterial communities on AB in comparison to ML and VB have a strong influence on the variations in Pb levels.

Cryoconite holes from AB may be more isolated than those from ML and VB (31). This could be due to differences in supraglacial drainage patterns of meltwater across the glaciers (31). A long cold polar glacier such as AB may have more distinct supraglacial drainage with fewer channels branching over the ablation zone of the glacier where cryoconite are located, in comparison to shorter glaciers such as ML and VB (31, 33). If the cryoconite holes were more hydrologically linked, a potentially higher degree of replenishment of dissolved elements, nutrients, cryoconite and microbial communities may occur (31, 33, 92, 115, 121). The replenishment of nutrients may support microbial growth within a hole, and thus potentially increase the OM (including EPS) content, which as a consequence may lead to increased Pb binding (31, 43). The replenishment of dissolved elements may also result in a higher degree of scavenging by cryoconite, leading to higher accumulation of elements such as Pb, As and Cd (96).

In contrast to Pb, As in the form As(V) has an affinity for Fe and Mn oxides in addition to clay (239). It could therefore be expected that higher concentrations of As would be found in cryoconite from AB given that the samples from AB contained statistically significantly higher concentrations of Fe than those from VB. However this was not the case, indicating that other processes were occurring in the cryoconite holes leading to the significantly lower concentrations of As on AB. Singh et al. (2017) also found concentrations of As to be elevated in VB compared to AB (98). Differences in for example pH, or redox potential, in CHs from AB, which impact speciation of As and thus its solubility, may alter the accumulation ability of the cryoconite (239).

Similar trends across glacier locations were observed in cryoconite hole water for elements Fe, Pb, As, Cd, and Cr (Fig. 5.11), some of which may be attributed to the relative concentrations of elements in the underlying cryoconite sediment. In contrast, the trend in the concentration of Al in CW did not reflect that of the underlying sediment. These findings indicate that other processes are occurring in CHs, influenced by for example pH, valence state of the metal, redox potential, the presence of DOM and colloids, and the presence of clays and organic matter with high surface areas and charges for binding (6, 74, 77). These properties may have an influence on the speciation of the elements, and may provide an explanation for the variations observed

(6). Overall the reflection of the trends in both the cryoconite sediment and water by location shows the influence of sediment dissolution, or scavenging, on the concentrations of elements in the overlying water contained within cryoconite holes.

6.4.4 The Carbon Content of Cryoconite

The total carbon (TC) content of cryoconite was low at an average of 2.6 %, which is comparable to reported results from Takeuchi et al. (2001) where a carbon content of 2.7 % was measured (21). Wind-blown material, the majority of which originates from mineral fragments, was also analysed by Takeuchi et al. (2001) and was found to have a TC content of 0.55 % (21). Given the dominance of the mineral fraction in cryoconite, supported by the high Fe and Al concentrations measured in this study, the low TC content determined is in agreement with the general composition of cryoconite. Of the TC present in cryoconite, the majority is dominated by TOC (mean TOC content = 1.6 %). It has been well documented that microbial communities are an important component of cryoconite (18, 102). A study by Stibal et al. (2008) suggested that the OC content of cryoconite is mostly related to microorganism cells, in addition to structureless organic particulate components (amorphous organic matter) (102). Microorganisms and their decaying components may therefore provide an explanation as to the high proportion of TOC in TC, and thus samples with low TOC content may represent a younger cryoconite hole, more recently formed (96).

The TIC content was lower than originally expected given the high proportion of inorganic matter in cryoconite. However, TIC in this study was found to be comparable with a study by Xu et al. (2010) which reported a TIC content of 0.05 ± 0.02 % in cryoconite from the Athabasca Glacier in the Canadian Rocky Mountains (259). Total inorganic carbon is predominantly carbon dioxide (CO_2), found in the atmosphere. In water, it dissolves and forms species such as carbonic acid (H_2CO_3), bicarbonate (HCO_3^-), and carbonate (CO_3^{2-}) (260). In soils, TIC originates from carbonate minerals, primarily dolomite ($MgCO_3$) and calcite ($CaCO_3$) (233). Carbon dioxide from the atmosphere, dissolved in the cryoconite hole water may act as an acid, dissolving the mineral particles present in the cryoconite to release dissolved inorganic carbon (DIC) species. For example, in the dissolution of calcite (260):

$$CO_2\,(aq) + H_2O + CaCO_3(s) \rightleftharpoons 2HCO_3^- + Ca^{2+}$$

The inorganic carbon fraction of cryoconite may therefore be in its dissolved form as DIC in the CW, rather than present in the solid material, thus providing a possible explanation for the low TIC content of cryoconite material. Indeed, Ca concentrations in cryoconite were significantly depleted compared to crustal levels, thus it is possible that due to the solubility of Ca, dissolution is likely to have occurred from the cryoconite into the cryoconite hole water (43). Sample 25 was found to contain high concentrations of Ca and Mg in both the cryoconite and CW, as well as an elevated conductivity (36.7 μS cm^{-1}). The correspondingly high TIC content of 6.6 % indicates that the sample may be very high in minerals such as dolomite and/or calcite. Indeed the local lithology of VB, as described in Section 4.1.1 contains dolomite and limestone (usually in the form of aragonite or calcite), which may well represent the mineral base of the cryoconite found in this sample (7).

Variations in the TOC, ROC, and TIC content in cryoconite between locations was observed (Table 5.5). The mean TOC content of cryoconite in ML was 2.2 ± 0.51 % which is of a similar value to TOC content (3.27 %) reported in cryoconite sampled on ML by Langford et al. (2010) (94). Total organic carbon content in cryoconite from AB and VB was slightly lower, particularly in cryoconite from AB. As previously discussed, Edwards et al. (2011) found significantly lower percentage organic content on AB in comparison to VB and ML (31). The TOC content, a component of OM, was also found at slightly lower average levels from AB when compared to VB and ML in this study, although due to small sample sizes it is not possible to determine statistical significance between locations. The lower OC content in cryoconite from AB may be due to a different microbial structure inhabiting this glacier (31). Residual oxidisable carbon was also slightly lower in cryoconite from AB, although marginally higher TIC was observed in cryoconite from AB and VB compared to ML. As previously discussed, the rock surrounding AB and VB, which contains among others dolomite and calcite, may explain the higher TIC content in cryoconite from the two glaciers (7).

6.5 Similarities and Differences in Supraglacial Deposits

Different forms of supraglacial debris exist on glaciers (33, 125). In this study, in addition to cryoconite, supraglacial debris from small mounds on the glacier surfaces (SGD-M) as well as small isolated pieces of debris were sampled and analysed. The isolated pieces of debris (SGD-P) had very clear and observable plant content, and as can be expected contained a significantly higher TOC content (mean 18 ± 15 %) than the other sample types analysed (Table 5.5). The

TIC and ROC content of the SGD-P samples were however comparable to both cryoconite and SGD-M. The SGD-M samples demonstrated a very similar TOC, ROC, and TIC content to cryoconite, in particular to cryoconite from ML.

The elements that dominated the composition of cryoconite were also present in similar proportions to both SGD-P and SGD-M samples as described in Section 5.1.2. Calcium however made up a smaller proportion of SGD-M in comparison to SGD-P and cryoconite, which were comparable (Table 5.2). Similarities in the concentrations of most elements was observed between cryoconite and SGD-M samples, although it was not possible to determine the statistical significance of any differences between the two sample types due to the small sample size of SGD-M. Lead was however present at higher concentrations in SGD-M and SGD-P samples (mean concentrations of 79.7 ± 23.4 µg g^{-1} and 71.2 ± 78.4 µg g^{-1} respectively) compared to the mean concentration in cryoconite (mean: 50.0 ± 25.0 µg g^{-1}). Supraglacial debris also showed higher EFs for Pb compared to cryoconite, with mean EFs of 10.4 and 15.0 for SGD-M and SGD-P respectively compared to a mean EF of 6.85 for cryoconite (Table 5.4). Both SGD-M and SGD-P samples were dark in colour, and as discussed in Section 6.1.1 the possible presence of larger quantities of quality OM may be responsible for both the dark colour and thus the elevated Pb concentrations (9, 22). The similarities in elemental concentrations, in addition to TOC, ROC, and TIC content between SGD-M and cryoconite samples is an indication that this material may originate from cryoconite melted out of cryoconite holes. In contrast, the large differences in mean elemental concentrations and TOC content in the SGD-P samples indicate a very different source than cryoconite. Finally, the SGD-M samples were of a similar appearance to the cryoconite mantles described by Hodson et al. (2008) and it is therefore possible that the debris sampled is melted out and accumulated cryoconite (33).

The concentrations of the polluting elements in SGD-M and SGD-P samples were compared to the Norwegian Environmental Agency quality standards for sediment (in freshwater) (238). Arsenic and Cd concentrations were found at ‘background’ levels in all samples. Chromium concentrations were also at ‘background’ levels in all SGD-P samples and three of the four SGD-M samples, the final SGD-M sample was categorised as having ‘good’ levels of Cr. Zinc concentrations in all SGD-P samples were at ‘background’ levels, whereas, all SGD-M samples contained ‘good’ levels of Zn. In agreement with cryoconite, SGD samples were also the most polluted with Pb. Two of the four SGD-M samples, and one SGD-P sample contained Pb at ‘moderate’ levels of pollution, only one SGD sample (SGD-P) contained ‘background’ levels of Pb, the remaining samples were classified as ‘good’ (238).

6.6 Sources of Error

Contamination and sources of error can occur in a project analysing trace levels of contaminants present in environmental samples, even with strong QA and QC measures in place. As a consequence of limitations in resource availability and the scale of a master project, some QC measures were not performed which would have strengthened the reliability of the data and the conclusions drawn. For example, the use of field blanks and transport blanks would have identified potential background contamination at the glacier during sampling, and during the transport of samples to the laboratory at NTNU. Despite quality control procedures in place, such as the use of method blanks during the sample pre-treatment step, and the use of reagent and solvent blanks, it is not possible to completely eliminate contamination throughout the entire process, and some error may therefore be present in the quantification of elements particularly those with many potential external sources for contamination.

The cryoconite solid samples were diluted 50 times for analysis by ICP-MS as a consequence of the high concentrations of Fe and Al present. This may have caused the levels of Hg present in cryoconite to fall below detection, thus preventing quantification. It is not possible to accurately conclude that cryoconite do not accumulate Hg given the high levels of dilution.

The use of HNO_3 for the digestion of cryoconite and SGD samples for ICP-MS analysis resulted in precipitation, and therefore a loss of analyte. This may mean that the concentrations of some elements may be underestimated, particularly silicon.

Matrix effects on the GC-MS column were high, and low accuracy was noted when analysing the reference material. It is possible that the GC column was contaminated by previous use, leading to the presence of additional active sites, and a reduction in elution of target analytes. If this is the case, then the concentrations of PCBs, and PAHs may be underestimated. The spiking of matrix matched samples should enable the compensation for matrix effects, however if the column was already dirty from previous analysis, then it may be difficult to accurately determine the specific contribution of the cryoconite matrix to reduction in the target analyte signal.

6.7 Limitations and Further Research

The discussions provide many unanswered questions and a number of assumptions. As a consequence of the limitations in both time and funds for a master project, decisions and

priorities were made on the number and type of samples, the parameters to be measured and the analysis performed. Assumptions have been made in this study as a consequence of unavailable data which may have provided a more complete picture of the various interactions occurring within cryoconite holes. Many studies have focussed on a few aspects of cryoconite holes, such as the water composition and microbial presence, or the cryoconite composition (both organic and inorganic), and these studies demonstrate the presence of important abiotic and biotic interactions. However to the best of our knowledge, there are no studies that provide the complete picture of interactions occurring within cryoconite holes, and as such there is still missing knowledge on exactly how these holes can accumulate certain trace elements, radionuclides and POPs. With this lack of knowledge, it is difficult to draw accurate conclusions on the impact that climate change and the accelerated melting of glaciers will have on the soil and water systems once the components of cryoconite holes are released from the ice. Given the heterogeneity of cryoconite holes and the many external factors that can influence the concentrations of both inorganic and organic matter within these holes, taking samples and parameters to analyse all the components mentioned below at a specific point in time may help to provide a more complete picture of all the interactions occurring within cryoconite.

The size and depth of the CHs may have provided interesting and additional insight into the accumulation ability of elements. It may have also provided an indication of the potential age of some of the CHs, as newer holes may be shallower. Variations in the concentration of elements in CW between locations and holes may be the result of variations in the speciation of these elements. Parameters such as pH, redox potential, turbidity, and analysis of DOM would have provided additional data to support the assumptions and conclusions made. Speciation studies may have also provided insight into the fate of the mineral fraction of cryoconite once contained within the holes.

Knowledge of the composition of the microbial communities and their biomass within the cryoconite holes would have provided information to support assumptions made regarding the influence of cyanobacteria on the ability of cryoconite to accumulate selected trace elements, and may have aided in the explanation of the differences identified in accumulation between locations.

Only a small number of samples were obtained for the mud deposits (SGD-M) on the surface of the glacier. Although only found at a low frequency on the glacier surface, a larger sample size would have enabled the use of statistical tools to compare this material to the cryoconite

collected from cryoconite holes, which would have helped support the conclusions drawn with respect to the origin of this material.

The detection of some PAHs indicate that the cryoconite are exposed to these airborne pollutants. As such further research could be performed on method development, in particular with respect to sample pre-treatment steps in-order to optimise the detection of these pollutants in cryoconite. This further research may be important in monitoring changes in the release of POPs into the atmosphere and their ability to be transported to the Arctic.

7 Conclusion

The results from cryoconite studied on Midtre Lovénbreen, and Austre and Vestre Brøggerbreen demonstrated accumulation of trace elements Cd, Pb, and As leading to elevated concentrations above average UCC levels. In contrast, Zn was only mildly enriched, and Cr levels in cryoconite were found to be depleted indicating a geological origin. Cryoconite were most polluted with Pb, demonstrating moderate pollution levels in several cryoconite samples. Lead was also found to be elevated in cryoconite compared to other matrices reviewed in the literature from the Ny-Ålesund area. Thus cryoconite may be of particular use in monitoring Pb, in addition to As contamination, derived from atmospheric deposition from anthropogenic sources.

The major elements in CW and snow differed, with CW being dominated by Ca, indicating a freshwater origin, whilst snow was dominated by elements Na and Cl indicating a marine influence. As such it may be assumed that cryoconite hole water is derived mostly from glacier ice melt water. The concentrations of Pb, Cr, and Cd were not significantly different between the two sample types, but As and Zn showed significantly higher concentrations in CW, indicating a potential influence from cryoconite dissolution.

Accumulation of contaminants from direct atmospheric deposition in addition to scavenging of impurities from glacier meltwater (also of atmospheric origin), generated from melted snow and ice, could be responsible for the elevated concentrations observed in cryoconite. The high binding capacity of OM (for example humic substances and EPS) contained within cryoconite may explain the scavenging ability for elements such as Pb. The age of the cryoconite may also impact levels of accumulation, with cryoconite holes containing elevated concentrations of certain elements such as Cd, Pb and As being older than those containing lower concentrations.

Large variation in the physical and chemical properties of cryoconite was observed both within and between glaciers. Differences in cryoconite colour and particle size were identified in addition to large variability in cryoconite hole shape. The concentrations of elements also showed spatial variability both within and between glaciers. In addition, dark coloured cryoconite, such as those found on ML and VB accumulated higher concentrations of Pb compared to the lighter coloured samples. Many factors may be responsible for the heterogeneity observed both within and between glaciers. For example, variations in cryoconite age, the presence and abundance of cyanobacteria, the OM content, the pH and redox potential

of the CHs (impacting speciation), the glacier structure, supraglacial drainage, and the local geology may all lead to spatial variability in the physical and chemical properties of cryoconite and cryoconite holes.

Although PCBs were not detected, it is possible that these contaminants were present, but at very low concentrations. Recoveries were reasonable, but large negative matrix effects were found. Development of a sample preparation method to include more extensive clean up and concentration steps may reduce matrix effects and enable PCB detection. The presence of PAHs indicates the ability of cryoconite to accumulate this contaminant group, and future research to analyse PAH concentrations will also be of importance for future monitoring.

Long term environmental monitoring in the Arctic can provide information on the natural levels of chemicals in the area, and can therefore be used as a warning system for alterations in the global distribution of contaminants. It is therefore important to regularly monitor the levels of contaminants present in the atmosphere in this remote Arctic region and the ability of cryoconite to accumulate trace elements and metalloids is important in its role as a potential monitoring tool.

8 References

1. Arctic Monitoring and Assessment Programme (AMAP). Arctic Pollution Issues: A State of the Arctic Environment Report [Internet, Report]. Oslo, Norway: AMAP; 1997 [cited 2022 3 May]. Available from: https://www.amap.no/documents/doc/arctic-pollution-issues-a-state-of-the-arctic-environment-report/67.
2. Aslam SN, Huber C, Asimakopoulos AG, Steinnes E, Mikkelsen Ø. Trace elements and polychlorinated biphenyls (PCBs) in terrestrial compartments of Svalbard, Norwegian Arctic. Science of the Total Environment. 2019;685:1127-38.
3. Arctic Monitoring and Assessment Programme (AMAP). Arctic Pollution 2002 [Internet, Report]. Oslo, Norway: AMAP; 2002 [cited 2022 3 May]. Available from: https://www.amap.no/documents/doc/arctic-pollution-2002/69.
4. Barbante C, Spolaor A, Cairns WRL, Boutron C. Man's footprint on the Arctic environment as revealed by analysis of ice and snow. Earth-Science Reviews. 2017;168:218-31.
5. Wania F, Mackay D. Global fractionation and cold condensation of low volatility organochlorine compounds in polar-regions. Ambio. 1993;22(1):10-8.
6. Ward NI. Trace elements. In: Fifield FW, Haines PJ, editors. Environmental Analytical Chemistry. 2nd ed: Blackwell Science Ltd; 2000. p. 360 - 92.
7. Hjelle A, Piepjohn K, Saalmann K, Ohta Y, Thiedig F, Salvigsen O, et al. Geological map of Svalbard 1:100,000, sheet A7G Kongsfjorden - With map description. Temakart nr. 30. [Internet]. 1999 [cited 2022 25 January]. Available from: https://geokart.npolar.no/geologi/GeoSvalbard/#11/78.9053/11.7776.
8. Wedepohl KH. The Composition of the Continental Crust. Geochimica Et Cosmochimica Acta. 1995;59(7):1217-32.
9. Lokas E, Zaborska A, Kolicka M, Rozycki M, Zawierucha K. Accumulation of atmospheric radionuclides and heavy metals in cryoconite holes on an Arctic glacier. Chemosphere. 2016;160:162-72.
10. Singh SM, Sharma J, Gawas-Sakhalkar P, Upadhyay AK, Naik S, Pedneker SM, et al. Atmospheric deposition studies of heavy metals in Arctic by comparative analysis of lichens and cryoconite. Environmental Monitoring and Assessment. 2013;185(2):1367-76.
11. de Voogt P, Brinkman UT. Production, properties and usage of polychlorinated biphenyls. In: Kimbrough RD, Jensen AA, editors. Halogenated biphenyls, terphenyls, naphthalenes, dibenzodioxins and related products. 2nd ed. Amsterdam: Elsevier Science Publishers B.V.; 1989. p. 3-45.
12. Eckhardt S, Breivik K, Mano S, Stohl A. Record high peaks in PCB concentrations in the Arctic atmosphere due to long-range transport of biomass burning emissions. Atmospheric Chemistry and Physics. 2007;7(17):4527-36.
13. Maturilli M, Herber A, Konig-Langlo G. Climatology and time series of surface meteorology in Ny-Alesund, Svalbard. Earth System Science Data. 2013;5(1):155-63.
14. Adakudlu M, Andresen J, Bakke J, Beldring S, Benestad R, Bilt W, et al. Climate in Svalbard 2100 - a knowledge base for climate adaptation. NCCS report no. 1/2019. [Internet]. Norwegian Centre for Climate Services (NCSS); 2019 [cited 2022 14 May]. Available from: https://www.miljodirektoratet.no/globalassets/publikasjoner/M1242/M1242.pdf.
15. Pfeffer WT, Arendt AA, Bliss A, Bolch T, Cogley JG, Gardner AS, et al. The Randolph Glacier Inventory: a globally complete inventory of glaciers. Journal of Glaciology. 2014;60(221):537-52.
16. Nuth C, Kohler J, Konig M, von Deschwanden A, Hagen JO, Kaab A, et al. Decadal changes from a multi-temporal glacier inventory of Svalbard. Cryosphere. 2013;7(5):1603-21.
17. Wharton RA, McKay CP, Simmons GM, Parker BC. Cryoconite holes on glaciers. Bioscience. 1985;35(8):499-503.
18. Gerdel RW, Drouet F. The Cryoconite of the Thule Area, Greenland. Transactions of the American Microscopical Society. 1960;79(3):256-72.

19. Sawstrom C, Mumford P, Marshall W, Hodson A, Laybourn-Parry J. The microbial communities and primary productivity of cryoconite holes in an Arctic glacier (Svalbard 79 degrees N). Polar Biology. 2002;25(8):591-6.
20. Zawierucha K, Ostrowska M, Vonnahme TR, Devetter M, Nawrot AP, Lehmann S, et al. Diversity and distribution of Tardigrada in Arctic cryoconite holes. Journal of Limnology. 2016;75(3):545-59.
21. Takeuchi N, Kohshima S, Seko K. Structure, formation, and darkening process of albedo-reducing material (cryoconite) on a Himalayan glacier: A granular algal mat growing on the glacier. Arctic, Antarctic, and Alpine Research. 2001;33(2):115-22.
22. Takeuchi N. Optical characteristics of cryoconite (surface dust) on glaciers: the relationship between light absorbency and the property of organic matter contained in the cryoconite. Annals of Glaciology. 2002;34:409-14.
23. Halbach K, Mikkelsen Ø, Berg T, Steinnes E. The presence of mercury and other trace metals in surface soils in the Norwegian Arctic. Chemosphere. 2017;188:567-74.
24. Humlum O, Instanes A, Sollid JL. Permafrost in Svalbard: a review of research history, climatic background and engineering challenges. Polar Research. 2003;22(2):191-215.
25. Hagen JO, Liestøl O, Roland E, Jørgensen T. Glacier Atlas of Svalbard and Jan Mayen. Meddelelser Nr. 129 [Internet]. Oslo: Norsk Polarinstitutt; 1993 [cited 2022 24 April]. Available from: https://brage.npolar.no/npolar-xmlui/handle/11250/173065.
26. Svendsen H, Beszczynska-Møller A, Hagen JO, Lefauconnier B, Tverberg V, Gerland S, et al. The physical environment of Kongsfjorden–Krossfjorden, an Arctic fjord system in Svalbard. Polar Research. 2002;21(1):133-66.
27. Shears J, Theisen F, Bjørdal A, Norris S. Environmental impact assessment: Ny-Ålesund international scientific research and monitoring station, Svalbard. Meddelelser no. 157 [Internet, Report]. Tromsø, Norway: Norsk Polarinstitutt; 1998 [cited 2022 14 May]. Available from: https://brage.npolar.no/npolar-xmlui/handle/11250/173051?locale-attribute=en.
28. Statistics Norway. Population of Svalbard [Internet]. Statistics Norway,; 2021 [updated 14 October 2021; cited 2022 24 April]. Available from: https://www.ssb.no/en/befolkning/folketall/statistikk/befolkningen-pa-svalbard.
29. Statistics Norway. This is Svalbard 2016. What the figures say. [Internet]. Statistics Norway; 2016 [cited 2022 24 April]. Available from: https://www.ssb.no/en/befolkning/artikler-og-publikasjoner/_attachment/294354?_ts=15a12de02c0.
30. Anesio AM, Mindl B, Laybourn-Parry J, Hodson AJ, Sattler B. Viral dynamics in cryoconite holes on a high Arctic glacier (Svalbard). Journal of Geophysical Research. 2007;112(G04S31).
31. Edwards A, Anesio AM, Rassner SM, Sattler B, Hubbard B, Perkins WT, et al. Possible interactions between bacterial diversity, microbial activity and supraglacial hydrology of cryoconite holes in Svalbard. Isme Journal. 2011;5(1):150-60.
32. National Snow & Ice Data Centre (NSIDC). All About Glaciers [Internet]. NSIDC; n.d. [updated 16 March 2020; cited 2022 13 May]. Available from: https://nsidc.org/cryosphere/glaciers.
33. Hodson A, Anesio AM, Tranter M, Fountain A, Osborn M, Priscu J, et al. Glacial ecosystems. Ecological Monographs. 2008;78(1):41-67.
34. Hambrey MJ, Glasser NF. Sediment Entrainment, Transport, and Deposition. In: Singh VP, Singh P, Haritashya UK, editors. Encyclopedia of Snow, Ice and Glaciers. Netherlands: Springer, Dordrecht; 2011. p. 984-1003.
35. Paterson WSB. Distribution of Temperature in Glaciers and Ice Sheets. The Physics of Glaciers. 3rd ed: Butterworth-Heinemann; 1994. p. 204 - 37.
36. Glasser NF. Polythermal Glaciers. In: Singh VP, Singh P, Haritashya UK, editors. Encyclopedia of Snow, Ice and Glaciers. Netherlands: Springer, Dordrecht; 2011. p. 865-7.
37. Blatter H, Hutter K. Polythermal conditions in arctic glaciers. Journal of Glaciology. 1991;37(126):261-9.
38. Hagen JO, Kohler J, Melvold K, Winther J-G. Glaciers in Svalbard: mass balance, runoff and freshwater flux. Polar Research. 2003;22(2):145-59.
39. Tranter M, Brown GH, Hodson AJ, Gurnell AM. Hydrochemistry as an indicator of subglacial drainage system structure: A comparison of Alpine and sub-polar environments. Hydrological Processes. 1996;10(4):541-56.

40. Fountain AG, Tranter M, Nylen TH, Lewis KJ, Mueller DR. Evolution of cryoconite holes and their contribution to meltwater runoff from glaciers in the McMurdo Dry Valleys, Antarctica. Journal of Glaciology. 2004;50(168):35-45.
41. van der Veen CJ. Fracture propagation as means of rapidly transferring surface meltwater to the base of glaciers. Geophysical Research Letters. 2007;34(1).
42. Blais JM, Schindler DW, Muir DCG, Sharp M, Donald D, Lafreniere M, et al. Melting glaciers: A major source of persistent organochlorines to subalpine Bow Lake in Banff National Park, Canada. Ambio. 2001;30(7):410-5.
43. Owens PN, Blake WH, Millward GE. Extreme levels of fallout radionuclides and other contaminants in glacial sediment (cryoconite) and implications for downstream aquatic ecosystems. Scientific Reports. 2019;9:1-9.
44. Bogdal C, Schmid P, Zennegg M, Anselmetti FS, Scheringer M, Hungerbuhler K. Blast from the Past: Melting Glaciers as a Relevant Source for Persistent Organic Pollutants. Environmental Science & Technology. 2009;43(21):8173-7.
45. Arctic Monitoring and Assessment Programme (AMAP). Snow, Water, Ice and Permafrost in the Arctic (SWIPA) 2017 [Internet, Report]. Oslo, Norway: AMAP; 2017 [cited 2022 13 May]. Available from: https://www.amap.no/documents/doc/snow-water-ice-and-permafrost-in-the-arctic-swipa-2017/1610.
46. Reddy AVB, Moniruzzaman M, Aminabhavi TM. Polychlorinated biphenyls (PCBs) in the environment: Recent updates on sampling, pretreatment, cleanup technologies and their analysis. Chemical Engineering Journal. 2019;358:1186-207.
47. Ballschmiter K, Zell M. Analysis of polychlorinated biphenyls (PCB) by glass capillary gas chromatography. Composition of technical Aroclor- and Clophen-PCB mixtures. Fresenius Zeitschrift Fur Analytische Chemie. 1980;302(1):20-31.
48. Erickson MD, Kaley RG. Applications of polychlorinated biphenyls. Environmental Science and Pollution Research. 2011;18(2):135-51.
49. Hutzinger O, Safe S, Zitko V. Chapter 1: Introduction. The Chemistry of PCB's: CRC press; 2018. p. 1-6.
50. Breivik K, Sweetman A, Pacyna JM, Jones KC. Towards a global historical emission inventory for selected PCB congeners — a mass balance approach: 1. Global production and consumption. Science of The Total Environment. 2002;290(1):181-98.
51. Poland JS, Mitchell S, Rutter A. Remediation of former military bases in the Canadian Arctic. Cold Regions Science and Technology. 2001;32(2-3):93-105.
52. Sundahl M, Sikander E, Ek-Olaussen B, Hjorthage A, Rosell L, Tornevall M. Determinations of PCB within a project to develop cleanup methods for PCB-containing elastic sealant used in outdoor joints between concrete blocks in buildings. Journal of Environmental Monitoring. 1999;1(4):383-7.
53. Norris G, Al-Dhahir Z, Birnstingl J, Plant SJ, Cui S, Mayell P. A case study of the management and remediation of soil contaminated with polychlorinated biphenyls. Engineering Geology. 1999;53(2):177-85.
54. Jartun M, Ottesen RT, Volden T, Lundkvist Q. Local Sources of Polychlorinated Biphenyls (PCB) in Russian and Norwegian Settlements on Spitsbergen Island, Norway. Journal of Toxicology and Environmental Health, Part A. 2009;72(3-4):284-94.
55. Gabrielsen GW, Skaare JU, Polder A, Bakken V. Chlorinated hydrocarbons in glaucous gulls (Larus-hyperboreus) in the southern part of Svalbard. Science of the Total Environment. 1995;160-61:337-46.
56. Braathen M, Derocher AE, Wiig O, Sormo EG, Lie E, Skaare JU, et al. Relationships between PCBs and thyroid hormones and retinol in female and male polar bears. Environmental Health Perspectives. 2004;112(8):826-33.
57. Breivik K, Sweetman A, Pacyna JM, Jones KC. Towards a global historical emission inventory for selected PCB congeners — A mass balance approach: 3. An update. Science of The Total Environment. 2007;377(2):296-307.
58. Secretariat of the Stockholm Convention. The 12 initial POPs under the Stockholm Convention. [Internet]. n.d. [cited 2022 15 May]. Available from: http://chm.pops.int/TheConvention/ThePOPs/The12InitialPOPs/tabid/296/Default.aspx.

59. Arctic Monitoring and Assessment Programme (AMAP). AMAP Assessment 2015: Temporal Trends in Persistent Organic Pollutants in the Arctic. [Internet, Report]. Oslo, Norway: AMAP; 2016 [cited 2022 3 May]. Available from: https://www.amap.no/documents/doc/amap-assessment-2015-temporal-trends-in-persistent-organic-pollutants-in-the-arctic/1521.
60. Hung H, Katsoyiannis AA, Brorstrom-Lunden E, Olafsdottir K, Aas W, Breivik K, et al. Temporal trends of Persistent Organic Pollutants (POPs) in arctic air: 20 years of monitoring under the Arctic Monitoring and Assessment Programme (AMAP). Environmental Pollution. 2016;217:52-61.
61. Megson D, Benoit NB, Sandau CD, Chaudhuri SR, Long TY, Coulthard E, et al. Evaluation of the effectiveness of different indicator PCBs to estimating total PCB concentrations in environmental investigations. Chemosphere. 2019;237.
62. Wania F, Mackay D. Tracking the distribution of persistent organic pollutants. Environmental Science & Technology. 1996;30(9):A390-A6.
63. Wang-Andersen G, Skaare JU, Prestrud P, Steinnes E. Levels and congener pattern of PCBs in Arctic Fox, Alopex-lagopus, in Svalbard. Environmental Pollution. 1993;82(3):269-75.
64. Wolkers H, Lydersen C, Kovacs KM. Accumulation and lactational transfer of PCBs and pesticides in harbor seals (Phoca vitulina) from Svalbard, Norway. Science of the Total Environment. 2004;319(1-3):137-46.
65. Granberg ME, Ask A, Gabrielsen GW. Local contamination in Svalbard: overview and suggestions for remediation actions. Brief Report no. 044. [Internet]. Tromsø, Norway: Norsk Polarinstitutt; 2017 [cited 2022 25 April]. Available from: http://hdl.handle.net/11250/2456307.
66. Aas W, Gallet J-C, Halse AK, Hermansen O, Mikkelsen Ø, Pedersen CA, et al. Effects of rocket launches in Ny-Ålesund, 2018 - 2019. Observations of snow and air samples. NILU report 07/2021. [Internet, Report]. Kjeller, Norway: Norwegian Institute for Air Research; 2021 [cited 2022 14 February]. Available from: https://nyalesundresearch.no/2021/08/report-on-effects-of-rocket-launches-in-ny-alesund-2018-2019/.
67. Ali H, Khan E. Trophic transfer, bioaccumulation, and biomagnification of non-essential hazardous heavy metals and metalloids in food chains/webs-Concepts and implications for wildlife and human health. Human and Ecological Risk Assessment. 2019;25(6):1353-76.
68. Shaw D, Reilly G, Muysson J, Pattenden G, Campbell F. An estimate of the chemical composition of the Canadian Precambrian Shield. Canadian Journal of Earth Sciences. 1967;4(5):829-53.
69. Shaw DM, Dostal J, Keays RR. Additional estimates of continental surface Precambrian shield composition in Canada. Geochimica et Cosmochimica Acta. 1976;40(1):73-83.
70. Nriagu JO. A global assessment of natural sources of atmospheric trace metals. Nature. 1989;338(6210):47-9.
71. Nriagu JO, Pacyna JM. Quantitative assessment of worldwide contamination of air, water and soils by trace metals. Nature. 1988;333(6169):134-9.
72. Tack FMG. Trace Elements: General Soil Chemistry, Principles and Processes. In: Hooda PS, editor. Trace elements in soils: Blackwell Publishing Ltd.; 2010. p. 9-38.
73. Bradl HB. Adsorption of heavy metal ions on soils and soils constituents. Journal of Colloid and Interface Science. 2004;277(1):1-18.
74. Stumm W, Morgan JJ. Metal Ions in Aqueous Solution: Aspects of Coordination Chemistry. In: Schnoor JL, Zehnder A, editors. Aquatic Chemistry: Chemical Equilibria and Rates in Natural Waters. 3rd ed: Wiley-Interscience; 1996. p. 252 - 348.
75. Buffle J, Leppard GG. Characterization of Aquatic Colloids and Macromolecules. 1. Structure and Behavior of Colloidal Material. Environmental Science & Technology. 1995;29(9):2169-75.
76. Stumm W, Morgan JJ. Particle-Particle Interaction: Colloids, Coagulation, and Filtration. In: Schnoor JL, Zehnder A, editors. Aquatic Chemistry: Chemical Equilibria and Rates in Natural Waters. 3rd ed: Wiley-Interscience; 1996. p. 818 - 71.
77. Mostofa KMG, Liu C-q, Feng X, Yoshioka T, Vione D, Pan X, et al. Complexation of Dissolved Organic Matter with Trace Metal Ions in Natural Waters. In: Mostofa KMG, Yoshioka T, Mottaleb A, Vione D, editors. Photobiogeochemistry of Organic Matter. Berlin, Heidelberg: Springer; 2013. p. 769-849.

78. Hartnett HE. Dissolved Organic Matter (DOM). In: White WM, editor. Encyclopedia of Geochemistry: A Comprehensive Reference Source on the Chemistry of the Earth. Cham: Springer; 2018. p. 375-8.
79. Kuhn M. The nutrient cycle through snow and ice, a review. Aquatic Sciences. 2001;63(2):150-67.
80. Wania F. Assessing the potential of persistent organic chemicals for long-range transport and accumulation in polar regions. Environmental Science & Technology. 2003;37(7):1344-51.
81. Mackay D, Wania F. Transport of contaminants to the Arctic - partitioning, processes and models. Science of the Total Environment. 1995;160-61:25-38.
82. Leo A, Hansch C, Elkins D. Partition coefficients and their uses. Chemical Reviews. 1971;71(6):525-616.
83. Li NQ, Wania F, Lei YD, Daly GL. A comprehensive and critical compilation, evaluation, and selection of physical-chemical property data for selected polychlorinated biphenyls. Journal of Physical and Chemical Reference Data. 2003;32(4):1545-90.
84. Wania F, Mackay D. The Global Fractionation of Persistent Organic Pollutants. Report No. TR 10/96 [Internet, Report]. Kjeller, Norway: NILU, Norwegian Insitute for Air Research; 1996 [cited 2022 15 June]. Available from: https://nilu.brage.unit.no/nilu-xmlui/bitstream/handle/11250/2762224/TR-10-96.pdf?sequence=1.
85. Macdonald RW, Harner T, Fyfe J. Recent climate change in the Arctic and its impact on contaminant pathways and interpretation of temporal trend data. Science of the Total Environment. 2005;342(1-3):5-86.
86. Law KS, Stohl A. Arctic air pollution: Origins and impacts. Science. 2007;315(5818):1537-40.
87. Barrie LA. Arctic air-pollution - an overview of current knowledge. Atmospheric Environment. 1986;20(4):643-63.
88. Klonecki A, Hess P, Emmons L, Smith L, Orlando J, Blake D. Seasonal changes in the transport of pollutants into the Arctic troposphere-model study. Journal of Geophysical Research-Atmospheres. 2003;108(D4).
89. Gajda RT. Cryoconite phenomena on the Greenland Ice Cap in the Thule area. Canadian Geographer/Le Géographe canadien. 1958;3(12):35-44.
90. Nordenskiöld AE. Nordenskiöld on the Inland Ice of Greenland. Science. 1883;2(44):732-8.
91. Zarsky JD, Stibal M, Hodson A, Sattler B, Schostag M, Hansen LH, et al. Large cryoconite aggregates on a Svalbard glacier support a diverse microbial community including ammonia-oxidizing archaea. Environmental Research Letters. 2013;8(3).
92. Webster-Brown JG, Hawes I, Jungblut AD, Wood SA, Christenson HK. The effects of entombment on water chemistry and bacterial assemblages in closed cryoconite holes on Antarctic glaciers. FEMS Microbiology Ecology. 2015;91(12):1-14.
93. Hodson A, Cameron K, Boggild C, Irvine-Fynn T, Langford H, Pearce D, et al. The structure, biological activity and biogeochemistry of cryoconite aggregates upon an Arctic valley glacier: Longyearbreen, Svalbard. Journal of Glaciology. 2010;56(196):349-62.
94. Langford H, Hodson A, Banwart S, Boggild C. The microstructure and biogeochemistry of Arctic cryoconite granules. Annals of Glaciology. 2010;51(56):87-94.
95. Samui G, Antony R, Thamban M. Chemical characteristics of hydrologically distinct cryoconite holes in coastal Antarctica. Annals of Glaciology. 2018;59(77):69-76.
96. Baccolo G, Di Mauro B, Massabo D, Clemenza M, Nastasi M, Delmonte B, et al. Cryoconite as a temporary sink for anthropogenic species stored in glaciers. Scientific Reports. 2017;7:1-11.
97. Lokas E, Zaborska A, Sobota I, Gaca P, Milton JA, Kocurek P, et al. Airborne radionuclides and heavy metals in high Arctic terrestrial environment as the indicators of sources and transfers of contamination. Cryosphere. 2019;13(7):2075-86.
98. Singh SM, Avinash K, Sharma P, Mulik RU, Upadhyay AK, Ravindra R. Elemental variations in glacier cryoconites of Indian Himalaya and Spitsbergen, Arctic. Geoscience Frontiers. 2017;8(6):1339-47.
99. Weiland-Brauer N, Fischer MA, Schramm KW, Schmitz RA. Polychlorinated Biphenyl (PCB)-Degrading Potential of Microbes Present in a Cryoconite of Jamtalferner Glacier. Frontiers in Microbiology. 2017;8.

100. Rozwalak P, Podkowa P, Buda J, Niedzielski P, Kawecki S, Ambrosini R, et al. Cryoconite - From minerals and organic matter to bioengineered sediments on glacier's surfaces. Science of the Total Environment. 2022;807.
101. Nagatsuka N, Takeuchi N, Uetake J, Shimada R. Mineralogical composition of cryoconite on glaciers in northwest Greenland. Bulletin of Glaciological Research. 2014;32:107-14.
102. Stibal M, Tranter M, Benning LG, Rehak J. Microbial primary production on an Arctic glacier is insignificant in comparison with allochthonous organic carbon input. Environmental Microbiology. 2008;10(8):2172-8.
103. Takeuchi N, Nishiyama H, Li ZQ. Structure and formation process of cryoconite granules on Urumqi glacier No. 1, Tien Shan, China. Annals of Glaciology. 2010;51(56):9-14.
104. Dong ZW, Qin DH, Kang SC, Liu YJ, Li Y, Huang J, et al. Individual particles of cryoconite deposited on the mountain glaciers of the Tibetan Plateau: Insights into chemical composition and sources. Atmospheric Environment. 2016;138:114-24.
105. Hodson A, Anesio AM, Ng F, Watson R, Quirk J, Irvine-Fynn T, et al. A glacier respires: Quantifying the distribution and respiration CO2 flux of cryoconite across an entire Arctic supraglacial ecosystem. Journal of Geophysical Research. 2007;112(G04S36).
106. Takeuchi N, Li ZQ. Characteristics of Surface Dust on Urumqi Glacier No. 1 in the Tien Shan Mountains, China. Arctic, Antarctic, and Alpine Research. 2008;40(4):744-50.
107. MacDonell S, Fitzsimons S. The formation and hydrological significance of cryoconite holes. Progress in Physical Geography. 2008;32(6):595-610.
108. Cook J, Edwards A, Takeuchi N, Irvine-Fynn T. Cryoconite: The dark biological secret of the cryosphere. Progress in Physical Geography. 2016;40(1):66-111.
109. Kastovska K, Stibal M, Sabacka M, Cerna B, Santruckova H, Elster J. Microbial community structure and ecology of subglacial sediments in two polythermal Svalbard glaciers characterized by epifluorescence microscopy and PLFA. Polar Biology. 2007;30(3):277-87.
110. Kamennaya NA, Ajo-Franklin CM, Northen T, Jansson C. Cyanobacteria as Biocatalysts for Carbonate Mineralization. Minerals. 2012;2(4):338-64.
111. Foreman CM, Sattler B, Mikucki JA, Porazinska DL, Priscu JC. Metabolic activity and diversity of cryoconites in the Taylor Valley, Antarctica. Journal of Geophysical Research. 2007;112(G04S32).
112. Stibal M, Sabacka M, Kastovska K. Microbial communities on glacier surfaces in Svalbard: Impact of physical and chemical properties on abundance and structure of cyanobacteria and algae. Microbial Ecology. 2006;52(4):644-54.
113. Langford H, Hodson A, Banwart S. Using FTIR spectroscopy to characterise the soil mineralogy and geochemistry of cryoconite from Aldegondabreen glacier, Svalbard. Applied Geochemistry. 2011;26:S206-S9.
114. Stibal M, Sabacka M, Zarsky J. Biological processes on glacier and ice sheet surfaces. Nature Geoscience. 2012;5(11):771-4.
115. Mueller DR, Pollard WH. Gradient analysis of cryoconite ecosystems from two polar glaciers. Polar Biology. 2004;27(2):66-74.
116. Pereira S, Zille A, Micheletti E, Moradas-Ferreira P, De Philippis R, Tamagnini P. Complexity of cyanobacterial exopolysaccharides: composition, structures, inducing factors and putative genes involved in their biosynthesis and assembly. FEMS Microbiology Reviews. 2009;33(5):917-41.
117. MacCarthy P. The principles of humic substances: an introduction to the first principle. In: Ghabbour EA, Davies G, editors. Humic Substances: Structures, Models and Functions. Special Publication No. 273. Cambridge UK: The Royal Society of Chemistry; 2001. p. 19-30.
118. Kumada K. Studies on the colour of humic acids. Soil Science and Plant Nutrition. 1965;11(4):11-6.
119. Adhikary S, Nakawo M, Seko K, Shakya B. Dust influence on the melting process of glacier ice: experimental results from Lirung Glacier, Nepal Himalayas. IAHS Publication. 2000(264):43-52.
120. Gribbon PWF. Cryoconite Holes on Sermikavsak, West Greenland. Journal of Glaciology. 1979;22(86):177-81.
121. Stibal M, Tranter M. Laboratory investigation of inorganic carbon uptake by cryoconite debris from Werenskioldbreen, Svalbard. Journal of Geophysical Research. 2007;112(G04S33).

122. Telling J, Anesio AM, Tranter M, Fountain AG, Nylen T, Hawkings J, et al. Spring thaw ionic pulses boost nutrient availability and microbial growth in entombed Antarctic Dry Valley cryoconite holes. Frontiers in Microbiology. 2014;5.
123. Tranter M, Fountain AG, Fritsen CH, Lyons WB, Priscu JC, Statham PJ, et al. Extreme hydrochemical conditions in natural microcosms entombed within Antarctic ice. Hydrological Processes. 2004;18(2):379-87.
124. Murugesan GP, Narayan V, Devaraj S. Spatial analysis of supraglacial debris cover in Svalbard, Arctic Region-a decadal study. Environmental Science and Pollution Research. 2021;28(18):22823-31.
125. Shroder JF, Bishop MP, Copland L, Sloan VF. Debris-covered glaciers and rock glaciers in the Nanga Parbat Himalaya, Pakistan. Geografiska Annaler: Series A, Physical Geography. 2000;82(1):17-31.
126. Spolaor A, Moroni B, Luks B, Nawrot A, Roman M, Larose C, et al. Investigation on the Sources and Impact of Trace Elements in the Annual Snowpack and the Firn in the Hansbreen (Southwest Spitsbergen). Frontiers in Earth Science. 2021;8.
127. Vecchiato M, Barbaro E, Spolaor A, Burgay F, Barbante C, Piazza R, et al. Fragrances and PAHs in snow and seawater of Ny-Alesund (Svalbard): Local and long-range contamination. Environmental Pollution. 2018;242:1740-7.
128. Nawrot AP, Migala K, Luks B, Pakszys P, Glowacki P. Chemistry of snow cover and acidic snowfall during a season with a high level of air pollution on the Hans Glacier, Spitsbergen. Polar Science. 2016;10(3):249-61.
129. Barbaro E, Koziol K, Bjorkman MP, Vega CP, Zdanowicz C, Martma T, et al. Measurement report: Spatial variations in ionic chemistry and water-stable isotopes in the snowpack on glaciers across Svalbard during the 2015-2016 snow accumulation season. Atmospheric Chemistry and Physics. 2021;21(4):3163-80.
130. de Caritat P, Hall G, Gislason S, Belsey W, Braun M, Goloubeva NI, et al. Chemical composition of arctic snow: concentration levels and regional distribution of major elements. Science of the Total Environment. 2005;336(1-3):183-99.
131. Schuler TV, Kohler J, Elagina N, Hagen JOM, Hodson AJ, Jania JA, et al. Reconciling Svalbard Glacier Mass Balance. Frontiers in Earth Science. 2020;8.
132. World Glacier Monitoring Service (WGMS). Latest glacier mass balance data [Internet]. n.d. [updated 3/11/2021; cited 2022 13 April]. Available from: https://wgms.ch/latest-glacier-mass-balance-data/.
133. The Grand Challenge Initiative. Project Cusp [Internet]. n.d. [updated 2 December 2021; cited 2022 14 February]. Available from: https://www.grandchallenge.no/project-cusp/.
134. Navarrete-Martin L, Krus P. Sounding Rockets: analysis, simulation and optimization of a solid propellant motor using Hopsan. Transportation Research Procedia. 2018;29:255-67.
135. Chaturvedi S, Dave PN. Solid propellants: AP/HTPB composite propellants. Arabian Journal of Chemistry. 2019;12(8):2061-8.
136. Dallas JA, Raval S, Gaitan JPA, Saydam S, Dempster AG. The environmental impact of emissions from space launches: A comprehensive review. Journal of Cleaner Production. 2020;255.
137. Dreschel TW, Hall CR. Quantification of hydrochloric acid and particulate deposition resulting from space shuttle launches at John F Kennedy Space Center, Florida, USA. Environmental Management. 1990;14(4):501-7.
138. Norwegian Polar Institute (NPI). TopoSvalbard [Internet]. NPI; n.d. [cited 2022 20 March]. Available from: https://toposvalbard.npolar.no/.
139. Anderson BJ, Keller VW. Space shuttle exhaust cloud properties. NASA Technical Paper 2258. 1983 [cited 2022 19 February]. Available from: https://ntrs.nasa.gov/citations/19840006538.
140. Potter A. Space shuttle environmental effects: the first five flights. Proceedings of the NASA/USAF Space Shuttle Environment Conference. Kennedy Space Center, Florida. 1983 [Available from: https://ntrs.nasa.gov/api/citations/19850002149/downloads/19850002149.pdf.
141. Boss EA, Filho RM, de Toledo ECV. Freeze drying process: real time model and optimization. Chemical Engineering and Processing. 2004;43(12):1475-85.
142. Guildner LA, Johnson DP, Jones FE. Vapor Pressure of Water at its Triple Point. Journal of Research of the National Bureau of Standards - A Physics and Chemistry. 1976;80A(3):505-21.

143. Barley J. Basic Principles of Freeze Drying [Internet]. SP Scientific; n.d. [cited 2022 7 February]. Available from: https://www.spscientific.com/freeze-drying-lyophilization-basics/.
144. International Organization for Standardization (ISO). ISO 16720:2005(E) Soil quality - Pretreatment of samples by freeze-drying for subsequent analysis [Internet, Report]. Geneva, Switzerland: ISO; 2005 [cited 2022 15 May]. Available from: https://www.standard.no/no/Nettbutikk/produktkatalogen/Produktpresentasjon/?ProductID=117086.
145. Beauchemin D. Environmental analysis by inductively coupled plasma mass spectrometry. Mass Spectrometry Reviews. 2010;29(4):560-92.
146. Bettinelli M, Beone GM, Spezia S, Baffi C. Determination of heavy metals in soils and sediments by microwave-assisted digestion and inductively coupled plasma optical emission spectrometry analysis. Analytica Chimica Acta. 2000;424(2):289-96.
147. Matusiewicz H. Chapter 3 - Systems for Microwave-Assisted Wet Digestion. In: Flores ÉMdM, editor. Microwave-Assisted Sample Preparation for Trace Element Analysis. Amsterdam: Elsevier; 2014. p. 77-98.
148. Müller EI, Mesko MF, Moraes DP, Korn MdGA, Flores ÉMM. Chapter 4 - Wet Digestion Using Microwave Heating. In: Flores ÉMdM, editor. Microwave-Assisted Sample Preparation for Trace Element Analysis. Amsterdam: Elsevier; 2014. p. 99-142.
149. International Organization for Standardization (ISO). ISO 16729:2013 (E) Soil quality - Digestion of nitric acid soluble fractions of elements. [Internet, Report]. Geneva, Switzerland: ISO; 2013 [cited 2022 16 June]. Available from: https://www.standard.no/no/Nettbutikk/produktkatalogen/Produktpresentasjon/?ProductID=668218.
150. Sneddon J, Masuram S, Richert JC. Gas chromatography-mass spectrometry-basic principles, instrumentation and selected applications for detection of organic compounds. Analytical Letters. 2007;40(6):1003-12.
151. Richter BE, Jones BA, Ezzell JL, Porter NL, Avdalovic N, Pohl C. Accelerated solvent extraction: A technique for sample preparation. Analytical Chemistry. 1996;68(6):1033-9.
152. Pintado-Herrera MG, Gonzalez-Mazo E, Lara-Martin PA. In-cell clean-up pressurized liquid extraction and gas chromatography-tandem mass spectrometry determination of hydrophobic persistent and emerging organic pollutants in coastal sediments. Journal of Chromatography A. 2016;1429:107-18.
153. Giergielewicz-Mozajska H, Dabrowski L, Namiesnik J. Accelerated Solvent Extraction (ASE) in the analysis of environmental solid samples - Some aspects of theory and practice. Critical Reviews in Analytical Chemistry. 2001;31(3):149-65.
154. Carabias-Martínez R, Rodríguez-Gonzalo E, Revilla-Ruiz P, Hernández-Méndez J. Pressurized liquid extraction in the analysis of food and biological samples. Journal of Chromatography A. 2005;1089(1-2):1-17.
155. Lundstedt S, van Bavel B, Haglund P, Tysklind M, Öberg L. Pressurised liquid extraction of polycyclic aromatic hydrocarbons from contaminated soils. Journal of Chromatography A. 2000;883(1-2):151-62.
156. Ramos L, Kristenson EM, Brinkman UAT. Current use of pressurised liquid extraction and subcritical water extraction in environmental analysis. Journal of Chromatography A. 2002;975(1):3-29.
157. Muir D, Sverko E. Analytical methods for PCBs and organochlorine pesticides in environmental monitoring and surveillance: a critical appraisal. Analytical and Bioanalytical Chemistry. 2006;386(4):769-89.
158. Al-Hakkani MF. Guideline of inductively coupled plasma mass spectrometry "ICP-MS": fundamentals, practices, determination of the limits, quality control, and method validation parameters. SN Applied Sciences. 2019;1(7).
159. Wilschefski SC, Baxter MR. Inductively Coupled Plasma Mass Spectrometry: Introduction to Analytical Aspects. The Clinical Biochemist Reviews. 2019;40(3):115-33.
160. Templeton DM. Inductively coupled plasma-atomic emission spectrometry (ICP-AES) and inductively coupled plasma-mass spectrometry (ICP-MS). In: Seiler HG, Sigel A, Sigel H, editors. Handbook on metals in clinical and analytical chemistry. New York: Marcel Dekker; 1994. p. 167 - 80.

161. Tanner SD, Baranov VI, Bandura DR. Reaction cells and collision cells for ICP-MS: a tutorial review. Spectrochimica Acta Part B: Atomic Spectroscopy. 2002;57(9):1361-452.
162. Santos FJ, Galceran MT. Modern developments in gas chromatography–mass spectrometry-based environmental analysis. Journal of Chromatography A. 2003;1000(1-2):125-51.
163. Schmid ER. Chromatography and mass-spectrometry - an overview. Chromatographia. 1990;30(9-10):573-6.
164. Ayris S, Currado GM, Smith D, Harrad S. GC/MS procedures for the determination of PCBs in environmental matrices. Chemosphere. 1997;35(5):905-17.
165. Fifield FW. Separation Techniques. In: Fifield FW, Haines PJ, editors. Environmental Analytical Chemistry. 2nd ed: Blackwell Science Ltd; 2000. p. 91 - 117.
166. Karasek F.W., Clement R.E. Gas Chromatography. Basic Gas Chromatography-Mass Spectrometry: Principles and Techniques. Amsterdam, The Netherlands: Elsevier Science B.V.; 2012. p. 5 - 40.
167. Medeiros PM. Gas Chromatography–Mass Spectrometry (GC–MS). In: White WM, editor. Encyclopedia of Geochemistry: A Comprehensive Reference Source on the Chemistry of the Earth. Cham: Springer International Publishing; 2018. p. 530-5.
168. Lang V. Polychlorinated biphenyls in the environment. Journal of Chromatography A. 1992;595(1-2):1-43.
169. Haines PJ. Molecular Spectrometry. In: Fifield FW, Haines PJ, editors. Environmental Analytical Chemistry. 2nd ed: Blackwell Science Ltd; 2000. p. 161-202.
170. Michalski R. Ion chromatography as a reference method for determination of inorganic ions in water and wastewater. Critical Reviews in Analytical Chemistry. 2006;36(2):107-27.
171. Tartari GA, Marchetto A, Mosello R. Precision and linearity of inorganic analyses by ion chromatography. Journal of Chromatography A. 1995;706(1-2):21-9.
172. Schnepf A, Kolb M, Seubert A, Läubli M. Practical Ion Chromatography - An Introduction. Switzerland: Metrohm Monograph; 2020.
173. Skalar Analytical. Skalar Methods - Total Organic Carbon, Residual Oxidisable Carbon, and Total Inorganic Carbon analysis in soil according to DIN19539 Norm. Lab Protocol. n.d. Report No.: Catnr. P06-001.
174. Zethof JHT, Leue M, Vogel C, Stoner SW, Kalbitz K. Identifying and quantifying geogenic organic carbon in soils - the case of graphite. Soil. 2019;5(2):383-98.
175. Skalar Analytical. Determination of different Carbon species according to DIN19539 [Internet]. Skalar Analytical B.V.; n.d. [cited 2022 16 May]. Available from: https://www.skalar.com/news/determination-of-different-carbon-species-according-to-din-19539.
176. Batley GE. Quality assurance in environmental monitoring. Marine Pollution Bulletin. 1999;39(1-12):23-31.
177. MacDougall D, Crummett WB. Guidelines for data acquisition and data quality evaluation in environmental chemistry. Analytical Chemistry. 1980;52(14):2242-9.
178. Fifield FW, Haines PJ. Introduction. In: Fifield FW, Haines PJ, editors. Environmental Analytical Chemistry. 2nd ed: Blackwell Science Ltd; 2000. p. 3-12.
179. Liabastre A.A., Carlberg K.A., Miller M.S. Quality Assurance for Environmental Assessment Activities. In: Hewitt C.N., editor. Methods of Envrionmental Data Analysis: Springer Science + Business Media, B.V.; 1992. p. 259 - 99.
180. Fifield FW. Analytical Environmental Data: Assessment and Interpretation. In: Fifield FW, Haines PJ, editors. Environmental Analytical Chemistry. 2nd ed: Blackwell Science Ltd; 2000. p. 13-35.
181. CITAC, Eurachem. CITAC/ Eurachem Guide: Guide to Quality in Analytical Chemistry. An Aid to Accreditation [Internet, Report]. 2002 [Available from: https://www.citac.cc/CITAC_EURACHEM_GUIDE.pdf.
182. International Organization for Standardization (ISO). Standards [Internet]. ISO; n.d. [cited 2022 14 April]. Available from: https://www.iso.org/standards.html.
183. International Organization for Standardization (ISO). ISO 5667-1:2020(E) Water quality - Sampling - Part 1: Guidance on the design of sampling programmes and sampling techniques. [Internet, Report]. Geneva, Switzerland: ISO; 2020 [cited 2022 14 April]. Available from: https://www.standard.no/en/webshop/productcatalog/productpresentation/?ProductID=1307032.

184. International Organization for Standardization (ISO). ISO 5667-4:2016(E) Water quality - Sampling - Part 4: Guidance on sampling from lakes, natural and man-made. [Internet, Report]. Geneva, Switzerland: ISO; 2016 [cited 2022 14 April]. Available from: https://www.standard.no/en/webshop/ProductCatalog/ProductPresentation/?ProductID=823632.
185. International Organization for Standardization (ISO). ISO 5667-8:1993(E) Water quality - Sampling - Part 8: Guidance on the sampling of wet deposition. [Internet, Report]. Geneva, Switzerland: ISO; 1993 [cited 2022 14 April]. Available from: https://www.standard.no/en/webshop/ProductCatalog/ProductPresentation/?ProductID=121366.
186. International Organization for Standardization (ISO). ISO 5667-12:2017(E) Water quality - Sampling - Part 12: Guidance on sampling of bottom sediments from rivers, lakes and estuarine areas [Internet, Report]. Geneva, Switzerland: ISO; 2017 [cited 2022 14 April]. Available from: https://www.standard.no/no/Nettbutikk/produktkatalogen/Produktpresentasjon/?ProductID=927243.
187. International Organization for Standardization (ISO). ISO 5667-15:2009(E) Water quality - Sampling - Part 15: Guidance on the preservation and handling of sludge and sediment samples [Internet, Report]. Geneva, Switzerland: ISO; 2009 [cited 2022 14 April]. Available from: https://www.standard.no/en/webshop/ProductCatalog/ProductPresentation/?ProductID=390634.
188. International Organization for Standardization (ISO). ISO 5667-3:2018 (E) Water quality - Sampling - Part 3: Preservation and handling of water samples. [Internet, Report]. Geneva, Switzerland: ISO; 2018 [cited 2022 14 April]. Available from: https://www.standard.no/no/Nettbutikk/produktkatalogen/Produktpresentasjon/?ProductID=975202.
189. International Organization for Standardization (ISO). ISO 5667-14:2014 (E) Water quality - Sampling - Part 14: Guidance on quality assurance and quality control of environmental water sampling and handling. [Internet, Report]. Geneva, Switzerland: ISO; 2014 [cited 2022 14 April]. Available from: https://www.standard.no/en/webshop/ProductCatalog/ProductPresentation/?ProductID=727650.
190. Raynie D.E. The Vital Role of Blanks in Sample Preparation. LCGC North America. 2018;36(8):494-7.
191. Simes GF, Harrington JS. The Measurement of Contamination in Environmental Samples. Air & Waste. 1993;43(8):1155-60.
192. Cantwell H (ed). Blanks in Method Validation - Supplement to Eurochem Guide The Fitness for Purpose of Analytical Methods. [Internet, Report]. 2019 [cited 2022 16 May]. 1st edition:[Available from: https://www.eurachem.org/images/stories/Guides/pdf/MV_Guide_Blanks_supplement_EN.pdf.
193. Rajakovic LV, Markovic DD, Rajakovic-Ognjanovic VN, Antanasijevic DZ. Review: The approaches for estimation of limit of detection for ICP-MS trace analysis of arsenic. Talanta. 2012;102:79-87.
194. Armbruster DA, Pry T. Limit of blank, limit of detection and limit of quantitation. The Clinical Biochemist Reviews. 2008;29(Suppl 1):S49-S52.
195. Wells G, Prest H, Russ IV C.W. Signal, Noise, and Detection Limits in Mass Spectrometry [Internet, Application Note - Chemical Analysis]. USA: Agilent Technologies, Inc.; 2021 [cited 2022 15 May]. Available from: https://www.agilent.com/cs/library/technicaloverviews/public/5990-7651EN.pdf.
196. Lundanes E, Reubsaet L, Greibrokk T. Quantitation. Chromatography: Basic Principles, Sample Preparations and Related Methods. Weinheim, Germany: Wiley-VCH; 2013. p. 189 - 99.
197. Quevauviller P, Griepink B. Reference Materials for Quality Assurance. In: Günzler H, editor. Accreditation and Quality Assurance in Analytical Chemistry. Berlin, Heidelberg: Springer; 1996. p. 195-208.
198. Willie S, Nadeau K, Pihillagawa IG, Yang L, Clancy V, Grinberg P, et al. Certificate of Analysis. Certified Reference Material MESS-4 [Report, Internet]. Ottawa, Canada: National Research Council Canada; 2014 [updated August 2021; cited 2022 2 April]. Available from: https://nrc-digital-repository.canada.ca/eng/view/object/?id=8a3fd39a-c068-4ce0-820c-d08cf742a20a.
199. Thompson M, Ellison SLR, Fajgelj A, Willetts P, Wood R. Harmonised guidelines for the use of recovery information in analytical measurement (technical report). Pure and Applied Chemistry. 1999;71(2):337-48.

200. Asimakopoulos AG, Wang L, Thomaidis NS, Kannan K. A multi-class bioanalytical methodology for the determination of bisphenol A diglycidyl ethers, p-hydroxybenzoic acid esters, benzophenone-type ultraviolet filters, triclosan, and triclocarban in human urine by liquid chromatography-tandem mass spectrometry. Journal of Chromatography A. 2014;1324:141-8.
201. Luthe GM, Schut BG, Aaseng JE. Monofluorinated analogues of polychlorinated biphenyls (F-PCBs): Synthesis using the Suzuki-coupling, characterization, specific properties and intended use. Chemosphere. 2009;77(9):1242-8.
202. Silvestro L, Tarcomnicu I, Savu SR. Matrix Effects in Mass Spectrometry Combined with Separation Methods—Comparison on HPLC, GC and Discussion on Methods to Control these Effects. In: Coelho AV, de Matos Ferraz Franco C, editors. Tandem Mass Spectrometry-Molecular Characterization. London: IntechOpen; 2013.
203. Garrido Frenich A, Martínez Vidal JL, Fernández Moreno JL, Romero-González R. Compensation for matrix effects in gas chromatography–tandem mass spectrometry using a single point standard addition. Journal of Chromatography A. 2009;1216(23):4798-808.
204. Erney DR, Gillespie AM, Gilvydis DM, Poole CF. Explanation of the matrix-induced chromatographic response enhancement of organophosphorus pesticides during open tubular column gas chromatography with splitless or hot on-column injection and flame photometric detection. Journal of Chromatography A. 1993;638(1):57-63.
205. Campbell MJ, Machin D, Walters SJ. Chapter 8: Tests for comparing two groups of categorical or continuous data. Medical statistics: a textbook for the health sciences. 4th ed: John Wiley & Sons Ltd; 2010. p. 117 - 47.
206. Statistics Kingdom. Shapiro-Wilk Test Calculator [Internet]. n.d. [cited 2022 10 June]. Available from: https://www.statskingdom.com/shapiro-wilk-test-calculator.html.
207. Campbell MJ, Machin D, Walters SJ. Chapter 5: Distributions. Medical statistics: a textbook for the health sciences. 4th ed: John Wiley & Sons Ltd; 2010. p. 64-77.
208. Campbell MJ, Machin D, Walters SJ. Chapter 9: Correlation, linear and logistic regression. Medical statistics: a textbook for the health sciences. 4th ed: John Wiley & Sons Ltd; 2010. p. 150 - 80.
209. Jolliffe IT, Cadima J. Principal component analysis: a review and recent developments. Philosophical Transactions of the Royal Society A. 2016;374(2065).
210. Ringnér M. What is principal component analysis? Nature Biotechnology. 2008;26(3):303-4.
211. Bro R, Smilde AK. Principal component analysis. Analytical Methods. 2014;6(9):2812-31.
212. Lever J, Krzywinski M, Altman N. Principal component analysis. Nature Methods. 2017;14(7):641-2.
213. Eckhardt S, Hermansen O, Grythe H, Fiebig M, Stebel K, Cassiani M, et al. The influence of cruise ship emissions on air pollution in Svalbard - a harbinger of a more polluted Arctic? Atmospheric Chemistry and Physics. 2013;13(16):8401-9.
214. Yr.no. Ny-Ålesund, Scientific research base, Svalbard (Norway), elevation 10 m [Internet]. n.d. [cited 2022 25 April]. Available from: https://www.yr.no/en/statistics/graph/1-2837778/Norway/Svalbard/Svalbard/Ny-%C3%85lesund.
215. Norwegian Meteorological Insitute. Annual mean temperature in Svalbard, filtered and unfiltered. Environmental monitoring of Svalbard and Jan Mayen [Internet]. MOSJ; 2022 [cited 2022 25 April]. Available from: http://www.mosj.no/en/climate/atmosphere/temperature-precipitation.html.
216. Norwegian Meteorological Insitute. Annual precipitation in Svalbard, Hopen and Jan Mayen, filtered. Environmental monitoring of Svalbard and Jan Mayen [Internet]. MOSJ; 2022 [cited 2022 25 April]. Available from: http://www.mosj.no/en/climate/atmosphere/temperature-precipitation.html.
217. Sadiq M, Dutta S, Kumar P, Jat S, Gajbhiye DY, Dharwadkar A. Ice dynamics of Vestre Broggerbreen glaciers, Ny-Alesund, Svalbard, Arctic. Journal of Earth System Science. 2022;131(1).
218. World Glacier Monitoring Service (WGMS). Midtre Lovénbreen, Svalbard. [Internet]. n.d. [updated 27 October 2016; cited 2022 29 April]. Available from: https://wgms.ch/products_ref_glaciers/midtre-lovenbreen-svalbard/.
219. Hjelle A. Introduction. Geology of Svalbard Polarhåndbok No 7. Oslo: Norsk Polarinstitutt; 1993. p. 1-8.
220. Hjelle A. The Kongsfjorden area. Geology of Svalbard Polarhåndbok No 7. Oslo: Norsk Polarinstitutt; 1993. p. 97-109.

221. Berthling I, Berti C, Mancinelli V, Stendardi L, Piacentini T, Miccadei E. Analysis of the paraglacial landscape in the Ny-Ålesund area and Blomstrandoya (Kongsfjorden, Svalbard, Norway). Journal of Maps. 2020;16(2):818-33.
222. Haldar SK, Tišljar J. Chapter 1 - Rocks and Minerals. In: Haldar SK, Tišljar J, editors. Introduction to Mineralogy and Petrology: Elsevier; 2014. p. 1-37.
223. Haldar SK, Tišljar J. Chapter 2 - Basic Mineralogy. In: Haldar SK, Tišljar J, editors. Introduction to Mineralogy and Petrology: Elsevier; 2014. p. 39-79.
224. Parsons I. Feldspars. In: Alderton D, Elias SA, editors. Encyclopedia of Geology. 2nd ed. Oxford: Academic Press; 2021. p. 271-86.
225. Rieder M, Cavazzini G, D'yakonov YS, Frank-Kamenetskii VA, Gottardi G, Guggenheim S, et al. Nomenclature of the micas. Clays and clay minerals. 1998;46(5):586-95.
226. Brigatti MF, Galán E, Theng BKG. Chapter 2 - Structure and Mineralogy of Clay Minerals. In: Bergaya F, Lagaly G, editors. Developments in Clay Science. 5: Elsevier; 2013. p. 21-81.
227. Wiewióra A, Weiss Z. Crystallochemical classifications of phyllosilicates based on the unified system of projection of chemical composition: II. The chlorite group. Clay Minerals. 1990;25(1):83-92.
228. Haldar SK, Tišljar J. Chapter 6 - Metamorphic Rocks. In: Haldar SK, Tišljar J, editors. Introduction to Mineralogy and Petrology: Elsevier; 2014. p. 213-32.
229. Dimri VP, Srivastava RP, Vedanti N. Chapter 5 - Reservoir Geophysics: Some Basic Concepts. In: Dimri VP, Srivastava RP, Vedanti N, editors. Handbook of Geophysical Exploration: Seismic Exploration. 41: Pergamon; 2012. p. 89-118.
230. Haldar SK, Tišljar J. Chapter 5 - Sedimentary Rocks. In: Haldar SK, Tišljar J, editors. Introduction to Mineralogy and Petrology: Elsevier; 2014. p. 121-212.
231. Weging S. Study of trace elements, natural organic matter and selected environmental toxicants in soil at Mitrahalvøya, to establish bias correction for studies of long-range atmospheric transported pollutants in Ny-Ålesund [Master Thesis]. Trondheim: Norwegian University of Science and Technology; 2021.
232. Balaram V. Rare earth elements: A review of applications, occurrence, exploration, analysis, recycling, and environmental impact. Geoscience Frontiers. 2019;10(4):1285-303.
233. Guo Y, Wang XJ, Li XL, Wang JP, Xu MG, Li DW. Dynamics of soil organic and inorganic carbon in the cropland of upper Yellow River Delta, China. Scientific Reports. 2016;6.
234. Sigma-Aldrich. Certificate of Analysis - Certified Reference Material PCB Congeners in Soil [Internet, Report]. 2015 [cited 2022 6 May]. Available from: https://www.sigmaaldrich.com/certificates/Graphics/COfAInfo/fluka/pdf/rtc/SQC068_LRAA7458.pdf .
235. Ryan MOL. Particulate matter released from Austre Broggerbreen; a study on the potential impact on chemical conditions in Bayelva and Kongsfjorden [Master Thesis]. Trondheim: Norwegian University of Science and Technology (NTNU); 2021.
236. Lo JM, Sakamoto H. Comparison of the acid combinations in microwave-assisted digestion of marine sediments for heavy metal analyses. Analytical Sciences. 2005;21(10):1181-4.
237. Steinnes E. Metal Contamination of the Natural Environment in Norway from Long Range Atmospheric Transport. Water, Air and Soil Pollution: Focus. 2001;1(3):449-60.
238. Miljødirektoratet. Grenseverdier for klassifisering av vann, sediment og biota - revidert 30.10.2020 [Internet, Report]. 2016 [Available from: https://www.miljodirektoratet.no/globalassets/publikasjoner/M608/M608.pdf
239. Arai Y, Chaney RL, Hough RL, Hooda PS, Ma Y, He ZL, et al. Characteristics and Behaviour of Individual Elements. In: Hooda PS, editor. Trace Elements in Soils: Blackwell Publishing Ltd; 2010. p. 381 - 575.
240. Jarup L. Hazards of heavy metal contamination. British Medical Bulletin. 2003;68:167-82.
241. Hiller E, Lalinska B, Chovan M, Jurkovic L, Klimko T, Jankular M, et al. Arsenic and antimony contamination of waters, stream sediments and soils in the vicinity of abandoned antimony mines in the Western Carpathians, Slovakia. Applied Geochemistry. 2012;27(3):598-614.
242. Hooda PS, Alloway BJ. Cadmium and lead sorption behaviour of selected English and Indian soils. Geoderma. 1998;84(1-3):121-34.

243. Pacyna JM, Pacyna EG. An assessment of global and regional emissions of trace metals to the atmosphere from anthropogenic sources worldwide. Environmental reviews. 2001;9(4):269-98.
244. Nam JJ, Gustafsson O, Kurt-Karakus P, Breivik K, Steinnes E, Jones KC. Relationships between organic matter, black carbon and persistent organic pollutants in European background soils: Implications for sources and environmental fate. Environmental Pollution. 2008;156(3):809-17.
245. Lima ALC, Farrington JW, Reddy CM. Combustion-Derived Polycyclic Aromatic Hydrocarbons in the Environment - A Review. Environmental Forensics. 2005;6(2):109-31.
246. Singh SM, Gawas-Sakhalkar P, Naik S, Ravindra R, Sharma J, Upadhyay AK, et al. Elemental composition and bacterial incidence in firn-cores at Midre Lovenbreen glacier, Svalbard. Polar Record. 2015;51(1):39-48.
247. Stumm W, Morgan JJ. Trace Metals: Cycling, Regulation, and Biological Role. In: Schnoor JL, Zehnder A, editors. Aquatic Chemistry: Chemical Equilibria and Rates in Natural Waters. 3rd ed: Wiley-Interscience; 1996. p. 614 - 71.
248. Cowan CE, Zachara JM, Resch CT. Cadmium Adsorption on Iron Oxides in the Presence of Alkaline-Earth Elements. Environmental Science & Technology. 1991;25(3):437-46.
249. Christensen TH. Cadmium Soil Sorption at Low Concentrations: V. Evidence of Competition by Other Heavy Metals. Water Air and Soil Pollution. 1987;34(3):293-303.
250. Scheinost AC. Metal Oxides. In: Hillel D, editor. Encyclopedia of Soils in the Environment. Oxford: Elsevier; 2005. p. 428-38.
251. Sutherland IW. Structure-function relationships in microbial exopolysaccharides. Biotechnology Advances. 1994;12(2):393-448.
252. Micheletti E, Pereira S, Mannelli F, Moradas-Ferreira P, Tamagnini P, Philippis RD. Sheathless Mutant of Cyanobacterium *Gloeothece* sp. Strain PCC 6909 with Increased Capacity To Remove Copper Ions from Aqueous Solutions. Applied and Environmental Microbiology. 2008;74(9):2797-804.
253. Headley AD. Heavy metal concentrations in peat profiles from the high Arctic. Science of the Total Environment. 1996;177(1-3):105-11.
254. Lu ZB, Cai MH, Wang J, Yin ZG, Yang HZ. Levels and distribution of trace metals in surface sediments from Kongsfjorden, Svalbard, Norwegian Arctic. Environmental Geochemistry and Health. 2013;35(2):257-69.
255. Blais JM, Kimpe LE, McMahon D, Keatley BE, Mattory ML, Douglas MSV, et al. Arctic seabirds transport marine-derived contaminants. Science. 2005;309(5733):445-.
256. Pacyna AD, Frankowski M, Kozioł K, Węgrzyn MH, Wietrzyk-Pełka P, Lehmann-Konera S, et al. Evaluation of the use of reindeer droppings for monitoring essential and non-essential elements in the polar terrestrial environment. Science of The Total Environment. 2019;658:1209-18.
257. Östrem G. Ice Melting under a Thin Layer of Moraine, and the Existence of Ice Cores in Moraine Ridges. Geografiska Annaler. 1959;41(4):228-30.
258. Cook J, Hodson A, Telling J, Anesio A, Irvine-Fynn T, Bellas C. The mass-area relationship within cryoconite holes and its implications for primary production. Annals of Glaciology. 2010;51(56):106-10.
259. Xu YP, Simpson AJ, Eyles N, Simpson MJ. Sources and molecular composition of cryoconite organic matter from the Athabasca Glacier, Canadian Rocky Mountains. Organic Geochemistry. 2010;41(2):177-86.
260. Stumm W, Morgan JJ. Dissolved Carbon Dioxide. In: Schnoor JL, Zehnder A, editors. Aquatic Chemistry: Chemical Equilibria and Rates in Natural Waters. 3rd ed: Wiley-Interscience; 1996. p. 148-205

Appendices

The appendices include supplementary material to the main report. Additional material from materials and methods is presented in Section A. Section B presents additional material from the results.

A Materials and Methods

The materials and methods supplementary material includes tables with respect to the sampling performed during fieldwork in Svalbard and details of the analytical techniques applied to each sample. In addition to this, data is provided with regards to pre-treatments steps: microwave assisted digestion, accelerated solvent extraction (ASE), and internal standards used for ICP-MS.

A.1 Sampling Information

Table A.1.1 *Information including sample type, location, and collection details for sampling performed on three glaciers: Midtre Lovénbreen, Austre Brøggerbreen, and Vestre Brøggerbreen in Ny-Ålesund, Svalbard from 24 to 27 August 2021. Altitude is displayed as meters above sea level (m.a.s.l). The 'NA' represents data that is not available. The table continues on the following pages.*

Sample Reference	Sample Type	Sample Location	Sample No.	GPS Latitude	GPS Longitude	Altitude (m.a.s.l)	Sampling Container
1a	Cryoconite	Midtre Lovénbreen	1	78.88976 N	12.04925 E	155	Cc-cup
2a	Cryoconite	Midtre Lovénbreen	2	78.88947 N	12.04848 E	159	Cc-cup
3a	Cryoconite	Midtre Lovénbreen	3	78.88892 N	12.04816 E	160	Cc-cup
4a	Cryoconite	Midtre Lovénbreen	4	78.88840 N	12.04666 E	167	Cc-cup
5a	Cryoconite	Midtre Lovénbreen	5	78.88816 N	12.04620 E	170	Cc-cup
6a	Cryoconite	Midtre Lovénbreen	6	78.88289 N	12.03512 E	230	Cc-cup
7a	Cryoconite	Midtre Lovénbreen	7	78.88170 N	12.03393 E	240	Cc-cup
8a	Cryoconite	Midtre Lovénbreen	8	78.87922 N	12.03309 E	267	Cc-cup
AB1a	Cryoconite	Austre Brøggerbreen	9	78.89920 N	11.83200 E	124	Cc-cup
AB2a	Cryoconite	Austre Brøggerbreen	10	78.89898 N	11.83178 E	124	Cc-cup
AB3a	Cryoconite	Austre Brøggerbreen	11	78.89877 N	11.83162 E	125	Cc-cup
AB4a	Cryoconite	Austre Brøggerbreen	12	78.89711 N	11.83126 E	133	Cc-cup
AB5a	Cryoconite	Austre Brøggerbreen	13	78.89474 N	11.83991 E	167	Cc-cup
AB6a	Cryoconite	Austre Brøggerbreen	14	78.89474 N	11.83991 E	167	Cc-cup
AB7a	Cryoconite	Austre Brøggerbreen	15	78.89474 N	11.83991 E	167	Cc-cup
AB8a	Cryoconite	Austre Brøggerbreen	16	78.89454 N	11.83995 E	168	Cc-cup
AB9a	Cryoconite	Austre Brøggerbreen	17	78.89454 N	11.83995 E	168	Cc-cup
AB10a	Cryoconite	Austre Brøggerbreen	18	78.89454 N	11.83995 E	168	Cc-cup
VB1a	Cryoconite	Vestre Brøggerbreen	19	78.91418 N	11.74567 E	92	Cc-cup
VB2a	Cryoconite	Vestre Brøggerbreen	20	78.91397 N	11.74550 E	96	Cc-cup
VB3a	Cryoconite	Vestre Brøggerbreen	21	78.91385 N	11.74593 E	97	Cc-cup
VB4a	Cryoconite	Vestre Brøggerbreen	22	78.91360 N	11.74593 E	98	Cc-cup
VB5a	Cryoconite	Vestre Brøggerbreen	23	78.91341 N	11.74608 E	99	Cc-cup

Sample Reference	Sample Type	Sample Location	Sample No.	GPS Latitude	GPS Longitude	Altitude (m.a.s.l)	Sampling Container
VB6a	Cryoconite	Vestre Brøggerbreen	24	78.91335 N	11.74623 E	99	Cc-cup
VB7a	Cryoconite	Vestre Brøggerbreen	25	78.91316 N	11.74630 E	99	Cc-cup
VB8a	Cryoconite	Vestre Brøggerbreen	26	78.91251 N	11.74650 E	102	Cc-cup
VB9a & b	Cryoconite	Vestre Brøggerbreen	27-28	78.91224 N	11.74693 E	104	Cc-cup
VB10a	Cryoconite	Vestre Brøggerbreen	29	78.91211 N	11.74660 E	107	Cc-cup
1	Cryoconite hole water	Midtre Lovénbreen	30	78.88976 N	12.04925 E	155	50mL HDPP tube
2	Cryoconite hole water	Midtre Lovénbreen	31	78.88947 N	12.04848 E	159	50mL HDPP tube
3	Cryoconite hole water	Midtre Lovénbreen	32	78.88892 N	12.04816 E	160	50mL HDPP tube
4	Cryoconite hole water	Midtre Lovénbreen	33	78.88840 N	12.04666 E	167	50mL HDPP tube
5	Cryoconite hole water	Midtre Lovénbreen	34	78.88816 N	12.04620 E	170	50mL HDPP tube
6	Cryoconite hole water	Midtre Lovénbreen	35	78.88289 N	12.03512 E	230	50mL HDPP tube
7	Cryoconite hole water	Midtre Lovénbreen	36	78.88170 N	12.03393 E	240	50mL HDPP tube
8	Cryoconite hole water	Midtre Lovénbreen	37	78.87922 N	12.03309 E	267	50mL HDPP tube
AB1	Cryoconite hole water	Austre Brøggerbreen	38	78.89920 N	11.83200 E	124	50mL HDPP tube
AB2	Cryoconite hole water	Austre Brøggerbreen	39	78.89898 N	11.83178 E	124	50mL HDPP tube
AB3	Cryoconite hole water	Austre Brøggerbreen	40	78.89877 N	11.83162 E	125	50mL HDPP tube
AB4	Cryoconite hole water	Austre Brøggerbreen	41	78.89711 N	11.83126 E	133	50mL HDPP tube
AB5	Cryoconite hole water	Austre Brøggerbreen	42	78.89474 N	11.83991 E	167	50mL HDPP tube
AB6	Cryoconite hole water	Austre Brøggerbreen	43	78.89474 N	11.83991 E	167	50mL HDPP tube
AB7	Cryoconite hole water	Austre Brøggerbreen	44	78.89474 N	11.83991 E	167	50mL HDPP tube
AB8	Cryoconite hole water	Austre Brøggerbreen	45	78.89454 N	11.83995 E	168	50mL HDPP tube
AB9	Cryoconite hole water	Austre Brøggerbreen	46	78.89454 N	11.83995 E	168	50mL HDPP tube
AB10	Cryoconite hole water	Austre Brøggerbreen	47	78.89454 N	11.83995 E	168	50mL HDPP tube
VB1	Cryoconite hole water	Vestre Brøggerbreen	48	78.91418 N	11.74567 E	92	50mL HDPP tube
VB2	Cryoconite hole water	Vestre Brøggerbreen	49	78.91397 N	11.74550 E	96	50mL HDPP tube
VB3	Cryoconite hole water	Vestre Brøggerbreen	50	78.91385 N	11.74593 E	97	50mL HDPP tube
VB4	Cryoconite hole water	Vestre Brøggerbreen	51	78.91360 N	11.74593 E	98	50mL HDPP tube

Table A.1.1 continued: Information including sample type, location, and collection details from sampling performed.

Sample Reference	Sample Type	Sample Location	Sample No.	GPS Latitude	GPS Longitude	Altitude (m.a.s.l)	Sampling Container
VB5	Cryoconite hole water	Vestre Brøggerbreen	52	78.91341 N	11.74608 E	99	50mL HDPP tube
VB6	Cryoconite hole water	Vestre Brøggerbreen	53	78.91335 N	11.74623 E	99	50mL HDPP tube
VB7	Cryoconite hole water	Vestre Brøggerbreen	54	78.91316 N	11.74630 E	99	50mL HDPP tube
VB8	Cryoconite hole water	Vestre Brøggerbreen	55	78.91251 N	11.74650 E	102	50mL HDPP tube
VB9	Cryoconite hole water	Vestre Brøggerbreen	56	78.91224 N	11.74693 E	104	50mL HDPP tube
VB10	Cryoconite hole water	Vestre Brøggerbreen	57	78.91211 N	11.74660 E	107	50mL HDPP tube
MLS1	Snow	Midtre Lovénbreen	58	78.88289 N	12.03512 E	230	50mL HDPP tube
MLS2	Snow	Midtre Lovénbreen	59	78.88289 N	12.03512 E	230	50mL HDPP tube
MLS3	Snow	Midtre Lovénbreen	60	78.88236 N	12.03441 E	231	50mL HDPP tube
MLS4	Snow	Midtre Lovénbreen	61	78.88236 N	12.03441 E	231	50mL HDPP tube
MLS5	Snow	Midtre Lovénbreen	62	78.88170 N	12.03393 E	240	50mL HDPP tube
MLS6	Snow	Midtre Lovénbreen	63	78.88170 N	12.03393 E	240	50mL HDPP tube
MLS7	Snow	Midtre Lovénbreen	64	78.87922 N	12.03309 E	267	50mL HDPP tube
MLS8	Snow	Midtre Lovénbreen	65	78.87922 N	12.03309 E	267	50mL HDPP tube
MLS9	Snow	Midtre Lovénbreen	66	78.87780 N	12.02964 E	285	50mL HDPP tube
MLS10	Snow	Midtre Lovénbreen	67	78.87780 N	12.02964 E	285	50mL HDPP tube
ABSN1	Snow	Austre Brøggerbreen	68	78.89359 N	11.84646 E	169	50mL HDPP tube
ABSN2	Snow	Austre Brøggerbreen	69	78.89359 N	11.84646 E	169	50mL HDPP tube
ABSN3	Snow	Austre Brøggerbreen	70	78.89359 N	11.84646 E	169	50mL HDPP tube
ABSN4	Snow	Austre Brøggerbreen	71	78.89359 N	11.84646 E	169	50mL HDPP tube
ABSN5	Snow	Austre Brøggerbreen	72	78.89359 N	11.84646 E	169	50mL HDPP tube
ABSN6	Snow	Austre Brøggerbreen	73	78.89359 N	11.84646 E	169	50mL HDPP tube
ABSN7	Snow	Austre Brøggerbreen	74	78.89359 N	11.84646 E	169	50mL HDPP tube
ABSN8	Snow	Austre Brøggerbreen	75	78.89359 N	11.84646 E	169	50mL HDPP tube

Table A.1.1 continued: Information including sample type, location, and collection details from sampling performed.

Sample Reference	Sample Type	Sample Location	Sample No.	GPS Latitude	GPS Longitude	Altitude (m.a.s.l)	Sampling Container
VBSN1	Snow	Vestre Brøggerbreen	76	78.91418 N	11.74567 E	92	50mL HDPP tube
VBSN2	Snow	Vestre Brøggerbreen	77	78.91418 N	11.74567 E	92	50mL HDPP tube
VBSN3	Snow	Vestre Brøggerbreen	78	78.91418 N	11.74567 E	92	50mL HDPP tube
VBSN4	Snow	Vestre Brøggerbreen	79	78.91418 N	11.74567 E	92	50mL HDPP tube
VBSN5	Snow	Vestre Brøggerbreen	80	78.91418 N	11.74567 E	92	50mL HDPP tube
VBSN6	Snow	Vestre Brøggerbreen	81	78.91418 N	11.74567 E	92	50mL HDPP tube
VBSN7	Snow	Vestre Brøggerbreen	82	78.91418 N	11.74567 E	92	50mL HDPP tube
ML1	Supraglacial debris	Midtre Lovénbreen	83	78.88340 N	12.03520 E	224	Cc-cup
ML2	Supraglacial debris	Midtre Lovénbreen	84	78.88340 N	12.03520 E	224	Cc-cup
ML3	Supraglacial debris	Midtre Lovénbreen	85	78.88170 N[a]	12.03393 E[a]	240[a]	Cc-cup
ML4	Supraglacial debris	Midtre Lovénbreen	86	78.87922 N	12.03309 E	267	PE-LD Ziplock bag
9a	Supraglacial debris	Midtre Lovénbreen	87	78.87922 N	12.03309 E	267	Cc cup
ABS1	Supraglacial debris	Austre Brøggerbreen	88	78.89640 N	11.83078 E	137	PE-LD Ziplock bag
ABS2	Supraglacial debris	Austre Brøggerbreen	89	78.89454 N[b]	11.83995 E[b]	168[b]	50mL HDPP tube
ABS3	Supraglacial debris	Austre Brøggerbreen	90	NA	NA	NA	PE-LD Ziplock bag

Table A.1.1 continued: Information including sample type, location, and collection details from sampling performed.

[a] No exact co-ordinates recorded, location of sample close to cryoconite 7 & 8 sampling location. GPS co-ordinates noted for location of sample 7.

[b] No exact GPS co-ordinates recorded, location of sample close to AB8-10 sampling location.

A.2 Analytical Techniques Performed

Several analytical techniques were performed on glacial samples collected from ML, AB, and VB. Analytical techniques included elemental analysis by ICP-MS, PCB determination by GC-MS, anion determination by IC, and carbon content determination (TOC/ROC/TIC) via combustion. Table A.2.1 presents all sample preparation and analytical techniques used for each sample type, including parameters measured during fieldwork.

Table A.2.1 *Sample preparation and analytical techniques performed on cryoconite hole water, cryoconite, supraglacial debris, and snow samples. The 'x' denotes where a method has been performed, 'n/a' where a method is not applicable, and '-' where the method was not selected for analysis of the sample.*

Sample Reference	Sample Type	Temp (ºC)	Conductivity ($\mu S\ cm^{-1}$)	Mortar & Pestel	Freeze Drying	Digestion (HNO_3)	ICP-MS	IC	GC-MS	TOC/ ROC/ TIC
1-8	Cryoconite hole water	x	x	n/a	n/a	n/a	x	x	-	-
AB1-10	Cryoconite hole water	x	x	n/a	n/a	n/a	x	x	-	-
VB1-10	Cryoconite hole water	x	x	n/a	n/a	n/a	x	x	-	-
1a	Cryoconite	n/a	n/a	-	x	x	x	-	x	x
2a	Cryoconite	n/a	n/a	-	x	x	x	-	x	-
3a	Cryoconite	n/a	n/a	-	x	x	x	-	x	-
4a	Cryoconite	n/a	n/a	-	x	x	x	-	x	-
5a	Cryoconite	n/a	n/a	-	x	x	x	-	x	x
6a	Cryoconite	n/a	n/a	-	x	x	x	-	x	-
7a	Cryoconite	n/a	n/a	-	x	x	x	-	x	x
8a	Cryoconite	n/a	n/a	-	x	x	x	-	x	x
AB1a	Cryoconite	n/a	n/a	-	x	x	x	-	x	x
AB2a	Cryoconite	n/a	n/a	-	x	x	x	-	x	-
AB3a	Cryoconite	n/a	n/a	-	x	x	x	-	x	-
AB4a	Cryoconite	n/a	n/a	-	x	x	x	-	x	-
AB5a	Cryoconite	n/a	n/a	-	x	x	x	-	x	x
AB6a	Cryoconite	n/a	n/a	-	x	x	x	-	x	-
AB7a	Cryoconite	n/a	n/a	-	x	x	x	-	x	-
AB8a	Cryoconite	n/a	n/a	-	x	x	x	-	x	x
AB9a	Cryoconite	n/a	n/a	-	x	x	x	-	x	-
AB10a	Cryoconite	n/a	n/a	-	x	x	x	-	x	x

Sample Reference	Sample Type	Temp (ºC)	Conductivity (µS cm^{-1})	Mortar & Pestel	Freeze Drying	Digestion (HNO_3)	ICP-MS	IC	GC-MS	TOC/ ROC/ TIC
VB1a	Cryoconite	n/a	n/a	-	x	x	x	-	x	-
VB2a	Cryoconite	n/a	n/a	-	x	x	x	-	x	x
VB3a	Cryoconite	n/a	n/a	-	x	x	x	-	x	-
VB4a	Cryoconite	n/a	n/a	-	x	x	x	-	x	-
VB5a	Cryoconite	n/a	n/a	-	x	x	x	-	x	-
VB6a	Cryoconite	n/a	n/a	-	x	x	x	-	x	x
VB7a	Cryoconite	n/a	n/a	x	x	x	x	-	x	x
VB8a	Cryoconite	n/a	n/a	-	x	x	x	-	x	-
VB9a & b	Cryoconite	n/a	n/a	-	x	x	x	-	x	x[a]
VB10a	Cryoconite	n/a	n/a	-	x	x	x	-	x	-
ML1	Supraglacial debris	n/a	n/a	-	x	x	x	-	-	x
ML2	Supraglacial debris	n/a	n/a	-	x	x	x	-	-	x
ML3	Supraglacial debris	n/a	n/a	x	x	x	x	-	-	x
ML4	Supraglacial debris	n/a	n/a	x	x	x	x	-	-	x
ABS1	Supraglacial debris	n/a	n/a	x	x	x	x	-	-	x
ABS2	Supraglacial debris	n/a	n/a	x	x	x	x	-	-	x
ABS3	Supraglacial debris	n/a	n/a	x	x	x	x	-	-	x
MLS1-10	Snow	-	-	n/a	n/a	n/a	x	x	-	-
ABSN1-8	Snow	-	-	n/a	n/a	n/a	x	x	-	-
VBSN1-7	Snow	-	-	n/a	n/a	n/a	x	x[b]	-	-

Table A.2.1 continued: Sample preparation and analytical techniques performed on cryoconite hole water, cryoconite, supraglacial debris, and snow samples.

[a] TOC/ROC/TIC content analysed for VB9a only.

[b] VBSN6 was not analysed by ion chromatography due to insufficient sample volume.

A.3 Microwave Assisted Digestion Measurements

Cryoconite and supraglacial debris required a digestion pre-treatment step prior to elemental analysis. Sample weights of between 250 and 350 mg were required for digestion. Following digestion, the sample was diluted with ultrapure water to approximately 109.8 g. The exact sample weights are presented in Table A.3.1 along with observations of any precipitation remaining following digestion. The Teflon vial number was recorded for identification of possible cross contamination between batches as a result of insufficient cleaning of vials between runs. Table A.3.2 contains details of the temperature, pressure and power program parameters for the microwave assisted digestion.

Table A.3.1 *Weights of cryoconite and supraglacial debris samples measured before digestion and on dilution of digested sample. Weights reported in g. Nitric acid digestion performed on samples. Precipitation relates to visible precipitation remaining following digestion. The 'n/a' represents entries that were not applicable. Reference materials are displayed as 'RM'. The table continues on the following page.*

Sample Reference	Sample No.	Teflon Vial No.	Batch No.	Sample Weight Before Digestion (g)	Weight on Dilution (g)	Visible Precipitation? (Yes/No)
Method Blank 1	n/a	121	1	-	109.8	No
Method Blank 2	n/a	122	1	-	111.4	No
Method Blank 3	n/a	123	1	-	109.9	No
1a	1	124	1	0.237	111.6	Yes
2a	2	125	1	0.258	115.6	Yes
3a	3	126	1	0.326	113.5	Yes
4a	4	127	1	0.250	109.9	Yes
5a	5	128	1	0.277	109.9	Yes
6a	6	129	1	0.278	111.2	Yes
7a	7	130	1	0.254	110.0	Yes
8a	8	131	1	0.267	109.9	Yes
9a	87	132	1	0.007[a]	111.8	No
AB1a	9	133	1	0.299	112.5	Yes
AB2a	10	134	1	0.261	117.7	Yes
AB3a	11	135	1	0.251	109.8	Yes
AB4a	12	136	1	0.284	109.9	Yes
AB5a	13	137	1	0.313	112.3	Yes
AB6a	14	138	1	0.251	109.9	Yes
AB7a	15	139	1	0.273	109.9	Yes
AB8a	16	140	1	0.292	109.8	Yes
AB9a	17	141	1	0.275	109.9	Yes
AB10a	18	142	1	0.288	109.9	Yes
VB1a	19	143	1	0.289	109.9	Yes
VB2a	20	144	1	0.329	109.9	Yes
VB3a	21	145	1	0.249	111.8	Yes
VB4a	22	146	1	0.272	110.1	Yes
VB5a	23	147	1	0.326	112.6	Yes
VB6a	24	148	1	0.265	110.4	Yes

Sample Reference	Sample No.	Teflon Vial No.	Batch No.	Sample Weight Before Digestion (g)	Weight on Dilution (g)	Visible Precipitation? (Yes/No)
VB7a	25	149	1	0.326	110.5	Yes
VB8a	26	150	1	0.336	109.9	Yes
VB9a	27	151	1	0.307	110.0	Yes
VB9b	28	152	1	0.295	109.8	Yes
VB10a	29	153	1	0.335	109.9	Yes
RM 1	n/a	154	1	0.234	110.7	Yes
RM 2	n/a	155	1	0.281	110.7	Yes
RM 3	n/a	156	1	0.282	110.8	Yes
RM 4	n/a	157	1	0.268	110.7	Yes
ML1	83	125	2	0.327	109.9	Yes
ML2	84	126	2	0.339	109.9	Yes
ML3	85	128	2	0.267	110.0	Yes
ML4	86	129	2	0.319	109.9	Yes
ABS1	88	131	2	0.233	109.8	Yes
ABS2	89	133	2	0.275	110.0	Yes
ABS3	90	136	2	0.258	109.9	Yes
Method Blank 1.1	n/a	123	2	-	110.2	No
Method Blank 2.2	n/a	127	2	-	109.8	No
RM 1.2	n/a	130	2	0.304	111.0	Yes
RM 2.2	n/a	138	2	0.303	110.3	Yes

Table A.3.1 continued: Weights of cryoconite and supraglacial debris samples measured before digestion and on dilution of digested sample.

[a] Low sample weight following freeze drying resulting in low weight used for digestion.

Table A.3.2 *Temperature, power, and pressure program parameters used in microwave assisted digestion of cryoconite and supraglacial debris samples.*

Time (min)	Power (W)	Temp 1 (°C)	Temp 2 (°C)	Pressure (bar)
00:05:00	1000	50	60	160
00:10:00	1000	50	60	160
00:10:00	1000	100	60	160
00:08:00	1000	110	60	160
00:15:00	1000	190	60	160
00:05:00	1000	210	60	160
00:15:00	1000	245	60	160
00:10:00	1000	245	60	160

A.4 Accelerated Solved Extraction Measurements and Parameters

A list of the materials and chemicals used in the accelerated solved extraction (ASE) procedure for the extraction of PCBs is presented in Table A.4.1 including specifications and suppliers. Internal and external standards were added for identification and quantification of PCBs in later analysis with GC-MS. The exact weights and volumes of internal and external standards are recorded in Table A.4.2.

Table A.4.1 *Materials with specifications used in the ASE procedure for PCB extraction.*

Material	Specification	Supplier
Copper Powder (Cu)	99.5 % trace metals basis <425 µm CAS-No: 7440-50-8 Lot: MKCK0242	Sigma-Aldrich (USA)
Aluminium Oxide (Al_2O_3)	Activated, basic Brockmann I, standard grade ~150 mesh CAS-No: 1344-28-1 Lot:BCCG3176	Sigma-Aldrich (USA)
Diatomaceous Earth (SiO_2)	Flux calcined, 150 mesh CAS-No: 68855-54-9 Lot: MKCJ8320	Sigma-Aldrich (USA)
Ottawa Sand (Quartz)	General purpose grade CAS-No: 14808-60-7 Lot: 2189898	Fisher Scientific (UK)
Dichloromethane	Analytical grade CAS-No: 75-09-2 Lot: 22A134017	VWR Chemicals (USA)
Ethyl Acetate	Analytical grade CAS-No: 141-78-6 Lot: 21A13027	VWR Chemicals (USA)
Acetone (cleaning use)	Technical grade	VWR Chemicals (USA)
3-Fluor-2,4,4'-Trichlorobiphenyl (F-PCB 28)	Internal standard 3-F-PCB, 0.1 mg mL^{-1} in 1 mL isooctane; Lot: 4220 Prod. No: 2228.12-100-IO CAS-No: 863314-89-0	CHIRON AS (Norway)
5-Fluoro 2,3',4,4',5 Pentachlorobiphenyl (F-PCB-118)	Internal standard 5-F-PCB, 10 µg mL^{-1} in isooctane Prod. No: 2865.12-10-IO CAS-No: 1023690-19-8 Batch: 5864 & 27065	CHIRON AS (Norway)
Dutch Seven PCBs (PCB-28, PCB52, PCB-101, PCB-118, PCB-138, PCB-153, PCB-180)	ISO10382 Multicomponent stock solution, external standard 100 µg mL^{-1} in isooctane Batch: 7336	CHIRON AS (Norway)
PCB congeners in soil	Certified reference material Lot:LRAA7458	Sigma Aldrich (USA)
Cellulose filters (ASE extraction)	For 1, 5, 10, 22 mL ASE 350/150 cell Lot: 114058	Thermo Scientific (USA)

Table A.4.2 *Weight in g of cryoconite samples, reference material, and cryoconite mixture added to extraction cells for PCB extraction using ASE. Includes volume (µL) of internal (IS) and external standard (ES) added.*

Type	Sample Reference	Sample ID	Weight	IS	ES
Blank	Method Blank 1	MB1	-	50	-
Blank	Method Blank 2	MB2	-	50	-
Blank	Method Blank 3	MB3	-	50	-
Cryoconite	1a	1	0.505	50	-
Cryoconite	2a	2	0.506	50	-
Cryoconite	3a	3	0.502	50	-
Cryoconite	4a	4	0.496	50	-
Cryoconite	5a	5	0.504	50	-
Cryoconite	6a	6	0.509	50	-
Cryoconite	7a	7	0.518	50	-
Cryoconite	8a	8	0.500	50	-
Cryoconite	AB1a	9	0.503	50	-
Cryoconite	AB2a	10	0.503	50	-
Cryoconite	AB3a	11	0.502	50	-
Cryoconite	AB4a	12	0.502	50	-
Cryoconite	AB5a	13	0.507	50	-
Cryoconite	AB6a	14	0.500	50	-
Cryoconite	AB7a	15	0.502	50	-
Cryoconite	AB8a	16	0.501	50	-
Cryoconite	AB9a	17	0.502	50	-
Cryoconite	AB10a	18	0.504	50	-
Cryoconite	VB1a	19	0.502	50	-
Cryoconite	VB2a	20	0.509	50	-
Cryoconite	VB3a	21	0.506	50	-
Cryoconite	VB4a	22	0.500	50	-
Cryoconite	VB5a	23	0.504	50	-
Cryoconite	VB6a	24	0.503	50	-
Cryoconite	VB7a	25	0.501	50	-
Cryoconite	VB8a	26	0.504	50	-
Cryoconite	VB9a	27	0.506	50	-
Cryoconite	VB10a	29	0.505	50	-
Method Blank	Method Blank 5	MB5	-	50	-
Method Blank	Method Blank 7	MB7	-	50	-
Reference	Reference Material 1	RM1	0.499	50	-
Reference	Reference Material 2	RM2	0.516	50	-
Reference	Reference Material 3	RM3	0.500	50	-
Cryoconite Mix	Recovery Test 1	REC1	0.499	50	-
Cryoconite Mix	Recovery Test 2	REC2	0.500	50	-
Cryoconite Mix	Recovery Test 3	REC3	0.503	50	-
Cryoconite Mix	Recovery Test 4	REC4	0.501	50	50
Cryoconite Mix	Recovery Test 5	REC5	0.504	50	50
Cryoconite Mix	Recovery Test 6	REC6	0.505	50	50
Cryoconite Mix	Recovery Test 7	REC7	0.509	50	100
Cryoconite Mix	Recovery Test 8	REC8	0.504	50	100
Cryoconite Mix	Recovery Test 9	REC9	0.503	50	100
Cryoconite Mix	Matrix Match 1	MM1	0.501	50[a]	50[a]
Cryoconite Mix	Matrix Match 2	MM2	0.501	50[a]	50[a]
Cryoconite Mix	Matrix Match 3	MM3	0.503	50[a]	100[a]
Cryoconite Mix	Matrix Match 4	MM4	0.501	50[a]	100[a]

[a] Internal and external standards added after extraction and concentration steps (post extraction spiking).

A.5 Concentration and Solvent Exchange

Table A.5.1 *Materials used in concentration and solvent exchange pre-treatment steps for PCB extraction including their specifications.*

Material	Specification	Supplier
Syringe Filter	25mm 0.2 µm Nylon membrane Batch No. 10282351A	VWR Chemicals (USA)
Sterican needles	0.90 x 70 mm; 20G x $2^3/_4$” Ref 4665791 Lot: 17H18G8841	B. Braun (Germany)
Centrifuge Tubes (ethyl acetate evaporation)	15mL, 12500g, Conical-bottom, clear, PP, Sterilized, metal free	VWR Chemicals (USA)
Syringe	10 mL, Luer Slip CAT No. 12931031	Fisher Scientific (Germany)
Dichloromethane	Analytical grade CAS-No: 75-09-2 Lot: 22A134017	VWR Chemicals (USA)
Ethyl Acetate	Analytical grade CAS-No: 141-78-6 Lot: 21A13027	VWR Chemicals (USA)

A.6 Internal Standards for ICP-MS

Table A.6.1 *Details of internal standards and corresponding elements for calibration by ICP-MS. Tuning modes are O_2, H_2 and no gas.*

Internal Standard	Elements
Ir (O_2 tune mode)	Yb, Pt, Hg, Tl, Pb, Bi and U
Re (O_2 tune mode)	Si, P S, Cl, Sc, Ti, V, As, Y, Ze, Nb, Mo, Sb La, Ce, Pr, Nd, Sm, Gd, Tb, Dy, Ho, Er, Tm, Lu, Hf, Ta, W
Rh (No gas tune mode)	Li, Be, B
Rh (H_2 tune mode)	Be, B, Al, Ca, Fe, Zn, Ga, Se, Sr
Rh (O_2 tune mode)	B, Na, Mg, K, Cr, Mn, Co, Ni. Cu, Br, Rb, Ru, Pd, Cd, In Sn, Cs, Ba, Eu

B Results

Tables and figures included within this section are supplementary material from the results of field measurements and observations. Results from elemental analysis of cryoconite, supraglacial debris, snow and cryoconite water, in addition to anion determination in cryoconite hole water and snow, TOC/ROC/TIC content in supraglacial debris and cryoconite, and PCB determination in cryoconite. The results are found in Section 5.

B.1 Temperature and Conductivity Measurements in Cryoconite Holes

Temperature and conductivity measurements were taken at each cryoconite hole after water sampling but prior to cryoconite sampling. Results for temperature and conductivity are presented in Table B.1.1

Table B.1.1 *Temperature and conductivity measurements of cryoconite hole water contained within individual cryoconite holes sampled from three glaciers near Ny-Ålesund. Temperature is displayed in ºC, and conductivity in µS cm^{-1}.*

Sample Reference	Sample No.	Temperature (ºC)	Conductivity (µS cm^{-1})
1	30	0.4	1.4
2	31	0.6	1.8
3	32	0.2	2.0
4	33	0.2	1.9
5	34	0.2	2.1
6	35	0.3	2.1
7	36	0.1	2.3
8	37	0.0	3.0
AB1	38	0.6	2.1
AB2	39	0.5	1.4
AB3	40	0.3	1.4
AB4	41	0.3	1.2
AB5	42	0.3	3.0
AB6	43	0.6	2.5
AB7	44	0.5	1.5
AB8	45	0.5	1.4
AB9	46	0.5	1.6
AB10	47	0.3	1.3
VB1	48	0.3	10.3
VB2	49	0.8	3.5
VB3	50	0.4	10.5
VB4	51	0.7	13.5
VB5	52	0.6	3.7
VB6	53	0.6	5.3
VB7	54	0.8	36.7
VB8	55	1.7	2.3
VB9	56	0.5	1.5
VB10	57	0.7	2.0

B.2 Physical Characteristics of Cryoconite

Visual observations of the physical properties of cryoconite sampled from cryoconite holes are presented in Table B.2.1. Samples have been categorised by colour and particle size. Those samples containing a mixture of particle sizes are represented by 'M'. The size group representing the highest proportion of particles within the sample is underlined.

Table B.2.1 *Visual observations of the physical characteristics of 28 cryoconite sampled from cryoconite holes and 8 supraglacial debris samples on three glaciers: Midtre Lovénbreen (ML), Austre Brøggerbreen (AB), and Vestre Brøggerbreen (VB) located near Ny-Ålesund, Svalbard. The particle size dominating in the mixed group (M) is underlined. Sample nos. 1 – 29 are cryoconite samples, and sample nos. 83 – 90 represent supraglacial debris samples.*

Sample Ref.	Sample No.	Location	Colour	Particle Size
1a	1	ML	Grey	M – Fine & granules
2a	2	ML	Grey	M – Fine & granules
3a	3	ML	Grey	M – Fine & granules
4a	4	ML	Grey	M – Fine & granules
5a	5	ML	Grey	M – Fine & granules
6a	6	ML	Grey	M – Fine & granules
7a	7	ML	Dark grey	Granules
8a	8	ML	Dark grey	Granules
AB1a	9	AB	Red-brown	M – Fine & granules
AB2a	10	AB	Red-brown	M – Fine & granules
AB3a	11	AB	Red-brown	M – Fine & granules
AB4a	12	AB	Red-brown	M – Fine & granules
AB5a	13	AB	Pale grey	Very fine particles
AB6a	14	AB	Pale grey	Very fine particles
AB7a	15	AB	Grey	Fine particles
AB8a	16	AB	Grey	Fine particles
AB9a	17	AB	Grey	Fine particles
AB10a	18	AB	Grey	M – Fine & granules
VB1a*	19	VB	Brown	M – Fine & granules
VB2a	20	VB	Brown	M – Fine & granules
VB3a	21	VB	Brown	M – Fine & granules
VB4a*	22	VB	Brown	M – Fine & granules
VB5a	23	VB	Brown	M – Fine & granules
VB6a	24	VB	Dark grey[a]	M – Fine & granules
VB7a	25	VB	Cream	Very fine particles
VB8a	26	VB	Brown	M – Fine & granules
VB9a*	27	VB	Dark grey	M – Fine & granules
VB10a	29	VB	Brown	Granules
ML1	83	ML	Dark brown	Granules
ML2	84	ML	Dark brown	Granules
ML3	85	ML	Black	Plant fibres
ML4	86	ML	Dark brown	Plant fibres
ABS1	88	AB	Black	Very fine particles
ABS2	89	AB	Dark brown	Granules
ABS3	90	AB	Brown	Plant fibres
9a	87	ML	Red-brown	Very fine particles

*Cryoconite holes with frozen lids found on VB;

[a] Sample turned container yellow after drying.

B.3 Elemental Analysis of Cryoconite and Supraglacial Debris

Cryoconite and supraglacial debris collected from cryoconite holes and the surface of three glaciers: Midtre Lovénbreen (ML), Austre Brøggerbreen, (AB) and Vestre Brøggerbreen (VB) were analysed for 64 elements by ICP-MS. Of these elements, 9 were selected for further investigation: Al, Fe, Ca, Mg, Zn, Pb, As, Cd, and Cr. The results of the elemental analysis for each sample are presented in Table B.3.1 and B.3.2

Table B.3.1 *Elemental concentrations detected in cryoconite from three glaciers in Ny-Ålesund. Locations are represented as ML (Midtre Lovénbreen), AB (Austre Brøggerbreen), and VB (Vestre Brøggerbreen). Concentration is displayed in μg g^{-1} for all elements. Samples were analysed by ICP-MS.*

Sample Reference	Sample No.	Location	Al μg g^{-1}	Fe μg g^{-1}	Ca μg g^{-1}	Mg μg g^{-1}	Zn μg g^{-1}	Pb μg g^{-1}	As μg g^{-1}	Cd μg g^{-1}	Cr μg g^{-1}
1a	1	ML	42082.89	40757.70	2726.85	13255.77	89.84	56.75	8.49	0.045	59.69
2a	2	ML	37938.64	37378.26	2684.04	12372.42	84.55	48.80	7.34	0.063	52.52
3a	3	ML	39456.89	40358.28	2812.33	13208.50	91.60	52.76	7.88	0.047	54.57
4a	4	ML	43319.81	41503.90	2453.55	13543.90	93.89	63.67	8.70	0.043	58.82
5a	5	ML	41213.80	38695.51	2402.65	12645.79	89.42	60.62	8.33	0.044	58.63
6a	6	ML	40601.48	40084.80	2516.33	13120.81	100.18	79.03	9.68	0.052	56.78
7a	7	ML	42192.89	40430.28	2530.21	13047.26	99.60	83.09	10.19	0.078	58.26
8a	8	ML	41164.00	39295.00	2698.98	13047.13	100.64	90.17	11.86	0.095	59.34
AB1a	9	AB	46770.71	42136.16	3951.43	13921.56	93.01	31.83	5.30	0.111	62.94
AB2a	10	AB	50693.14	46619.03	3673.37	15118.05	98.04	32.51	4.56	0.143	67.72
AB3a	11	AB	45954.24	43122.92	3306.67	13660.92	95.02	36.04	7.10	0.078	64.38
AB4a	12	AB	45143.39	44127.11	4287.57	13530.35	96.05	39.86	6.41	0.065	62.57
AB5a	13	AB	45522.13	40587.96	10497.69	18239.35	88.57	25.15	2.77	0.198	59.20
AB6a	14	AB	52107.31	41884.40	3388.25	14894.51	91.43	25.69	3.16	0.146	63.71
AB7a	15	AB	44132.01	40255.33	5126.39	14596.00	90.03	31.74	4.61	0.122	60.99
AB8a	16	AB	40641.93	45021.23	6283.99	15955.09	98.81	33.42	3.53	0.078	57.47
AB9a	17	AB	40344.02	47832.97	6662.10	16865.45	96.13	31.55	3.21	0.067	58.19
AB10a	18	AB	40576.27	43808.02	5511.98	14970.50	97.63	35.50	4.87	0.089	58.35

Sample Reference	Sample No.	Location	Al μg g^{-1}	Fe μg g^{-1}	Ca μg g^{-1}	Mg μg g^{-1}	Zn μg g^{-1}	Pb μg g^{-1}	As μg g^{-1}	Cd μg g^{-1}	Cr μg g^{-1}
VB1a	19	VB	38362.90	31213.12	2218.28	9110.78	84.41	49.08	9.19	0.155	65.64
VB2a	20	VB	35656.29	29369.50	2609.86	9235.15	79.74	45.56	8.15	0.161	63.28
VB3a	21	VB	36263.07	29933.17	10208.58	11915.60	79.62	43.85	8.55	0.196	64.78
VB4a	22	VB	35371.71	29275.96	7997.54	11789.14	81.43	46.32	8.21	0.146	60.38
VB5a	23	VB	31623.12	27721.66	2663.57	8730.04	72.24	42.61	7.55	0.141	54.91
VB6a	24	VB	35391.77	29365.95	2028.24	8854.20	75.80	135.20	9.05	0.088	60.36
VB7a	25	VB	32674.31	14028.12	150507.72	48883.97	60.55	8.33	5.91	0.532	84.05
VB8a	26	VB	32249.71	27144.68	2472.03	8732.51	75.17	42.71	8.03	0.124	59.90
VB9a	27	VB	35461.12	38654.25	2014.45	9129.80	76.43	69.86	8.82	0.121	61.19
VB10a	29	VB	36058.04	28466.49	2022.24	9196.51	77.51	57.61	8.45	0.109	64.97

Table B.3.1 continued: Elemental concentrations detected in cryoconite from three glaciers in Ny-Ålesund.

Table B.3.2 *Elemental concentrations detected in supraglacial debris from three glaciers in Ny-Ålesund. Locations are represented as ML (Midtre Lovénbreen) and AB (Austre Brøggerbreen). Concentrations are displayed in μg g^{-1} for all elements. Samples were analysed by ICP-MS. Supraglacial debris samples collected from mud mound deposits (SGD-M) are represented by ML1, ML2, ABS1 and ABS2. Supraglacial debris with observable plant content (SGD-P) are represented by ABS3, ML3 and ML4. Sample 9a represents debris collected from a small supraglacial stream on ML.*

Sample Reference	Sample No.	Location	Al μg g^{-1}	Fe μg g^{-1}	Ca μg g^{-1}	Mg μg g^{-1}	Zn μg g^{-1}	Pb μg g^{-1}	As μg g^{-1}	Cd μg g^{-1}	Cr μg g^{-1}
ML1	83	ML	41796.11	44399.87	2217.89	13633.06	122.60	83.53	9.12	0.117	55.98
ML2	84	ML	34273.27	35310.20	1786.55	11885.61	97.90	63.61	7.07	0.078	47.42
ABS1	88	AB	46250.56	36921.30	3337.81	13043.75	100.96	111.30	13.56	0.099	64.68
ABS2	89	AB	40327.78	36917.96	3263.04	13024.75	90.61	60.48	8.41	0.074	60.04
ABS3	90	AB	44976.83	32784.94	5223.40	10337.83	77.01	45.63	3.88	0.171	52.99
ML3	85	ML	4640.61	5042.60	7988.76	2228.94	15.62	8.83	0.38	0.066	6.45
ML4	86	ML	29262.53	25073.47	1806.03	8017.01	63.80	159.24	5.44	0.060	39.12
9a	87	ML	70608.12	61447.74	4851.86	22615.67	150.37	144.08	22.36	0.340	89.87

B.4 Comparison of Elemental Concentrations in Cryoconite to Literature

Table B.4.1 *Comparison of elemental concentrations in cryoconite with studies from glaciers located in both Svalbard and worldwide. Mean, minimum (min) and maximum (max) concentrations of elements are presented where available. Units are presented as reported in the studies, as either µg g^{-1}, mg kg^{-1}, or ppm (all being equivalent). The 'NA' represents those elements which have not been analysed in the studies, and 'n' represents the number of samples. The analytical techniques used in each study are presented below the table.*

Location	Units		Al	Fe	Ca	Zn	Pb	As	Cd	Cr	Reference
Midtre Lovénbreen, Svalbard[a]											
(n = 8)	µg g^{-1}	Mean	41000	39800	2600	93.7	66.9	9.06	0.0583	57.3	This
	µg g^{-1}	Min	37900	37400	2400	84.6	48.8	7.34	0.0432	52.5	Study
	µg g^{-1}	Max	43300	41500	2810	101	90.2	11.9	0.0947	59.7	
Austre Brøggerbreen, Svalbard[a]											
(n = 10)	µg g^{-1}	Mean	45200	43500	5270	94.5	32.3	4.55	0.110	61.6	
	µg g^{-1}	Min	40300	40300	3310	88.6	25.2	2.77	0.0648	57.5	
	µg g^{-1}	Max	52100	47800	10500	98.8	39.9	7.10	0.198	67.7	
Vestre Brøggerbreen, Svalbard[a]											
(n = 10)	µg g^{-1}	Mean	34900	27500	18500	76.3	54.1	8.19	0.177	63.9	
	µg g^{-1}	Min	31600	14000	2010	60.6	8.33	5.91	0.0881	54.9	
	µg g^{-1}	Max	38400	31200	151000	84.4	135	9.19	0.532	84.1	
Austre Brøggerbreen, Svalbard[a,e]											
(n = 14)	µg g^{-1}	Mean	45400	45500	4090	105	55.8	6.79	0.0946	63.9	(235)
	µg g^{-1}	Min	39100	37200	2580	88.1	34.6	3.68	0.0529	56.9	
	µg g^{-1}	Max	55800	52200	5610	123	122	13.0	0.147	79.3	
Midtre Lovénbreen, Svalbard[a]											
(n = 4)	ppm	Mean	NA	NA	NA	NA	NA	NA	NA	NA	(10)
	ppm	Min	38603	28186	NA	132	49.87	11.01	0.043	52.37	
	ppm	Max	42870	32413	NA	150	85.08	14.22	0.145	60.68	
Austre Brøggerbreen, Svalbard[a]											
(n = 6)	mg kg^{-1}	Mean	NA	NA	NA	NA	NA	NA	NA	NA	(98)
	mg kg^{-1}	Min	NA	21058.7	1347	61.7	18.5	3.6	0.01	20.7	
	mg kg^{-1}	Max	NA	24722.9	1713	66.1	20.5	5.3	0.05	60.6	

Location	Units		Al	Fe	Ca	Zn	Pb	As	Cd	Cr	Reference
Vestre Brøggerbreen, Svalbard[a]											
(n = 5)	mg kg^{-1}	Mean	NA	NA	NA	NA	NA	NA	NA	NA	(98)
	mg kg^{-1}	Min	NA	15892.9	325	44.7	25.5	5.0	0.00	18.8	
	mg kg^{-1}	Max	NA	18305.4	1692	66.2	36.3	5.7	0.14	35.3	
Hansbreen, Hornsund, Svalbard[b]											
(n = 14)	mg kg^{-1}	Mean	NA	54280	NA	96.33	54.38	NA	0.420	NA	(9)
	mg kg^{-1}	Min	NA	40497	NA	84.31	16.26	NA	0.065	NA	
	mg kg^{-1}	Max	NA	63994	NA	108.45	82.74	NA	1.529	NA	
Waldemarbreen, Kaffiøyra, Svalbard[c]											
(n = 12)	mg kg^{-1}	Mean	NA	NA	NA	NA	NA	NA	NA	NA	(97)
	mg kg^{-1}	Min	63570	29380	NA	59.57	19.87	NA	0.190	47.55	
	mg kg^{-1}	Max	91870	51270	NA	97.55	97.70	NA	0.600	84.04	
Morteratsch Glacier, Swiss Alps[d]											
(n = 10)	µg g^{-1}	Mean	NA	NA	NA	NA	NA	NA	NA	NA	(96)
	µg g^{-1}	Min	NA	27700	10000	81	NA	16	NA	NA	
	µg g^{-1}	Max	NA	50500	26000	275	NA	31	NA	NA	
Sutri Dhaka, Himalayas[a]											
(n = 12)	mg kg^{-1}	Mean	NA	NA	NA	NA	NA	NA	NA	NA	(98)
	mg kg^{-1}	Min	NA	21921	203	98.93	16.43	18.87	0.18	37.88	
	mg kg^{-1}	Max	NA	28897	733	206.23	52.98	35.34	0.57	77.08	

Table B.4.1 continued: Comparison of the elemental concentrations in cryoconite with studies from glaciers located in both Svalbard and worldwide.

[a] Elemental concentrations measured by ICP-MS.

[b] Pb, Zn and Fe analysed by flame atomic absorption spectrometry (AAS), Cd measured by ICP-MS.

[c] Elemental concentrations measured by flame AAS.

[d] Elemental concentrations measured by instrumental neutron activation analysis (INAA).

[e] Includes supraglacial debris.

B.5 Comparison of Ca and Mg Concentrations in Cryoconite by Location

Differences in Ca and Mg concentrations in cryoconite determined by ICP-MS are presented by location. Results are presented with and without sample 25, a sample with significantly higher concentrations of Ca and Mg than other cryoconite sampled, in Fig. B.5.1 and B.5.2 respectively.

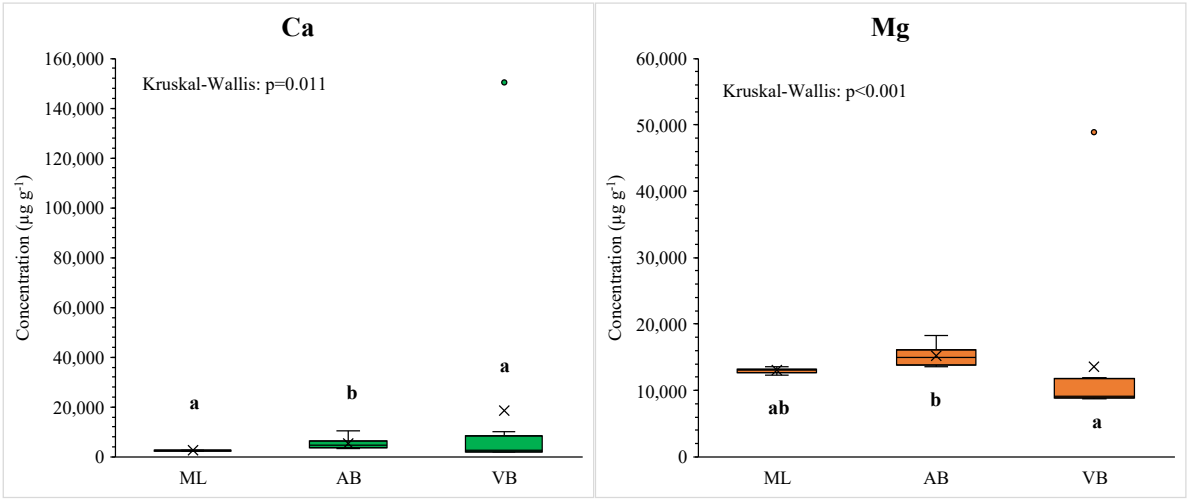

Figure B.5.1 *Box and Whisker plot of Ca and Mg concentrations determined in cryoconite from Midtre Lovénbreen (ML), Austre Brøggerbreen (AB) and Vestre Brøggerbreen (VB). Concentrations of all elements are in µg g^{-1}. Study locations with the same letter were not statistically significantly different from each other (Kruskal-Wallis and Dunn's post hoc test with Bonferroni correction, $p < 0.05$). The mean is represented by the 'x', the median by the line within the box, and the interquartile range by the box itself. Outliers are identified as circular coloured markers.*

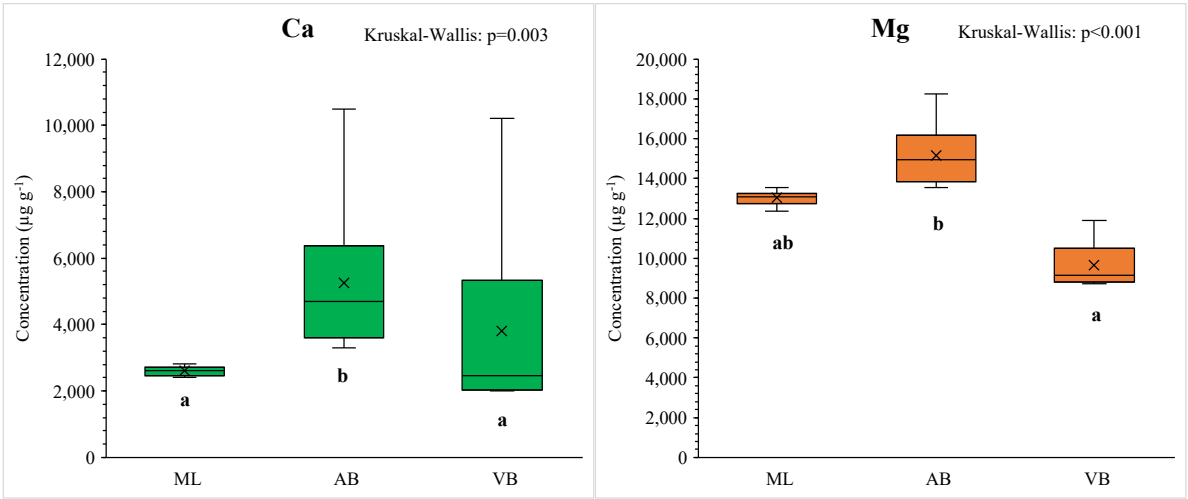

Figure B.5.2 *Box and Whisker plot of Ca and Mg concentrations in cryoconite from ML, AB, and VB excluding outlier sample 25 from Vestre Brøggerbreen. Concentrations of all elements are in µg g^{-1}. Study locations with the same letter were not significantly different from each other (Kruskal-Wallis and Dunn's post hoc test with Bonferroni correction, $p < 0.05$).*

B.6 Correlations Between Nine Selected Elements Determined in Cryoconite

A non-parametric Spearman correlation was performed for all cryoconite samples in order to identify significant correlations between elements in cryoconite, including sample no. 25. The results are presented in Table B.6.1.

Table B.6.1 *Non-parametric Spearman correlation between concentrations of elements determined in cryoconite by ICP-MS. The correlation coefficient is represented by R^2. Statistically significant correlations with a p value < 0.05 are represented by * and statistically significant correlations with a p value < 0.01 are represented by **. Sample size of n = 28 in all correlation tests. Statistically significant correlations are in bold.*

		Al	Fe	Ca	Mg	Zn	Pb	As	Cd
Al	R^2								
	p								
Fe	R^2	**0.809****							
	p	<0.001							
Ca	R^2	0.232	**0.386***						
	p	0.235	0.042						
Mg	R^2	**0.632****	**0.714****	**0.706****					
	p	<0.001	<0.001	<0.001					
Zn	R^2	**0.697****	**0.814****	0.192	**0.530****				
	p	<0.001	<0.001	0.329	0.004				
Pb	R^2	-0.270	-0.344	**-0.761****	**-0.666****	0.025			
	p	0.164	0.073	<0.001	<0.001	0.899			
As	R^2	-0.351	**-0.483****	**-0.673****	**-0.692****	-0.087	**0.920****		
	p	0.067	0.009	<0.001	<0.001	0.660	<0.001		
Cd	R^2	-0.256	**-0.394***	0.338	-0.042	**-0.489****	**-0.473***	-0.234	
	p	0.189	0.038	0.079	0.834	0.008	0.011	0.231	
Cr	R^2	0.091	-0.153	0.074	0.020	-0.309	-0.264	-0.041	**0.603****
	p	0.646	0.436	0.707	0.919	0.110	0.174	0.836	<0.001

B.7 TOC/ROC/TIC Content Determination

Calibration results for TOC, ROC, and TIC are presented in Table B.7.1. The DIN A standard was prepared at concentrations of 10, 25, 51, 75, 100, 125, and 150 mg to obtain calibration curves. Results of TOC, ROC, and TIC content in supraglacial debris and cryoconite, in both ppm and percentage content are presented in Table B.7.2. A selection of four cryoconite samples were analysed from each glacier. Samples weighed to between 75 – 125 mg.

Table B.7.1 *Results of DIN A calibration standard for TOC, ROC, and TIC determination shown in both ppm and % content.*

Sample Reference	Sample No.	Weight (mg)	TOC (ppm)	ROC (ppm)	TIC (ppm)	TOC (%)	ROC (%)	TIC (%)
Standard	n/a	10.0	0.19	0.16	0.19	1.93	1.61	1.88
Standard	n/a	24.9	0.52	0.55	0.52	2.10	2.19	2.09
Standard	n/a	50.9	1.00	1.05	1.06	1.97	2.07	2.09
Standard	n/a	75.3	1.50	1.48	1.47	1.99	1.97	1.96
Standard	n/a	100.1	2.00	1.92	1.88	2.00	1.92	1.88
Standard	n/a	125.4	2.52	2.58	2.62	2.01	2.06	2.09
Standard	n/a	149.7	2.99	2.99	2.98	2.00	1.99	1.99

Table B.7.2 *Results of TOC, ROC, and TIC determination in cryoconite and supraglacial debris shown in both ppm and % content. Samples weighed to between 75-125 mg. Information includes blanks for quality control.*

Sample Reference	Sample No.	Weight (mg)	TOC (ppm)	ROC (ppm)	TIC (ppm)	TOC (%)	ROC (%)	TIC (%)
Blank	n/a	1	0.01	<LOD	<LOD	0.59	<LOD	<LOD
Blank	n/a	1	<LOD	<LOD	<LOD	<LOD	<LOD	<LOD
Blank	n/a	1	<LOD	<LOD	<LOD	<LOD	<LOD	<LOD
ML1	83	90.9	2.23	0.30	0.01	2.45	0.33	0.01
ML2	84	86.2	1.75	0.42	0.00	2.03	0.48	0.01
ML3	85	78.4	27.09	0.45	<LOD	34.56	0.58	<LOD
ML4	86	81.1	12.36	0.33	0.01	15.25	0.41	0.01
ABS1	88	112.6	2.02	0.69	0.02	1.79	0.62	0.02
ABS2	89	83.6	1.74	0.25	0.01	2.08	0.30	0.01
ABS3	90	103.1	5.82	0.33	0.02	5.65	0.32	0.02
1a	1	86.3	1.60	0.22	0.01	1.86	0.26	0.01
5a	5	95.1	1.70	0.25	0.02	1.78	0.26	0.02
7a	7	110.0	2.54	0.57	0.02	2.31	0.51	0.02
8a	8	87.7	2.53	0.69	0.01	2.89	0.79	0.02
AB1a	9	80.1	0.84	0.08	0.01	1.05	0.11	0.01
AB5a	13	76.0	0.14	0.16	0.20	0.18	0.22	0.26
AB8a	16	97.7	0.54	0.03	0.02	0.55	0.03	0.02
AB10a	18	93.7	1.05	0.12	0.02	1.12	0.13	0.02
VB2a	20	96.4	2.24	0.31	<LOD	2.32	0.32	<LOD
VB6a	24	119.3	2.86	0.83	0.01	2.40	0.69	0.01
VB7a	25	93.0	0.22	1.22	6.15	0.24	1.31	6.62
VB9a	27	84.4	1.55	0.56	<LOD	1.84	0.67	<LOD

B.8 Ion Chromatography

Anion concentrations in cryoconite hole water and snow samples were determined using ion chromatography (IC). Standards were used to obtain calibration curves for the anions: F^-, Cl^-, NO_3^-, Br^-, NO_2^-, PO_4^{3-}, and SO_4^{2-} at concentrations of 0.2, 0.5, 1.0, 2.0, 5.0 and 10.0 ppm. An example of a chromatogram is presented in Fig. B.8.1. Blank information is not displayed as all results were below the limit of detection. The results for cryoconite hole water and snow are

presented in Tables B.8.1 and B.8.2 respectively. Many of the concentrations were very low and although quantified by IC, were outside of the calibration range but have been included for information purposes. Examples of one cryoconite hole water and snow chromatogram per location are presented in Fig. B.8.2 – B.8.4 and Fig. B.8.5 – B.8.7 respectively.

Table B.8.1 *Concentrations of anions present in cryoconite hole water samples collected from cryoconite holes located on Midtre Lovénbreen, Austre Brøggerbreen, and Vestre Brøggerbreen in August 2021. Anion concentrations analysed by IC. All concentrations displayed in mg L^{-1}. Concentrations recorded outside the calibration range can be identified by [a].*

Sample Ref.	Sample No.	Cl^- (mg L^{-1})	SO_4^{2-} (mg L^{-1})	NO_3^- (mg L^{-1})	Figure No.
1	30	-	0.286[a]	-	
2	31	0.168[a]	0.317[a]	-	
3	32	0.167[a]	0.331	-	
4	33	0.168[a]	0.333	-	
5	34	0.170[a]	0.334	-	
6	35	0.176[a]	0.337	-	
7	36	0.198[a]	0.336	-	
8	37	0.300	0.349	-	B.8.2
AB1	38	0.304[a]	0.628[a]	-	
AB2	39	0.317[a]	0.697	-	
AB3	40	0.324[a]	0.700	-	B.8.3
AB4	41	-	-	-	
AB5	42	0.351[a]	0.647	-	
AB6	43	0.353[a]	0.633	-	
AB7	44	0.319[a]	0.617[a]	-	
AB8	45	0.323[a]	0.661	-	
AB9	46	0.346[a]	0.682	-	
AB10	47	0.315[a]	0.649	-	
VB1	48	0.370[a]	0.888	-	B.8.4
VB2	49	0.357[a]	0.730	-	
VB3	50	0.386[a]	0.646	-	
VB4	51	0.386[a]	0.616[a]	0.318[a]	
VB5	52	0.355[a]	0.741	-	
VB6	53	0.363[a]	0.641	-	
VB7	54	0.379[a]	0.613[a]	-	
VB8	55	0.361[a]	0.828	-	
VB9	56	0.320[a]	0.523[a]	-	
VB10	57	0.343[a]	0.680	-	

[a] Concentrations quantified, but below calibration.

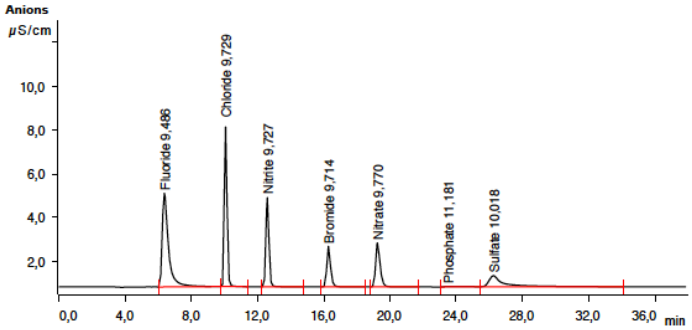

Peak number	Retention time min	Area (µS/cm) x min	Height µS/cm	Concentration mg/L	Component name
1	6,357	1,8854	4,288	9,486	Fluoride
2	10,053	1,3206	7,312	9,729	Chloride
3	12,575	0,8614	4,081	9,727	Nitrite
4	16,262	0,4967	1,850	9,714	Bromide
5	19,225	0,6306	2,011	9,770	Nitrate
6	23,475	0,0264	0,023	11,181	Phosphate
7	26,240	0,5275	0,505	10,018	Sulfate

Figure B.8.1 *10ppm standard ion chromatogram.*

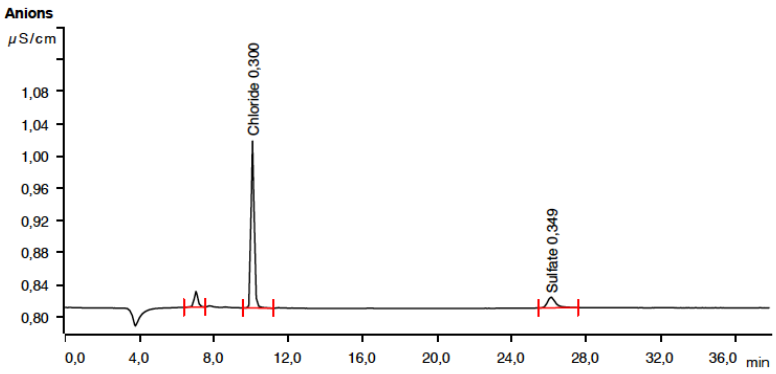

Peak number	Retention time min	Area (µS/cm) x min	Height µS/cm	Concentration mg/L	Component name
1	7,025	0,0045	0,019	invalid	
2	10,067	0,0387	0,208	0,300	Chloride
3	26,108	0,0069	0,013	0,349	Sulfate

Figure B.8.2 *Cryoconite hole water sample 8 ion chromatogram.*

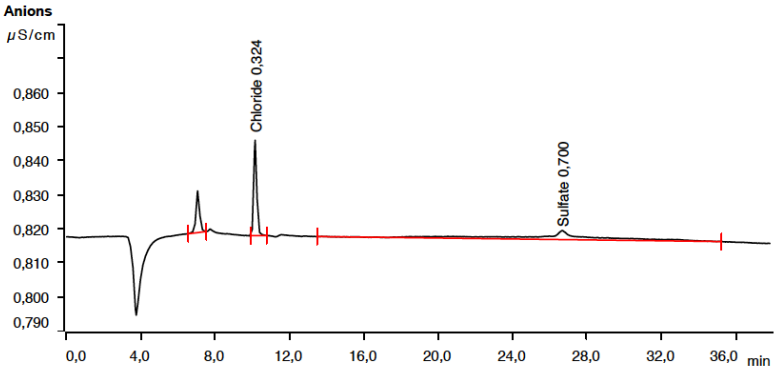

Peak number	Retention time min	Area (µS/cm) x min	Height µS/cm	Concentration mg/L	Component name
1	7,072	0,0028	0,012	invalid	
2	10,163	0,0053	0,028	0,324	Chloride
3	26,645	0,0098	0,003	0,700	Sulfate

Figure B.8.3 *Cryoconite hole water sample AB3 ion chromatogram.*

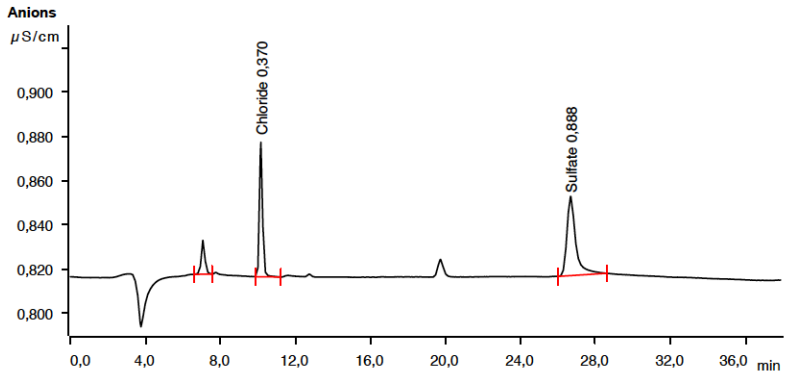

Peak number	Retention time	Area	Height	Concentration	Component name
	min	(µS/cm) x min	µS/cm	mg/L	
1	7,067	0,0035	0,015	invalid	
2	10,160	0,0116	0,061	0,370	Chloride
3	26,650	0,0195	0,036	0,888	Sulfate

Figure B.8.4 *Cryoconite hole water sample VB1 ion chromatogram.*

Table B.8.2 *Concentrations of anions present in snow samples collected from Midtre Lovénbreen, Austre Brøggerbreen, and Vestre Brøggerbreen in August 2021. Anion concentrations analysed by IC. All concentrations displayed in mg L^{-1}. Concentrations recorded outside the calibration range can be identified by [a]. No analysis was performed for snow sample no. 81 due to insufficient volume of sample. Dilution factor included for samples diluted with ultra-pure water where insufficient melted snow volume was available for analysis. Concentrations have been adjusted for dilution.*

Sample Ref.	Sample No.	Dilution Factor	Cl^- (mg L^{-1})	SO_4^{2-} (mg L^{-1})	NO_3^- (mg L^{-1})	Figure No.
MLS1	58	-	0.369	-	-	
MLS2	59	-	0.525	-	-	B.8.5
MLS3	60	-	0.357	-	-	
MLS4	61	-	0.396	0.278[a]	0.150[a]	
MLS5	62	-	0.325	-	-	
MLS6	63	-	0.403	-	-	
MLS7	64	-	0.525	0.276[a]	0.158[a]	
MLS8	65	-	0.488	-	-	
MLS9	66	-	0.420	-	0.153[a]	
MLS10	67	-	0.496	-	0.150[a]	
ABSN1	68	-	0.414	-	-	B.8.6
ABSN2	69	-	0.458	0.275[a]	0.149[a]	
ABSN3	70	-	0.439	0.276[a]	0.197[a]	
ABSN4	71	-	0.407	-	0.191[a]	
ABSN5	72	-	0.449	-	0.167[a]	
ABSN6	73	-	0.419	-	0.184[a]	
ABSN7	74	-	0.441	-	0.165[a]	
ABSN8	75	-	0.442	-	0.151[a]	
VBSN1	76	-	0.190[a]	0.279[a]	0.153[a]	
VBSN2	77	1:2	0.532[b]	-	-	B.8.7
VBSN3	78	-	0.187[a]	0.287[a]	-	
VBSN4	79	1:1.5	0.309[a,b]	0.449[a,b]	0.219[a,b]	
VBSN5	80	1:2.7	0.515[a,b]	0.796[a,b]	0.398[a,b]	
VBSN7	82	1:2.3	0.388[a,b]	0.637[a,b]	-	

[a] Concentrations quantified, but below calibration;

[b] Concentrations have been adjusted with respect to dilution factor.

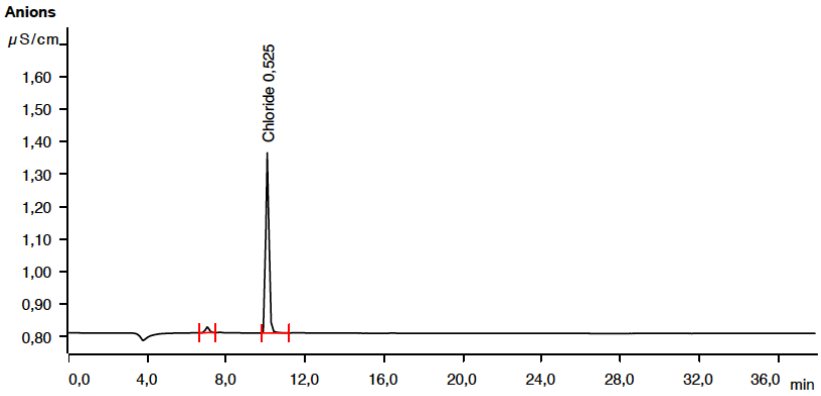

Peak number	Retention time	Area	Height	Concentration	Component name
	min	(µS/cm) x min	µS/cm	mg/L	
1	7,027	0,0037	0,017	invalid	
2	10,070	0,1003	0,555	0,525	Chloride

Figure B.8.5 *Snow sample MLS2 ion chromatogram.*

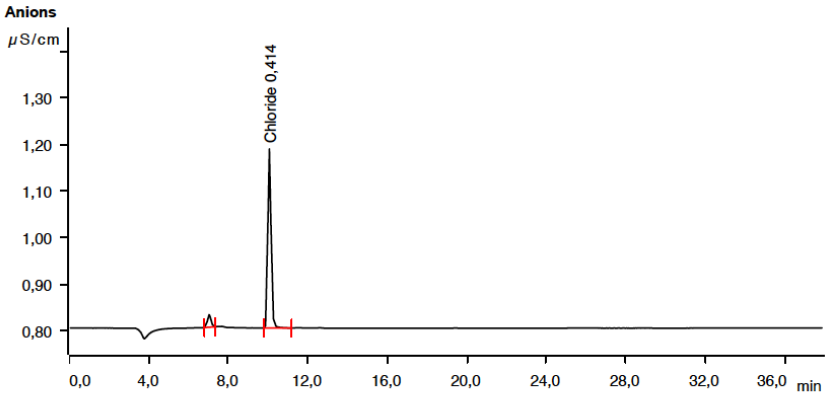

Peak number	Retention time	Area	Height	Concentration	Component name
	min	(µS/cm) x min	µS/cm	mg/L	
1	7,032	0,0056	0,027	invalid	
2	10,062	0,0698	0,384	0,414	Chloride

Figure B.8.6 *Snow sample ABSN1 ion chromatogram.*

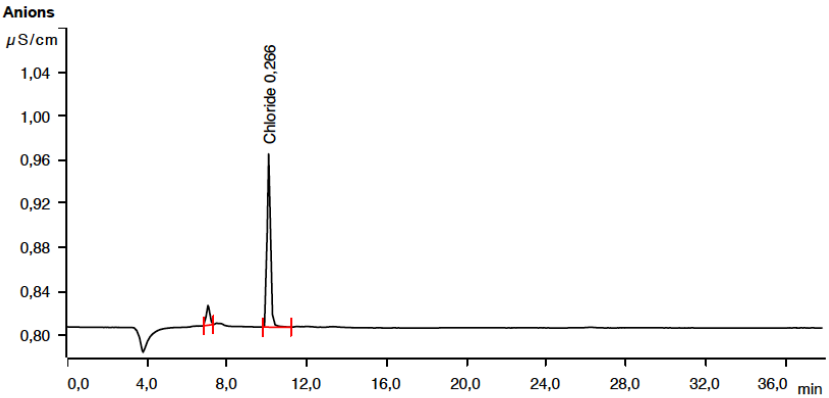

Peak number	Retention time	Area	Height	Concentration	Component name
	min	(µS/cm) x min	µS/cm	mg/L	
1	7,032	0,0037	0,018	invalid	
2	10,077	0,0296	0,158	0,266	Chloride

Figure B.8.7 *Snow sample VBSN2 ion chromatogram.*

B.9 Elemental Analysis of Cryoconite Hole Water and Snow

Cryoconite hole water and snow collected from the surface of three glaciers: Midtre Lovénbreen (ML), Austre Brøggerbreen (AB), and Vestre Brøggerbreen (VB) were analysed for 62 elements by ICP-MS. Of these elements, 11 were selected for further investigation: Na, Cl, Al, Fe, Ca, Mg, Zn, Pb, As, Cd, and Cr. The results of the elemental analysis for each sample are presented in Tables B.9.1 and B.9.2.

Table B.9.1 *Elemental concentrations detected in cryoconite hole water from three glaciers in Ny-Ålesund. Locations are represented as ML (Midtre Lovénbreen), AB (Austre Brøggerbreen), and VB (Vestre Brøggerbreen). Concentration is displayed in μg L^{-1} for all elements. Samples analysed by ICP-MS.*

Sample Ref.	Sample No.	Location	Na μg L^{-1}	Cl μg L^{-1}	Ca μg L^{-1}	Mg μg L^{-1}	Al μg L^{-1}	Fe μg L^{-1}	As μg L^{-1}	Cd μg L^{-1}	Cr μg L^{-1}	Pb μg L^{-1}	Zn μg L^{-1}
1	30	ML	3.03	<LOD	34.31	3.20	0.315	1.003	0.003	0.0004	<LOD	0.007	1.135
2	31	ML	11.03	<LOD	34.70	5.47	0.516	2.001	0.005	0.0003	<LOD	0.020	1.095
3	32	ML	9.75	<LOD	41.86	8.58	0.727	2.373	0.007	0.0007	<LOD	0.028	1.253
4	33	ML	12.37	<LOD	44.07	9.36	1.084	3.129	0.006	0.0007	<LOD	0.033	1.136
5	34	ML	12.85	<LOD	41.43	9.06	1.309	2.823	0.005	0.0007	<LOD	0.052	0.481
6	35	ML	17.97	<LOD	29.10	7.50	0.740	2.379	0.008	0.0006	<LOD	0.055	0.567
7	36	ML	44.18	<LOD	46.37	13.14	0.920	2.825	0.013	0.0008	<LOD	0.106	0.993
8	37	ML	141.06	210.97	57.86	23.43	1.100	2.677	0.016	0.0012	<LOD	0.099	1.689
AB1	38	AB	24.88	<LOD	62.67	16.29	2.253	0.864	<LOD	0.0006	<LOD	<LOD	2.237
AB2	39	AB	40.06	<LOD	110.56	27.86	1.499	2.285	0.006	0.0016	0.032	<LOD	1.430
AB3	40	AB	49.50	<LOD	56.95	11.25	3.611	1.841	0.003	0.0003	<LOD	<LOD	1.066
AB4	41	AB	10.38	<LOD	39.36	5.18	0.336	0.756	<LOD	0.0004	<LOD	<LOD	0.780
AB5	42	AB	72.11	198.61	673.53	273.39	1.775	2.061	0.005	0.0046	<LOD	<LOD	0.712
AB6	43	AB	73.99	125.86	258.05	89.19	1.356	2.346	0.006	0.0024	0.016	<LOD	1.040
AB7	44	AB	40.83	<LOD	161.04	47.07	0.941	2.003	<LOD	0.0011	<LOD	<LOD	1.803
AB8	45	AB	46.76	<LOD	42.05	6.14	1.396	2.290	0.004	0.0004	0.030	0.006	0.979
AB9	46	AB	68.63	103.53	60.99	16.16	1.172	1.758	0.004	0.0005	<LOD	0.004	1.427
AB10	47	AB	44.79	<LOD	53.52	9.78	2.134	1.695	0.003	0.0009	<LOD	<LOD	1.576

Sample Ref.	Sample No.	Location	Na µg L^{-1}	Cl µg L^{-1}	Ca µg L^{-1}	Mg µg L^{-1}	Al µg L^{-1}	Fe µg L^{-1}	As µg L^{-1}	Cd µg L^{-1}	Cr µg L^{-1}	Pb µg L^{-1}	Zn µg L^{-1}
VB1	48	VB	79.89	114.49	853.54	311.56	1.724	1.374	0.012	0.0037	<LOD	<LOD	1.676
VB2	49	VB	73.96	134.30	1695.76	532.23	2.846	2.183	0.015	0.0035	0.032	<LOD	1.822
VB3	50	VB	99.47	138.71	1436.69	466.02	3.340	1.140	0.014	0.0042	0.006	<LOD	0.882
VB4	51	VB	92.96	146.29	1620.01	773.70	3.502	1.477	0.016	0.0028	0.018	<LOD	0.654
VB5	52	VB	70.76	114.55	330.28	129.88	1.558	1.409	0.010	0.0022	<LOD	0.004	0.800
VB6	53	VB	78.16	96.22	570.40	262.07	1.621	1.515	0.011	0.0017	0.028	0.007	0.632
VB7	54	VB	89.17	119.55	5533.57	1700.11	7.714	1.207	0.021	0.0055	0.077	<LOD	0.185
VB8	55	VB	71.07	<LOD	199.50	81.22	1.365	1.349	0.015	0.0030	<LOD	0.017	0.897
VB9	56	VB	36.94	<LOD	55.03	20.82	0.982	1.267	0.006	0.0010	0.014	0.017	0.691
VB10	57	VB	62.63	<LOD	218.57	36.21	1.144	1.056	0.011	0.0014	<LOD	0.027	0.836

Table B.9.1 continued: Elemental concentrations detected in cryoconite hole water from three glaciers in Ny-Ålesund

Table B.9.2 *Elemental concentrations detected in snow from three glaciers in Ny-Ålesund. Locations are represented as ML (Midtre Lovénbreen), AB (Austre Brøggerbreen), and VB (Vestre Brøggerbreen). Concentrations are displayed in µg L^{-1} for all elements. Samples analysed by ICP-MS.*

Sample Ref.	Sample No.	Location	Na µg L^{-1}	Cl µg L^{-1}	Ca µg L^{-1}	Mg µg L^{-1}	Al µg L^{-1}	Fe µg L^{-1}	As µg L^{-1}	Cd µg L^{-1}	Cr µg L^{-1}	Pb µg L^{-1}	Zn µg L^{-1}
MLS1	58	ML	292.51	513.18	17.25	1.75	0.176	0.436	0.003	<LOD	<LOD	<LOD	0.101
MLS2	59	ML	424.61	667.19	39.54	3.77	0.216	0.569	0.003	0.0003	<LOD	<LOD	0.638
MLS3	60	ML	242.74	458.57	30.15	3.20	0.665	2.053	<LOD	<LOD	<LOD	<LOD	2.345
MLS4	61	ML	281.93	475.96	69.27	7.96	0.954	1.293	<LOD	0.0013	0.027	0.014	1.864
MLS5	62	ML	205.43	317.53	43.93	3.35	0.042	0.748	<LOD	0.0001	<LOD	<LOD	0.298
MLS6	63	ML	290.31	436.48	53.12	6.13	0.178	0.987	<LOD	0.0006	0.025	<LOD	0.814
MLS7	64	ML	421.08	662.53	55.77	2.65	0.108	0.975	<LOD	0.0002	<LOD	<LOD	0.304
MLS8	65	ML	442.61	758.93	43.02	3.50	0.558	1.651	0.004	0.0004	<LOD	0.005	0.219
MLS9	66	ML	347.73	552.50	47.51	2.13	0.032	1.350	<LOD	0.0003	0.013	<LOD	0.365
MLS10	67	ML	409.59	705.75	43.65	3.14	0.526	1.785	0.003	0.0007	<LOD	0.004	0.366

Sample Ref.	Sample No.	Location	Na µg L^{-1}	Cl µg L^{-1}	Ca µg L^{-1}	Mg µg L^{-1}	Al µg L^{-1}	Fe µg L^{-1}	As µg L^{-1}	Cd µg L^{-1}	Cr µg L^{-1}	Pb µg L^{-1}	Zn µg L^{-1}
ABSN1	68	AB	292.96	512.77	77.98	15.95	2.742	3.564	0.006	0.0010	<LOD	0.025	1.589
ABSN2	69	AB	323.68	642.50	87.50	23.03	1.109	3.614	0.006	0.0020	0.051	0.024	1.398
ABSN3	70	AB	293.87	457.85	54.16	11.98	1.140	2.708	0.005	0.0007	<LOD	0.018	0.606
ABSN4	71	AB	272.12	400.12	55.75	11.59	0.968	3.483	0.008	0.0007	<LOD	0.028	0.749
ABSN5	72	AB	342.86	491.94	73.84	15.11	0.816	3.010	0.005	0.0010	0.010	0.029	1.446
ABSN6	73	AB	290.55	462.69	57.73	13.15	0.965	2.777	0.012	0.0007	<LOD	0.020	0.846
ABSN7	74	AB	307.85	617.95	64.17	12.50	0.857	2.511	0.007	0.0005	<LOD	0.024	0.913
ABSN8	75	AB	305.17	507.20	66.54	11.96	1.001	3.200	0.009	0.0007	<LOD	0.026	1.869
VBSN1	76	VB	41.21	<LOD	90.00	26.91	2.929	13.258	0.006	0.0015	0.144	0.018	1.572
VBSN2	77	VB	289.20	420.47	69.47	22.86	4.094	7.827	0.013	0.0014	0.205	0.046	0.588
VBSN3	78	VB	27.14	<LOD	38.90	16.80	3.324	4.185	0.009	0.0012	0.029	0.017	0.267
VBSN4	79	VB	79.95	96.55	204.96	93.40	5.560	8.141	0.011	0.0021	0.022	0.035	0.494
VBSN5	80	VB	57.24	125.22	111.95	51.57	3.810	5.511	0.008	0.0014	0.037	0.022	0.695
VBSN6	81	VB	43.84	<LOD	167.73	84.58	3.377	4.944	0.008	0.0018	0.019	0.022	0.671
VBSN7	82	VB	22.12	<LOD	32.09	12.53	2.797	3.969	0.008	0.0009	0.009	0.019	0.351

Table B.9.2 continued: Elemental concentrations detected in snow from three glaciers in Ny-Ålesund.

B.10 Gas Chromatography - Mass Spectrometry Calibration and PAH Data

Calibration curves established for the seven indicator PCBs are presented in Fig. B.10.1 based on the relative response, using calibration solutions with concentrations of 'Dutch Seven' ES dissolved in ethyl acetate of: 0.5, 5, 10, 30, 50, and 100 ng mL^{-1}. Internal standards (3'-F-PCB and 5'-F-PCB) were added at concentrations of 50 ng mL^{-1} to each calibration solution.

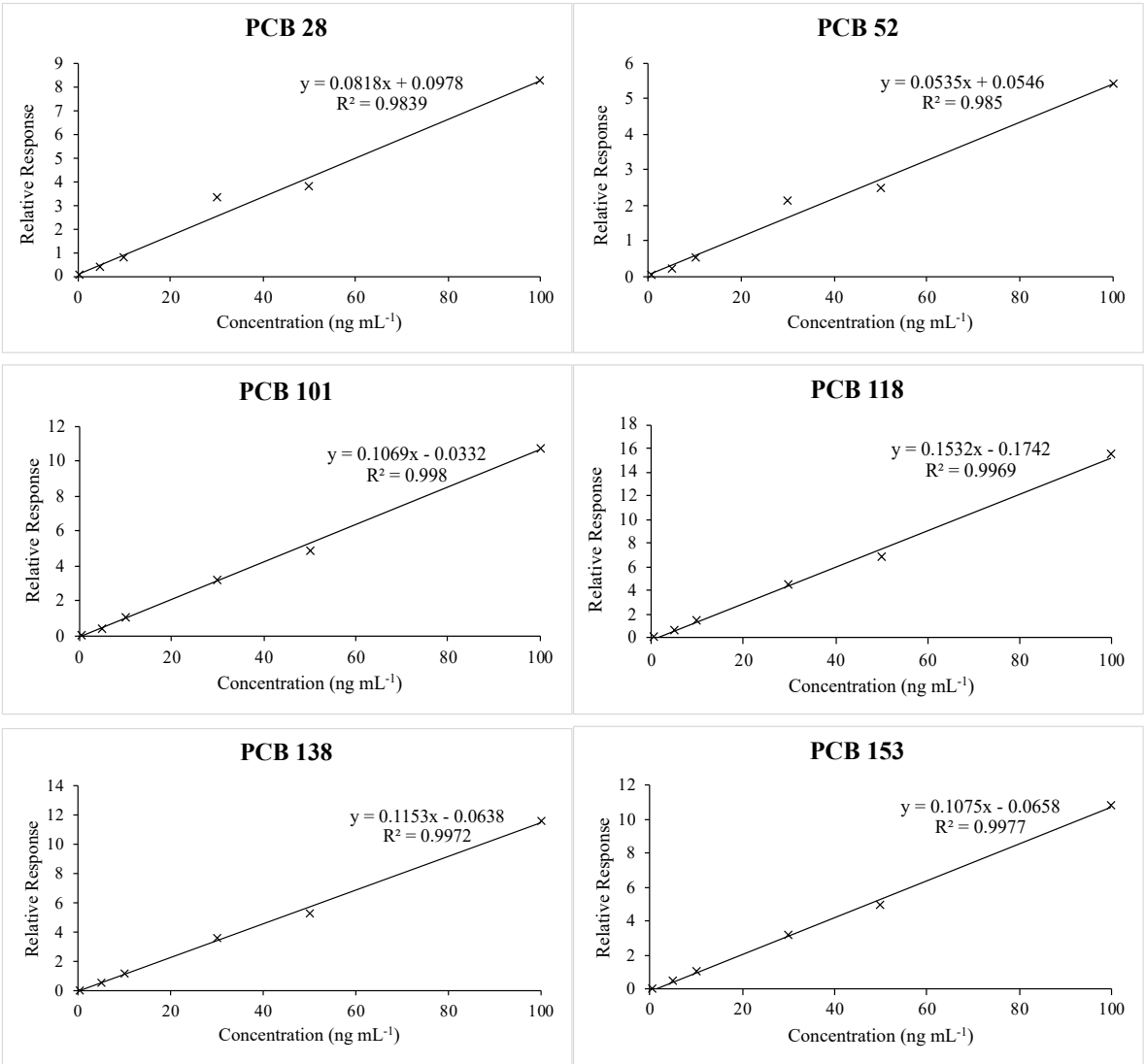

Figure B.10.1 *Calibration curves for the seven indicator PCBs: PCB 28, 52, 101, 118, 138, 153, and 180 established using the relative response based on the peak area of the target analyte relative to the peak area of the internal standard in the standard solution. Calibration concentrations prepared at concentrations of 0.5, 5, 10, 30, 50, and 100 ng mL^{-1} of 'Dutch Seven' PCBs in ethyl acetate. Internal standard concentration in each standard solution of 50 ng mL^{-1} for both 3'-F-PCB and 5'-F-PCB. The co-efficient of determination is represented by R^2.*

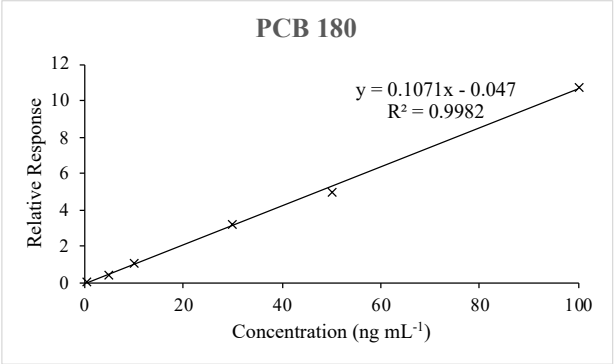

Figure B.10.1 continued: Calibration curves for the seven indicator PCBs: PCB 28, 52, 101, 118, 138, 153, and 180 established using the relative response based on the peak area of the target analyte relative to the peak area of the internal standard in a standard solution.

Table B.10.1 *Raw calibration data for the four PAHs detected in cryoconite by GC-MS. Calibration concentrations of 0.5, 5, 10, 30, 50, and 100 ng mL^{-1} of 16 PAHs dissolved in ethyl acetate. The retention time (RT) is given in minutes. Information on peak area, signal to noise ratio (S/N) and peak height is also presented for each concentration.*

PAH	Concentration (ng mL^{-1})	RT	Peak Area	S/N	Peak Height
Naphthalene					
	0.5	7.717	368.53	3.27	145.50
	5	7.717	912.66	10.93	585.43
	10	7.717	1,111.79	24.24	788.47
	30	7.717	4568.75	84.82	3351.39
	50	7.717	6742.13	169.12	5364.68
	100	7.717	14551.07	356.44	11821.69
Phenanthrene					
	0.5	11.190	219.83	1.68	96.93
	5	11.190	1184.04	5.46	640.20
	10	11.190	1698.57	5.92	906.02
	30	11.190	6569.32	160.80	3830.57
	50	11.190	10198.49	109.37	5441.28
	100	11.181	22047.59	217.52	12743.04
Fluoranthene					
	0.5	13.331	99.86	1.98	50.44
	5	13.331	1566.96	25.71	570.04
	10	13.331	2153.81	31.94	782.95
	30	13.331	8480.08	91.91	3258.68
	50	13.322	13447.08	150.29	4984.42
	100	13.322	30001.92	383.41	11856.38
Pyrene					
	0.5	13.880	135.66	1.79	45.44
	5	13.880	1578.56	25.84	573.04
	10	13.889	2274.46	32.83	804.95
	30	13.880	8987.02	88.85	3150.15
	50	13.880	14264.86	157.74	5231.74
	100	13.880	31059.52	389.33	12039.39

Table B.10.2 *Peak areas for each of the four PAHs detected in cryoconite by GC-MS. PAHs are represented by NAP = naphthalene, PHEN = phenanthrene, FLTH = fluoranthene, and PYR = pyrene. The retention time (RT) is presented in minutes. Method blank data (MB1 – MB5) is provided for reference. Where the retention time differs by > 0.02 minutes from the RT identified in calibration, or where the GC software flagged an uncertainty in the peak retention time, the peak area has been assigned 'NA' indicating no peak was identified.*

Sample Ref.	RT (min)	NAP Peak Area	RT (min)	PHEN Peak Area	RT (min)	FLTH Peak Area	RT (min)	PYR Peak Area
MB1	7.591	NA	11.172	829.06	13.313	199.05	13.861	221.03
MB2	7.591	NA	11.172	789.59	13.313	195.96	13.861	199.43
MB3	7.591	NA	11.172	446.78	13.313	102.32	13.861	153.20
MB4	7.591	NA	11.181	540.04	13.322	144.60	13.880	223.51
MB5	7.717	538.58	11.181	760.96	13.322	219.09	13.871	409.17
ML1	7.717	1293.33	11.172	1571.60	13.313	753.96	13.862	570.13
ML2	7.717	1250.57	11.172	1395.57	13.313	626.17	13.861	499.89
ML3	7.717	1602.16	11.172	1865.65	13.304	NA	13.861	647.72
ML4	7.717	1951.40	11.172	2160.98	13.313	1100.82	13.861	713.10
ML5	7.717	1641.86	11.172	1897.28	13.313	1006.09	13.862	723.34
ML6	7.717	1565.96	11.172	2420.42	13.313	1232.96	13.861	746.62
ML7	7.716	2529.33	11.172	3736.86	13.303	NA	13.861	1785.96
ML8	7.717	3116.30	11.172	5322.72	13.304	NA	13.861	2785.00
AB1	7.717	703.95	11.172	1267.11	13.305	NA	13.863	440.82
AB2	7.717	727.41	11.172	1260.59	13.305	NA	13.863	429.46
AB3	7.717	506.65	11.172	1124.44	13.304	NA	13.861	426.33
AB4	7.717	783.69	11.172	1451.81	13.313	694.08	13.862	481.71
AB5	7.717	552.06	11.172	1454.11	13.313	384.14	13.862	522.16
AB6	7.717	563.87	11.172	1815.00	13.313	477.68	13.861	666.41
AB7	7.717	590.08	11.172	1450.75	13.313	417.25	13.861	456.15
AB8	7.717	546.30	11.172	931.22	13.313	338.63	13.861	295.77
AB9	7.717	558.08	11.172	1045.32	13.313	358.91	13.861	326.49
AB10	7.717	667.24	11.172	1244.58	13.313	529.83	13.861	413.24
VB1	7.717	2316.65	11.172	4734.23	13.304	NA	13.861	1186.40
VB2	7.628	NA	11.172	3450.82	13.304	NA	13.861	1153.92
VB3	7.717	2151.34	11.172	4029.78	13.304	NA	13.861	1434.99
VB4	7.717	2670.73	11.172	4318.89	13.313	1,635.19	13.861	1496.32
VB5	7.717	1781.81	11.172	3635.58	13.304	NA	13.861	873.41
VB6	7.717	14795.24	11.172	18129.72	13.304	NA	13.852	NA
VB7	7.717	789.59	11.172	3768.59	13.304	NA	13.862	2560.11
VB8	7.717	1680.35	11.172	3258.90	13.303	NA	13.861	1058.14
VB9	7.717	6149.67	11.172	12234.34	13.305	NA	13.863	4713.18
VB10	7.628	NA	11.172	4232.82	13.304	NA	13.861	1379.84

B.11 A Comparison of Elemental Concentrations in Cryoconite with Other Matrices in Svalbard

Table B.11.1 *Comparison of elemental concentrations in cryoconite with studies of different matrices located in Svalbard. Mean, minimum (min) and maximum (max) concentrations of elements are presented where available. Units are presented as reported in the studies, as either µg g^{-1}, mg kg^{-1} or ppm. The 'NA' represents those elements which have not been analysed in the studies, and 'n' represents the number of samples. The analytical techniques used in each study are presented below the table.*

Location	Units		Al	Fe	Ca	Zn	Pb	As	Cd	Cr	Reference
Ny-Ålesund, Svalbard											
Cryoconite[a]	µg g^{-1}	Mean	40300	36800	9220	87.8	50.0	7.14	0.119	61.2	This
(n = 28)	µg g^{-1}	Min	31600	14000	2010	60.6	8.33	2.77	0.0432	52.5	Study
	µg g^{-1}	Max	52100	47800	151000	101	135	11.9	0.532	84.1	
Ny-Ålesund & Adventdalen											
Surface soil[a]	µg g^{-1}	Mean	14400	10900	NA	66	11.9	3.47	0.44	18.4	(23)
(n = 37)	µg g^{-1}	Min	1500	1300	NA	16	5.6	0.93	0.13	2.2	
	µg g^{-1}	Max	36500	23600	NA	106	25.1	9.99	1.00	47.8	
Mineral soil[a]	µg g^{-1}	Mean	31900	25800	NA	55	11.4	6.6	0.12	42.1	
(n = 37)	µg g^{-1}	Min	6600	4900	NA	25	2.9	0.7	0.04	8.8	
	µg g^{-1}	Max	56800	43100	NA	105	22.7	14.1	0.50	72.3	
Midtre Lovénbreen											
Lichen[a]	ppm	Mean	NA	NA	NA	NA	NA	NA	NA	NA	(10)
(n = 8)	ppm	Min	88.6	74.15	NA	26.39	2.09	0.11	0.126	0.75	
	ppm	Max	1937	1566	NA	93.14	79.69	1.76	0.584	15.25	
Ny-Ålesund											
Vegetation[a]	µg g^{-1}	Mean	7896.18	6742.5	NA	69.86	8.37	1.36	0.54	10.59	(2)
(n = 33)	µg g^{-1}	Min	1868.79	1619.3	NA	33.76	3.33	0.32	0.13	2.79	
	µg g^{-1}	Max	16049.26	12460.7	NA	96.66	18.59	3.26	0.96	19.29	
Organic soil[a]	µg g^{-1}	Mean	20895.47	1566.58	NA	45.70	11.84	3.22	0.25	26.70	
(n = 13)	µg g^{-1}	Min	5029.48	3322.32	NA	11.62	3.84	1.95	0.005	9.00	
	µg g^{-1}	Max	46976.43	33021.46	NA	95.55	25.77	6.99	0.59	54.82	
Adventdalen											
Vegetation[a]	µg g^{-1}	Mean	21666.47	15301.65	NA	79.80	7.68	8.89	0.63	30.19	(2)
(n = 41)	µg g^{-1}	Min	4119.00	3226.08	NA	46.57	3.38	1.71	0.15	6.88	
	µg g^{-1}	Max	34753.53	27846.66	NA	125.47	12.16	17.66	2.16	52.38	

Location	Units		Al	Fe	Ca	Zn	Pb	As	Cd	Cr	Reference
Adventdalen											
Organic soil[a]	µg g^{-1}	Mean	47715.81	30520.59	NA	71.83	15.46	18.03	0.18	61.58	(2)
(n = 22)	µg g^{-1}	Min	27631.92	19482.74	NA	51.51	8.80	7.50	0.03	40.50	
	µg g^{-1}	Max	68509.33	46292.62	NA	99.14	19.31	28.39	0.54	81.36	
Kongsfjorden surface sediment[b]											
	mg kg^{-1}	Mean	NA	NA	NA	85.50	22.60	NA	0.19	64.70	(254)
	mg kg^{-1}	Min	NA	NA	NA	50.28	10.68	NA	0.13	48.65	
	mg kg^{-1}	Max	NA	NA	NA	199.07	36.59	NA	0.63	81.84	
Bayelva overbank sediment[a]											
	µg g^{-1}	Mean	20500	18300	49300	47.5	12.4	4.35	0.174	35.3	(235)
	µg g^{-1}	Min	1220	1030	14400	32.5	5.50	3.35	0.0971	26.8	
	µg g^{-1}	Max	28600	24900	155500	56.0	17.8	5.89	0.301	45.3	
Ny-Ålesund											
Coal[c]	µg g^{-1}	Mean	NA	1015	NA	16.6	5.0	NA	NA	NA	(253)
	µg g^{-1}	Min	NA	910	NA	16	4.8	NA	NA	NA	
	µg g^{-1}	Max	NA	1120	NA	17	5.2	NA	NA	NA	
Continental Crust											
	ppm		79600	43200	38500	65	14.8	1.7	0.1	126	(8, 68, 69)

Table B.11.1 continued: Comparison of the elemental composition of cryoconite with studies of different matrices located in Svalbard.
[a] Elemental analysis by ICP-MS.
[b] ICP-OES, Pb and Cd measured using graphite furnace atomic absorption spectroscopy.
[c] Atomic absorption spectroscopy (AAS).

B.12 Principal Component Analysis for Snow and Cryoconite Hole Water Samples

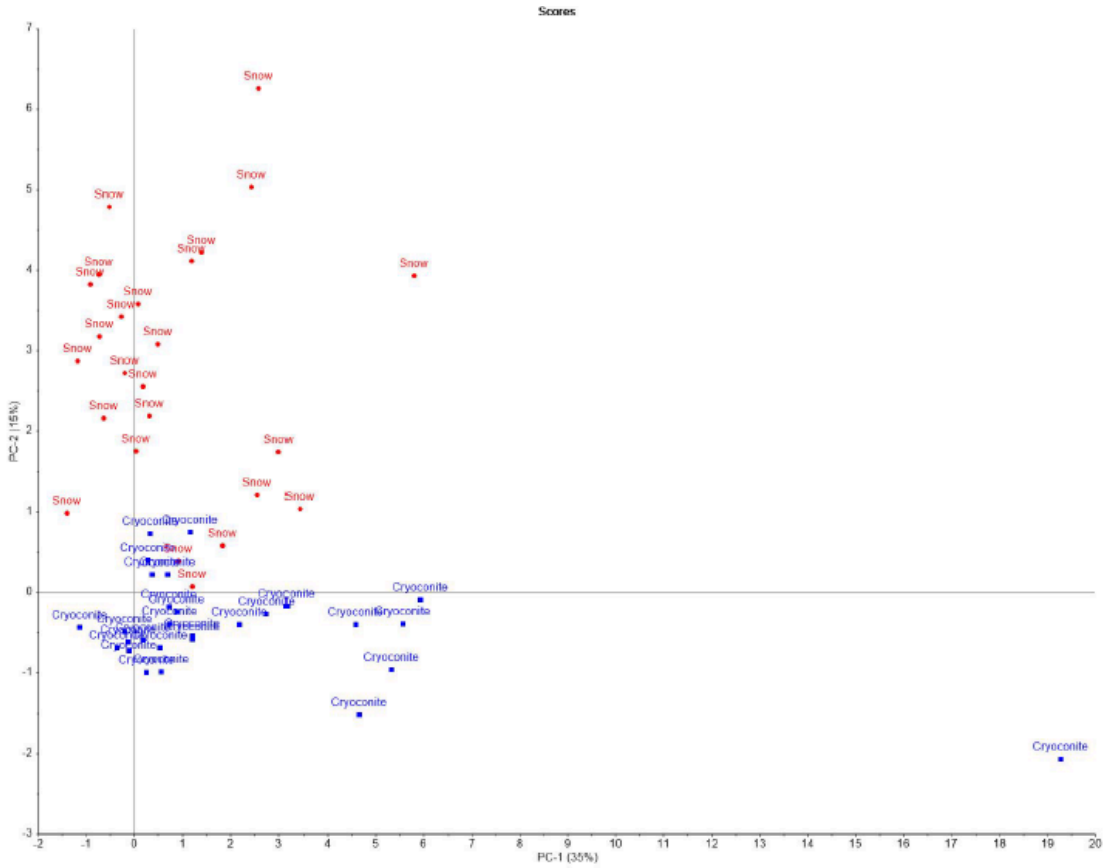

Figure B.12.1 *Principal Component Analysis (PCA) score and loadings plot for cryoconite hole water and snow. The PC1 and PC2 make up 50 % of the total data variance. The loadings plot shows the original variable influence (the elements analysed) and the score plot shows the cryoconite hole water and snow samples. Snow samples are displayed in red and cryoconite hole water samples are labelled 'cryoconite' in blue in the scores plot.*

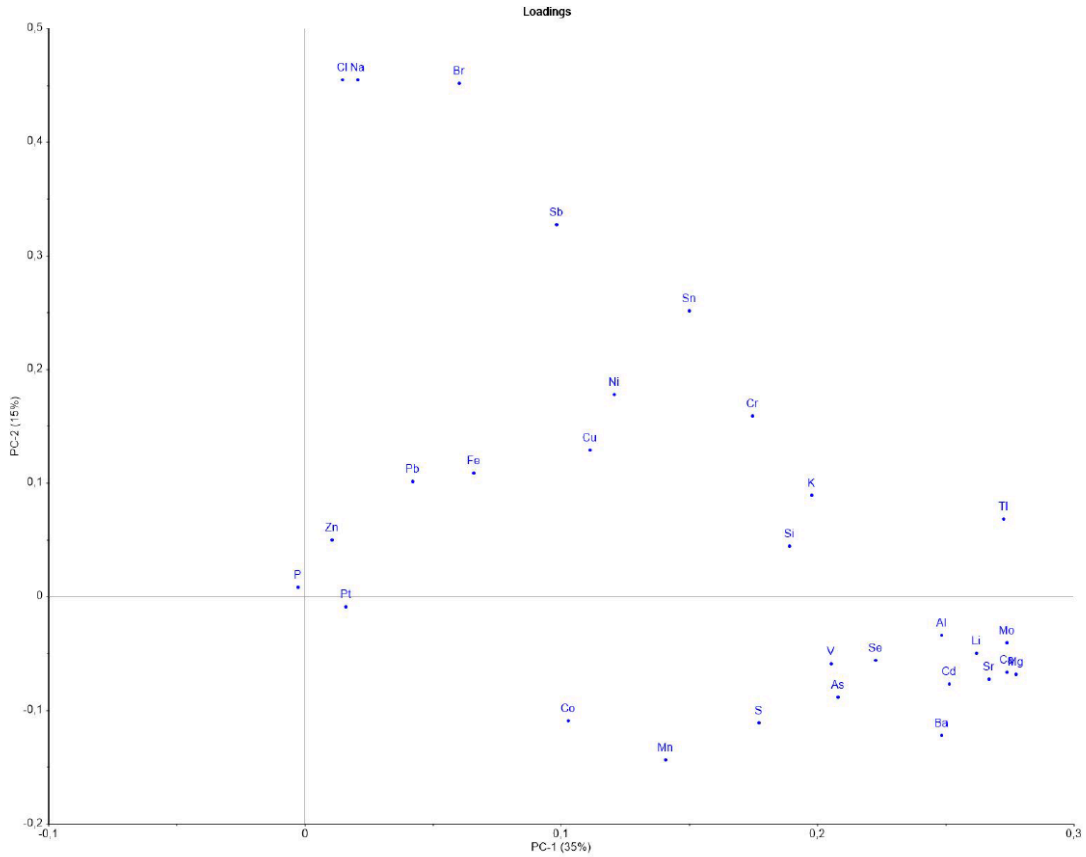

Figure B.12.1 continued: Principal Component Analysis (PCA) score and loadings plot for cryoconite hole water and snow. The PC1 and PC2 make up 50 % of the total data variance. The loadings plot shows the original variable influence (the elements analysed) and the score plot shows the cryoconite hole water and snow samples. Snow samples are displayed in red and cryoconite hole water samples are labelled 'cryoconite' in blue in the scores plot.

Sara Johnson

Cryoconite Holes as Potential Tools for Environmental Monitoring in the Arctic.

NTNU
Norwegian University of
Science and Technology